AFSWC-TN-61-29
Part I







# HEADQUARTERS
# AIR FORCE SPECIAL WEAPONS CENTER
# AIR FORCE SYSTEMS COMMAND
# KIRTLAND AIR FORCE BASE, NEW MEXICO



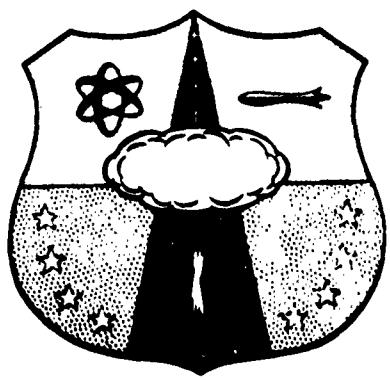

## AFSWC SECOND HYDRODYNAMIC CONFERENCE

**Numerical Methods of Fluid Flow Problems**

16-18 May 1961



Compiled by

John C. Rich
Lt USAF

AFSWC-TN-61-29
Part I

# AFSWC SECOND HYDRODYNAMIC CONFERENCE

## Numerical Methods of Fluid Flow Problems

16-18 May 1961

Compiled by

John C. Rich
Lt USAF

Research Directorate
AIR FORCE SPECIAL WEAPONS CENTER
Air Force Systems Command
Kirtland Air Force Base
New Mexico

Approved:

DONALD I. PRICKETT
Colonel USAF
Director, Research Directorate

Project No. 5776

## ABSTRACT

The second AFSWC Hydrodynamic Conference was held at Kirtland Air Force Base for the purpose of discussing numerical techniques which have become an important and widely used tool for solving fluid flow problems. A large number of the papers presented dealt with the problems of the finite difference analogs of the differential equations of motion. A few papers discussed work toward analytic solutions of these equations. Topics included hydrodynamics, magnetohydrodynamics, radiation transport, and solid material motion. (U)

The Proceedings are published in two parts: Part I is unclassified and Part II is classified. (U)

## PUBLICATION REVIEW

**This report has been reviewed and is approved.**

John J. Dishuck

JOHN J. DISHUCK
Colonel USAF
Deputy Chief of Staff for Operations

# AGENDA

AFSWC Second Hydrodynamic Conference
Numerical Methods of Fluid Flow Problems

16-18 May 1961

## FIRST SESSION

Moderator, Dr. Olen Nance, E. H. Plesset Associates

Welcoming Address, Col David R. Jones, AFSWC

The AFSWC Hydro-code, Lt Richard G. Allen, AFSWC

Use of the AFSWC Hydro-code, Dr. Louis Bothell, McAllister and Associates

Semi-Analytical Approximations and Scaling Rules for the X-Ray Problem, Dr. Jerrold Yos, AVCO-RAD

On the Treatment of Rarefaction Using a Dissipative Hydrodaynamics Code, Mr. Gunning Butler, Jr. and Mr. Daniel M. Young, Boeing Airplane Company

## SECOND SESSION

Moderator, Capt Jasper A. Welch, Jr., AFSWC

Analytic Methods and Approximations of MHD Problems, Dr. J. D. Cole and Dr. Carl Greifinger, The RAND Corporation

Numerical Approximations for Weak Solutions of Mixed Initial-Boundary Value Problems of Fluid Flows, Dr. W. McIlroy and Mr. Milton Halem, Republic Aviation Corporation

Early Solar Evolution, Dr. Arthur N. Cox, Los Alamos Scientific Laboratory

## THIRD SESSION

Moderator, Maj Lew Allen, Jr., AFSWC

The Aeronutronic HOP Program for Fluid Flow, Dr. R. A. Grandey, Aeronutronic

The Theory of Air Blasts, Dr. Walter Gibson, Cornell Aeronautical Laboratory

Some Comments on Convair's Work on Numerical Methods of Fluid Flow Problems, Dr. William F. Brown, et al., Convair, San Diego

FOURTH SESSION

Moderator, Capt Jasper A. Welch, Jr., AFSWC

Fluid Dynamics and Radiation Flow in the SPUTTER Code, Dr. Charles C. Loomis, General Atomic, Division of General Dynamics

The SHELL Radiation Hydrodynamics Code, Dr. Burton E. Freeman, General Atomic, Division of General Dynamics.

Problems of Radiation Transport, R. K. M. Landshoff and R. E. Meyerott, Lockheed Missiles and Space Division

Numerical Methods for Hydrodynamics with Radiation Transport, Dr. R. A. Grandey, Aeronutronic

FIFTH SESSION

Moderator, Dr. John G. Trulio, Lawrence Radiation Laboratory

Analysis of Hypervelocity Pellet Impacts, Lt John A. Davies, AFSWC

Shock Induced Reactions, Dr. Olen Nance, E. H. Plesset Associates

Calculation of Spall Based on a One-Dimensional Model, Dr. Mark L. Wilkins, Lawrence Radiation Laboratory

Dynamic Large Deflection of Shell Structures, Dr. Walter Herrmann, et al., Massachusetts Institute of Technology

Motion of an Elastic Half-Space, Dr. C. M. Ablow and Dr. Roy Alverson, Stanford Research Institute

Comments by the Moderator, Dr. John G. Trulio, Lawrence Radiation Laboratory

Attendance at the
AFSWC Second Hydrodynamic Conference
Numerical Methods of Fluid Flow Problems

16-18 May 1961

Kirtland Air Force Base, New Mexico

Dr. C. M. Ablow
Stanford Research Institute
Menlo Park, California

Dr. George Abrahamson
Stanford Research Institute
Menlo Park, California

Lt John Ahearne
AFSWC
Kirtland AFB
New Mexico

Mr. Frank J. Allen
BRL
Aberdeen Proving Ground, Md.

Maj Lew Allen
AFSWC
Kirtland AFB
New Mexico

Lt Richard G. Allen
AFSWC
Kirtland AFB
New Mexico

Capt M. C. Atkins
AFSWC
Kirtland AFB
New Mexico

Mr. Walter Atkins
Naval Research Laboratory
Washington, D. C.

Capt Harry Auld
AFSWC
Kirtland AFB
New Mexico

Dr. L. Evan Bailey
Stanford Research Institute
Menlo Park, California

Mr. Robert Banaugh
Lawrence Radiation Laboratory
Livermore, California

Mr. Patrick Blewett
AFSWC
Kirtland AFB
New Mexico

Dr. Robert L. Bjork
The RAND Corporation
Santa Monica, California

Dr. Louis E. Bothell
McAllister and Associates
Albuquerque, New Mexico

Dr. William F. Brown
Convair
San Diego, California

Mr. Gunning Butler
Boeing Airplane Company
Seattle, Washington

Dr. Ernest G. Chilton
Stanford Research Institute
Menlo Park, California

Mr. Philip Cooley
AFSWC
Kirtland AFB
New Mexico

Dr. Arthur Cox
LASL
Los Alamos, New Mexico

Mrs. Geraldine Creasey
McAllister and Associates
Albuquerque, New Mexico

Lt John A. Davies
AFSWC
Kirtland AFB
New Mexico

Mr. John O. Erkman
Stanford Research Institute
Menlo Park, California

Mr. Joseph Fleck
Lawrence Radiation Laboratory
Livermore, California

Mr. G. R. Fowles
Stanford Research Institute
Menlo Park, California

Dr. Burt Freeman
General Atomics
San Diego, California

Mr. Gilbert Fryklund
American Science & Engineering
Cambridge, Massachusetts

Lt J. D. Garcia
AFSWC
Kirtland AFB
New Mexico

Dr. Walter Gibson
Cornell Aeronautical Lab
Buffalo, New York

Capt C. M. Gillespie
AFSWC
Kirtland AFB
New Mexico

Dr. Ray Grandey
Aeronutronic
Newport Beach, California

Dr. Carl Greifinger
The RAND Corporation
Santa Monica, California

Mr. Milton Halem
Republic Aviation Corporation
Farmingdale, New York

Dr. J. Gordon Hall
Cornell Aeronautical Lab
Buffalo, New York

Dr. Walter Herrmann
MIT
Cambridge, Massachusetts

Lt T. L. Hershey
ASD
Wright-Patterson AFB, Ohio

Mr. Fred Herzfeld
RCA
Princeton, New Jersey

Dr. Donald Hicks
Boeing Airplane Company
Seattle, Washington

Lt Paul R. Hoffman
AFSWC
Kirtland AFB
New Mexico

Mr. John Jarem
RCA
Princeton, New Jersey

Lt John D. Johnston
AFSWC
Kirtland AFB
New Mexico

Col David R. Jones
AFSWC
Kirtland AFB
New Mexico

Mr. Sheldon Kahalas
Allied Research Assoc.
Boston, Massachusetts

Capt Donald L. Lamberson
AFSWC
Kirtland AFB
New Mexico

Dr. R. K. M. Landshoff
Lockheed Missiles & Space Div.
Palo Alto, California

Mr. John W. Lipford
Aeronutronic
Newport Beach, California

Lt P. M. Livingston
AFSWC
Kirtland AFB
New Mexico

Dr. Charles Loomis
General Atomic
San Diego, Calif

Lt Fred Lowery
AFSWC
Kirtland AFB
New Mexico

Mr. C. D. Lundergan
Sandia Corporation
Sandia Base, New Mexico

Maj William M. McCormac
DASA
Washington, D. C.

Dr. William McIlroy
Republic Aviation Corporation
Farmingdale, New York

Dr. R. E. Meyerott
Lockheed Missile & Space Div.
Palo Alto, California

Lt Col M. Morgan
DASA/FC
Sandia Base, New Mexico

Dr. Olen Nance
E. H. Plesset Associates
Los Angeles, California

Maj Marion R. Nadler
AFSWC
Kirtland AFB
New Mexico

Lt William J. Niles
AFSWC
Kirtland AFB
New Mexico

Capt Joseph O'Brien
AFSWC
Kirtland AFB
New Mexico

Mr. Carroll Porter
Naval Research Laboratory
Washington, D. C.

Mr. James Quong
Lawrence Radiation Laboratory
Livermore, California

Lt Roy Reichenbach
AFSWC
Kirtland AFB
New Mexico

Lt Robert Reynolds
AFSWC
Kirtland AFB
New Mexico

Lt John C. Rich
AFSWC
Kirtland AFB
New Mexico

Lt Patrick Roszel
AFSWC
Kirtland AFB
New Mexico

Dr. Donald Sachs
Aeronutronic
Newport Beach, California

Dr. Marion Schuler
Edgerton, Germeshausen & Grier
Boston, Mass

Capt Thomas Soapes
AFSWC
Kirtland AFB
New Mexico

Mr. Kenneth Schwartz
The RAND Corporation
Santa Monica, California

Dr. Harry E. Stubbs
Geophysics Corporation of America
Bedford, Massachusetts

Capt Frank Sulkowski
AFSWC
Kirtland AFB
New Mexico

Maj Marvin B. Sullivan
AFSWC
Kirtland AFB
New Mexico

Lt Paul N. Swarztrauber
AFSWC
Kirtland AFB
New Mexico

Mr. Nigel Thomas
Aerojet
Downey, California

Dr. John G. Trulio
Lawrence Radiation Laboratory
Livermore, California

Mr. Mark Wagner
Aerojet
Downey, California

Capt Raymond B. Walker
ASD
Wright-Patterson AFB, Ohio

Capt Jasper A. Welch, Jr.
AFSWC
Kirtland AFB
New Mexico

Capt Leland Welsh
AFSWC
Kirtland AFB
New Mexico

Lt Col Jack Whitener
AFSWC-RAND
Santa Monica, California

Dr. Mark Wilkins
Lawrence Radiation Laboratory
Livermore, California

Dr. Max Williams
Cal Tech
Pasadena, California

Dr. Arthur W. Winston
Allied Research Assoc.
Boston, Massachusetts

Lt Donald Wunsch
AFSWC
Kirtland AFB
New Mexico

Dr. Jerrold Yos
AVCO-RAD
Wilmington, Massachusetts

Mr. Daniel Young
Boeing Airplane Company
Seattle, Washington

Dr. Louis Zernow
Aerojet
Downey, California

# TABLE OF CONTENTS

# WELCOMING ADDRESS

Col David R. Jones
Chief, Physics Division, AFSWC

I would like to welcome you to Kirtland on behalf of General McCorkle, the Research Directorate, and the Physics Division.

This conference can very well be considered as the second AFSWC Hydrodynamics Conference. The first was held in March of 1960. At that time we were primarily concerned with the X-ray effects of a nuclear burst, and needed to arrive at new levels of common understanding before embarking on an integrated large-scale in-house and contractual research program.

This year we are not concerning ourselves with an individual program, but are attempting to discuss one aspect of a number of the Physics Division's programs. This aspect is hydrodynamics. We have chosen to concentrate on numerical methods and techniques of hydrodynamics, but have included some topics dealing with the physics involved and with non-numerical methods of solution to these problems.

The overall purpose of this meeting should be toward the exchange of methods and techniques of approaching and solving various problems. We hope that the idea of a working meeting can be kept in mind and that impromptu discussion of unresolved topics will flow freely.

Again, I repeat my welcome to Kirtland, and offer our services to you.

# ON THE TREATMENT OF RAREFACTION USING A DISSIPATIVE HYDRODYNAMICS CODE

Gunning Butler, Jr., and Daniel M. Young
Boeing Airplane Company

One of the methods being used to study the response of materials to the X-ray impulse is slapping the material with a thin flying plate. The Boeing group working on this problem is accelerating the flyer plates by discharging a condenser bank through a thin metallic foil and using the pressure developed in the exploded foil to accelerate the flyer. After the plate has moved a sufficient distance it is essentially at initial density and moving with constant velocity. When the plate impinges on the target material, a square pressure pulse is generated in the material with a width equal to the time for the resulting shock to travel back through the flyer plate and the rarefaction from the free surface to travel back to the contact surface. As the shock progresses into the target material it will develop into a normal triangular shock because of rarefactions from the surface relieving the back of the pulse and degrading the peak pressure.

In order to understand the details of these processes and the subsequent details of the flow, a hydrodynamic code was developed at Boeing. The code is based on the Richtmyer-Von Neumann method and the details of the code are reported in the proceedings of the Air Force Special Weapons Center Hydrodynamics Conference (AFSWC TR-60-12) which was held here about a hear ago.[3]

The manner in which a dissipative hydrodynamics code such as that of Von-Neumann and Richtmyer[1] or Ludford, Polachek, and Seeger[2] handles one-dimensional shocks is well established and fully reported in the literature. The usual set of basic difference equation is

$$\rho_o \frac{U_j^{n+\frac{1}{2}} - U_j^{n-\frac{1}{2}}}{\Delta t^n} = - \frac{P_{j+\frac{1}{2}}^{n} + Q_{j+\frac{1}{2}}^{n-\frac{1}{2}} - P_{j-\frac{1}{2}}^{n} - Q_{j-\frac{1}{2}}^{n-\frac{1}{2}}}{\Delta a} ,$$

$$\frac{E_{j+\frac{1}{2}}^{n+1} - E_{j+\frac{1}{2}}^{n}}{\Delta t} = - \left[ \tfrac{1}{2} \left( P_{j+\frac{1}{2}}^{n+1} + P_{j+\frac{1}{2}}^{n} \right) + Q_{j+\frac{1}{2}}^{n+\frac{1}{2}} \right] \frac{(V_{j+\frac{1}{2}}^{n+1} - V_{j+\frac{1}{2}}^{n})}{\Delta t} .$$

$$\rho_o \frac{V^{n+1}_{j+1/2} - V^{n}_{j+1/2}}{\Delta t} = \frac{U^{n+1/2}_{j+1} - U^{n+1/2}_{j}}{\Delta a} ,$$

and an equation of state

$$P^{n+1}_{j+1/2} = f\left(E^{n+1}_{j+1/2}, V^{n+1}_{j+1/2}\right) .$$

For reference, the pertinent phenomenological features are shown in figure 1, which is a synoptic view of a shock in terms of fluid particle velocity as calculated by the Boeing hydrodynamics code and compared with the idealized shock in a perfect fluid. The independent variable here is the Lagrangian coordinate. One notes the spreading of the shock front by the code and the oscillations or ripples induced in the flow after passage of the shock. Figure 2 shows the pressure time history of a mass-zone after the shock has passed. It is well known that as the dissipation terms in the equations are increased in magnitude, the amplitude of the oscillations is decreased and the shock thickness is increased.

Originally it was decided to start the calculations by dumping the energy based on the measurements of the current and voltage versus time into the foil. However, it was not possible to treat this situation with sufficient accuracy. The results of dumping the energy into the foil are extremely sensitive to the equation of state of the foil. A series of runs was done in which the foil was treated as an ideal gas and the peak pressures and peak free-surface velocities varied quite widely with a small change in gamma. This effort was then dropped because of lack of knowledge of the foil equation of state. At the present time the input is taken as the flyer plate at normal density and constant velocity at the time it impinges on the target, because measurements of the flyer plate velocity are readily measurable and quite reproducible. Also by using the flyer plate in motion as input, the equation of state of the foil need not be known and only the equation of state of the flyer over a relatively small pressure range is required.

The Boeing group is particularly interested in the mechanism of spall. Spall occurs when a material is in tension. For this reason it is important to know how a Von-Neumann-type code treats rarefactions. If these codes do not handle rarefactions properly then there are problems in determining the location of the maximum tension and its absolute magnitude. For this reason

a series of numerical experiments on centered rarefactions has been conducted at Boeing. Mr. Daniel M. Young will now present the results of these studies.

At the suggestion of Dr. John G. Trulio of the Lawrence Radiation Laboratory, Livermore, the Boeing group has undertaken what can best be described as a series of numerical experiments on simple centered waves using the Boeing hydrodynamics code. The treatment of these types of flow by such codes is of some interest, but does not seem to have been reported in the literature, at least in the available recent and near-recent sources. For normal materials, simple centered waves are rarefactions and are represented by similarity solutions of the equations of motion; i. e., the equations are reduced to a set of ordinary differential equations which can be integrated by standard methods. For certain equations of state such solutions are expressable in closed form.

Simple centered waves are of interest primarily because they occur frequently as integral parts of more complicated flow fields which require a hydrodynamic code for solution. The manner in which a code handles simple centered waves in cases where the solution is known should be indicative to some extent of the error introduced in the more complicated flows which include them. This is particularly important when one is trying to look at spall which is largely determined by crossing rarefactions. The exact similarity solution representing a simple centered wave is presented in figure 3 which is a synoptic view of a rarefaction moving into a medium at rest. The material in this case has a Hooke's law equation of state. Both pressure and particle velocity are shown as functions of the Lagrangian coordinate.

If the dissipation terms in the above set of difference equations are set to zero and the same problem is calculated with the hydrodynamics code, the results are those shown in figure 4. The features contrasting the analytical and code solutions are the overshoot in the flow behind the wave and the spreading of the wave over too wide a region. If the dissipation terms are included in the calculation, the amplitude of the overshoot is markedly decreased but the spreading is increased, as is indicated in figure 5 which shows the rarefaction wave both with and without dissipation. As in the case of shock compressions, increasing the magnitude of the dissipation terms enhances these effects. That this should be the case also for rarefactions is

not altogether obvious, since for such flows the Von Neumann-Richtmyer dissipation is negative. The inclusion of such terms, therefore, corresponds to a physically unreal situation, since a negative dissipation implies violation of the second law of thermodynamics. It should be recalled, however, that the dissipation terms were originally introduced into the equations only as a mathematical device, not as an attempt to simulate physical reality. The magnitude of these terms required to allow the shock calculation to proceed is greatly in excess of the real physical magnitude.

Figure 6 is a wave diagram in Lagrangian coordinates of the development of a simple centered wave from a pressure discontinuity as computed by the hydrodynamics code without dissipation. It resembles somewhat grossly the early history of the development of a shock compression from a pressure discontinuity, shown for comparison in figure 7. The effect of the dissipation term is shown by the wave diagrams of figure 8. The parameter C is the constant in the Richtmyer-Von Neumann dissipation term. Comparison with the wave diagram of the analytical solution indicates that, as calculated by the code, the head of the wave initially propagates too quickly and the tail too slowly. Finally the wave settles down to a stable fan-shaped structure with all parts traveling at their correct speeds. The center of the wave seems to travel at the right speed from the beginning.

There seem, then, to be two problems associated with the treatment of simple centered waves by dissipative-type hydrodynamic codes: (1) there is a spurious overshoot and subsequent decaying ripple induced on the flow following the wave, which if the dissipative terms are small or ignored completely, can be of significant magnitude; and (2) the trajectories of the head and tail of the wave are incorrect because they are initially of the wrong slope, a situation aggravated by increasing the dissipation.

Inspection of the details of the difference equations at the contact surface across which the pressure discontinuity originally exists leads one to suspect that some of the difficulty is the result of the way in which the velocity of that surface is computed. The usual difference equation for the velocity of a mass zone boundary is

$$\frac{U_j^{n+1/2} - U_j^{n-1/2}}{\Delta t^n} = - \frac{P^n_{j+1/2} + Q^{n-1/2}_{j+1/2} - P^n_{j-1/2} - Q^{n-1/2}_{j-1/2}}{\rho_o \, \Delta a} ,$$

where the nomenclature is essentially that of Von Neumann and Richtmyer. The customary way of handling a surface is to use this same form of difference equation. Letting $P_b$ denote the outside pressure on the boundary, the equation for the velocity of the surface is

$$\frac{U_b^{n+1/2} - U_b^{n-1/2}}{\Delta t^n} = \frac{P^n_{b-1/2} + Q^{n-1/2}_{b-1/2} - P_b}{1/2 \, \rho_o \, \Delta a} , \qquad (*)$$

where the boundary has been assumed to be on the right.

Actually the right hand side of the above equation (*) represents the secant centered one quarter of a mass zone from the surface. For simplicity consider the case where $P_b$ is zero. Then according to (*) the pressure in the first zone adjacent to the surface must be completely relieved before the acceleration of the surface will cease. Thus the velocity of the surface will overshoot, a tension will develop to slow it down, etc. This effect will then propagate along with the tail of the wave. The early history of the surface velocity is shown in figure 9. It is interesting to note that when dissipation is included, the magnitude of the initial overshoot is decreased as it should be according to (*), since the dissipation term will always be opposite in sign to the pressure difference for a rarefaction wave.

When, in the hydrodynamics code, the rarefaction is initiated by the reflection of a shock wave from a free pressure boundary, it is not a simple centered wave. The structure of the shock prevents the wave from being centered. This is shown in figure 10, which is a wave diagram in Eulerian coordinates of this process. However, since the resulting wave is not centered, it is not liable to such violent overshoots in its formative stages and one of the problems has been alleviated. The cost however, is a larger error in the trajectories of the head and the tail.

The effect of such errors in a rather simple problem is illustrated in figure 11. The problem is that of an unstrained flyer plate impacting against a semi-infinite slab of identical material. The quantities of interest are the distance and time at which the rarefaction overtakes the shock, and the trajectory and shape of the subsequently decaying shock pulse. The sort of error that is prone to occur is too short a catch-up distance after which the pulse calculated by the code continues to fall behind because of its early loss of driving pressure. The effect of some of the program parameters upon the results is shown in figure 12. The parameter to which the catch-up distance is most sensitive is the dissipation constant C. The reason is, as has been shown, that the smaller the dissipation the more accurately localized are the waves. However, simultaneously the amplitudes tend to become rather ill-defined because of the overshoots and subsequent oscillations in the flow regions immediately following the waves.

It seems, then, that some care should be taken in interpreting the results of problems calculated with dissipative hydrodynamics codes when simple centered waves are features of the resulting flows. In particular, tension regions following rarefactions should be examined by an independent method to establish their validity. Also, if possible, catch-up distances should be checked.

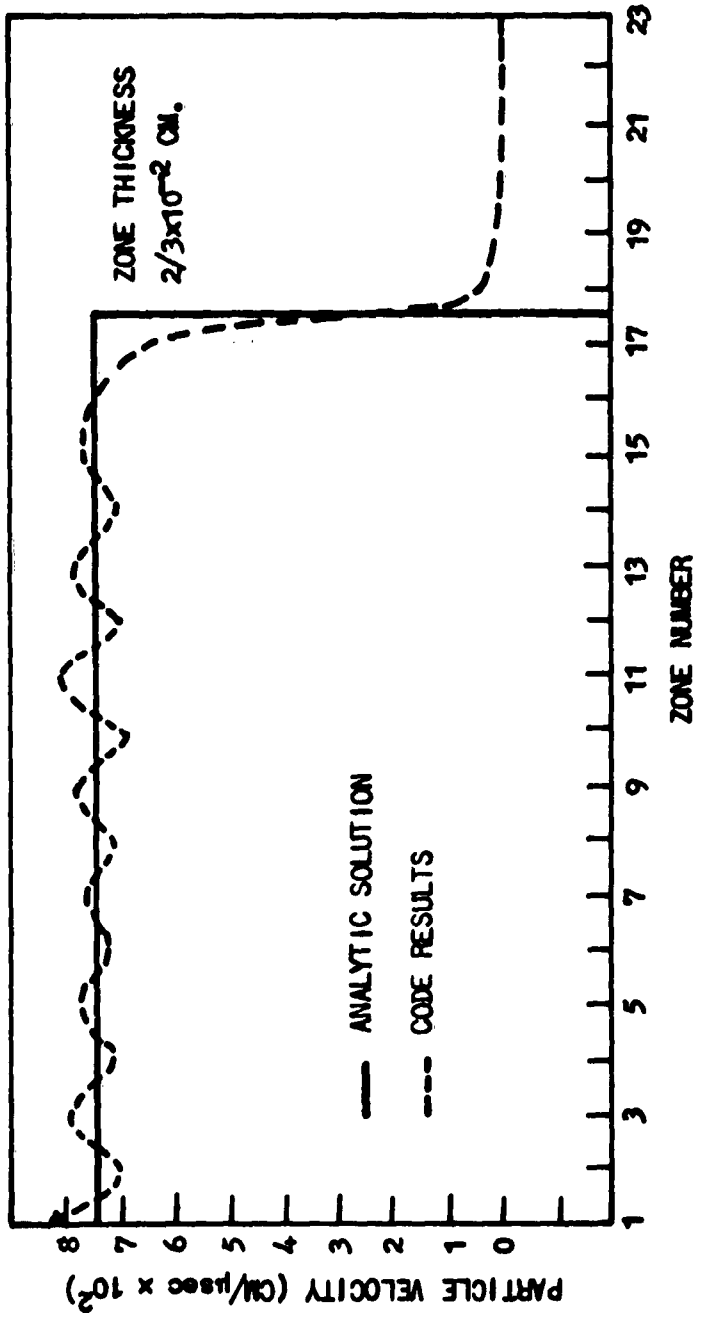


Figure 1. Particle velocity vs. zone number

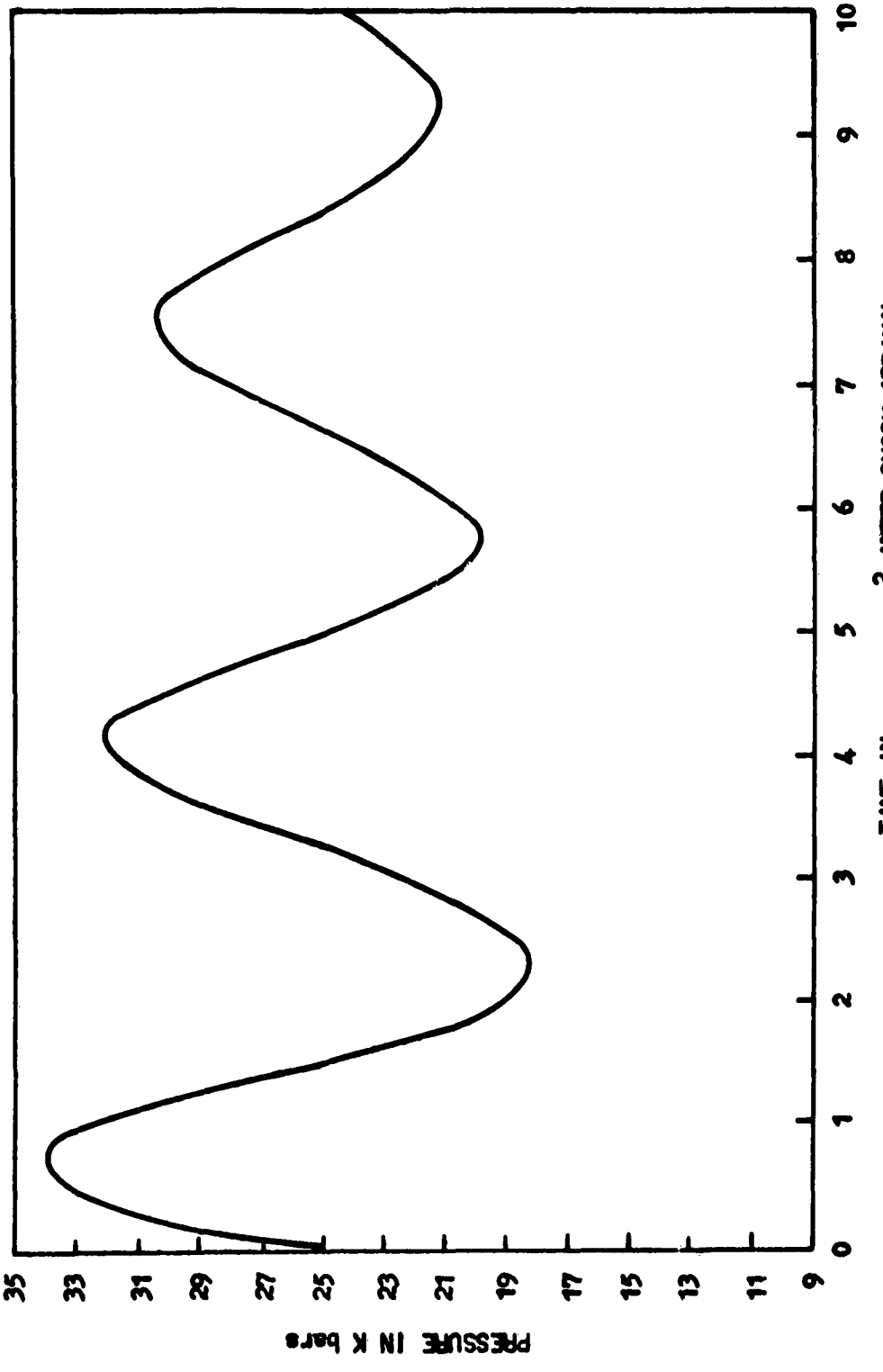


Figure 2. Pressure vs. time after shock arrival for a mass zone

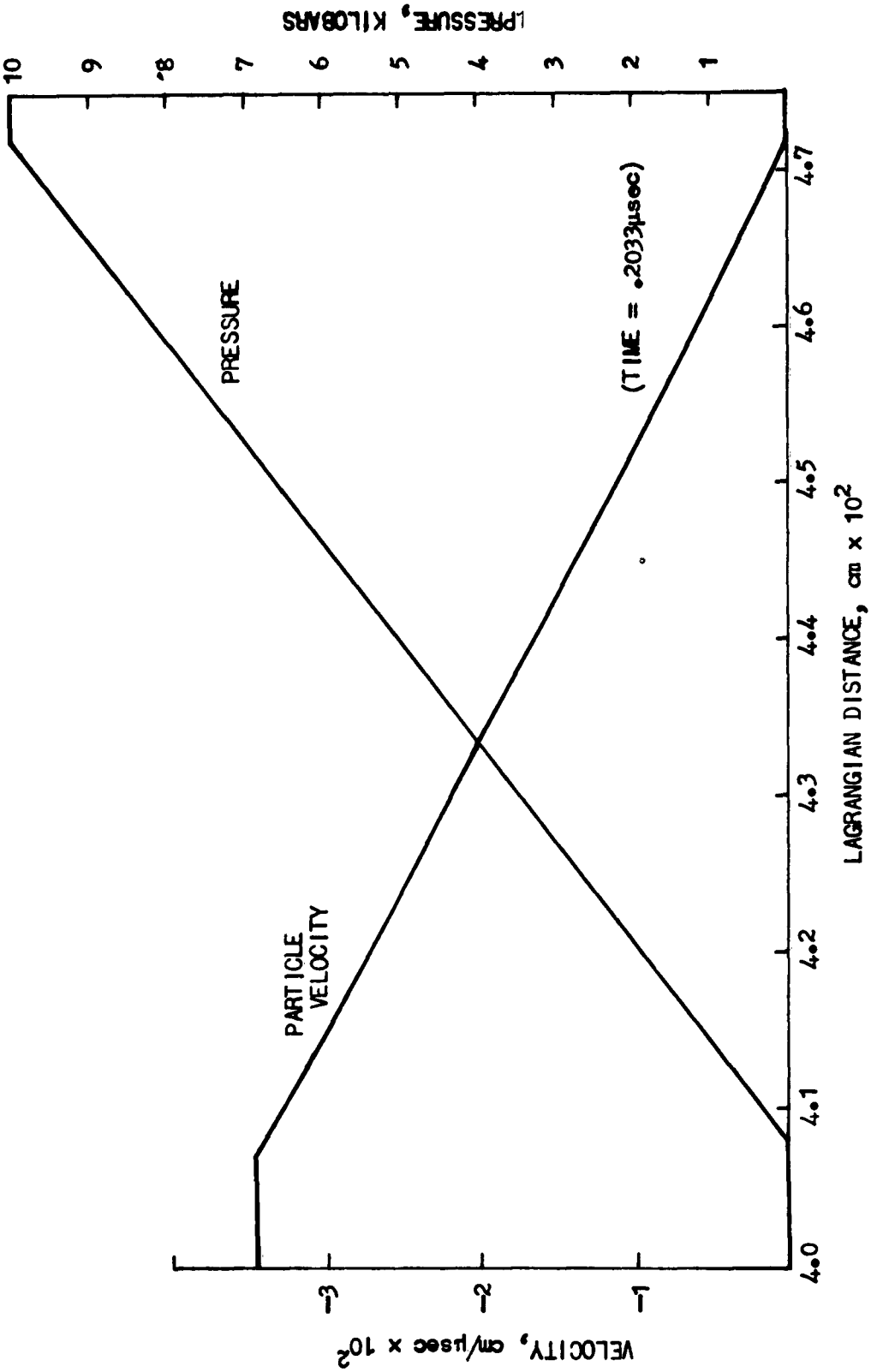


Figure 3. Analytic solution of simple centered wave for Hooke's Law material

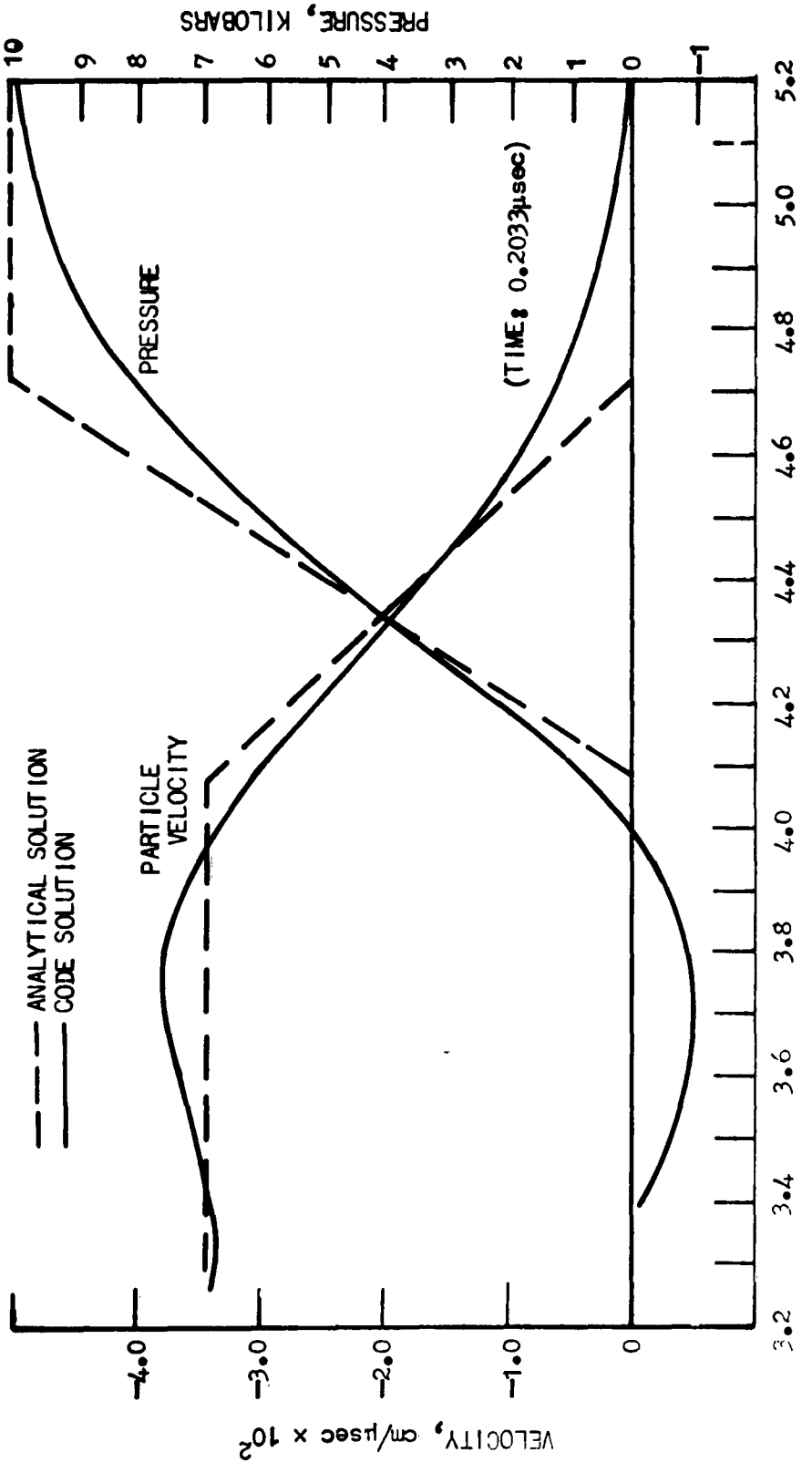


Figure 4. Comparison of analytical and code solution for a centered simple wave in a Hooke's Law material. No dissipation in code

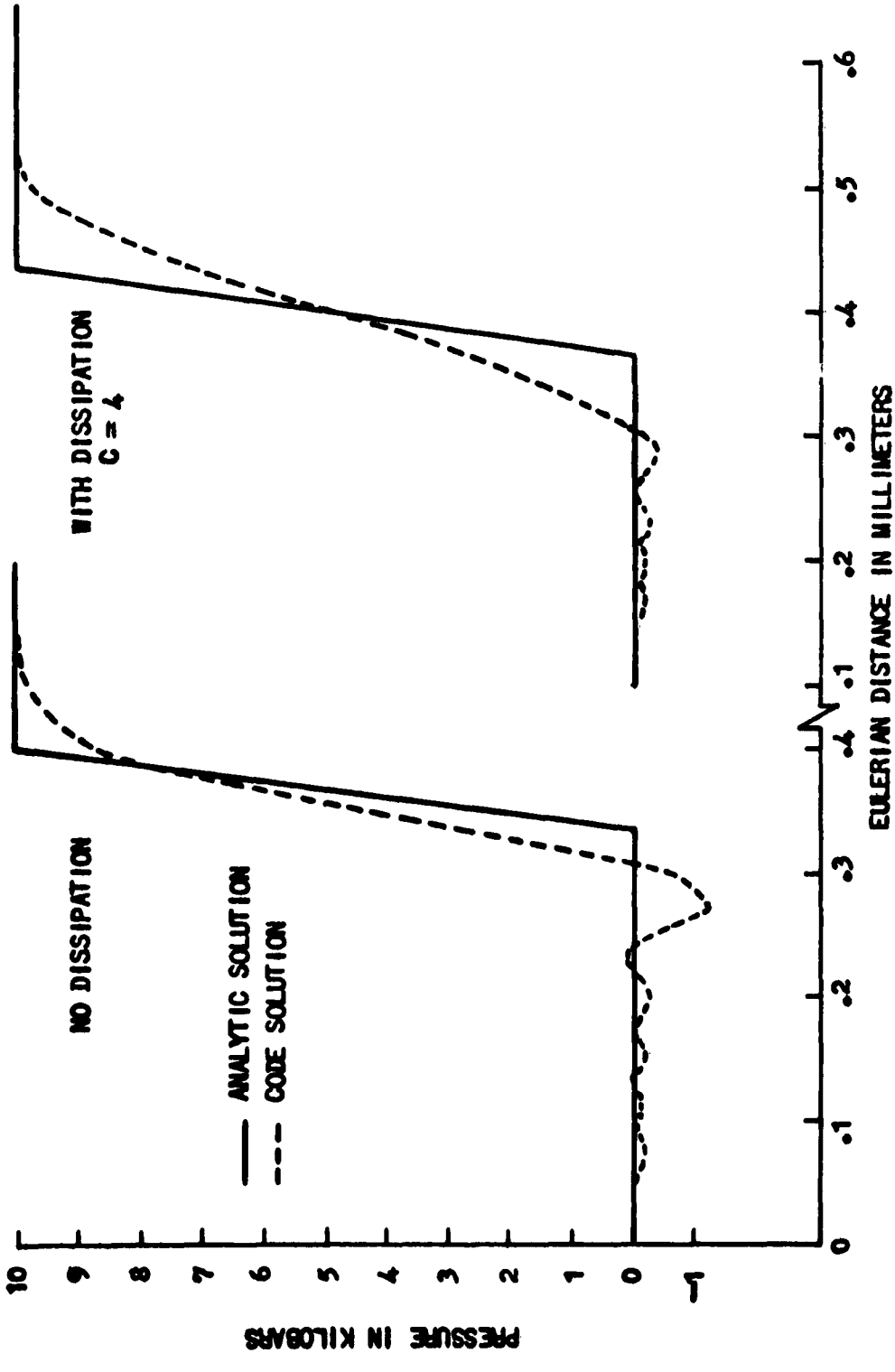


Figure 5. Pressure vs. Eulerian distance

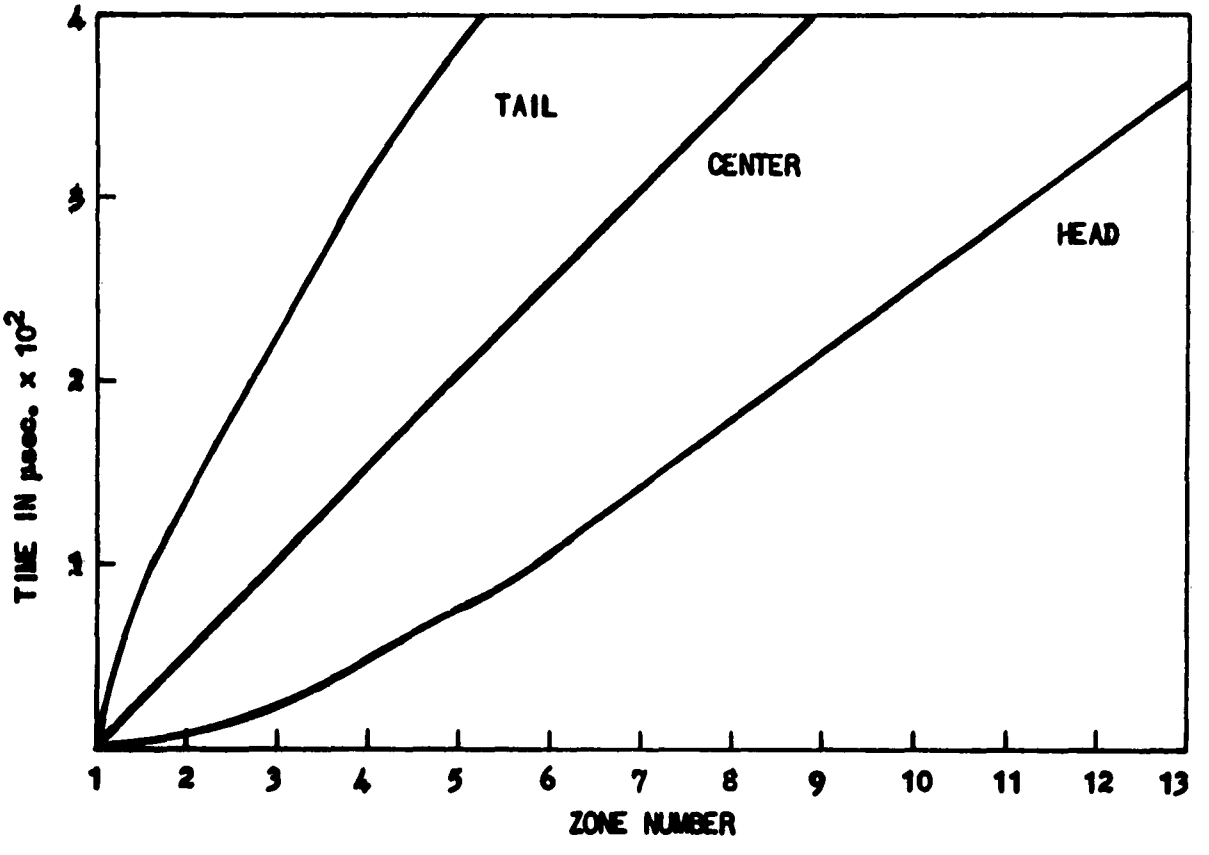


Figure 6. Early history of development
of a rarefaction from a pressure discontinuity

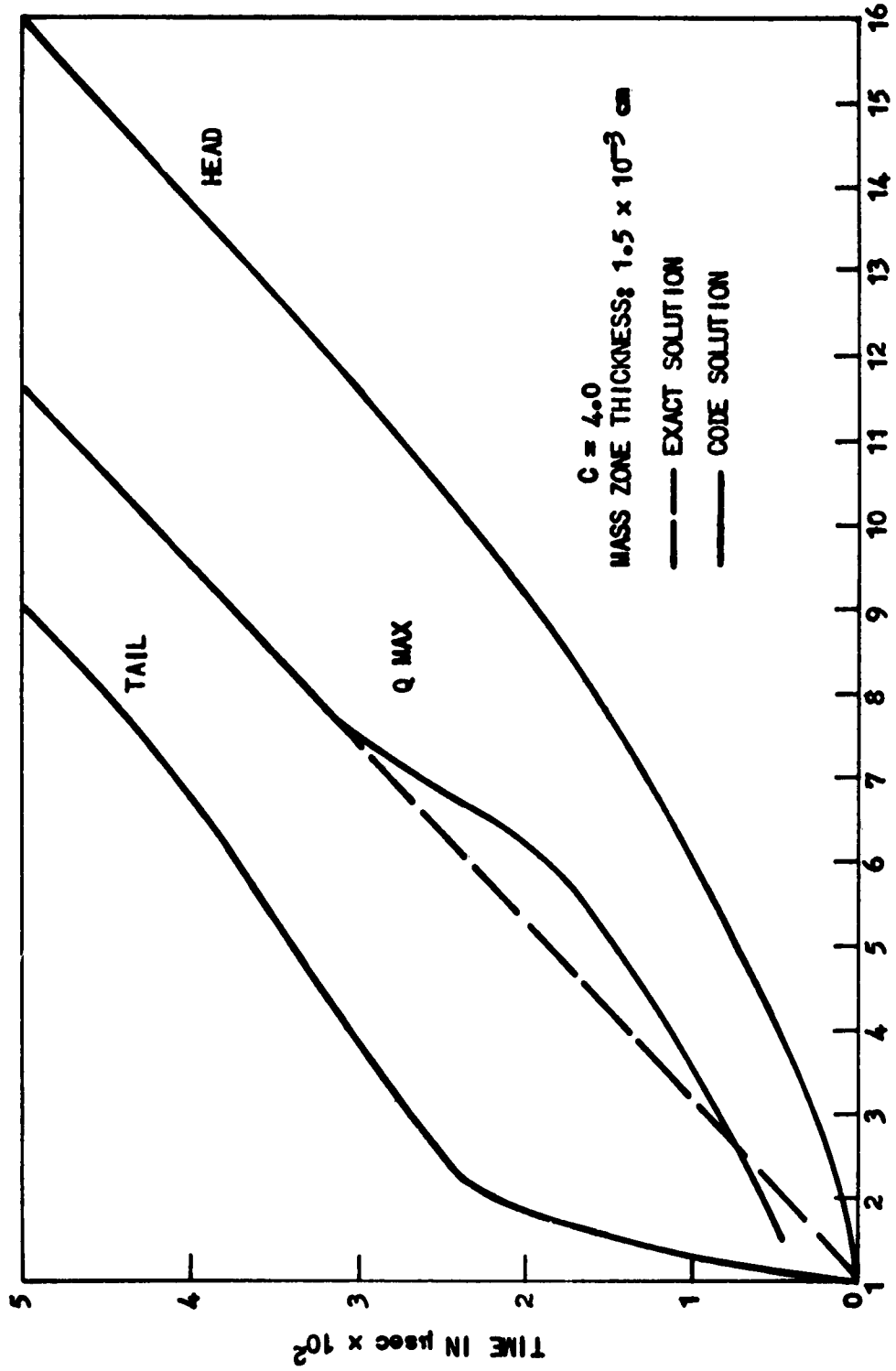


Figure 7. Early history of the development of a shock wave from a velocity discontinuity

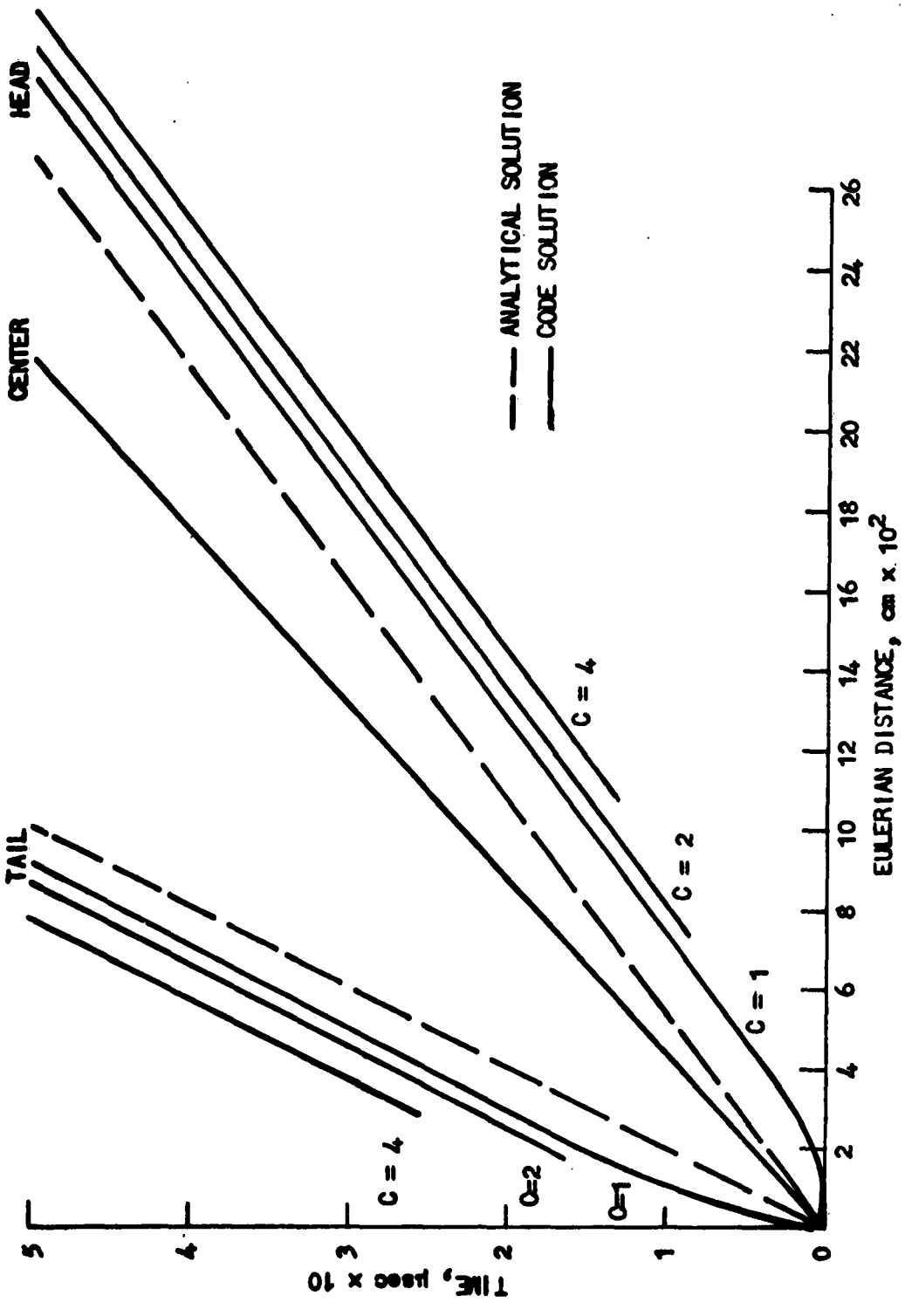


Figure 8. Wave diagram of a simple centered wave

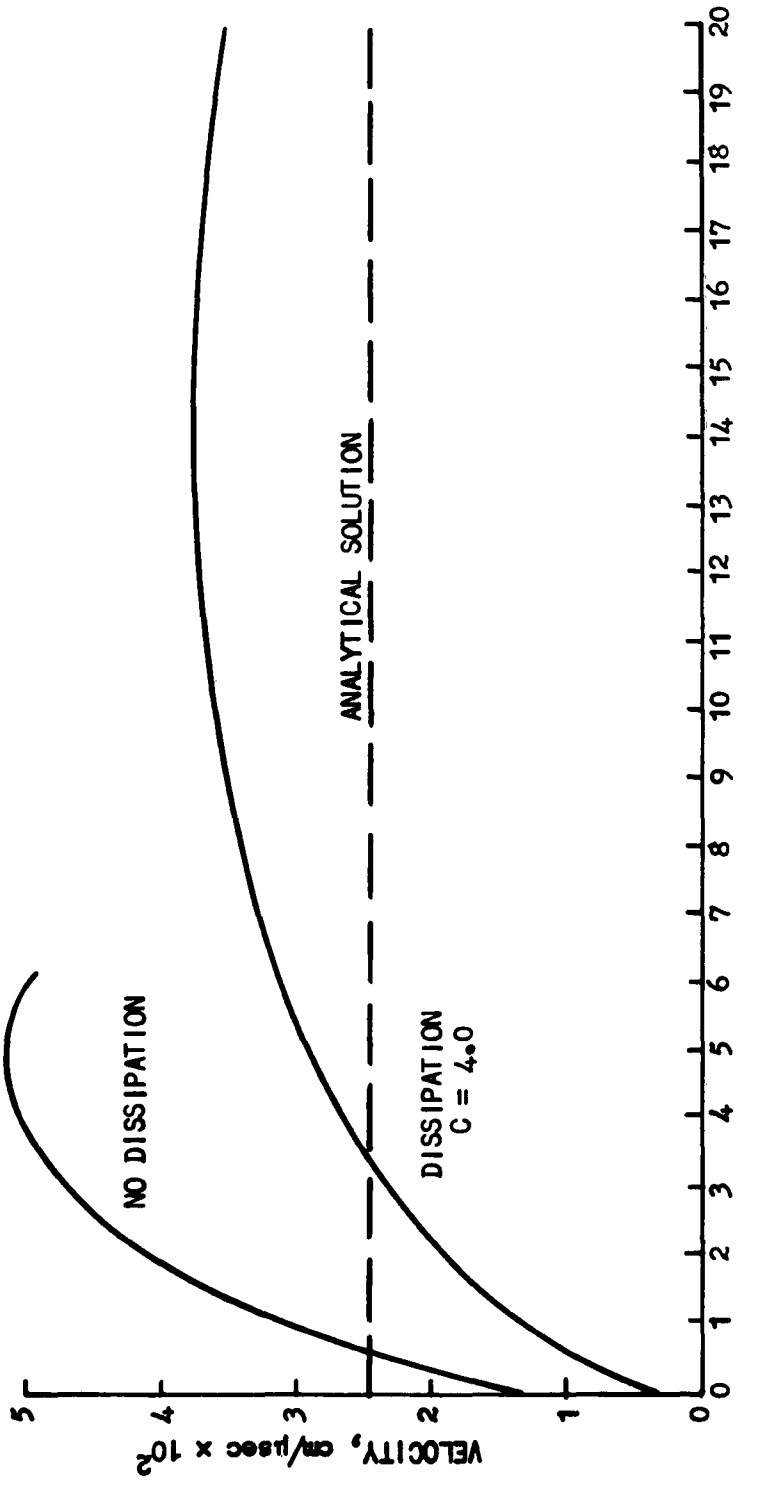


Figure 9. Free surface velocity as a function of time for a rarefaction centered at the surface

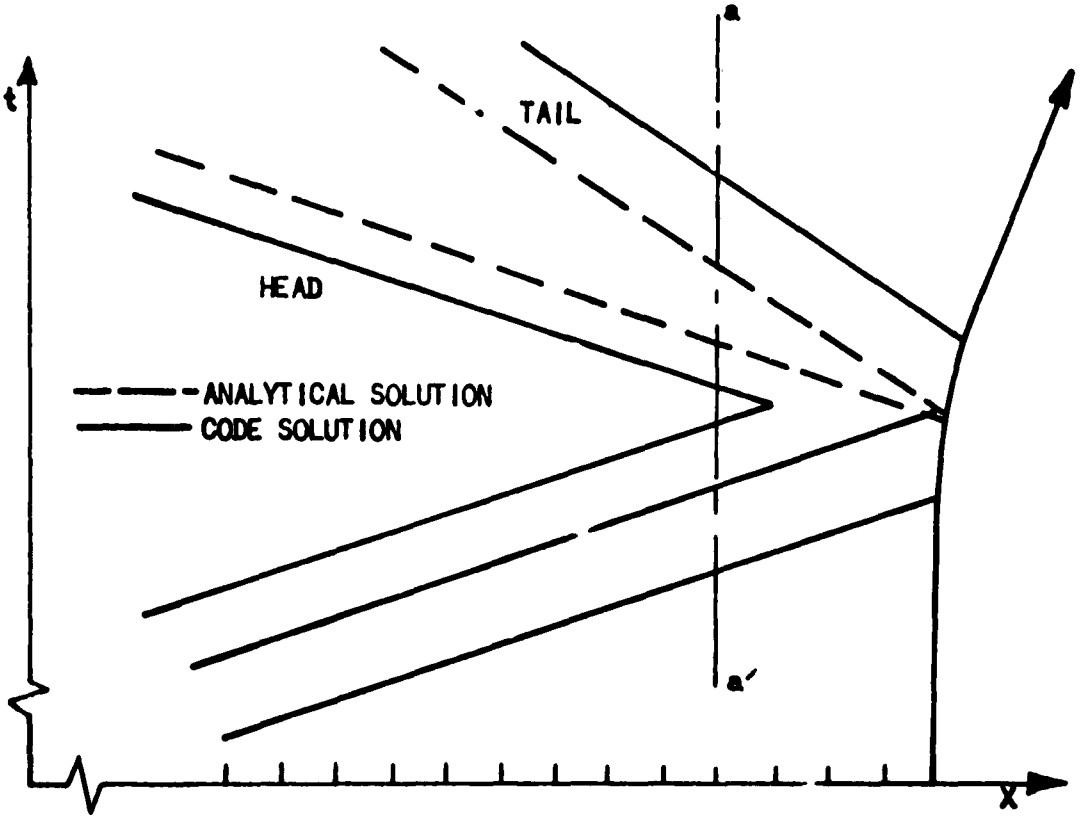


Figure 10. Rarefaction caused by shock reflection at a free pressure boundary

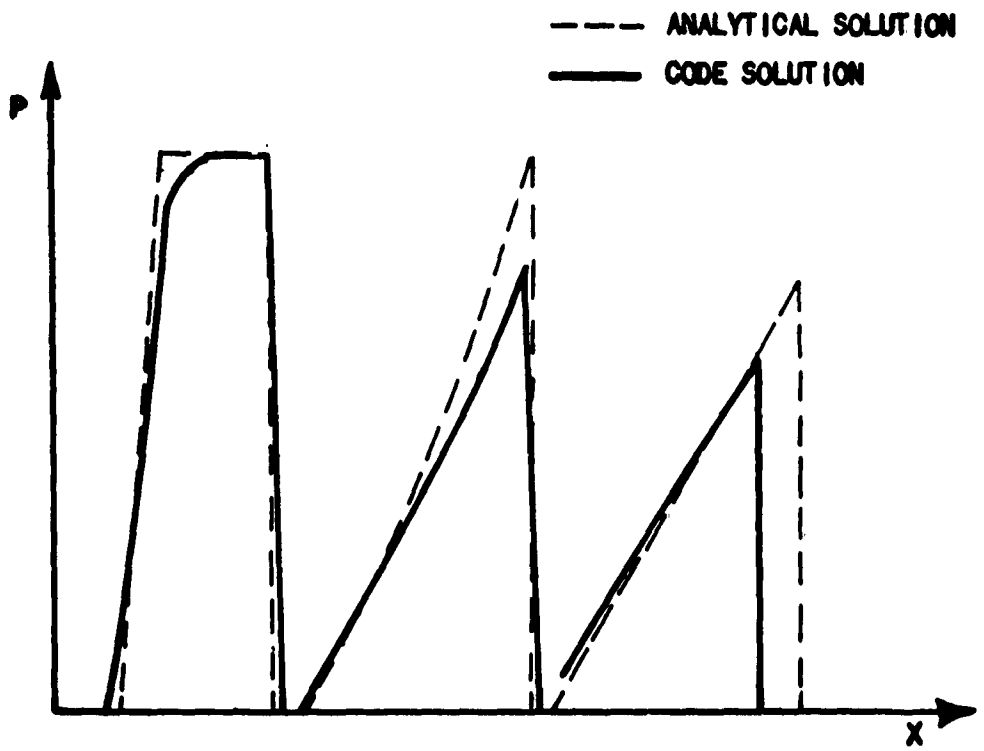


Figure 11. Degrading of shock by overtaking rarefaction

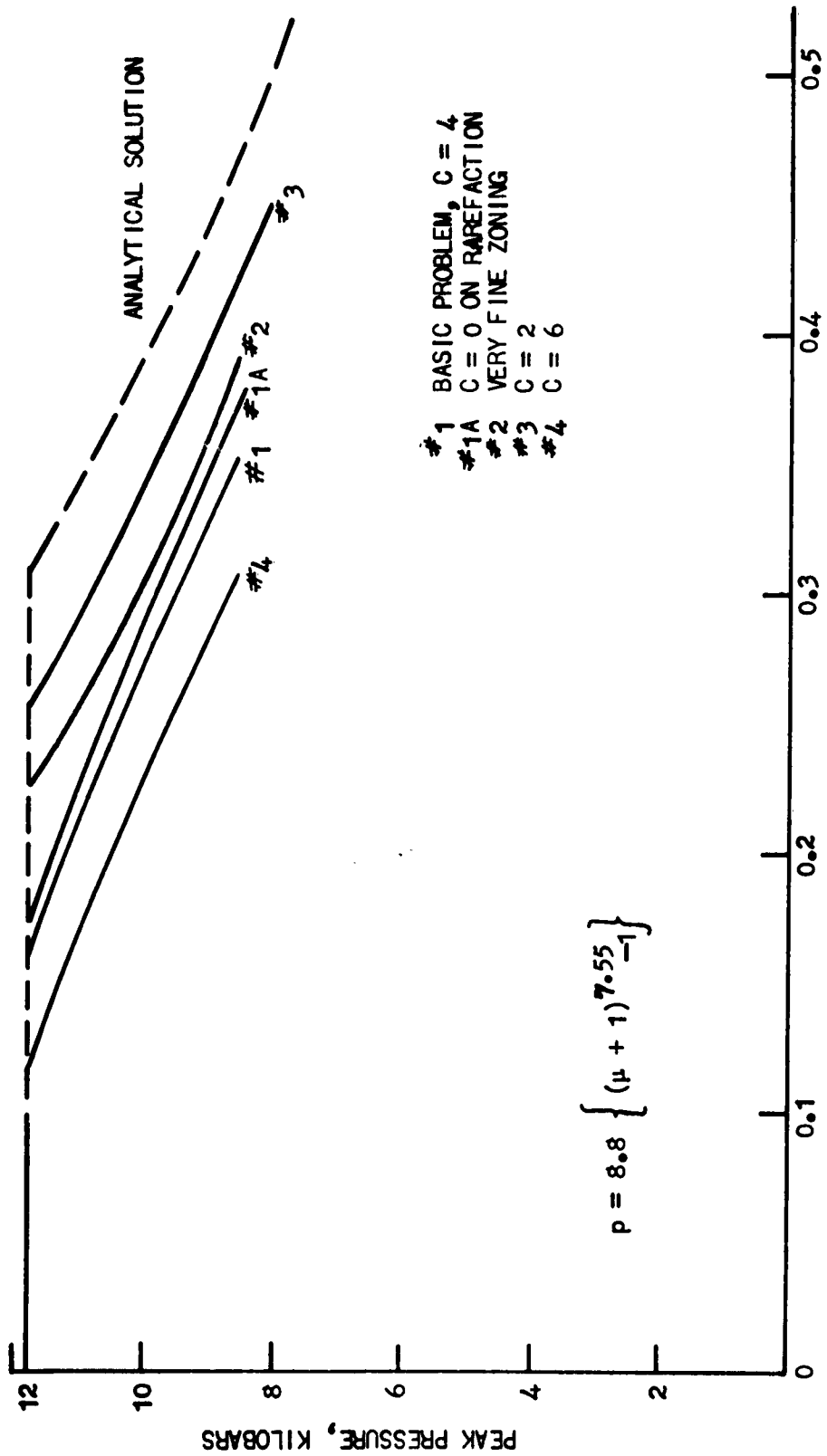


Figure 12. Effect of program parameters on catch-up distance

## REFERENCES

1. Von Neumann, J., and Richtmyer, R. D., A Method of Numerical Calculation of Hydrodynamic Shocks, Journal of Applied Physics, Vol. 21, pp. 232-237, 1950

2. Ludford, G., Polachek, H., and Seeger, R. J., On Unsteady Flow of Compressible Viscous Fluids, Journal of Applied Physics, Vol. 24, pp. 490-495, 1953

3. Butler, G., Jr. in Proceedings of the AFSWC Hydrodynamics Conference, AFSWC TR-60-12, (Secret-RD Report)

# ANALYTIC METHODS AND APPROXIMATIONS OF MHD PROBLEMS

Dr. J. D. Cole
California Institute of Technology
and
Dr. C. Greifinger
The RAND Corporation

## I. INTRODUCTION.

In recent years, largely because of the interest in controlled thermonuclear reactions, many devices have been designed to accelerate gases to thermonuclear energies (~10 kev). In the operation of most of these devices, the gas is driven electromagnetically, it being possible in this manner to achieve much higher gas velocities than by mechanical or gas-dynamic means.

In the usual mode of operation, electrical energy, stored in a charged capacitor, is delivered to the apparatus containing the gas. The gas is rapidly broken down by the applied voltage, and currents flow through it. A magnetic field is thereby generated which interacts with the currents in the gas and sets the gas into motion. Generally, the currents are confined to a rather thin sheet at the boundary of the gas. The magnetic field then acts as a piston, pushing the boundary inward and leaving behind a region of vacuum. The boundary is preceded by a shock wave which compresses, ionizes, and sets into motion the enveloped gas.

To analyze quantitatively the operation of such devices, it is obviously necessary to make a number of simplifying approximations, the most common of which are the following:

(a) idealization of the geometry of the apparatus,

(b) idealization of the physical properties of the gas,

(c) neglect of the reaction of the gas on the external circuit, and

(d) idealization of the mechanical properties of the gas.

The geometrical idealization always involves the neglect of end effects and occasionally involves other idealizations, one of which will be illustrated below in the analysis of the inverse pinch. Such approximations do not usually impose serious limitations on the validity of the analysis, but merely limit that validity to some, usually large, portion of the apparatus.

The idealization of the physical properties of the gas generally consists in the assumptions that the plasma is a nonviscous, non-heat-conducting, ideal gas and that it has infinite electrical conductivity. These approximations limit the validity of the analysis to some range of operating conditions; fortunately, under normal conditions, the devices to be discussed operate well within the necessary range. This point is best illustrated by considering in some detail the assumption of infinite conductivity.

The infinite conductivity approximation is equivalent to the assumption that the currents in the plasma are confined to an infinitely thin sheet on the boundary which excludes the driving magnetic field from the plasma. Actually however, because of the finite conductivity of the plasma, the field diffuses into it. The diffusion distance $\delta$ at a time t is roughly

$$\delta \sim \left(\frac{t}{\mu \sigma}\right)^{1/2} \tag{1}$$

where $\sigma$ is the conductivity of the gas and $\mu$ the permeability of free space. For a shock of roughly constant speed c, the separation $\Delta$ of the shock and the current carrying contact front is

$$\Delta \sim (c - u)t \tag{2}$$

where u is the speed of the contact front. The density ratio across the shock is

$$\frac{\rho_o}{\rho} = 1 - \frac{u}{c} = \frac{\gamma - 1}{\gamma + 1} \tag{3}$$

where the last equality holds for a very strong shock in a perfect gas ($\gamma$ is the usual ratio of specific heats). For a real gas (with partial dissociation and ionization), $(\gamma - 1)/(\gamma + 1) > 1/15$, so that

$$\Delta > \frac{1}{15} ct . \tag{4}$$

The approximation should be valid so long as (taking an average for $\Delta$ )

$$\frac{\delta}{\Delta} \simeq \frac{10}{c} \left(\frac{1}{\mu \sigma t}\right)^{1/2} < 1 . \tag{5}$$

If this is to apply to a shock traveling a distance D, than $t \sim D/c$ and

$$\frac{\delta}{\Delta} \sim \frac{10}{(\mu \sigma Dc)^{1/2}} \tag{6}$$

Thus, a magnetic Reynolds number $R_M$ based on the dimensions of the device and the shock speed must be fairly large,

$$R_M = \mu \sigma D c > 100 , \qquad (7)$$

say. As a typical case, for a Mach 20 shock (10-ev temperature) progressing through cold deuterium $c \sim 4 \times 10^4$ m/sec and $\sigma \sim 6 \times 10^4$ mho/m, so that the inequality required by equation (7) is well satisfied for dimensions D greater than about 2 inches. The relevant dimension of all the devices to be discussed is at least this large, so that the approximation may be expected to apply rather well.

The approximation of neglecting the reaction of the gas on the external circuit is effected by replacing the external circuit by a boundary condition. That is, the current through the gas, and hence the driving field, is taken to be some prescribed function of time, and the dynamical equations of motion are solved subject to this boundary condition. This assumption limits the validity of the analysis to the time during which the prescribed current can be maintained experimentally — usually not the entire period of operation. It also involves a considerable loss of detail, such as, for example, the division of energy at arbitrary times between magnetic field and mechanical motion. If a detailed description of such physical quantities is desirable for design or diagnostic purposes, the reaction must obviously be taken into account.

The final approximation, that of idealizing the mechanical properties of the gas, consists of replacing the full fluid dynamic equations by a single equation based on some simplified mechanical model. One such model in current use, the snowplow model, will be discussed below. Such idealizations have the advantage of allowing a rather simple calculation of the gross dynamics of the gas enveloped by the shock. However, an analysis based on this kind of simplification is clearly not capable of providing the detailed description of the flow which is contained in a solution of the full equations. The latter, unfortunately, cannot usually be solved analytically.

Of the assumptions discussed above, the first two are essentially unavoidable if any analytic results are to be obtained. Of the last two, at least one must be made for the analysis to be tractable. If both (c) and (d) are assumed, the analysis may become particularly simple while still yielding

results which are quite adequate for many purposes. However, if quantitative information is needed concerning the interrelation between gas and circuit, the reaction of the gas must be included. The desired results may then be obtained with somewhat more effort. Finally, there are special cases where similarity solutions of the full fluid dynamic equations can be obtained describing the flow in complete detail. To obtain these solutions, it is again necessary to replace the external circuit by a boundary condition. Moreover, the form of the boundary condition is no longer arbitrary; it is determined by the form the solution must take.

Of course, in addition to the approximations described above, which are of a more or less general nature, there are also those which are specific to a particular device.

The points discussed above will now be illustrated by specific examples.

## II. SNOWPLOW THEORY WITHOUT CIRCUIT REACTION.

As mentioned in the Introduction, the greatest analytical simplification results when assumptions (c) and (d) are both made. A particularly useful mechanical simplification is the so-called snowplow model, which was first applied by Rosenbluth[1] to the ordinary pinch effect. It is assumed, in this model, that all the mass swept up by the shock is compressed into an infinitely thin layer immediately behind the shock, so that the contact front and shock are the same interface. The motion of the interface is determined from the principle that the time rate of change of momentum of the accumulated mass is equal to the force on the interface.

It is interesting to note that snowplow theory can be derived from the full gas-dynamic equations as the limit shock strength $\longrightarrow \infty$, specific heat ratio $\longrightarrow 1$. This limit is called Newtonian theory[2]. The model should therefore be a valid approximation for strong shocks in gases in which ionization and dissociation are taking place, since the additional degrees of freedom provided by these processes result in a specific heat ratio which approaches unity. It is clear that under these conditions the compression $(\gamma + 1)/(\gamma - 1)$ becomes very large, as required by the theory.

In the devices to be analyzed below, the flow is approximately one-dimensional; that is, the location of the shock at a time t is describable by a single coordinate, X(t). If the mass of gas which has been swept up by the

shock is denoted by M(t), the basic equation of snowplow theory can be written

$$\frac{d}{dt}\left(M\frac{dX}{dt}\right) = F\ , \tag{8}$$

where F is the force on the interface. This equation will now be used to analyze the two devices known as inverse pinch[3] and Scylla[4].

A) Inverse pinch

A diagram of the apparatus for this device is shown in figure 1. A current is passed through the gas and returns along the central conducting rod. This current produces an azimuthal magnetic field which pushes the gas away from the rod, leaving behind a cylindrical vacuum region. In such a device, the gas can be pre-ionized, and an axial magnetic field produced by an external solenoid can be trapped in the plasma region. The resulting shock wave will then be a transverse magnetohydrodynamic one. This more general case will in fact be considered.

The additional geometrical idealization will be made of replacing the central rod by a line. This is done first because an exact solution of the resulting equation can then be obtained, but mainly so that a comparison can be made with the similarity solution of the same problem. In practice, the solution thus obtained should become a good approximation to the flow at distances from the rod of several times its radius.

If the plasma is initially at a uniform pressure $p_o$ and density $\rho_o$, and in a uniform axial magnetic field of strength $B_0$, the accumulated mass per unit length of the sheath is

$$M = \pi\,\rho_o X^2\ , \tag{9}$$

where X is the distance of the sheath from the axis, while the net outward pressure on the sheath is (mks units)

$$p = \frac{B_\theta^{\,2}}{2\mu} - \frac{B_o^{\,2}}{2\mu} - p_o = \frac{\mu I^2}{8\pi^2} - \frac{B_o^{\,2}}{2\mu} - p_o \tag{10}$$

The first term on the right hand side of equation (10) is the magnetic pressure of the aximuthal field $B_\theta$ produced by the pinch current I, while the second term is the magnetic pressure of the external field.

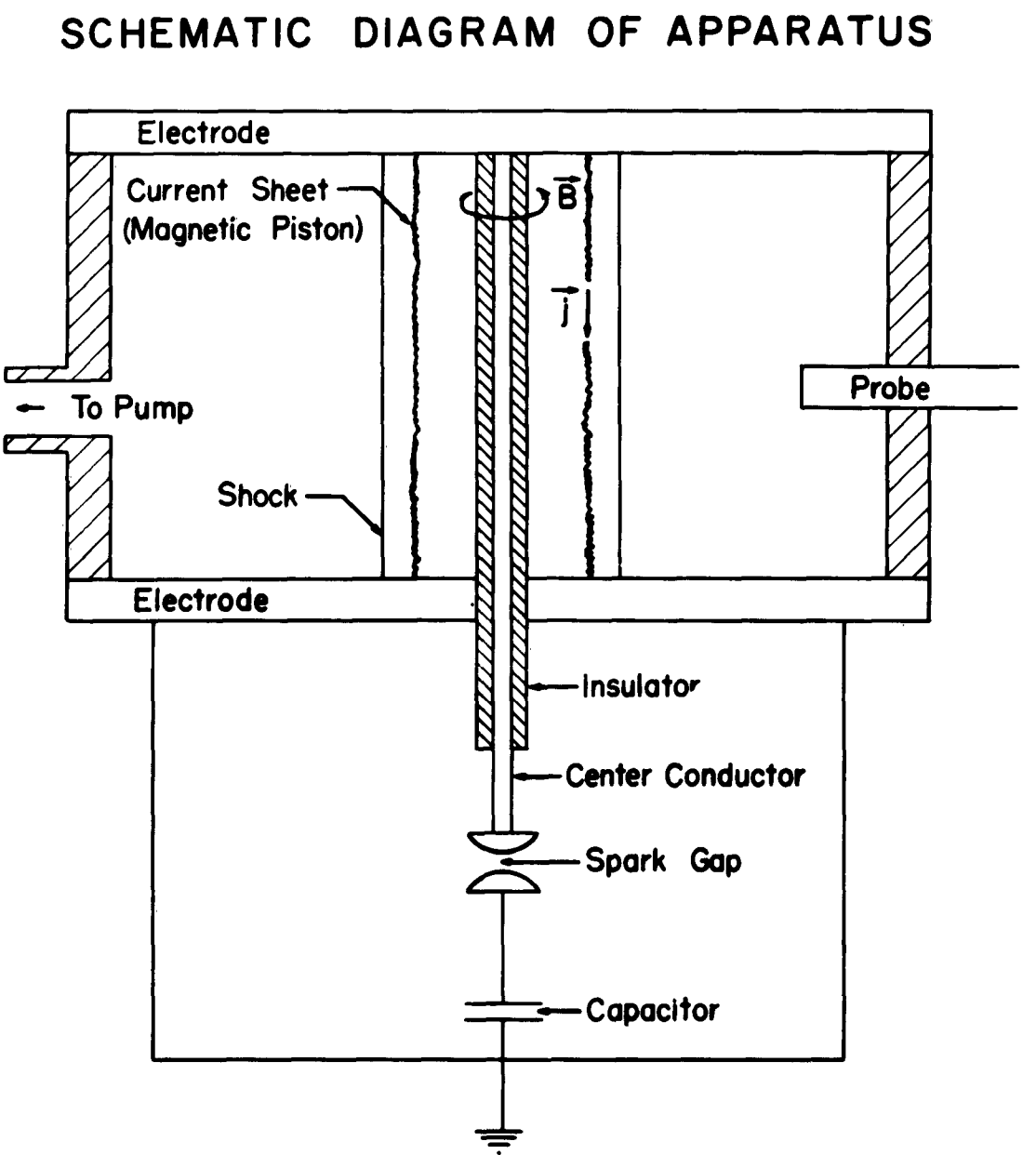


Figure 1. Diagram of apparatus for inverse pinch

It is now necessary to make some assumption concerning the form of $I(t)$. Although under typical experimental conditions the current is usually sinusoidal, the ringing time of the circuit can be made sufficiently long that the current rises linearly over a large portion of the time of interest. If one then assumes a linear pinch current, $I = I_o \omega t$, and introduce as parameters the sound speed $a_o = (\gamma p_o/\rho_o)^{1/2}$ and the Alfvén speed $b_o = (B_o^2/\mu\rho_o)^{1/2}$, equation (8) with $F = 2\pi Xp$ becomes

$$\frac{d}{dt}\left(X^2 \frac{dX}{dt}\right) = c_o^4 \frac{t^2}{X} - X\left(b_o^2 + \frac{2}{\gamma} a_o^2\right) \tag{11}$$

where

$$c_o = (\mu I_o^2 \omega^2/4\pi^2 \rho_o)^{1/4} \tag{12}$$

is a characteristic quantity with the dimensions of a speed. The solution of equation (12) which passes through $X(o) = 0$ is

$$X = kt, \quad k^2 = \frac{1}{4}\left\{-\left(b_o^2 + \frac{2}{\gamma} a_o^2\right) + \left[\left(b_o^2 + \frac{2}{\gamma} a_o^2\right)^2 + 8 c_o^4\right]^{1/2}\right\} \tag{13}$$

Thus, according to the theory, the front moves with the constant speed $\frac{dX}{dt} = k$.

In the limit of strong shocks, where the snowplow theory should give reasonably accurate results, $a_o^2/c_o^2 << 1$; and $b_o^2/c_o^2 << 1$; equation (13) becomes

$$k \cong 2^{-1/4} c_o \left[1 - \frac{2^{-11/4}}{c_o^2}\left(b_o^2 + \frac{2}{\gamma} a_o^2\right)\right] \tag{14}$$

From equation (14) and the definition of $c_o$ the scaling laws for the device are obtained; the shock speed scales as the square root of the rate of current rise and inversely as the fourth root of the density. A comparison of the snowplow result (for $a_o = b_o = o$) with experiments of Liepmann and Vlases[12] is shown in figure 2. The agreement is good indeed, verifying the scaling law with respect to both current rise and initial density.

In addition to providing the scaling laws for the device, the theory also provides a fair idea of the shock speeds to be expected under typical experimental conditions. For example, if the working gas is deuterium at

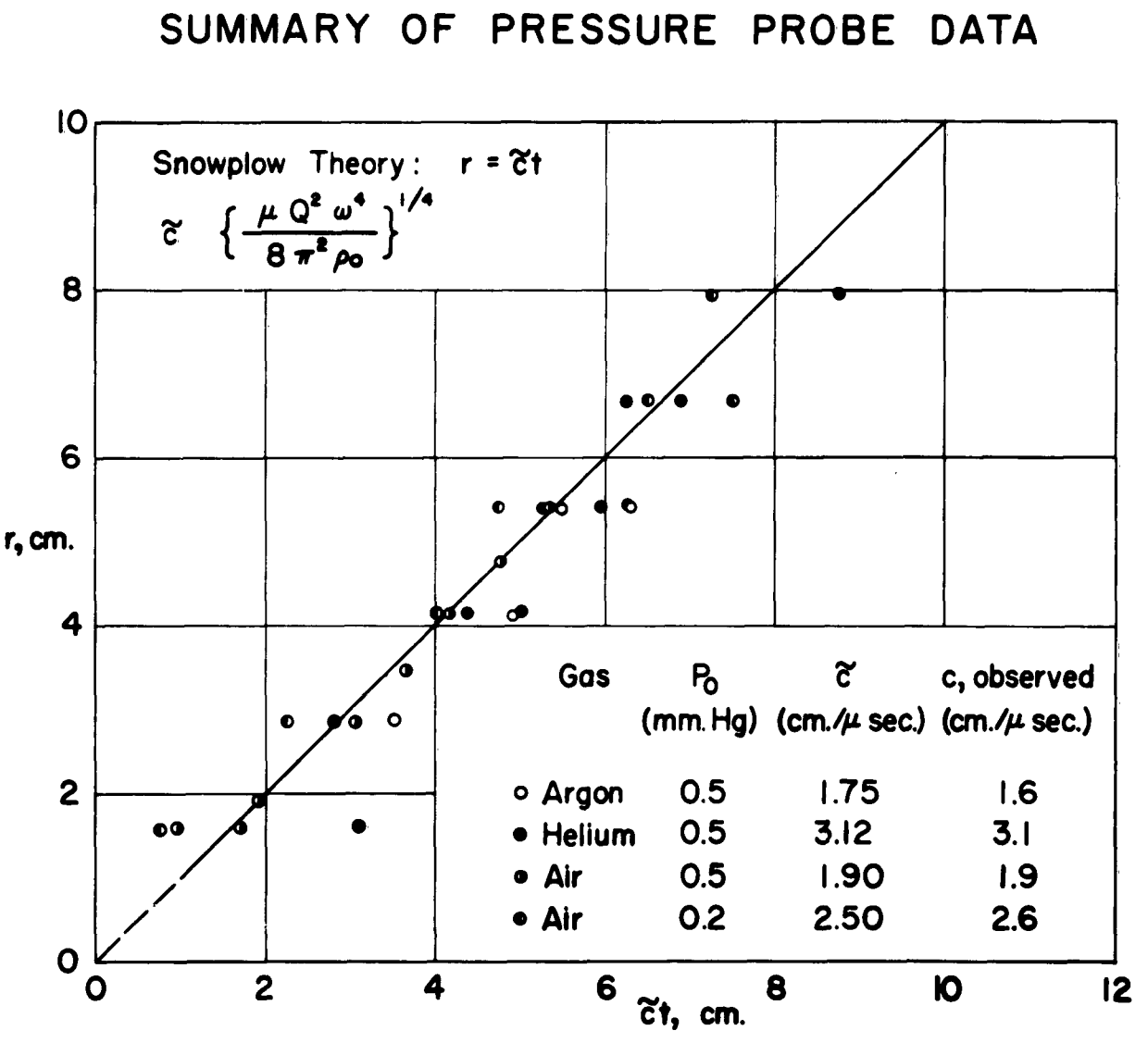


Figure 2. Comparison of snowplow theory of inverse pinch with experiments of Liepmann and Vlases

100-$\mu$ initial pressure and if the rate of current rise is 250 ka/$\mu$-sec, the predicted shock speed is about 9 cm/$\mu$-sec, again in good agreement with experiment.

Finally, although the theory provides no information about the detail of the flow, the internal energy in the gas may, within the framework of the theory, still be calculated. This is the energy which is available to heat, dissociate, and ionize the gas. The total energy per unit length, E(t), delivered to the gas in the time t is just the work done on it by the magnetic piston, i. e.,

$$E(t) = \int_0^{X(t)} F\, dX = \int_0^{X(t)} \frac{d}{dt}\left(M \frac{dX}{dt}\right) dX$$

$$= M\left(\frac{dX}{dt}\right)^2 - \int_0^{X} M \frac{d^2X}{dt^2}\, dX \qquad (15)$$

With the aid of equation (8) the last integral can be transformed to

$$\int_0^{X} M \frac{d^2X}{dt^2} = E(t) - \int_0^{M} \left(\frac{dX}{dt}\right)^2 dM \qquad (16)$$

so that finally

$$E(t) = \frac{1}{2} M\left(\frac{dX}{dt}\right)^2 + \frac{1}{2} \int_0^{M} \left(\frac{dX}{dt}\right)^2 dM\,. \qquad (17)$$

The first term on the right-hand side of equation (17) is the kinetic energy of the gas; the second term is the internal energy. Internal energy is thus acquired at the rate of $\frac{1}{2}\left(\frac{dX}{dt}\right)^2$ per unit mass. (The dissipative mechanism responsible for the production of internal energy is the shock wave.) The internal energy at any time depends on the history of the motion to that time, whereas the kinetic energy depends only on the velocity at that instant. When, as in the case under consideration, the velocity $\frac{dX}{dt}$ is constant, the in-

tegral in equation (17) is trivially evaluated, and the internal energy is evidently just equal to the kinetic energy. In such cases, then, there is exact equipartition between kinetic and internal energy.

B) Scylla

In this device, shown in figure 3, the external circuit drives a circumferential current around the outside of the cylindrical discharge tube. When the switch is closed, the rising current induces an electric field which drives a surface current around the gas, opposite in direction to the primary current. The resulting magnetic field is axial, and drives the gas radially inward from the wall. As in the case of the inverse pinch, such a device can be used to generate magnetohydrodynamic shock waves if the gas has been pre-ionized and an axial field established in it prior to the discharge. This will again be the case considered.

If the azimuthal current per unit length is denoted by i, the driving axial field is uniform between the current sheet and the outer wall, and is given by

$$B_z = \mu i , \tag{18}$$

and the snowplow equation of motion becomes

$$\frac{d}{dt}\left[\pi \rho_o (X_o^2 - X^2)\frac{dX}{dt}\right] = -2\pi X\left(\frac{\mu i^2}{2} - \frac{B_o^2}{2\mu} - p_o\right) , \tag{19}$$

where X(t) is the radius of the current sheet and $X_o$ is the radius of the tube. The other quantities are defined as before, and the equation is to be solved with the boundary condition $X(o) = X_o$ .

An analytic solution of equation (19) can be obtained if it is assumed that the current i(t) rises instantaneously from zero to a constant value $i_1$. (This can be approximated fairly well in practice if the external inductance is made sufficiently small.) The desired solution of equation (19) is then

$$X = X_o - k_1 t \tag{20}$$

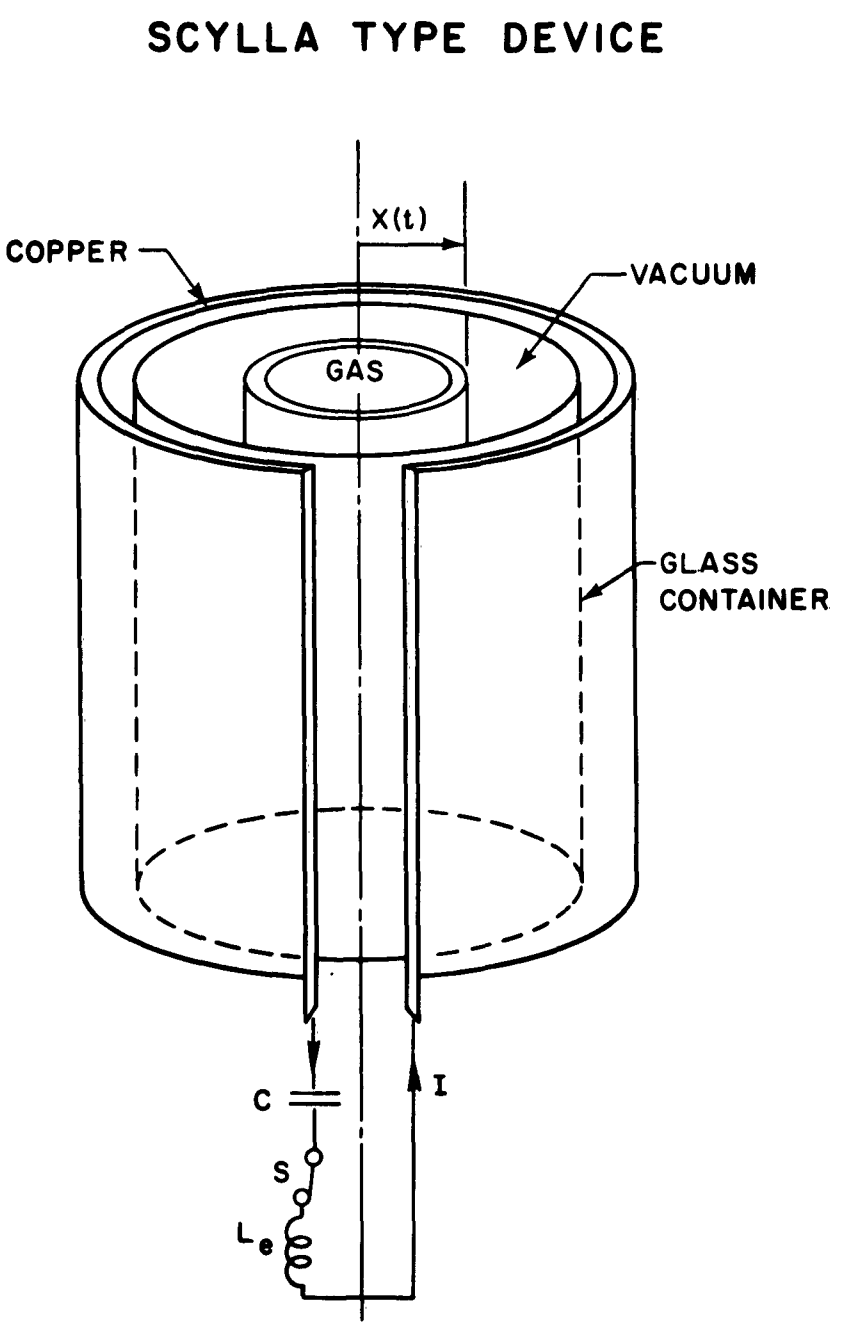


Figure 3. Diagram of apparatus for Scylla

where

$$k_1 = 2^{-1/2} c_1 \left[ 1 - \frac{b_o^2}{c_1^2} - \frac{2}{\gamma} \frac{a_o^2}{c_1^2} \right]^{1/2} \tag{21}$$

and

$$c_1 = \left( \frac{\mu i_1^2}{\rho_o} \right)^{1/2} \tag{22}$$

is the characteristic speed for the device.

The result of the theory, then, is that the gas moves radially inward with the constant speed $\frac{dX}{dt} = k_1$. It is interesting to note that the speed is independent of the dimension $X_o$ of the apparatus. Moreover, the scaling laws are once again obtained; the shock speed scales linearly as the current per unit length and inversely as the square root of the density. Once again typical shock speeds can be estimated; for deuterium at an initial pressure of 100-$\mu$ and currents of about $10^6$ amps/m, shock speeds of about 25-30 cm/$\mu$-sec are to be expected. Finally, the internal energy may be calculated just as in the case of the inverse pinch; here again there is equipartition of energy.

An analysis of the operation of either of the above devices for other forms of the driving current in general requires a numerical integration of the snowplow equation. The same is true if the solution of the inverse pinch is desired near the central rod.

## III. SNOWPLOW THEORY WITH CIRCUIT REACTION.

As mentioned in the Introduction, it is desirable for many purposes to have a detailed description of the interchange of energy between source and device, the division of energy between magnetic field and mechanical motion, etc. When this is the case, the analysis must be modified to include the reaction of the gas back on the energy source. This modification makes it necessary to replace the single equation of motion of the last section by two coupled equations, one equation for the electric circuit and the other for the mechanical system. A detailed analysis of this type has been carried out

for the ordinary pinch by Killeen and Lippman.[5]

As circuit elements, the devices in question are essentially variable inductances which, under normal operating conditions, can be considered to be connected simply in series with the energy source.[5] The inductance of the device at any instant depends on the location of the plasma boundary, and it is this dependence which couples the electric circuit and the mechanical system. If the inductance of the device is denoted by $L_i(t)$, and the external source is taken to be a capacitor of capacitance C in series with an (unavoidable) inductance $L_e$, the circuit equation becomes

$$\frac{d}{dt}\left[(L_e + L_i)\frac{dQ}{dt}\right] + \frac{Q}{C} = 0 \qquad (23)$$

where Q(t) is the charge on the capacitor. If the initial pressure of the gas is neglected, the rate at which mechanical work is done on the plasma is

$$W = F \cdot \frac{dX}{dt} = \frac{1}{2}\left(\frac{dQ}{dt}\right)^2 \cdot \frac{dL_i}{dt} \qquad (24)$$

so that the snowplow equation of motion (8) becomes

$$\frac{d}{dt}\left(M\frac{dx}{dt}\right) = \frac{1}{2}\frac{dLi}{dX} \cdot \left(\frac{dQ}{dt}\right)^2 \qquad (25)$$

The system is thus described by the two coupled equations, (23) and (25). In these equations, dissipation in the resistance of the walls of the device and in resistance in the external circuit has been neglected. Such dissipation could easily be included but in practice is usually small. The main dissipative mechanism, the shock wave, is included however.

These equations will now be applied to the analysis of a specific device.

MAST (Magnetic Annular Shock Tube[6])

This device (figure 4) is also called a linear plasma accelerator. The gas is contained between two coaxial electrodes which are connected to the external circuit. When the switch is closed, the gas breaks down near the end of the tube and a radial current flows in a thin disk between the inner and outer cylinders. The discharge current gives rise to an azimuthal magnetic field which pushes the current disk down the tube. The disk sweeps up the gas ahead of it, leaving vacuum behind.

# LINEAR PLASMA ACCELERATOR

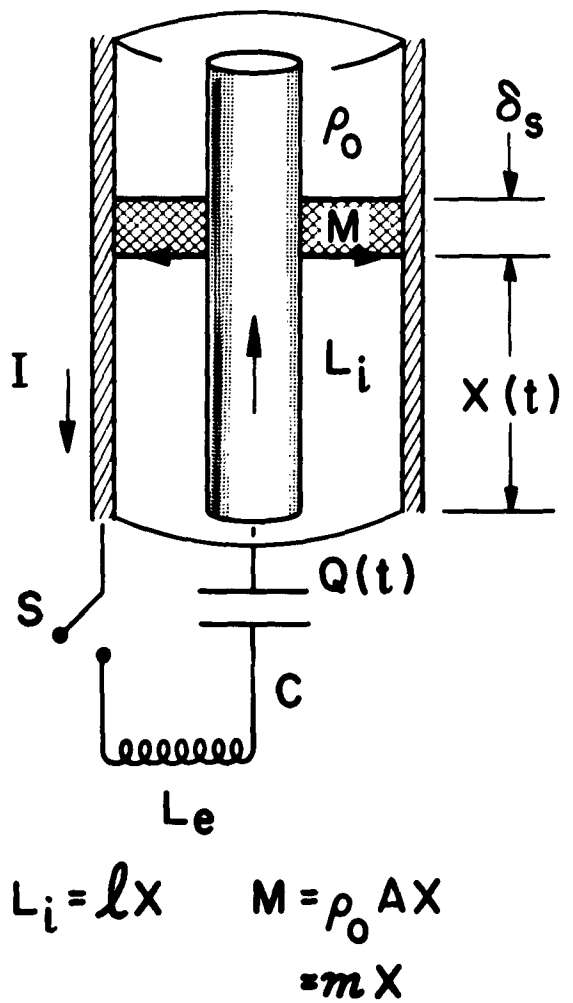


Figure 4. Diagram of apparatus for linear plasma accelerator

Other devices for the linear acceleration of plasma, in which the mass of accelerated gas could be considered constant, have been analyzed by various authors [7, 8, 9] along these same lines. These analyses differ from that presented below mainly in that they do not contain the mechanism of shock dissipation. One treatment, however, [7] does take into account electrical resistance. The device considered here has been discussed by Dattner [9] whose treatment, however, is somewhat inconsistent in that it is assumed that the internal energy of the gas is always some fixed fraction of the kinetic energy. It is clear from equation (17) that this is not generally the case.

If X(t) denotes the distance of the current disk from the end of the tube, the inductance of the device is

$$L_i(t) = \ell X(t) \tag{26}$$

where

$$\ell = \frac{dL_i}{dX} = \frac{\mu}{2\pi} \ln \frac{d_2}{d_1} \tag{27}$$

is the inductance per unit length, $d_1$ and $d_2$ being the inner and outer diameters, respectively. Furthermore,

$$M(t) = \rho_o A X(t) \equiv m X(t) \tag{28}$$

where A is the area of the annulus, so that m as defined by equation (28) is the mass per unit length of the tube. If the initial charge on the capacitor is $Q_o$, the equations of motion must now be solved subject to the boundary conditions.

$$Q(0) = Q_O, \quad \dot{Q}(0) = 0, \quad X(0) = 0, \quad \dot{X}(0) = 0 \tag{29}$$

A study of the problem in dimensionless variables shows that the operation of the device can be described in terms of a single parameter. If one introduces as dimensionless variables

$$x = \frac{\ell}{L_e} X \quad \text{(length)}$$

$$\tau = \frac{t}{\sqrt{L_e C}} \quad \text{(time)} \tag{30}$$

$$q = \frac{\ell^{3/2}}{\sqrt{2m}L_e} \quad Q \quad \text{(charge)}$$

the equations of motion become

$$\frac{d}{d\tau}\left[(1 + x)\frac{dq}{d\tau}\right] + q = 0 \tag{31}$$

$$\frac{d}{d\tau}\left(x\frac{dx}{d\tau}\right) = \left(\frac{dq}{d\tau}\right)^2 \tag{32}$$

and the initial conditions are

$$q(0) = \frac{Q_o \ell^{3/2}}{\sqrt{2m}\, L_e} = q_o \tag{33}$$

$$\dot{q}(0) = x(0) = \dot{x}(0) = 0$$

The equations and boundary conditions thus contain the single parameter $q_o$, the ratio of the initial charge on the capacitor to the characteristic charge for the system. The time-dependence of all nondimensional variables is therefore determined, once the value of this single quantity has been specified.

A general analytic discussion of the system (31) and (32) presents formidable difficulties. However, some general remarks can be made. For very small times, $x << 1$, that is, the inductance of the device is small compared to the external inductance. The external circuit is thus essentially shorted through the device and starts to ring at its natural frequency. From the resulting driving force, the initial motion of the gas is readily calculated. For $x << 1$, the solution of the circuit equation is

$$q = q_o \cos \tau, \tag{34}$$

and with this as the driving term, the solution of the mechanical equation is

$$x = \frac{q_o}{\sqrt{2}}\left(\tau^2 - \sin^2\tau\right)^{1/2} \tag{35}$$

This initial phase of the system can persist for a considerable time if $q_o$ is made sufficiently small. Since a small $q_o$ implies a weak driving force, the condition $x << 1$ can then be satisfied to values of $\tau^2 >> 1$, in which case the velocity of the front $\frac{dx}{d\tau} \longrightarrow \frac{q_o}{2}$. If $\tau$ becomes too large, however, this initial description breaks down and a period of strong coupling occurs. Ultimately, however, the driving force $\left(\frac{dq}{d\tau}\right)^2$ must become small; the gas

will then decelerate while conserving its momentum. Thus, in the final phase

$$x \sim k\sqrt{\tau} \tag{36}$$

The varying inductance now "drives" the external circuit, the equation for which becomes

$$\frac{d}{d\tau}\left[k\sqrt{\tau}\,\frac{dq}{d\tau}\right] + q = 0 \tag{37}$$

The asymptotic solution of equation (37) for large times is

$$q \sim \tau^{-1/8} \sin\left(\frac{4}{3k^{1/2}}\,\tau^{3/4} - \varphi\right) \tag{38}$$

A numerical solution of equations (31) and (32) has been carried out on an IBM 7090 for a number of different values of the parameter $q_o$. The results are shown in figures 5-8. The dashed curve is the asymptotic solution for $x << 1$ given by equations (34) and (35). It is evident that, for the small values of $q_o$, the asymptotic solution is a very good approximation indeed to the actual solution over the entire range shown. The numerical solution has also been carried to values of $\tau >> 1$; the results verify the validity of equations (36) and (38) in this limit.

An energy integral of the system (31) and (32) is readily obtained, namely

$$\frac{1}{2}q^2 + \frac{1}{2}\left(\frac{dq}{d\tau}\right)^2 + \frac{1}{2}x\left(\frac{dq}{d\tau}\right)^2 + \frac{1}{4}x\left(\frac{dx}{d\tau}\right)^2 + \frac{1}{4}\int_0^x \left(\frac{dx}{d\tau}\right)^2 dx = \frac{1}{2}q_o^2 \tag{38a}$$

The integral in equation (38a) is the internal energy in nondimensional form. The internal energy can be calculated from this equation once the equations of motion have been integrated. The result for $q_o = 1$ is shown in figure 9, where for comparison the kinetic energy has also been plotted. It is seen that there is no simple relationship in this case between internal and kinetic energy.

The predictions of the theory may be compared with the experiments of Dattner.[9] These experiments, with deuterium as the working gas, covered a range of pressures of 200-1000 μ and a range of voltages of 3-7 kv. With

# POSITION OF PLASMA FRONT AS A FUNCTION OF TIME FOR VARIOUS VALUES OF THE INITIAL CHARGE

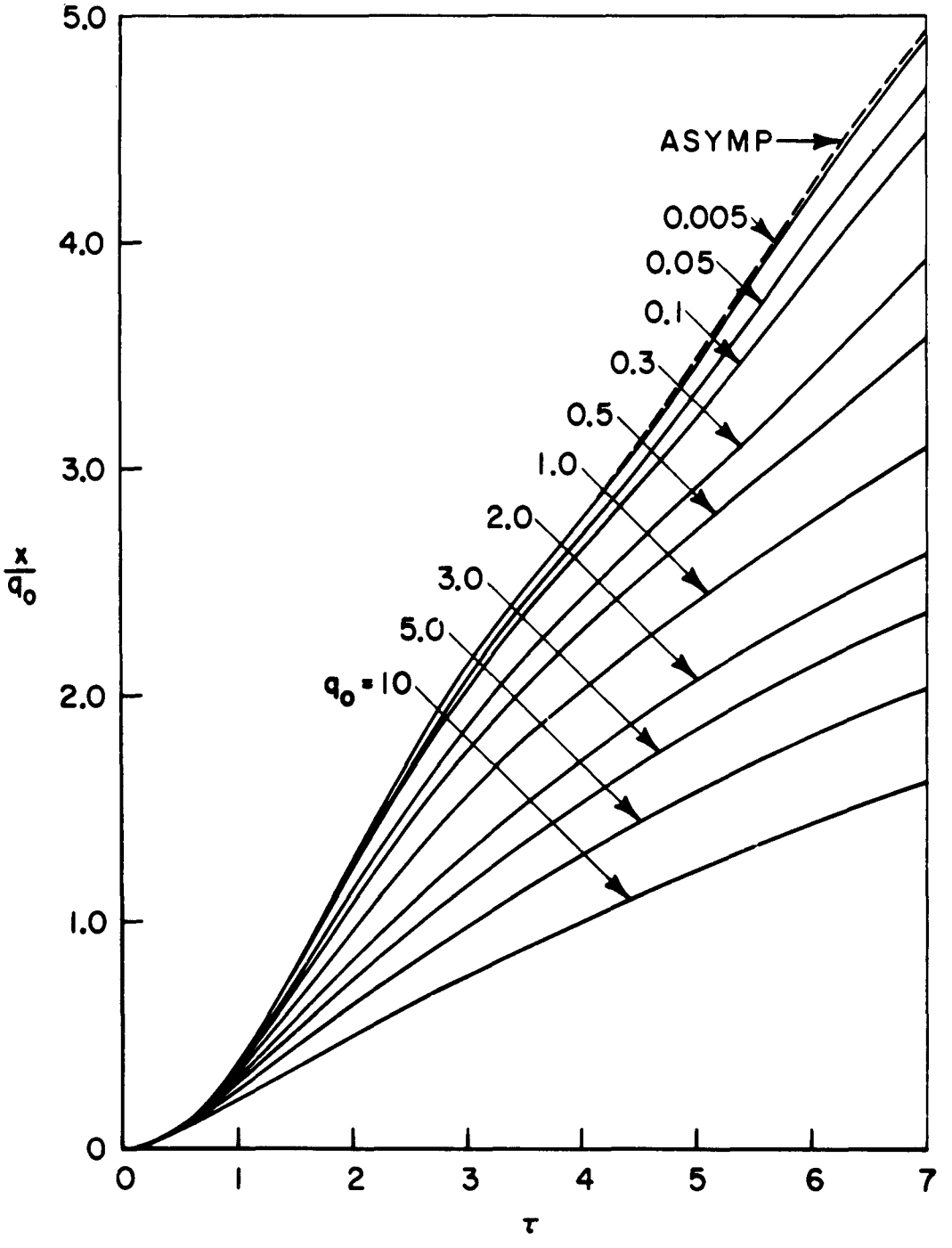


Figure 5. Position of front as a function of time for various values of $q_0$

# VELOCITY OF PLASMA FRONT AS A FUNCTION OF TIME FOR VARIOUS VALUES OF THE INITIAL CHARGE

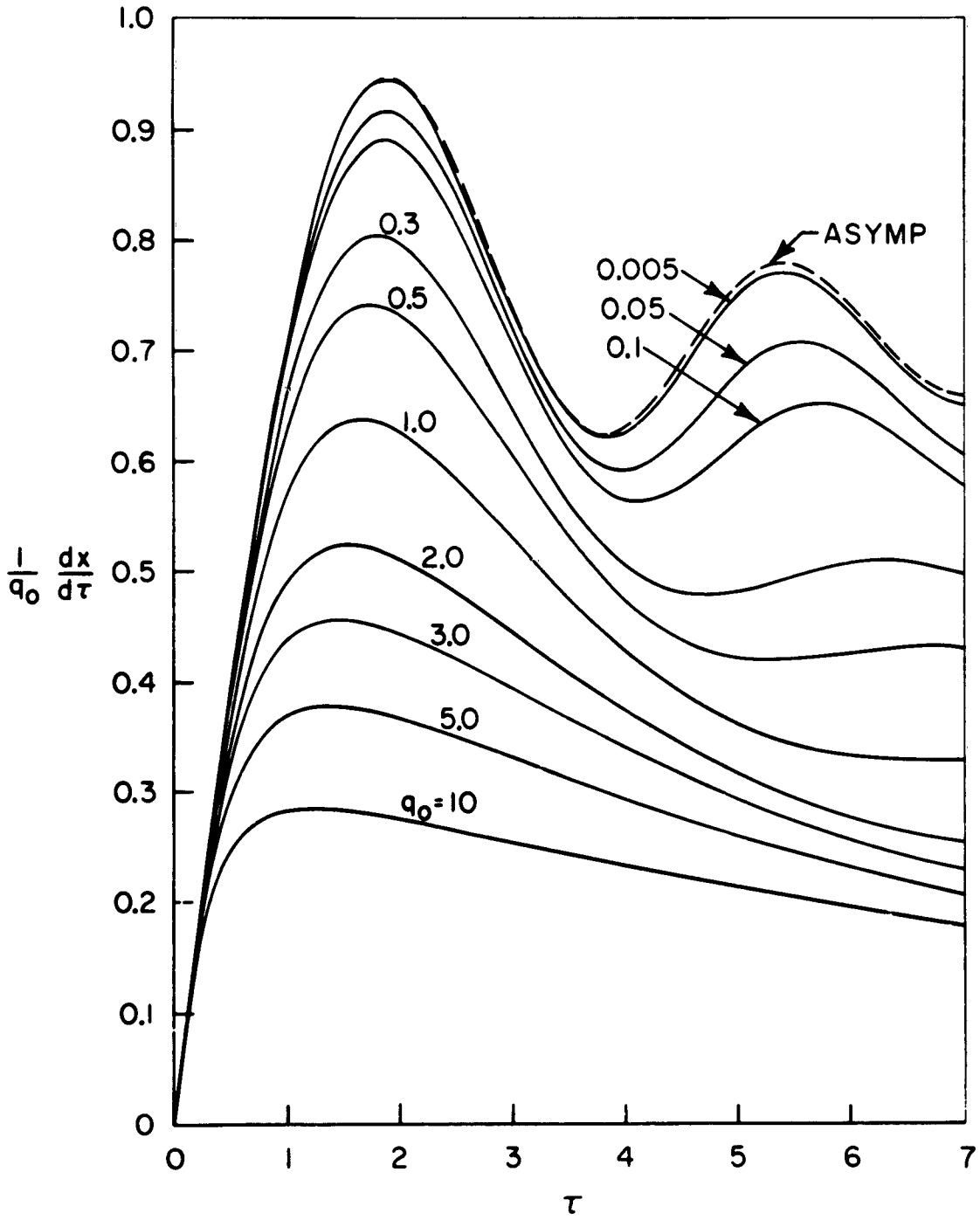


Figure 6. Velocity of front as a function of time for various values of $q_o$

# CHARGE ON CONDENSER AS A FUNCTION OF TIME FOR VARIOUS VALUES OF THE INITIAL CHARGE

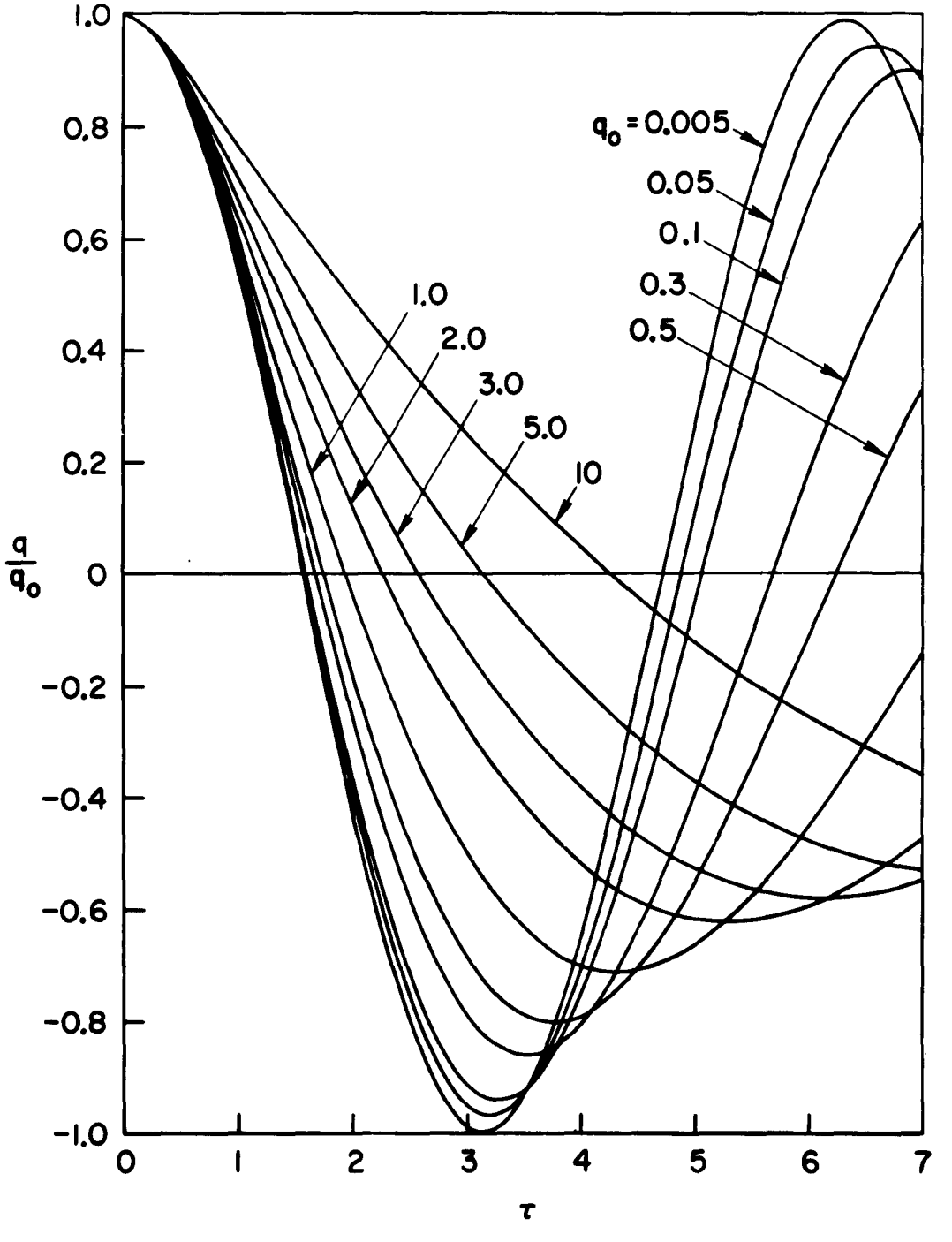


Figure 7. Charge as a function of time for various values of $q_0$

# CURRENT AS A FUNCTION OF TIME FOR VARIOUS VALUES OF THE INITIAL CHARGE

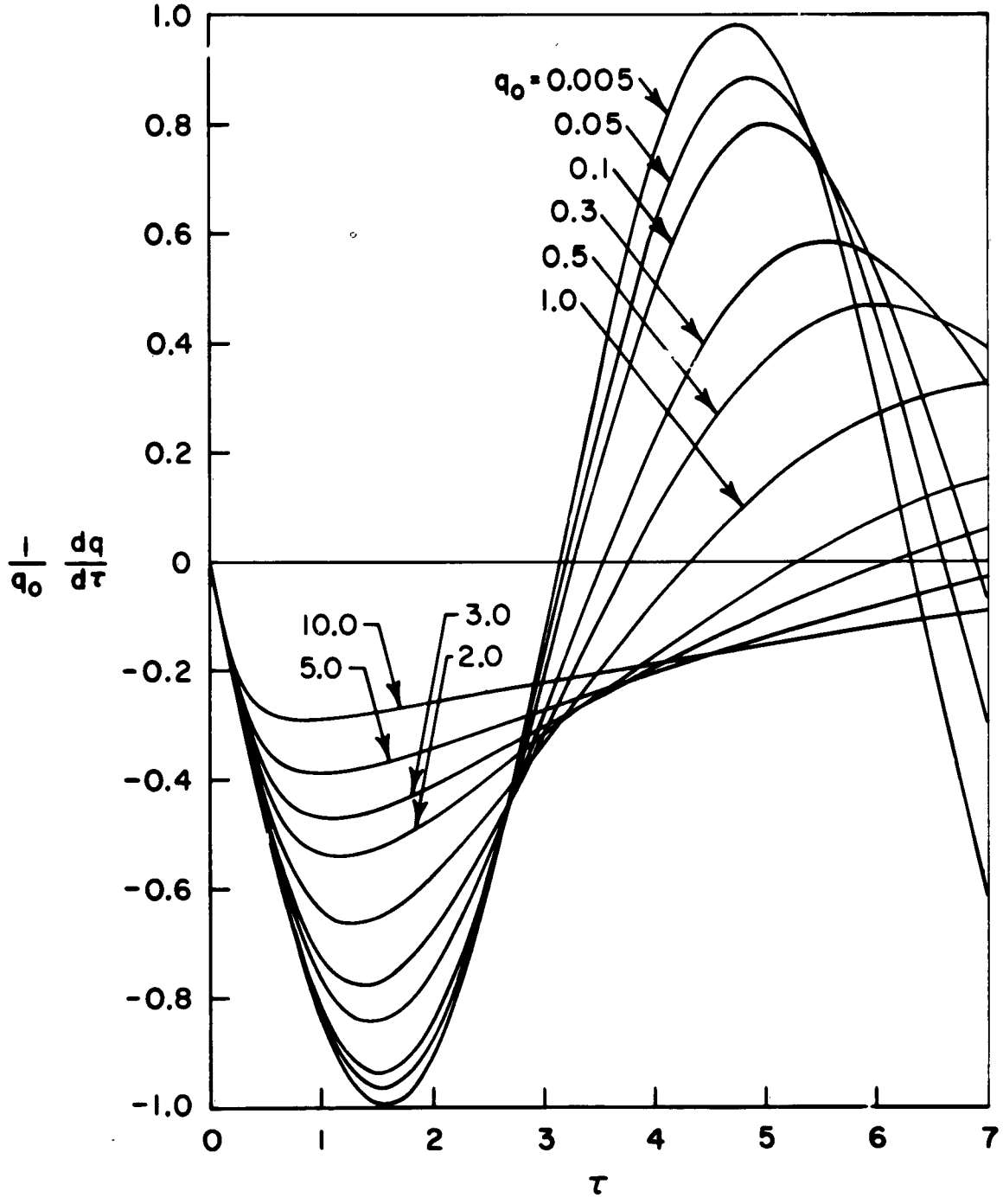


Figure 8. Current as a function of time for various for various values of $q_0$

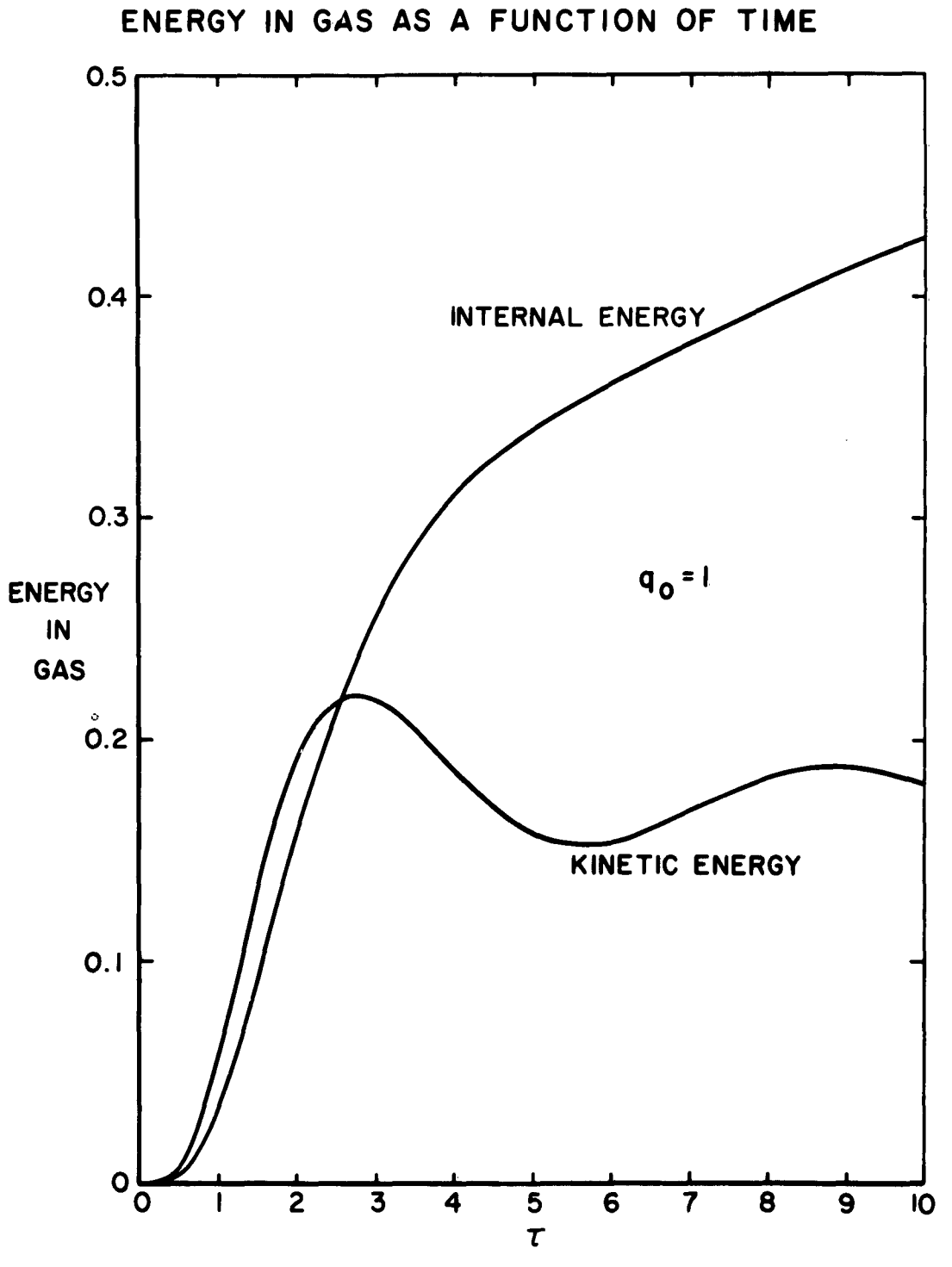


Figure 9. Energy distribution in the gas as a function of time for $q_0 = 1$

circuit parameters of $C = 12.5 \times 10^{-6}$ f and $L_e = 57.4 \times 10^{-9}$ h, this range of pressures and voltages corresponds to a range of values of $q_o$ of 0.8 - 4.2. It was observed that the velocity of the gas became roughly constant after about 1/4 of a cycle, with the velocities attained by the gas ranging from 6 to 11 cm/$\mu$sec. The maximum calculated velocities occur at about the proper time and range from 4 to 14 cm/$\mu$sec. Thus, there is rough agreement between theory and experiment.

One of the sources of discrepancy between theory and experiment lies in the assumption that the flow is one-dimensional, that is, that the current interface is a plane disk. The magnetic pressure across the annulus varies as $1/r^2$, where r is the radius, and therefore decreases from the inner electrode to the outer. This pressure distribution is incompatible with the uniform dynamic pressure which exists across a plane disk. It is actually not difficult to modify the theory to take this effect into account. The shape of the interface can be calculated[10] by requiring that the magnetic pressure across the interface is everywhere balanced by the dynamic pressure given by snowplow theory. The shape calculated in this manner turns out to be a paraboloid of revolution, in agreement with experiment.

## IV. SIMILARITY SOLUTION FOR INVERSE PINCH.

As mentioned in the Introduction, special cases exist for which a similarity solution of the full magnetohydrodynamic equations may be obtained describing the flow in complete detail. Of course, the external circuit must be replaced by an appropriate boundary condition. One such case is that of the inverse pinch with just those initial and boundary conditions for which the snowplow solution was obtained above, namely an initial uniform axial field in the plasma and a discharge current which increases linearly with time. Details and results of the calculation appear elsewhere.[11] It is sufficient to say that the solution is of the form

$$\begin{aligned} \rho(x,t) &= \rho_o \sigma(\Phi) \\ u(x,t) &= c^* U(\Phi) \\ p(x,t) &= \rho_o c^{*2} P(\Phi) \\ B_z(x,t) &= \rho_o c^{*2} \beta(\Phi) \end{aligned} \qquad (39)$$

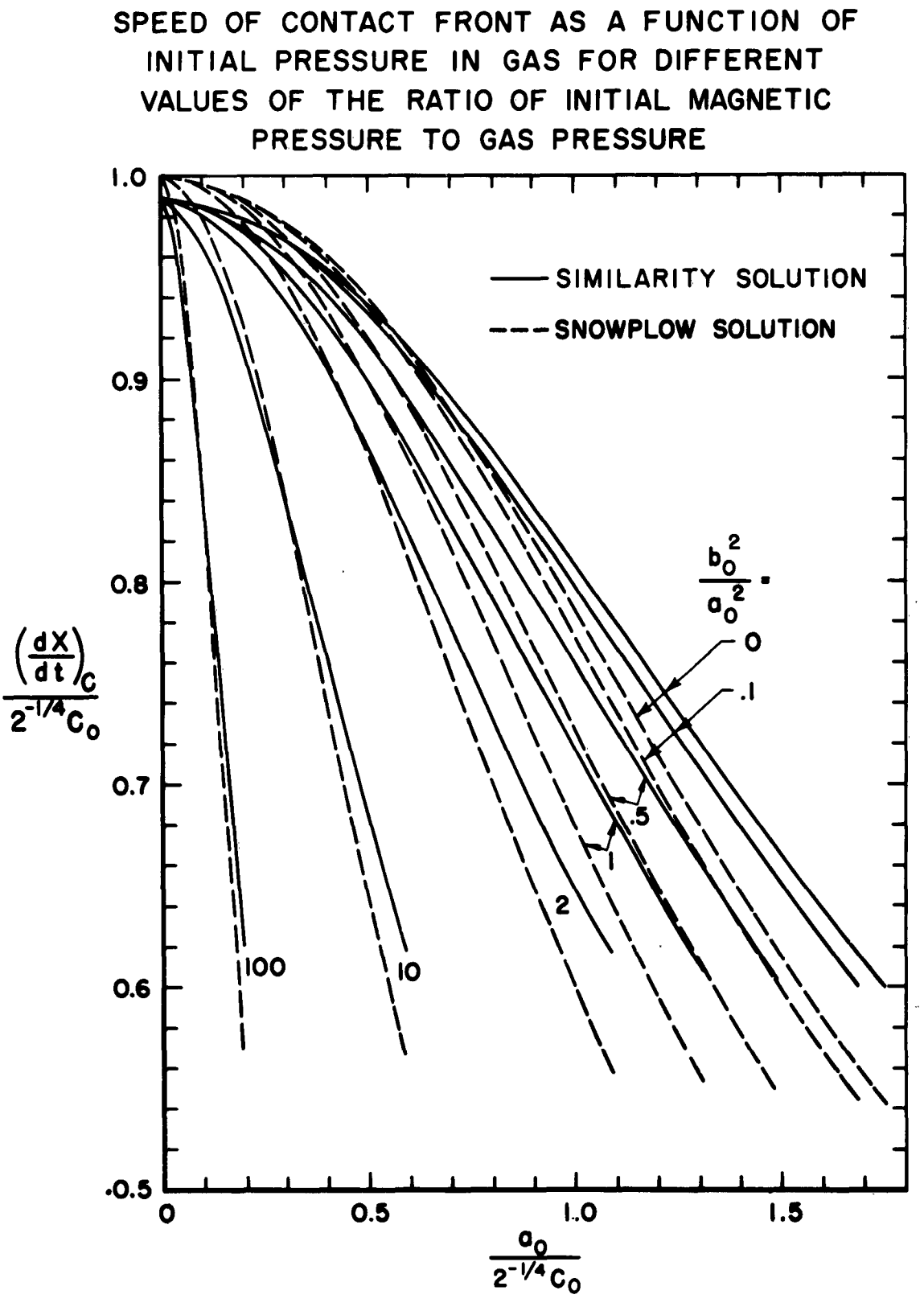


Figure 10. Comparison of speed predicted by snowplow theory with speed of contact front obtained from a similarity solution of the full equations

where $\sigma$, U, P, and $\beta$ are nondimensional functions of a single nondimensional variable $\Phi$. Two exact integrals of the four magnetohydrodynamic equations are obtained, and the remaining two equations integrated numerically. The full detail of the flow between the shock and the contact front is thus obtained.

Of particular interest is the result shown in figure 10. Here the speed of the contact front obtained from the solution of the full equations is compared with the speed predicted by the snowplow theory, equation (13). It is seen that there is remarkably good agreement between the snowplow solution and the similarity solution over the entire range of shock strength. The reason for this uniformly good agreement is that, independent of shock strength and specific heat ratio, most of the momentum in the flow is carried by the fluid very close to the contact front where the density and velocity are greatest. Snowplow theory, being simply a statement of momentum balance, predicts rather accurately the motion of this portion of the fluid. This accounts for the success of the theory noted in the preceding sections.

## REFERENCES


1. Rosenbluth, M. with Garwin, R. and Rosenbluth, A., Infinite Conductivity Theory of the Pinch, Los Alamos Report LA-1850, September 1954
2. Cole, J. D., Newtonian Flow Theory for Slender Bodies, Journal of Aeronautical Science 24, 448, 1957
3. Anderson, O. A., Furth, H. P., Stone, J. M., and Wright, R. E., Physics Fluids 1, 489, 1958
4. Elmore, W. C., Little, E. M., and Quinn, W. E., Neutrons of Possible Thermonuclear Origin, Physical Review Letters 1, 32, 1958
5. Killeen, J. and Lippman, B. A., Circuit Dynamics of the Pinch, Journal of Applied Physics 31, 1549, 1960
6. Patrick, R. M., High-Speed Shock Waves in a Magnetic Annular Shock Tube, Physics Fluids 2, 599, 1960
7. Mostov, P. M., Neuringer, J. L., and Rigney, D. S., Electromagnetic Acceleration of a Plasma Slug, Plasma Propulsion Laboratory, Republic Aviation Corporation, TR-61-5, February 24, 1961
8. Artsimovich, L. A., Luk'ianov, S. Iu., Podgorny, I. M., and Chuvatin, S. A., Electrodynamic Acceleration of Plasma Bunches, Soviet Physics JETP 6, 1, 1958; Podgorny, I. M., Chuvatin, S. A., Bykov, G. A., and Pis'menny, V. D., Study of the Process of Electrodynamic Acceleration of Plasma Bunches II, Plasma Physics and the Problem of Controlled Thermonuclear Reactions, Vol. IV, Pergamon Press, London, p. 262, 1960
9. Dattner, A., Acceleration of Plasma, Proceedings of the Fourth International Conference on Ionization Phenomena in Gases, Vol. II, Uppsala, p. 1151, 1959
10. Kech, J. C., Fishman, F., and Petschek, H. E., Experimental Study of the Flow Field in a MAST of Large Radius Ratio, Bulletin of American Physical Society II, 278, 1961
11. Greifinger, C. and Cole, J. D., On Cylindrical Magnetohydrodynamic Shock Waves, Physics Fluids 4, 527, 1961
12. Liepmann, H., and Vlases, G. to be published in the Physics of Fluids

# NUMERICAL APPROXIMATIONS FOR WEAK SOLUTION OF MIXED INITIAL-BOUNDARY VALUE PROBLEMS OF FLUID FLOWS

Dr. W. McIlroy
Mr. M. Halem
Republic Aviation Corporation

## 1. INTRODUCTION.

This paper will present a brief survey of some of the problems that are under investigation by the Plasma Propulsion Lab, in conjunction with the Digital Computing Division at Republic Aviation. Each of the problems represent a special case of a more general system of conservative hyperbolic equations with moving boundaries.

In support of the work being carried out in developing a pulsed plasma accelerator, a number of studies have been made of the pinch process using various models with varying degrees of sophistication. In the present paper emphasis will be placed on the analytical solution obtained by Chu[1] and the numerical gasdynamic treatment using the technique of the pseudo viscosity term of Lax[2] for application to an IBM 7090. The analytical approach is based upon the assumption that one shock, and only one, exists. The numerical approach makes no such restriction. It is conceivable in the general case that more than one could exist, resulting in shock collisions and violation of the constant entropy condition for piston problems. On using the numerical technique, however, if more than one shock does arise they are immediately recognizable as areas across which rapid changes in the variables take place, and are automatically accounted for in the analysis. This technique is therefore a very powerful one, especially in cases where the actual physical processes are not completely understood. This same method has been applied to the study of hydromagnetic shocks generated by the relative motions of fluids in the presence of magnetic fields. Here again the shocks are readily identified and can be categorized into the fast, slow, or Alfven variety, without the necessity of prior shock fitting. The technique is applicable to fluid flows for arbitrary dimensions.

The analytical approach is presently being extended to the compression of a sphere of plasma by an external magnetic field, where the field intensity

is a function of the plasma shape at any instant. This problem is being studied in support of project Cantaloupe under contract with AFSWC.

A further problem that fits into the general numerical procedure is the Stefan problem of heat conduction, which is extremely important in reentry studies. The program that has been developed makes it possible to treat arbitrary geometries in one, two, or three dimensions, with layers of different materials and moving boundaries. A similar problem also arises in the studies of the initial ionization processes and skin formations in the pinch, as was described by Killeen, Gibson and Colgate[3].

## 2.1 HYPERBOLIC SYSTEMS OF CONSERVATION FORM.

Consider the hyperbolic systems of equations from gasdynamics and magnetogasdynamics which have the following form governing the basic flow equations:

$$U_t + \nabla \cdot F + B = 0 \tag{2.1}$$

where $U$ is a column vector of the unknown functions, $F$ and $B$ are vector valued functions of $x_i$, $t$ and $U$, where $x_i$ represents the spatial coordinates $x$, $y$, $z$ and the symbol $\nabla$ is the customary del operator. The initial condition $U(x, 0) = \varphi(x)$, is assumed to satisfy equation (2.1). Such systems of equations are said to be of conservative form.

To illustrate such systems, consider the nonsteady, non-isentropic, dimensionless ideal gas flow equations in Eulerian coordinates which are

$$\begin{aligned}
&\frac{\partial \rho}{\partial t} + \frac{\partial m}{\partial r} + \frac{\sigma m}{r} = 0 \\
&\frac{\partial m}{\partial t} + \frac{\partial}{\partial r}\left\{\frac{p}{\gamma} + \frac{m^2}{\rho}\right\} + \frac{\sigma m^2}{\rho r} = 0 \\
&\frac{\partial E}{\partial t} + \frac{\partial}{\partial r}\left\{\frac{m(p+E)}{\rho}\right\} + \frac{\sigma m(E+p)}{\rho r} = 0
\end{aligned} \tag{2.1.1}$$

where

$$u = u^*/a_0$$

$$r = r^*/R_0$$

$$\rho = \rho^*/\rho_0$$

$$E = E^*/p_0$$

$$p_0 = (\gamma - 1)\left\{E - \frac{\gamma m^2}{\rho}\right\}$$

and where $u^*, r^*, \rho^*$ are dimensional quantities and $\sigma = 0, 1, 2$ for the one-dimensional, axisymmetric, spherically symmetric cases respectively.

The familiar Lundquist equations (for infinitely conducting, nondissipative, inviscid ideal gas) in dimensionless form are:

$$\frac{\partial}{\partial t} B_Y + \frac{\partial}{\partial x}\left\{B_Y \frac{m_x}{\rho} - \frac{m_Y}{\rho}\right\} = 0$$

$$\frac{\partial}{\partial t} B_Z + \frac{\partial}{\partial x}\left\{B_Z \frac{m_x}{\rho} - \frac{m_Z}{\rho}\right\} = 0 \qquad (2.1.2)$$

$$\frac{\partial}{\partial t} m_x + \frac{\partial}{\partial x}\left\{\frac{m_x^2}{\rho} + \frac{p a}{\gamma} + \left(B_Y^2 + B_Z^2\right)\frac{b}{2}\right\} = 0$$

$$\frac{\partial}{\partial t} m_Y + \frac{\partial}{\partial x}\left\{\frac{m_Y m_x}{\rho} - bB_Y\right\} = 0$$

$$\frac{\partial}{\partial t} m_z + \frac{\partial}{\partial x}\left\{\frac{m_x m_z}{\rho} - bB_z\right\} = 0$$

$$\frac{\partial}{\partial t}\rho + \frac{\partial}{\partial x} m_x = 0$$

$$\frac{\partial}{\partial t}\left\{\frac{m^2}{2\rho} + \frac{\rho e a}{\gamma(\gamma-1)} + (B_Y^2 + B_z^2)\frac{b}{2}\right\} + \frac{\partial}{\partial x}\left\{\frac{m_x}{\rho}\left(\frac{m^2}{2\rho} + \frac{\rho e a}{\gamma(\gamma-1)}\right.\right.$$

$$\left.\left. + \frac{pa}{\gamma} + [B_Y^2 + B_z^2]\frac{b}{2}\right) - \frac{b}{\rho}(m_x + B_Y m_Y + B_z m_z)\right\} = 0$$

where $a = \left\{\frac{a_o}{U_{Y_o}}\right\}^2$, $b = \left\{\frac{b_o}{U_{Y_o}}\right\}^2$ and $U_{yo}$ is the initial value of $U_y$.

The equations for a steady, two-dimensional, nonviscous, adiabatic, rotational flow are:

$$\nabla\cdot(\rho u) = 0$$

$$\frac{\partial}{\partial x}(u\rho u) + \frac{\partial}{\partial y}(v\rho u) - \frac{\partial}{\partial Y} p = 0$$

$$\frac{\partial}{\partial x}(u\rho v) + \frac{\partial}{\partial Y}(v\rho v) - \frac{\partial}{\partial Y} p = 0 \qquad (2.1.3)$$

$$\frac{\partial}{\partial x} u\left\{\rho\frac{(u^2+v^2)}{2} + \rho e + p\right\} +$$

$$\frac{\partial}{\partial Y} v\left\{\rho\frac{(u^2+v^2)}{2} + \rho e + p\right\} = 0$$

where p, $\rho$, u are the unknowns.

These particular systems are only a sample of those which lend themselves to a general method of numerical solution which is directly applicable to the actual form of the physical problems. The occurrence of these problems in nature usually involves at least one moving boundary and more often two free boundaries. Almost any attempt at their solutions has led to simplifying assumptions which usually are not physically realizable.

For such systems a complete mathematical theory exists, since they are all of hyperbolic type. However, the existence and uniqueness of solutions of such systems are all of a local nature. The physical nature of the problems, because of neglecting such notions as viscosity and heat conduction, gives rise to the mathematical notion of "shocks" or discontinuities. These discontinuities in the solutions do, however, have certain algebraic properties derived from the conservation principles. It is these curves which become the free boundaries in many important physical problems and they have led to a host of analytical and numerical techniques for effecting their solutions.

## 2.2 THE "LAX DIFFERENCE SCHEME".

The method adopted for the numerical solution of such a class of free boundary problems is essentially due to Lax[2]. The notion of weak solution is introduced, since one is interested in solutions in the large which need not have continuous first derivatives. A solution is defined as weak if it satisfies

$$\iint \{W_t U + F \nabla \cdot W - WB\}\, dx\, dt + \int W(x,0)\,\phi(x)\, dx = 0 \qquad (2.21)$$

where W is a test function with continuous first derivatives and is zero outside some interval. It can be shown that for two genuine solutions on two adjacent domains separated by a smooth curve, where the slope of the curve satisfies the Rankine-Hugoniot shock conditions with respect tc these two solutions, the smooth curve forms a weak solution over the entire domain.

As so often happens when one generalizes the notion of solutions in mathematics, a penalty is imposed. In this case the initial values for conservative systems do not determine a unique weak solution. However, an additional principle asserted by Lax to determine the unique solution is that "weak solutions for fluid problems are limits of viscous flows".

Using this principle one can enlarge equations (2.21) to a nonlinear parabolic system

$$U_t + \nabla \cdot F + B = \lambda \nabla^2 U \qquad (2.2.2)$$

For a fixed initial value of U(x, o), the solution exists for a range of t independent of $\lambda$ . If corresponding solutions $U_\lambda$ (x, t) converge boundedly to a limit U(x, t) as $\lambda \to 0$, then this limit will be a weak solution.

The difference scheme is derived by choosing $\lambda = \frac{(\Delta r)^2}{2\Delta t}$ and using a forward difference approximation with respect to t and centered difference approximations with respect to x.

This difference method gives rise to the following recipe for differencing the equations.

Replace $\frac{\partial U}{\partial t}$ by

$$\frac{1}{\Delta t}\left\{U(x,t+\Delta t) - \frac{U(x+\Delta x,t) + U(x-\Delta x,t)}{2}\right\} \qquad (2.2.3)$$

and $\frac{\partial F}{\partial x}$ by

$$\frac{1}{\Delta x}\left\{\frac{F[U(x+\Delta x,t)] - F[U(x-\Delta x,t)]}{2}\right\} \qquad (2.2.4)$$

This difference scheme when viewed as an approximation to equation (2.2.2) satisfies the stability condition for parabolic equations;

i.e., $$\lambda \frac{\Delta t}{(\Delta r)^2} < \frac{1}{2}$$

The difference equations can also be shown to be stable for the hyperbolic systems.

Since it is desired to select the unique solution in nature, it is conjectured that one should try to satisfy the stability criteria of Courant-Friedricks-Lewy for hyperbolic systems (i.e., $\frac{\Delta t}{\Delta x} < \frac{1}{u + c}$ ).

It is our aim to extend this method to mixed initial value problems. For free and fixed boundary value problems one usually has integral forms of the conservative systems determining the behavior of the boundaries. The system of integral equations take the following form

$$\int_{V(t)} U_t \, dV + \int_{S(t)} F \vec{n} \cdot d\vec{S} = 0 \qquad (2.2.5)$$

These integral forms lead to equations (2.1.1) by application of Gauss' Theorem. However, the equations being solved are of the form (2.2.2). Thus, equations (2.2.5) should be modified if they are to lead to equation (2.2.2). A natural generalization of the integral forms leading to this system takes the form

$$\int_{V(t)} U_t \, dV + \int_{S(t)} F \vec{n} \cdot d\vec{S} = \int_{S(t)} \lambda \nabla U \vec{n} \cdot d\vec{S} \qquad (2.2.6)$$

From this form it is possible to obtain equations governing the motion of the free boundaries.

Questions as to the existence of solutions of equations (2.2.2) subject to conditions (2.2.5) have been only partially answered for specific problems. That such solutions $U_\lambda$ of the equations (2.2.2) with boundary conditions (2.2.6) converge to solutions of equations (2.1.1) subject to boundary conditions (2.2.5) can only be conjectured at this moment. However, for many of the cases tried so far, the method seems to give promising results.

## 3. APPLICATIONS TO PHYSICAL PROBLEMS.

The general difference scheme just described will be applied to various problems which have already been solved by special techniques. A summary of the technique by which analytic solutions have been obtained will be described, and then the application of the generalized Lax method to the same problem will be presented. The following selection of problems includes some of those that have been of theoretical concern to the Plasma Propulsion Lab and of numerical interest to the Digital Computing Division of Republic Aviation Corporation.

### 3.1 STEFAN'S PROBLEM.

The first type of application to be considered includes those physical problems governed by parabolic equations with moving boundary conditions. Missile reentry problems for bodies with ablating materials, melting of ice, recrystallization of metals, are some examples of problems now considered as Stefan's problem. The problem also arises in studies of the initial ionization processes in a plasma[3]. Consider the simplest form of the Stefan

problem described by the following equations:

$$\frac{\partial V}{\partial t} = \lambda \frac{\partial^2 V}{\partial x^2} \qquad (3.1.1)$$

for $0 < x < b(t)$ where b (t) is the position of the boundary subject to the following initial and boundary conditions

$$\frac{\partial V}{\partial x}(0,t) = -1 \quad ; \; t > 0$$

$$V(x,0) = x \qquad (3.1.2)$$

$$V[b(t), t] = 1$$

$$\frac{\partial V}{\partial x}[b(t), t] = -\frac{db}{dt}$$

$$b(0) = 1$$

This is almost the form considered by Douglas and Gallie[4] for which a numerical difference scheme is shown to converge to a solution whose existence and uniqueness have already been established by Evans[5] Theirs is a series method that resolves the solution. However, the coefficients of this series are difficult to obtain and no radius of convergence is available.

Applying the recipe for the equation of form (2. 2. 2)to the equations (3. 1. 1) where U = v and F = 0 leads to the following difference equation at some point x, t in the interior of the domain $0 \le x \le b(t)$ , $0 < t < \infty$

$$V(x, t+\Delta t) = \lambda \frac{\Delta t}{(\Delta x)^2} \left\{ V(x+\Delta x, t) - 2V(x,t) + V(x-\Delta x, t) \right\} \qquad (3.1.3)$$

Additional equations are now needed for the boundary points [b (t), t] . Equations (2. 2. 6)applied to (3. 1. 1)lead to the following equations

$$-\frac{db}{dt}\lambda + \lambda = \int_0^{b(t)} \frac{\partial V}{\partial t}\, dx \qquad (3.1.4)$$

Since v $\left[b(t),\ t\right]$ is known for all t, (3.1.4) gives an equation for b(t). Approximating the integral by a trapezoidal rule and replacing time derivatives of the quantities by forward differences lead to the following

$$b(t+\Delta t) = b(t) + \Delta t \left\{ 1 - \frac{1}{\lambda} \sum_{i=1}^{N-1} \frac{V(i\Delta x, t+\Delta t) - V(i\Delta x, t)}{\Delta t} \Delta X \right\} \quad (3.1.5)$$

where $N\Delta X = b(t)$

The general recipe for the solution of free boundary value problems for hyperbolic systems obtained from the integral conservation laws was an outgrowth of this problem. The effectiveness of this approach for a single nonlinear parabolic equation, with boundary conditions general enough to include radiation terms and ablation, is described in an RAC report by Pines, Halem and Broder.[6]

It was natural to try to extend this approach to nonlinear parabolic systems. Other numerical schemes for such systems are presently being investigated, and as yet many open questions remain to be answered.

## 3.2 HYDROMAGNETIC SHOCKS

The next class of problems that the general numerical procedure will be applied to are the problems leading to magnetic shocks caused by relative motions. Consider a conducting pole face of an electromagnet adjacent to an infinitely conducting fluid with a magnetic field normal to the face and where no relative motion between magnet and fluid is assumed. (Figure 1.)

Suppose the magnet is suddenly set in motion with a velocity $-U_y$. A motion will result because of the presence of the x-component of the magnetic field. The magnetic lines of force can be regarded as fixed between magnet and fluid. The motion of the magnet pulls down the lines of magnetic intensity and the fluid in a thin layer adjacent to the pole. This produces a component of the magnetic field $B_y$ in the layer. The variation of $B_y$ with x in the layer results in a current density in the z direction of magnitude $\left| \frac{\partial H_y}{\partial x} \right|$. Thus the fluid experiences a magnetic force $\vec{J} \times \vec{B}$ which is in the x direction of magnitude $B_y \left| \frac{\partial H_y}{\partial x} \right|$. This force produces a motion in the layer which then propagates out. One can consider the motion of the

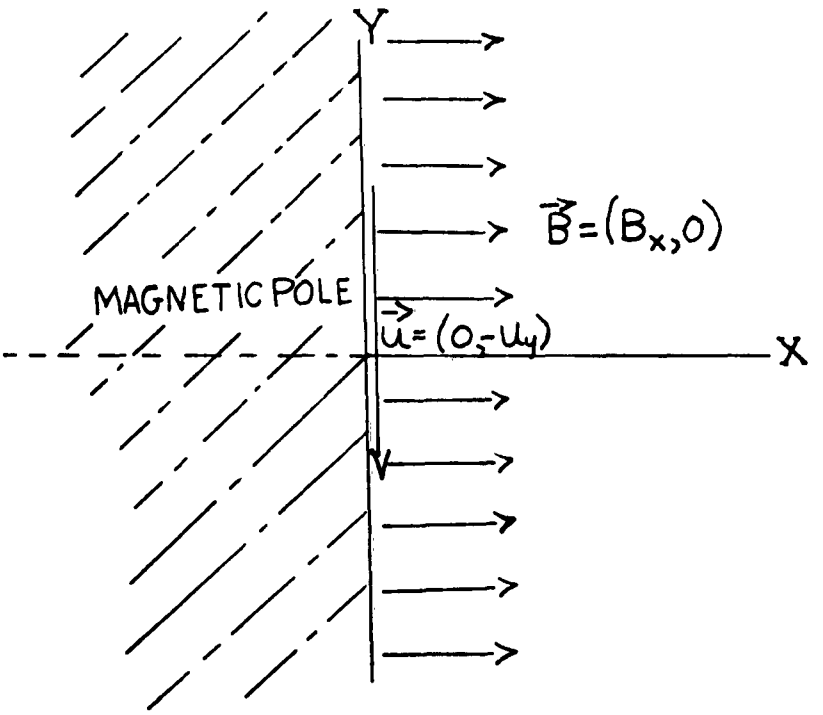


Figure 1.

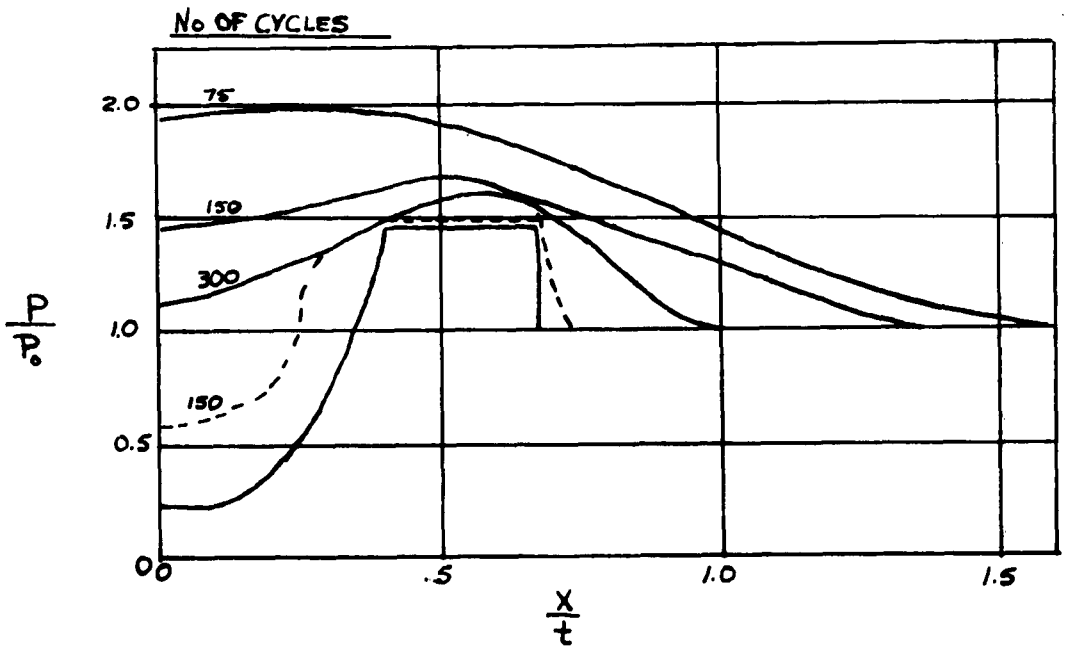


PRESSURE PROFILE SHEAR FLOW DISCONTINUITY

Figure 2.

electromagnet in the x direction, which leads to a pure gas dynamic problem, or in some arbitrary direction leading to more complicated shock and wave patterns.

The resultant flows will give rise to fast, slow, and Alfven hydromagnetic shocks as well as various wave motions. The particular problem for motion in the Y direction was first formulated by K. O. Friedrichs and leads to resolution of shear flow discontinuities. J. Bazer was the first to obtain numerical solutions of these problems[7]. The method used was that of piecing together fast shock and simple wave solutions.

The general approach described in Section 2, when applied to the Lundquist equations (2.1.2) leads to the following system of difference equations.

$$B_{y_i}^{j+1} = \left(\frac{B_{y_{i+1}}^{j} + B_{y_{i-1}}^{j}}{2}\right) - \frac{1}{2}\left[\frac{\left(B_{y_{i+1}}^{j} m_{x_{i+1}}^{j} - m_{y_{i+1}}^{j}\right)}{\rho_{i+1}^{j}} - \frac{\left(B_{y_{i-1}}^{j} m_{x_{i-1}}^{j} - m_{y_{i-1}}^{j}\right)}{\rho_{i-1}^{j}}\right]\frac{\Delta t}{\Delta x}$$

$$m_{x_i}^{j+1} = \frac{\left(m_{x_{i+1}}^{j} + m_{x_{i-1}}^{j}\right)}{2} - \frac{1}{2}\left[\left(\frac{m_{x_{i+1}}^{2}}{\rho_{i+1}^{j}} + \frac{\rho_{i+1} a}{\gamma} + B_{y_{i+1}}^{2}\frac{b}{2}\right) - \left(\frac{m_{x_{i-1}}^{2}}{\rho_{i-1}^{j}} + \frac{\rho_{i-1} a}{\gamma} + B_{y_{i-1}}^{2}\frac{b}{2}\right)\right]\frac{\Delta t}{\Delta x} \qquad (3.2.1)$$

$$m_{y_i}^{j+1} = \frac{\left(m_{y_{i+1}}^{j} + m_{y_{i-1}}^{j}\right)}{2} - \frac{1}{2}\left[\left(\frac{m_{y_{i+1}}^{j} m_{x_{i+1}}^{j}}{\rho_{i+1}^{j}} - B_{y_{i+1}} b\right) - \left(\frac{m_{y_{i-1}}^{j} m_{x_{i-1}}^{j}}{\rho_{i-1}^{j}} - B_{y_{i-1}} b\right)\right]\frac{\Delta t}{\Delta x}$$

$$\rho_i^{j+1} = \frac{\rho_{i+1}^{j} + \rho_{i-1}^{j}}{2} - \frac{1}{2}\left[m_{x_{i+1}}^{j} - m_{x_{i-1}}^{j}\right]\frac{\Delta t}{\Delta x}$$

(3. 2. 1)con't.

$$E^* = \frac{1}{2}\left[\left\{\left(\frac{m_{x_{i+1}}^2 + m_{y_{i+1}}^2}{2\rho_{i+1}^j}\right) + \frac{\rho_{i+1}^j E_{i+1}^j A}{\gamma(\gamma-1)} + B_{y_{i+1}}^2 \frac{b}{2}\right\} + \right.$$

$$\left. + \left\{\left(\frac{m_{x_{i-1}}^2 + m_{y_{i-1}}^2}{2\rho_{i-1}^j}\right) + \frac{\rho_{i-1}^j E_{i-1} A}{\gamma(\gamma-1)} + B_{y_{i-1}}^2 \frac{b}{2}\right\}\right]$$

$$- \frac{1}{2}\left[\frac{m_{x_{i+1}}^j}{\rho_{i+1}^j}\left\{\left(\frac{m_{x_{i+1}}^2 + m_{y_{i+1}}^2}{2\rho_{i+1}^j}\right) + \frac{\rho_{i+1}^j E_{i+1} A}{\gamma(\gamma-1)} + B_{y_{i+1}}^2 \frac{b}{2} + \rho_{i+1}^j \frac{A}{\gamma}\right\}\right.$$

$$- b\left(\frac{m_{x_{i+1}}^j + B_{y_{i+1}}^j m_{y_{i+1}}^j}{\rho_{i+1}^j}\right) - \frac{m_{x_{i-1}}^j}{\rho_{i-1}^j}\left\{\left(\frac{m_{x_{i-1}}^2 + m_{y_{i-1}}^2}{2\rho_{i-1}^j}\right) + \frac{\rho_{i-1}^j E_{i-1} A}{\gamma(\gamma-1)}\right.$$

$$\left.\left. + B_{y_{i-1}}^2 \frac{b}{2} + \rho_{i-1}^j \frac{A}{\gamma}\right\} - b\left(\frac{m_{x_{i-1}}^j + B_{y_{i-1}}^j m_{y_{i-1}}^j}{\rho_{i-1}^j}\right)\right] \frac{\Delta t}{\Delta X}$$

$$E_i^{j+1} = \left[E^* - \left(B_{y_i}^2\right)^{j+1} \frac{b}{2} - \left\{\frac{\left(m_{x_i}^2\right)^{j+1} + \left(m_{y_i}^2\right)^{j+1}}{2\rho_i^{j+1}}\right\}\right] \frac{\gamma(\gamma-1)}{a\rho_i^{j+1}}$$

Select a coordinate system that moves with the mean velocity of the thin layer. The initial vector is $U(B_{Y_0}, m_{x_0}, m_{y_0}, \rho_0, E_0)$ for $X<0$ and $U(B_{Y_0}, m_{x_0}=m_{Y_0}, \rho_0, E_0)$ for $X>0$. The numerical solution with this difference method gave very good agreement with the numerical analytical solution of Bazer (figure 2). For better agreement in the neighbor-

hood of the shock, larger values of $\frac{\Delta t}{\Delta x}$ are needed whereas for the steady state region, smaller mesh spacings should be used.

This approach is now being used in resolving other hydromagnetic shock flows and seems very promising.

The method gives numerical answers which are sufficiently accurate to be used directly in shock fitting techniques. Quite often the knowledge of the strength of some parameters across magnetic shocks of arbitrary types, as well as the relations which are known[8], enables one to actually compose the flows from the pieces directly. These techniques are now being developed for arbitrary motions of the magnetic poles moving into infinitely conducting plasmas.

## 3.3 MAGNETIC PISTON PROBLEM (PINCH EFFECT)

Consider a pair of circular electrodes in an electrical circuit containing capacitive, resistive, and inductive elements. When a sufficiently high voltage is applied across electrodes, the gas between them ionizes and a current sheath confined to a thin cylindrical shell at the edge of the electrodes is produced enclosing column of gas between electrodes. The magnetic field produced by current sheath then interacts with the current to produce a radially inward Lorentz force, $\vec{J} \times \vec{B}$, and compresses the enclosed gas. If the ionized gas has high conductivity, a current sheath of approximately zero thickness is formed, which enables one to think of this sheath as a magnetic piston. Since the magnetic pressure and gas pressure should be continuous across the infinitely thin current sheath, we obtain gas pressure

$$p_g = \frac{\mu I^2}{8\pi^2 r^2} + p_B$$

where $p_B$ is static gas pressure behind the piston which varies in time. It will be assumed initially that I (t) is given from external circuit characteristics and the time varying inductance due to movement of sheath is neglected. Assuming no leakage through the magnetic piston (or current sheath) equations (2.1.1) govern the flow. Prescribing $p_g$ on the curve OP in (figure 3) and the initial state on OA is a well posed problem.

BS represents the shock curve arising from the compression by the piston. The positions of the curves OP and BS as well as the flow between them is to be determined.

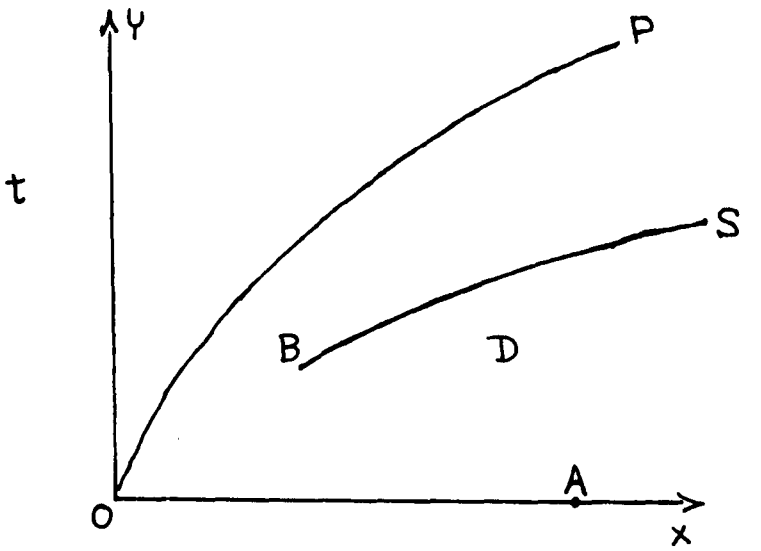


Figure 3.

Several approximate methods for solving this problem have been developed, but a complete solution to the physical problem is still open. A widely used technique for approximating the solution is the snowplow model. This thoery assumes that all the mass swept up by the shock is compressed into a thin layer so that the piston and shock curves can be treated coincidentally. The motion of this layer is governed by the momentum equation. This model gives valid approximations when the shock is sufficiently strong and the specific heat ratio of the gas is close to unity.

Another approach is that described in the paper by Drs. Greifinger and Cole[9] which makes use of similarity solutions. Assuming the solution has conical similarity, and introducing a coordinate system employing the stream function and a certain mass ratio parameter, one obtains two coupled ordinary differential equations.

3.3A An Analytical Formulation of the Pinch Problem.

Employing a somewhat different approach by B. T. Chu[1] it is also possible to reduce the partial differential equations governing the flow to a coupled system of ordinary differential equations. By labeling the particles as when they are traversed by the shock (figure 4)

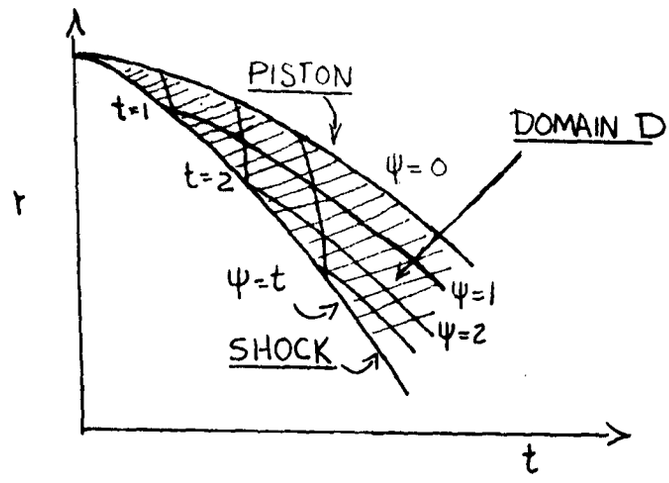


Figure 4.

a Lagrangian formulation of the equations for cylindrical geometry is obtained in the form

$$p_\psi = -\rho r_\psi r_{tt} \tag{3.3.1}$$

$$p_t = a^2 \rho_t$$

$$\rho r_\psi r = u_o r_s$$

$$u = r_t$$

where the subscript S indicates that the quantity to which it is affixed is evaluated just behind the shock. For a strong shock the density ratio

$$\epsilon \sim \frac{\gamma - 1}{\gamma + 1}$$

The boundary condition to be satisfied, obtained from the usual shock conditions and magnetic piston in dimensionless form, are

$$r^2 p = I^2(t) \qquad @ \quad \psi = 0$$

$$p = \frac{2}{\gamma+1} u_0^2 \qquad @ \quad \psi = t$$

$$\frac{1}{\rho} = \frac{\gamma-1}{\gamma+1} \qquad @ \quad \psi = t \qquad (3.3.2)$$

$$u = \frac{2}{\gamma+1} u_0 \qquad @ \quad \psi = t$$

$$r = 1 \qquad @ \quad \psi = t = 0$$

where $U_0$ is the shock speed (Note: $u_0 = (r_\psi)_s + u_s$ @ $t = \psi$ )

Assuming strong shocks one can write the solution in a power series $\epsilon$

$$p = p^{(0)} + \epsilon p^{(1)} + \epsilon^2 p^{(2)} + \ldots\ldots$$

$$r = r^{(0)} + \epsilon r^{(1)} + \epsilon^2 r^{(2)} + \ldots\ldots \qquad (3.3.3)$$

$$\tau = \epsilon(\tau^{(0)} + \epsilon\tau^{(1)} + \epsilon^2\tau^{(2)} + \ldots\ldots)$$

$$u = u^{(0)} + \epsilon u^{(1)} + \epsilon^2 u^{(2)} + \ldots\ldots$$

$$u_0 = u_0^{(0)} + \epsilon u_0^{(1)} + \epsilon^2 u_0^{(2)} + \ldots\ldots$$

Substituting into the equations (3.3.2) and collecting like terms of $\epsilon$, the lowest order terms are found to satisfy the differential equation

$$f\left[\frac{I^2}{f^2} - f'^2\right] = -\frac{f''}{2}(1 - f^2) \qquad (3.3.4)$$

WHERE $r^{(0)} = f(t)$ AND $u^{(0)} = f'(t)$

This equation is identical to that obtained from the snowplow model.

Since the initial condition of f=1 at t=0 is singular, the solutions of these equations are determined by the single condition that $f''(0) < 0$. When I(t) = sin $\alpha$ t one can derive a power series approximation for f (t) which for small $\alpha$t is

$$f(t) = 1 - \frac{\alpha}{\sqrt{6}} t^2 + \mathcal{O}(t^4) + \qquad (3.3.5)$$

from which one obtains f'' (0) as a starting condition.

Making the substitutions and equating first order terms then leads to the following integrodifferential equation

$$f_1''(f-1) + 2f'f_1' + f_1\left(\frac{2I^2}{f^3} + f''\right) =$$

$$f'^2 - \frac{2I}{f^3}\int_0^t F(\psi,t)\,d\psi + \int_0^t G(\psi,t)\,d\psi \qquad (3.3.6)$$

$$F(\psi,t) = -f'(\psi)^3 \Big/ \left\{f'^2 + f''\left(f(t) - f(\psi)\right)\right\}$$

$$G(\psi,t) = -\bar{f}'\left\{\frac{\partial^2}{\partial t^2}\int_\psi^t F(\psi,t)\,d\psi\right\}$$

$$r^{(1)} = f_1(t) + \int_\psi^t F(\psi,t)\,d\psi$$

$$u^{(1)} = f_1' - f' + \int_\psi^t F(\psi,t)\,d\psi$$

$$u_0^{(1)} = f_1'(\psi)$$

At t = 0, f = 1 is a singular point, and the solution is determined from the condition $f_1$ (o) = o.

To obtain initial values one again obtains a power series representation of $f_1(t)$ for small $\alpha t$ as

$$f_1(t) = \sqrt{6}\,\alpha\left[\frac{7}{6} - 3\log\frac{3}{2}\right]t^2 +$$

The numerical technique used to solve the coupled system of differential equations was a general self-starting, Cowell (double sum) second order integration scheme with eighth order accuracy. The routine has the option of using a fixed step or variable step size for better corrections. This method is more rapid and has greater accuracy than Runge-Kutta schemes. The integrals are evaluated by Simpsen's rule and the partial differential operator on the integrals by a backward second order difference scheme. The power series solution for small $\alpha t$ is used to allow for a sufficient number of points to build up good integral and differential approximations. The integration scheme is used with a sufficiently small fixed step size to avoid exceeding the memory storage requirements of the 7090 which might occur if variable time steps were used. The size of the steps was determined by solving special cases of these equations with the variable time step option. The solutions give the snowplow results as the zeroth order approximation, while the first order result gives the separation distance betwen the piston and the shock (figure 5.). This distance is relatively small, so that the dynamics are well satisfied by the snowplow. However, the first order solution gives the distribution of density, pressure, temperature and velocity in this small piston-shock space. Because of the assumption of strong shocks, the density at the piston is infinite initially, and remains so for the rest of the motion.

The basic assumption of such analytical solutions is that only one shock is formed during the piston acceleration. It is conceivable that a number of shocks could develop in the general case, and under these conditions reflected waves could change the constant entropy condition at the piston. It is in this respect that the Lax procedure represents an extremely powerful tool, since high gradients throughout the flow field will become immediately evident.

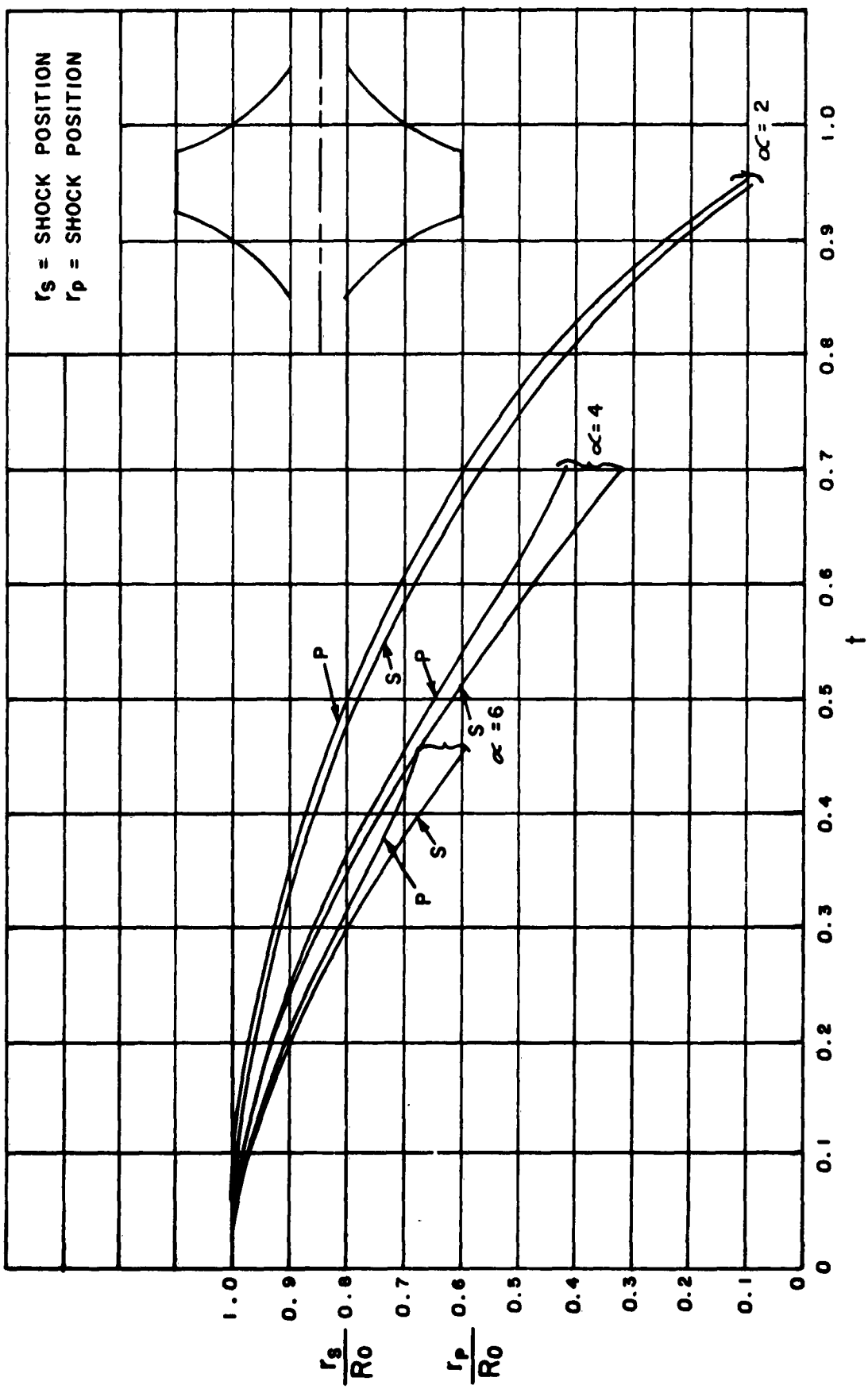


Figure 5. Pinch dynamics on a constant area channel

## 3.4 THE LAX DIFFERENCE APPROXIMATIONS FOR THE PISTON PROBLEM.

For the present purposes the difference equations will be specialized to treat one-dimensional flow.

Consider a subdivision $\Omega$ of the domain D of figure 3 and denote the mesh points $r = \sum \Delta_i r$ and $t = \sum \Delta_j t$ where i and j are non-negative integers. Let U (r, t) at these points be denoted as $U_i$. Using the recipe described in (2.2.3, 2.4) the following system of difference equations over the interior points with $\lambda = (\Delta r)^2 / 2\Delta t$ and $\sigma = 0$ can be derived from equations (2.1.1)as

$$\rho_i^{j+1} = \frac{\beta_j}{2}\left(\rho_{i+1}^j + \rho_{i-1}^j\right) + \frac{\beta_j \Delta t}{2\Delta r}\left(m_{i+1}^j - m_{i-1}^j\right) + \left(\rho_i^j - \beta_j \rho_i^j\right)$$

$$m_i^{j+1} = \frac{\beta_j}{2}\left(m_{i+1}^j + m_{i-1}^j\right) + \frac{\beta_j \Delta t}{2\Delta r}\left\{\frac{1}{\gamma}\left(\rho_{i+1}^j - \rho_{i-1}^j\right) + \frac{(m_{i+1}^j)^2}{\rho_{i+1}^j} - \frac{(m_{i-1}^j)^2}{\rho_{i-1}^j}\right\}$$

$$+\left(m_i^j - \beta_j m_i^j\right)$$

(3.4.1)

$$E_i^{j+1} = \frac{\beta_j}{2}\left(E_{i+1}^j + E_{i-1}^j\right) + \frac{\beta_j \Delta t}{2\Delta r}\left\{\frac{m_{i+1}^j\left(\rho_{i+1}^j + E_{i+1}^j\right)}{\rho_{i+1}^j} - \frac{m_{i-1}^j\left(\rho_{i-1}^j + E_{i-1}^j\right)}{\rho_{i-1}^j}\right\}$$

$$+\left(E_i^j + \beta_i E_i^j\right)$$

$$\rho_i^{j+1} = (\gamma - 1)\left\{E_i^{j+1} - \frac{\gamma}{2}\frac{(m_i^{j+1})^2}{\rho_i^{j+1}}\right\}$$

The time centered difference approximation over unequally spaced distance intervals $\Delta r$ and $\alpha\Delta r$ at the mesh points adjacent to the piston path (figure 6) can be derived from the Taylor series expansion in both directions; and eliminating the second order terms, one obtains for a function $\varphi(r, t)$

$$\phi_r\Big]_{i,j} \simeq \left\{\phi^j_{i-1} - (1-\alpha^2)\phi^j_i - \alpha^2\phi^j_{i+1}\right\} \Big/ \alpha(\alpha+1)\Delta r \qquad (3.4.2)$$

and similarly

$$\phi_{rr}\Big]_{i,j} \simeq \left\{\frac{\alpha(\alpha^2-1)\phi^j_{i+2} - 2(\alpha^3-4\alpha)\phi^j_{i+1} + (\alpha^3-7\alpha-6)\phi^j_i + 6\phi^j_{i-1}}{\alpha(\alpha+1)(\alpha+2)\Delta r}\right\} \qquad (3.4.3)$$

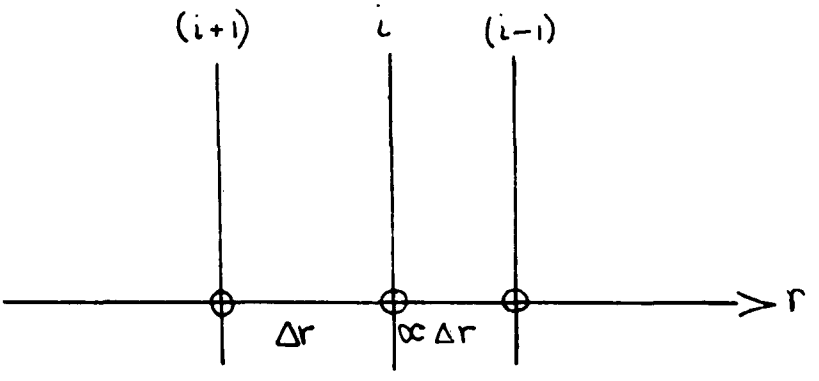


Figure 6

Denote the difference operator in (3.4.2) by $\nabla^1_i$ and in (3.4.3) by $\nabla^2_i$.

Apply these approximations to (2.1.1) one obtains the following system for the points adjacent to the piston path:

$$\rho^{J+1}_i = \beta_j \Delta t \left\{-\nabla_i' m_i + \lambda \nabla_i^2 \rho^j_i\right\} + \rho^j_i$$

$$m_i^{J+1} = -\beta_j \Delta t \left\{ -\nabla_i' \left( \frac{1}{\gamma} P_i^j + \frac{(m_i^j)^2}{\rho_i^j} \right) + \lambda \nabla_i^2 m_i^j \right\} + m_i^j$$

$$E_i^{J+1} = -\beta_j \Delta t \left\{ -\nabla_i' \left[ \frac{m_i^j (P_i^j + E_i^j)}{\rho_i^j} \right] + \lambda \nabla_i^2 E_i^j \right\} + E_i^j$$

$$P_i^{J+1} = (\gamma - 1) \left\{ E_i^{J+1} - \frac{\gamma}{2} \frac{(m_i^{J+1})^2}{\rho_i^{J+1}} \right\} \qquad (3.4.4)$$

## 3.5 NUMERICAL APPROXIMATIONS AT THE BOUNDARY.

The fundamental disturbances of the fluid arise and propagate from the moving boundary and present the inherent difficulties of the problem. Various numerical techniques were attempted and the appropriate approximations will be discussed.

### 3.5A Direct Methods for Boundary Computations.

The generalized system of integral equations to be used is:

$$(a) \quad \int_0^{r(t)} \rho(r,t)\, dr = \int_0^{r(0)} \rho\, dr + \int_0^t (\lambda \rho_r)\, dt \qquad (3.5A1)$$

$$(b)\quad \int_0^{r(t)} m(r,t)\,\delta r = \int_0^{r(0)} m\,dr + \int_0^t \left[\lambda m_r - p\{r(t),t\} + p\{0,t\}\right] dt$$

$$(c)\quad \int_0^{r(t)} E(r,t)\,\delta r = \int_0^{r(0)} E\,dr + \int_0^t \left[\lambda E_r - \frac{p\{r(t),t\}\, m\{r(t),t\}}{\rho\{r(t),t\}}\right] dt$$

The additional boundary conditions arise from the equation of state and the equation for the magnetic pressure.

These equations are analogous to the generalized integral forms for fluid equations considering viscosity and heat conduction. (3.5Ala) says there is a mass source. In the treatment of Von Neumann and Richtmeyer[10] this term does not appear, since they were particularly careful to maintain a close analogy with the physical description. It is one of the aims of the present studies to investigate t he present scheme with and without this effect.

A first derivative approximation for $U_r$ at a boundary point is required in terms of computed values of U at the interior points. Denote by P, A, i = I, ... N, the piston point, adjacent point, and subsequent interior points. Expanding U at P (j) with increments of $\alpha\ \Delta r$ and $(1+\alpha)\Delta r$ one obtains on eliminating second order terms

$$\left.\frac{\partial U}{\partial r}\right|_{P,j} = \frac{\alpha^2 U_I - (1+\alpha)^2 U_A + (1+2\alpha) U_P}{\alpha(1+\alpha)\Delta r} \qquad (3.5A2)$$

Let this derivative expression be denoted by $\Delta_p^j U$. An iteration procedure will be described to evaluate U at the piston boundary. One obtains as a

first approximation for $p_p$ in dimensionless form

$$P_p(j) = \left\{ I^2(j) / r_p^2(j-1) \right\} + 1 \qquad (3.5A3)$$

remembering that rarefactions behind the piston are to be neglected until a later date. This approximation uses the value of r at the previous time (j-1) and will be improved once $r_p$ (j) is computed.

The remaining variables to be determined are $\rho\{r(t), t\}$, $m\{r(t), t\}$, $E\{r(t), t\}$ and r(t). Two procedures were followed at this point.

As an initial approximation it is assumed that the specific entropy is a constant at the piston (as it would be in absence of $\lambda$ ). Therefore, knowing $P_p$ (j), $\rho_p$ can be computed from

$$\rho_p\{r(t), t\} \simeq \exp\left\{ \frac{1}{\gamma} \ln_e P_p(j) \right\} \qquad (3.5A4)$$

Since the density is now determined over the entire mesh at time, t , one can now compute the total mass. From the equation of mass conservation (3.5A1a) the position of r (j$\Delta$t) can be determined. However, there are certain possible positions of the piston for a given $\Delta$t.

The position of the piston

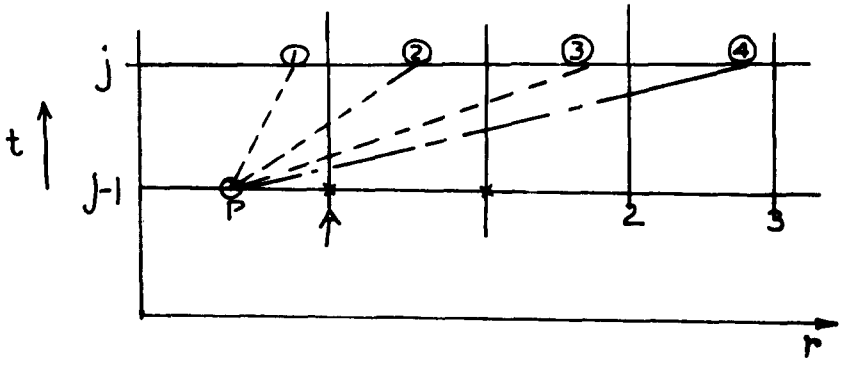


Figure 7

at the time (j$\Delta$t) might lie between the points p, A of time (j-1)$\Delta$t or between (A, 1), or (1, 2), etc., as indicated in figure 7.

Since a fixed mesh is used for all time, and the quantities for all interior and adjacent points are computed independently of the piston position, it is possible to integrate over a region with too many points. Assume the first case described, use a trapezoidal approximation for the integrals in equation (3.5A1a) and solve for $\alpha \Delta r$ to obtain the following expression for $\alpha_{j+1}$:

$$\alpha_{j+1} = \left\{ 1 + \frac{\lambda}{2} \sum_{j=0}^{j+1} \Delta_j t \left[ \frac{\{\alpha_{j+1} \rho_i^{j+1} - (1+\alpha_{j+1})^2 \rho_A^{j+1} + (1+2\alpha_{j+1}) \rho_P^{j+1}\}}{\alpha_{j+1}(1+\alpha_{j+1}) \Delta r} + \right.\right. \tag{3.5A5}$$

$$\left.\left. + \frac{\{\alpha_j \rho_i^j - (1+\alpha_j)^2 \rho_A^j + (1+2\alpha_j) \rho_P^j\}}{\alpha_j (1+\alpha_j) \Delta r} \right] - \sum_{i=A}^{N-1} \frac{(\rho_i + \rho_{i+1})}{2} \Delta r \right\}$$

$$\div \frac{1}{2}(\rho_P + \rho_A)$$

where the initial approximation $\alpha_{j+1} \simeq \alpha_j$ ; is used.

Since it is necessary to evaluate $\nabla_1 \rho$ at (j+1), an iteration procedure for $\alpha_{j+1}$ was introduced. If $0 \leq \alpha_{j+1} \leq 1$ then the points over which the integral is evaluated is valid for a first approximation. Knowing $\alpha_{j+1}$ and the number of points one easily computes r(j). It remains to co pute $m_p$ (j).

Using a trapesoidal approximation once more for equation (35A1b), one obtains

$$m_\rho^{j+1} = -\left\{ \sum_{j=0}^{j} \left\{ \frac{P_i^{j+1} - 1}{\gamma} - \lambda \left[ \frac{\alpha_{j+1}^2 m_i^{j+1} - (1+\alpha_{j+1})^2 m_A^{j+1} + (1+2\alpha_{j+1}) m_P^{j+1}}{\alpha_{j+1}(1+\alpha_{j+1}) \Delta r} \right] \right.\right. \tag{3.5A6}$$

$$\left.\left. + \frac{P_i^j - 1}{\gamma} - \lambda \left[ \frac{\alpha_j^2 m_i^j - (1+\alpha_j)^2 m_A^j + (1+2\alpha_j) m_P^j}{\alpha_j (1+\alpha_j) \Delta r} \right] \right\} \Delta_j t \right.$$

$$\left. + \sum_{i=A}^{N-1} (m_i^{j+1} + m_{i+1}^{j+1}) \Delta r + m_A^{j+1} \alpha_{j+1} \Delta r \right\} \div \alpha_{j+1} \Delta r .$$

where $m_p^{j+1}$ is initially computed as $r(j+1)-r(j)/\Delta_j t$.

At this stage $E_p$ can be computed from the equation of state knowing p, $m_p$, $\rho_p$. However, since the interior points have computed $E_i^j$ with the quasi-viscosity term included, it would seem to maintain the consistency of the technique that $E_p$ be also computed from an integral equation.

Similarly, one obtains

$$E_p^{j+1} = \left\{ \sum_{j=0}^{j} \left\{ - \frac{p_p^{j+1} m_p^{j+1}}{\rho_p^{j+1}} + \lambda \frac{\left[\alpha_{j+1}^2 E_1^{j+1} - (1+\alpha_{j+1})^2 E_A^{j+1} + (1+2\alpha_{j+1}) E_p^{j+1}\right]}{\alpha_{j+1}(1+\alpha_{j+1})\Delta r} \right.\right.$$

$$\left. - \frac{p_p^j m_p^j}{\rho_p^j} + \lambda \frac{\left[\alpha_j^2 E_1^j - (1+\alpha_j)^2 E_A^j + (1+2\alpha_j) E_p^j\right]}{\alpha_j(1+\alpha_j)\Delta r} \right\} \Delta_j t \qquad (3.5A7)$$

$$\left. + 2E_0 R_0 - \sum_{i=A}^{N-1} \left(E_i^{j+1} + E_{i+1}^{j+1}\right)\Delta r - E_A^{j+1} \alpha_{j+1} \Delta r \right\} \div \alpha_{j+1} \Delta r$$

where $E_p^{j+1}$ is initially computed from the equation of state.

This determines all the values for the boundary point. Equating the equations (3.5A3) and the equation of state, one obtains the following formula for r(t) at time j+1

$$r^2(j+1) = \frac{I^2(j)}{\left\{(\gamma-1)\left[E_p^{j+1} - \frac{\gamma}{2}\frac{(m_p^{j+1})^2}{\rho_p^{j+1}}\right] - 1\right\}} \qquad (3.5A8)$$

The iteration proceeds by repeating the sequence of calculations for $p_p$, $\rho_p$, $M_p$, $E_p$, $r_p$ using the latest computed values, averaged with the preceding values. It is also possible to avoid the use of the assumption of constant specific entropy. Again use r(j-1) for evaluating $P_p$. Now, only the assumption of constant entropy at the piston, as a first guess for $P_p^j$, is used.

3.5B Indirect Methods for Boundary Computations.

The alternate procedure that was tried was the indirect approach. This method has the advantage of simplified boundary conditions, but requires a compensating amount of computing time for iteration on finding the true boundary.

R(t) is prescribed for $t_o < t < T$, and assuming the piston path is the particle path of the point initially at the piston, one obtains $U_p(t)$ as well. Knowing the variables at the adjacent point A and the piston point P, at some time t, the values of the variables are computed by linear interpolation at some intermediate point C determined by the position R(t+ Δt)
figure 8 as

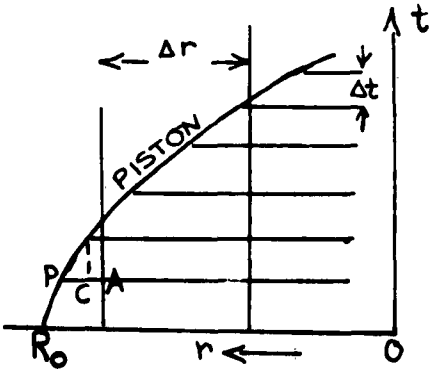


Figure 8

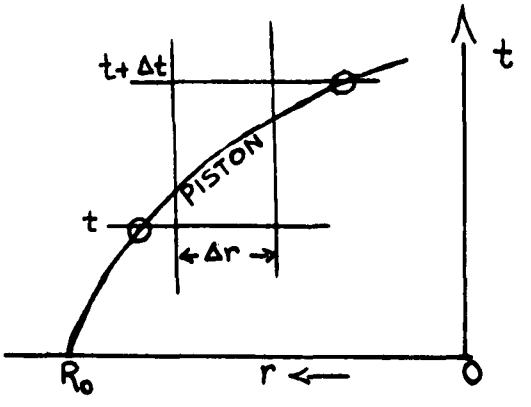


Figure 9

$$U_C = \frac{\Delta r_N U_P + \left\{ r_p(t) - r_p(t+\Delta t) \right\} U_A}{\Delta r_N + \left\{ r_p(t) - r_p(t+\Delta t) \right\}} \qquad (3.5B1)$$

where U is the vector ρ, m, E and $\Delta r_n$ is $\overline{PA}$. Using the unequally spaced difference approximations (3. 4.2) and (3. 4.3), and applying them at the point C gives rise to the following system

$$U_P^{J+1} = -\nabla_i \left\{ F(U_c^j) \right\} \frac{\Delta t}{\Delta r_{N_{J+1}}} \pm \nabla_i^2 (U_c^j) \alpha_{J+1}^2 + U_c^j \qquad (3.5B2)$$

where $F(U_c^j)$ is the vector $m_c^j, \left\{ \frac{p_c^j}{\gamma} + \frac{(m_c^j)^2}{\rho_c^j} \right\}, \left\{ \frac{(p_c^j + E_c^j) m_c^j}{\rho_c^j} \right\}$

and $p_c = (\gamma - 1) \left\{ E_c - \frac{\gamma}{2} \frac{m_c^2}{\rho_c} \right\}$ and for the 2nd component of $U_i^{J+1}$ the prescribed value of $U_p$ is used to compute $m_P^{J+1}$, $m_P^{J+1} = \rho_P^{J+1} u_P^{J+1}$. Having computed $\rho_p$, $m_p$, $E_p$ the value $P_p$ is computed again from the ideal gas law.

Since the equations for unequally spaced intervals may blow up as $\Delta r_{N_{J+1}} \to 0$ a Lagrangean interpolation is performed to compute the adjacent point when $\Delta r_N < \epsilon \Delta r$ . This has the tendency to greatly stabilize the unequally spaced difference approximations. This feature was not incorporated in the direct approach, though it is now being introduced.

In the case, as shown in figure 9 where R(t) may pass through several points for one time step, two features have been adopted. If only one point is passed, the newly computed adjacent point is omitted. If more than one point is passed, a refinement of the mesh spacing is performed by modifying $\Delta t$.

This explicitly defined numerical scheme can now continue to the next time step and so on to T. Since the magnetic pressure has been defined for all t, comparing the computed pressure on R(t) with the prescribed pressure enables one to fit the solution by modifying R(t).

Using the results obtained from the snowplow model as the first approximation for R(t), and then interpolating at certain intervals to obtain the necessary agreements on the prescribed pressure, leads to improved approximations for the desired solutions.

A much more exact procedure for determining the initial piston motion when the piston is driven by the magnetic pressure is by using the method of characteristics prior to formation of a shock wave.

When this is done for a linear current relationship (since the shock form is an extremely short period of time) it is found that the piston velocity varies as $t^2$; $u_p(t) = at^2$, where $a = (2c_o/\gamma)\ \mu i_o^2 / 16\pi^2 R_o^2 P_o$. The shock first forms at a time $t_s = \sqrt{\frac{2c_o}{a}}\ f(\gamma)$ at a distance from the outside radius $X_s = 2c_o \sqrt{\frac{2c_o}{a}}\ g(\gamma)$. From characteristic theory, therefore, the distribution of velocity, pressure, and density in the fluid between the piston and the point of formation of the shock can be readily derived. This enables one to have a more precise numerical procedure around small times.

Figures 10, 11, 12 show some of the numerical results that have been obtained using these approximation schemes.

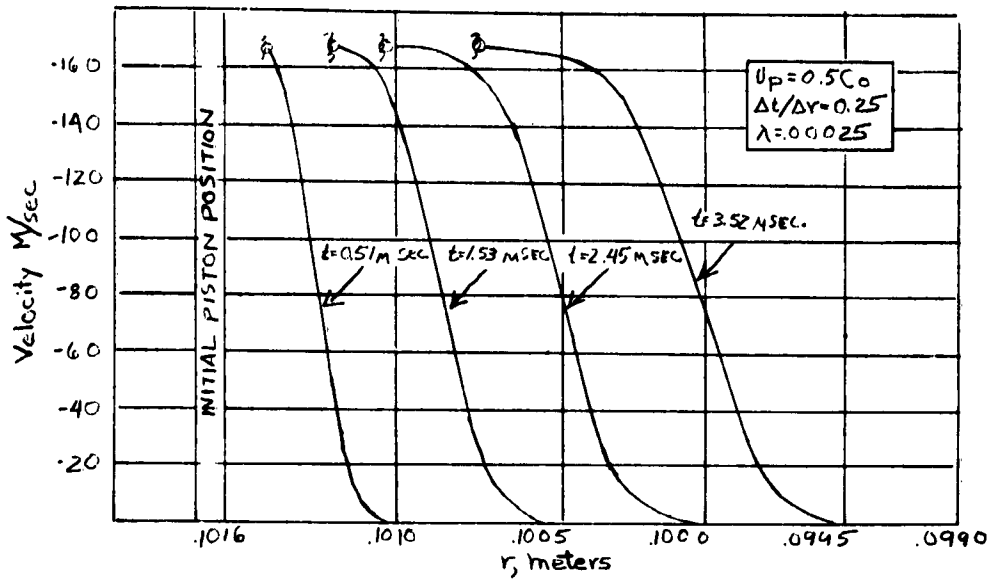


VELOCITY DISTRIBUTION FOR CONSTANT PISTON VELOCITY

**Figure 10**

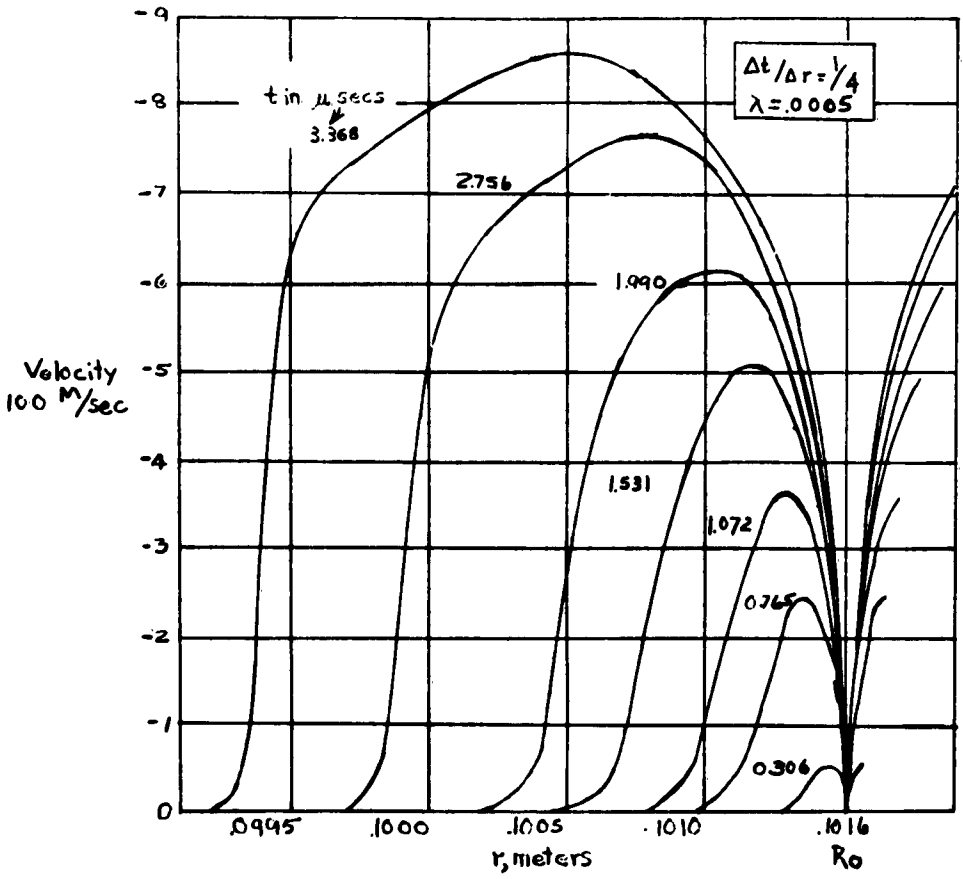


VELOCITY DIST.N FOR PRESSURE SOURCE $\propto I^2$ ($\lambda = .0005$)

**Figure 11**

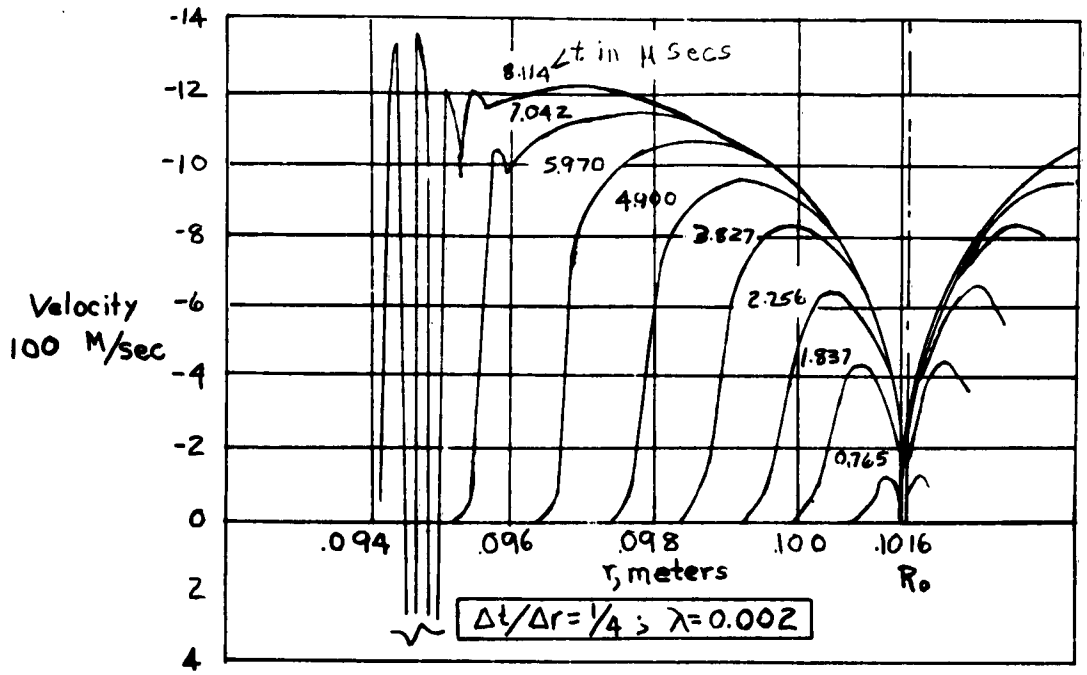


VELOCITY DIST'N FOR PRESSURE SOURCE $\propto I^2$

($\lambda = .002$)

Figure 12

## REFERENCES


1. Chu, B. T., Analytical Approach to Problem of Pinch Dynamics, RAC report, PPL-TR-60-9(185), November 1960
2. Lax, P., Weak Solution of Non-Linear Hyperbolic Equations and Their Numerical Computation, Transactions of Symposia in Applied Mathematics (Vol i), 1953
3. Killeen, Gibson and Colgate, Boundary Layer Formation in the Pinch, Physics of Fluids, Vol. 3, Number 3, May 1960
4. On the Numerical Integration of a Parabolic Differential Equation Subject to a Moving Boundary Condition," Duke Math Journal, 22. 1955
5. A note on the existence of a solution to a problem of Stefan, Quart. of Applied Math, Vol. 9, 1951
6. A Numerical Procedure for Solving a Class of Nonlinear Stefan problems, RAC Digital Computing Division Report, November 1959
7. Bazer, J., Resolution of an Initial Shear Flow Discontinuity in One-Dimensional Hydromagnetic Flow, Astrophysics Journal, Vol. 128, No. 3, November 1958
8. Ericsen and Bazer, Hydromagnetic Shocks, AFCRC-TN-58-241, Research Report No. MH-8 New York University, Institute of Math Science, January 1958
9. Greifinger and Cole, Similarity Solutions for Cylindrical Magneto-hydrodynamic Shock Waves Produced By a Line Current Which Increases Linearly With Time, RAND Corporation, November 1960
10. Richtmeyer, Difference Methods for Initial Value Problem, Chapter 10, pg 209, 1957

# EARLY SOLAR EVOLUTION

Dr. Arthur N. Cox
Los Alamos Scientific Laboratory

For a number of years several of us at Los Alamos Scientific Laboratory have been interested in applying to astrophysical problems some of the techniques developed for bomb design. Conditions in stellar interiors are somewhat similar to those in bombs, and in some cases it has proved possible to modify the time-dependent energy and mass flow equations so that they can be applied to stellar structure problems. With the current ban on nuclear bomb testing, we now have effort available to spend on these astrophysical applications.

There is much work to do in the field of stellar structure and stellar evolution; and one of the current interesting problems is an understanding of the complete history of the sun. Our calculations reported here start at a time when probably the solar system was condensing out of material shed from a collapsing cloud of matter. We watch this cloud increase its surface temperature from just a few hundred degrees to the present solar effective temperature close to 6,000°K. Our future work is to be directed to the late evolution of the sun when the increased solar radius and luminosity will make planetary conditions much different than they are now. The results I have today ignore the presence of the planets and the rotation of the sun. Actually our data apply only to the rapid evolution during the first few hundred million years of the solar life.

To study stellar structure it is necessary to consider a large number of physical processes. The equations that describe these phenomena are of three types. Those of the first type in figure 1 give the flux of energy due to radiation, convection, and conduction. The radiation flux is that given when the photons diffuse from one region to another region with only a slightly different temperature. The Rosseland mean absorption coefficient or opacity appears in this radiative flux expression. The other quantities are a, the radiation constant; c, the velocity of light; $\rho$, the density; and T, the temperature which changes in our one-dimensional calculations only in the direction r.

For convective energy transport we use the Prandtl mixing length theory. The flux is proportional to the 1.5 power of the excess of the

existing temperature gradient over the temperature gradient followed by an adiabatically expanding turbulent element. The element persists only for one mixing length L, and the mixing length is taken to be 1.5 times the local scale height. In the flux expression $c_p$ is the constant pressure specific heat; v the turbulent element velocity; $\Gamma$ the specific heat ratio; $\left(\frac{\partial E}{\partial T}\right)_v$ the constant volume specific heat; and g the local acceleration due to gravity.

The conduction equation is the usual one with $\nu$ the conductivity. We note that this equation can be combined with the radiative flux equation if a conductive opacity is properly defined.

The second set of equations given in figure 2 contains the hydrodynamic equations. Our calculations are done in a Lagrangian coordinate system where we follow the motions of mass shells, and it is not necessary to write an equation for the conservation of mass. The conservation of momentum law gives a force equation which indicates the magnitude and direction of the acceleration, $\ddot{r}$, of an interface between two mass shells when the pressure gradient, $\frac{\partial P}{\partial r}$, and local gravity are not balanced. The Navier-Stokes hydrodynamics equations also include the conservation of energy equation where Q is the heat put into a shell by the flux equations or by energy production.

The equations just described which govern the flow of energy and matter contain a large number of variables, but through various relations one can reduce the independent variables for a mass point of fixed composition to only the temperature and density. These required relations are the pressure and energy equations of state, the opacity law, and energy production formulas all of which depend on the composition of the matter, the temperature, and the density. These relations are given in figure 3. Here b' is the gas constant which includes electron degeneracy, and $E_I$ and $E_{EX}$ are the ionization and excitation energies. Radiation pressure and energy have been included.

To illustrate some of these relations, there are shown in figure 4 pressure data for a mixture of 0.744 by mass of H, .236 by mass of He, and .02 by mass of heavier elements distributed as given on the diagrams. If the electrons are nondegenerate (nuclei are always nondegenerate) then

$$b' = b = \frac{R}{\mu}$$

and the pressure equation of state is obtained only from the state of ionization

of the mixture. At low densities the b has a plateau around a kT of a few volts because of the complete ionization of hydrogen and HeI. At higher temperatures the helium and other rarer elements are ionized to produce more particles for pressure.

In figure 5 the ionization energy of this mixture for various temperatures and densities is given. Again, steps occur in the variation with temperature with constant density, because of the successive ionization of the important elements in the mixture.

Finally in figure 6 we show the opacity of the material at various temperatures and densities. A much more detailed table of opacities than shown has actually been used, and the table has been inserted in the machine during the computation. Enough points are included so that linear interpolation for log K versus log T and log $\rho$ is accurate to 10 percent. Simple fits have never proved very accurate over reasonable ranges of temperature and density.

The total solar mass is divided into 30 spherical shells of approximately equal thickness but not of equal mass. The thickness of these shells now is allowed to vary as the usual time integration of the energy and matter flow requires. Independent variables for a shell of fixed mass are composition, temperature, and density. The boundaries between the shells will take positions such that the net force at an interface is zero.

From a starting array of mass, composition, temperature, density, position, etc. for each mass shell, the flux equations and the force equation can be evaluated to give net energy flow in the time step $\Delta t$ and the net motion in time $\Delta t$. There is also to be considered the thermonuclear energy production in the time step. The energy equation of state and the conservation of energy equation can be used to evaluate the temperature changes in the individual mass shells. Likewise the new positions of the interfaces determine the new densities in the shells. Any composition change can also be noted, and in some cases this may change the opacity law and equation of state somewhat. The variable now can all be advanced to be ready for the next time step.

After some difficulty with the hydrodynamics as described above, we have converted to a method which places the interfaces in hydrostatic balance at the end of each time step. Thus when going from time n to time n + 1 with

a step of $\Delta t$,

$$\ddot{r}_i^{n+1} = \ddot{r}_i^{n} + \sum_{j=i-1}^{i+1} \frac{\partial \ddot{r}_i}{\partial r_j} \Delta r_j + \sum_{j=i-1/2}^{i+1/2} \frac{\partial \ddot{r}_i}{\partial T_j} \Delta T_j = 0$$

where $\ddot{r}_i^n$ for interface i is obtained from the conservation of momentum equation, and the partial derivatives are rather elaborate analytic expressions. Solution for the $\Delta r$ and $\Delta T$ values are made by an implicit method coupled with the usual implicit method of computing radiation flow. Never do motions in stellar interiors get so rapid that this assumption of constant perfect balance is invalid.

There is another violation of the fundamental equations that we make, and that is in the equation for the convective flux. The convection is so efficient that a very slight excess of the existing temperature gradient over the adiabatic gradient can carry all the energy required. Spurious fluctuations due to the integration procedure can then cause very large excursions in the convective flux. Thus, we divide the convective flux by a large factor so that to carry the flux required of it, convection makes the existing temperature gradient somewhat steeper than the adiabat. This steeper temperature gradient only slightly affects the structure of the star. There is more room for small integration errors with this steeper gradient, and wild fluctuations are largely eliminated.

The results I show today are all in the May 1961 issue of Sky and Telescope. For the details one should consult this article.

By manipulation of methods previously developed and by the addition of a few new features, we have a machine code capable of doing this early evolution of stars with both more and less mass than the sun. The later evolution of stars is another current problem which is also being studied by these time dependent methods.

$$F_R = - \frac{ac}{3K_R\rho} \frac{dT^4}{dr}$$

$$F_{CONV} = c_p(\Delta\nabla T) \frac{L}{2} \rho v$$

$$= \Gamma\left(\frac{\partial E}{\partial T}\right)_V \rho(\Delta\nabla T)^{3/2} \left(\frac{g}{T}\right)^{1/2} \frac{L^2}{4}$$

$$F_{COND} = - \nu \frac{dT}{dr} = - \frac{ac}{3K_{COND}\rho} \frac{dT^4}{dr}$$

Figure 1

$$\frac{dQ}{dt} = \left(\frac{\partial E}{\partial T}\right)_V \frac{dT}{dt} + \left(\frac{\partial E}{\partial V}\right)_T \frac{dV}{dt} + P \frac{dV}{dt}$$

$$\rho r = -\frac{\partial p}{\partial r} - \rho g$$

Figure 2

$$P = b'(\rho,T)\,\rho T + \frac{a}{3} T^4$$

$$E(\rho,T) = E_I(\rho,T) + E_{EX}(\rho,T) + \frac{3}{2} b'T + \frac{aT^4}{\rho}$$

$$K(\rho,T)$$

$$\epsilon(\rho,T)$$

Figure 3

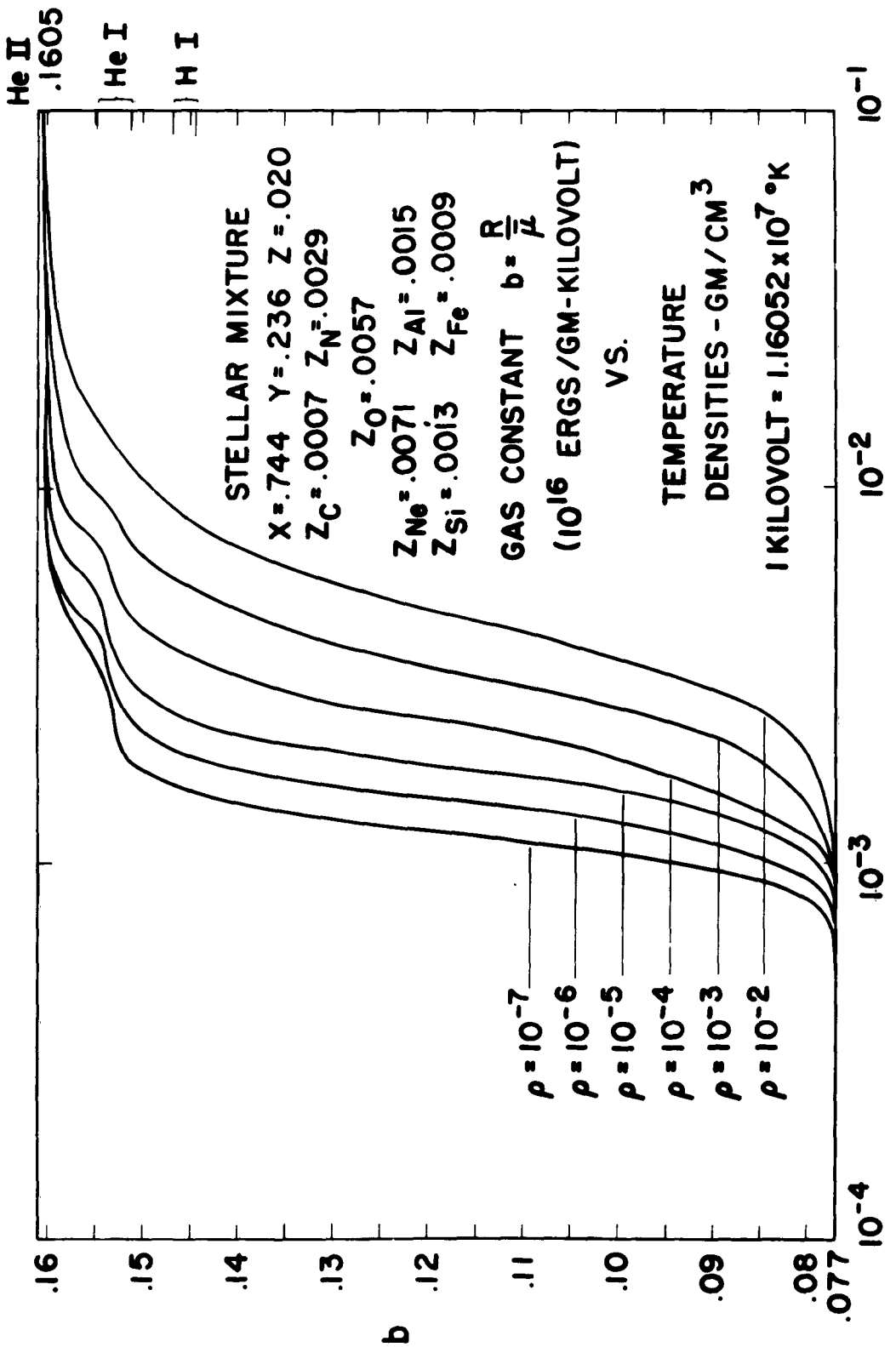
He II
.1605
He I
H I
STELLAR MIXTURE
X=.744 Y=.236 Z=.020
$Z_C$=.0007 $Z_N$=.0029
$Z_O$=.0057
$Z_{Ne}$=.0071 $Z_{Al}$=.0015
$Z_{Si}$=.0013 $Z_{Fe}$=.0009
GAS CONSTANT b = $\frac{R}{\mu}$
($10^{16}$ ERGS/GM-KILOVOLT)
VS.
TEMPERATURE
DENSITIES - GM/CM$^3$
1 KILOVOLT = 1.16052x$10^7$ °K
$\rho = 10^{-7}$
$\rho = 10^{-6}$
$\rho = 10^{-5}$
$\rho = 10^{-4}$
$\rho = 10^{-3}$
$\rho = 10^{-2}$
b
.16
.15
.14
.13
.12
.11
.10
.09
.08
.077
$10^{-4}$
$10^{-3}$
$10^{-2}$
$10^{-1}$
θ(KILOVOLTS)

Figure 4

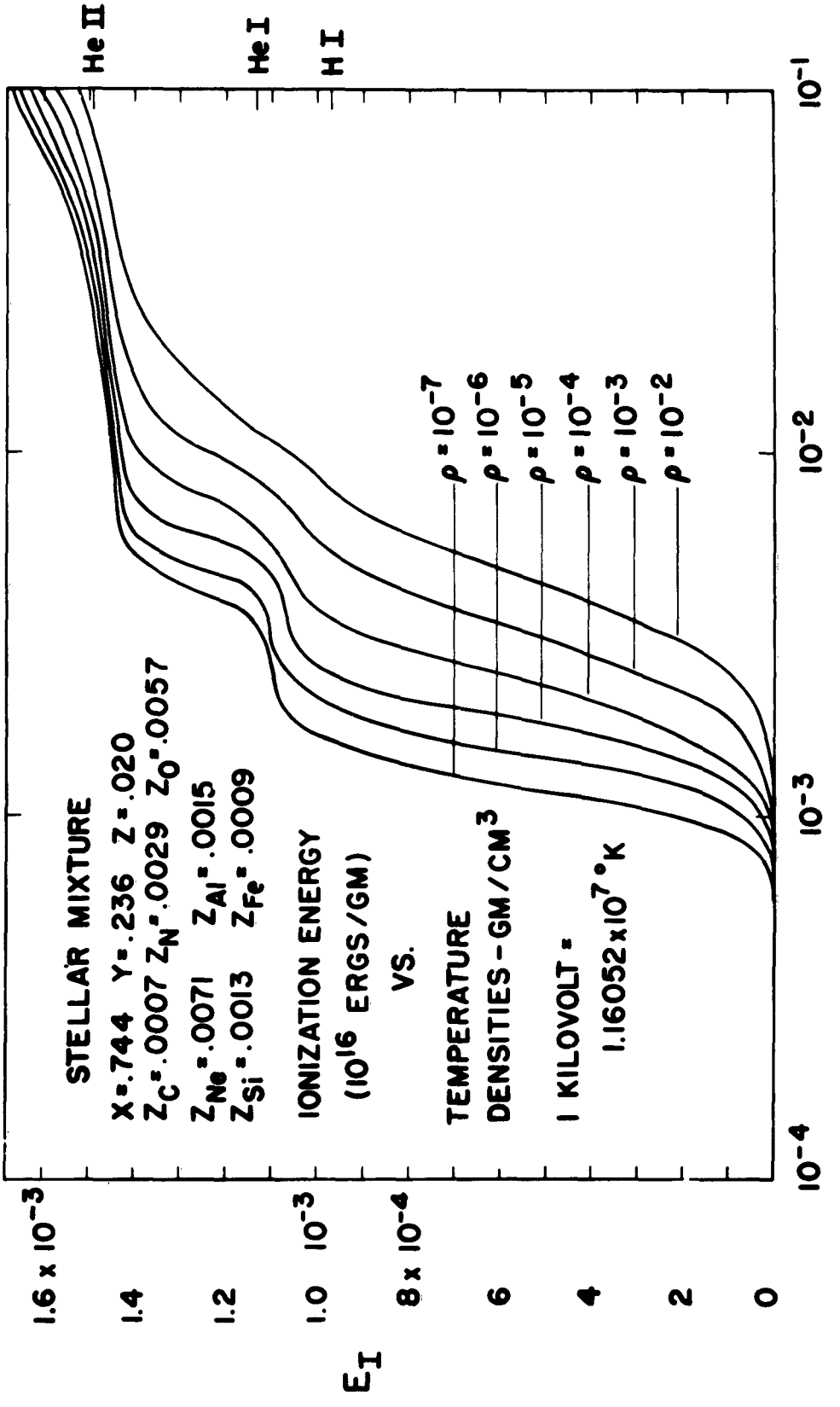
He II
He I
H I
STELLAR MIXTURE
X=.744 Y=.236 Z=.020
$Z_C$=.0007 $Z_N$=.0029 $Z_O$=.0057
$Z_{Ne}$=.0071 $Z_{Al}$=.0015
$Z_{Si}$=.0013 $Z_{Fe}$=.0009
IONIZATION ENERGY
($10^{16}$ ERGS/GM)
VS.
TEMPERATURE
DENSITIES - GM/CM$^3$
1 KILOVOLT =
1.16052x10$^7$ °K
$\rho = 10^{-7}$
$\rho = 10^{-6}$
$\rho = 10^{-5}$
$\rho = 10^{-4}$
$\rho = 10^{-3}$
$\rho = 10^{-2}$
$E_I$
1.6 x $10^{-3}$
1.4
1.2
1.0 $10^{-3}$
8 x $10^{-4}$
6
4
2
0
$10^{-4}$
$10^{-3}$
$10^{-2}$
$10^{-1}$
θ (KILOVOLTS)

Figure 5

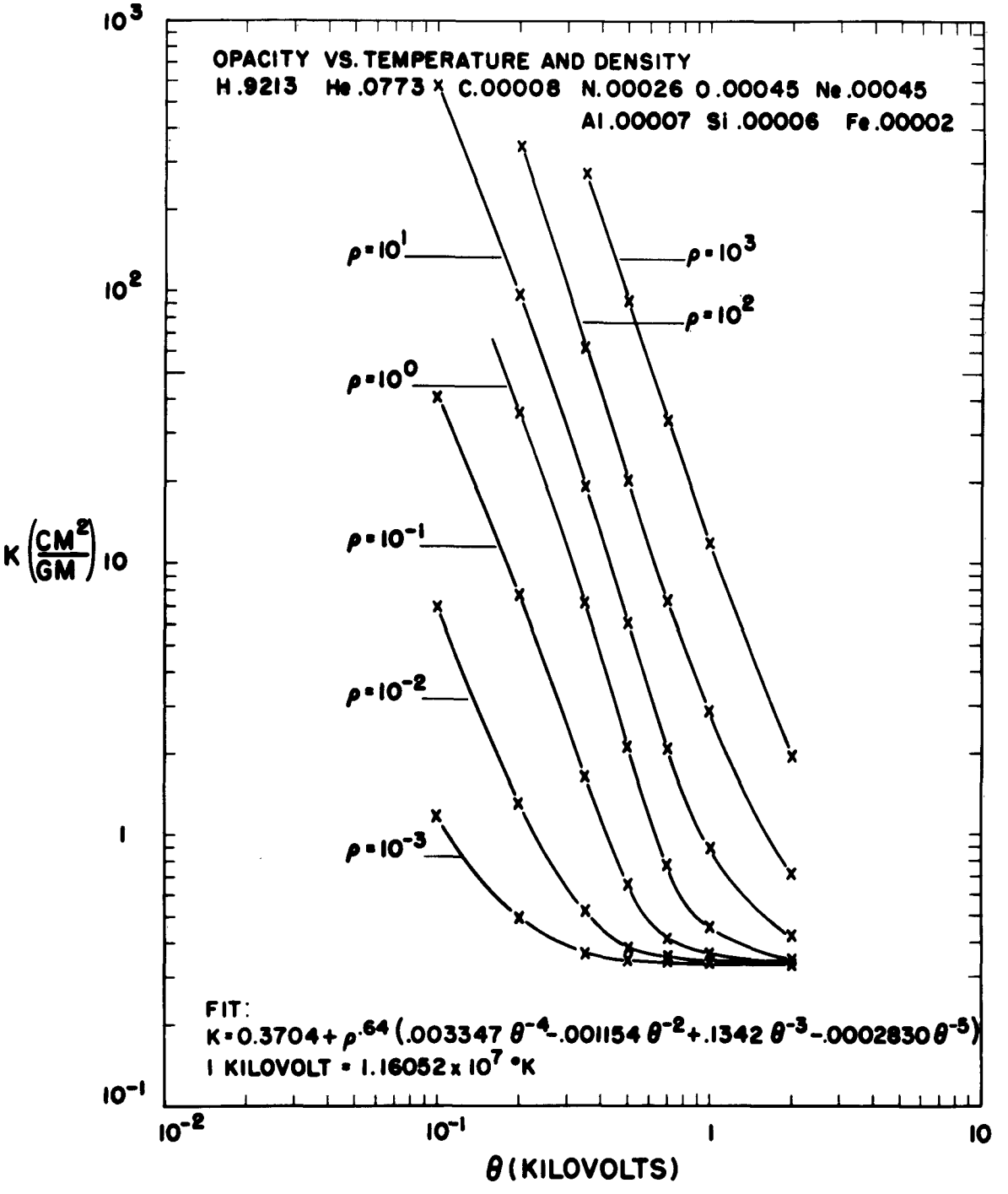
OPACITY VS. TEMPERATURE AND DENSITY
H .9213 He .0773 C.00008 N.00026 O.00045 Ne.00045
Al.00007 Si .00006 Fe.00002
ρ = 10^1
ρ = 10^3
ρ = 10^2
ρ = 10^0
ρ = 10^-1
ρ = 10^-2
ρ = 10^-3
FIT:
K = 0.3704 + ρ^.64 (.003347 θ^-4 - .001154 θ^-2 + .1342 θ^-3 - .0002830 θ^-5)
1 KILOVOLT = 1.16052 x 10^7 °K
K (CM^2/GM)
10^3
10^2
10
1
10^-1
10^-2
10^-1
1
10
θ (KILOVOLTS)

Figure 6

# THE AERONUTRONIC HOP PROGRAM FOR FLUID FLOW

Dr. R. A. Grandy
Aeronutronic Division, Ford Motor Company

The differential equations of hydrodynamics are

$$\frac{d\vec{q}}{dt} + \frac{1}{\rho}\nabla P = 0 \qquad \text{(The momentum equation)} \qquad (1)$$

$$\frac{d\rho}{dt} + \rho\nabla\cdot\vec{q} = 0 \qquad \text{(The continuity equation)} \qquad (2)$$

$$\frac{de}{dt} + P\frac{dV}{dt} = 0 \qquad \text{(The energy equation)} \qquad (3)$$

$$\frac{d\vec{r}}{dt} = \vec{q} \qquad \text{(The transformation equation)} \qquad (4)$$

$$P = F(\rho, s) = g(\rho, e) \qquad \text{(The equation of state)} \qquad (5)$$

In the above $\vec{q}$ is the flow velocity, $\rho$ the density, P the hydrodynamic pressure, $V = 1/\rho$ the specific volume, S the entropy, e the energy density per unit mass, and $\vec{r} = \hat{i}x + \hat{j}y + \hat{k}z$ is the Eulerian radius vector defining the location of an element of the fluid. We may also write $\vec{q} = \hat{i}u + \hat{j}v + \hat{k}w$.

Equations (1) to (5) are called the Lagrange equations of hydrodynamics. In this scheme, x, y, and z are considered functions of the fluid element in question.

Finite difference methods for the hydro equations break both the space and time continuum into finite intervals.[1] The hydrodynamic variables are sampled at various points in space and at various times. Let us restrict attention to one-dimensional flows for purposes of illustration. In this case a one-dimentional spatial mesh is sufficient to define the problem. The above equations, for example, are most commonly differenced in the form:

$$U_j^{n+1/2} = U_j^{n-1/2} + \frac{\Delta t^n (P'^n_{j-1/2} - P^n_{j+1/2})}{(\rho \Delta x)^n_j} \qquad \text{(momentum)} \quad (1')$$

$$\rho_{j-1/2}^{n+1}\left[(X_j^{n+1})^{\alpha+1}-(X_{j-1}^{n+1})^{\alpha+1}\right]=\rho_{j-1/2}^{o}\left[(X_j^{o})^{\alpha+1}-(X_j^{o})^{\alpha+1}\right]$$

(continuity) (2')

$$e_{j-1/2}^{n+1}=e_{j-1/2}^{n}-\tfrac{1}{2}(P_{J-1/2}^{n}+P_{j-1/2}^{n+1})(V_{j-1/2}^{n+1}-V_{j-1/2}^{n})$$

(energy) (3')

$$X_j^{n+1}=X_j^{n}+U_j^{n+1/2}\Delta t^{n+1/2}$$

(transformation) (4')

$$P_{j-1/2}^{n+1}=g(\rho_{j-1/2}^{n+1},\ e_{j-1/2}^{n+1})$$

(equation of state) (5')

The superscripts n and subscripts j represent the temporal and spatial mesh points under consideration respectively. Time centering of the above equations has been achieved by defining the velocity and coordinate of a mesh point a half cycle apart in time. The superscript $\alpha$ equals 0, 1, or 2 for slab, cylindrical, or spherical symmetry. These difference equations are well known and, with minor modifications, are used by the AFSWC in their SHARP program and by Aeronutronic in our HOP code. The equations used include an additional term in the pressure, the von Neumann-Richtmyer Q, to allow the equations to treat shocks, but the presence of this term unnecessarily complicates an illustrative discussion.

The conditional stability of finite difference approximations to linear partial differential equations is well known, having first been discussed by Courant, Friedrichs, and Lewy in 1928.[2] A mathematically rigorous analysis of the stability of nonlinear equations has never been realized, although nonrigorous stability criteria have been established which work in practice. It is found that as $\Delta x$, the mesh size, and $\Delta t$, the time interval, separately approach zero in the finite difference equations, the solution of the difference equations does not necessarily uniformly approach the solution of the differential equations. In most cases there must be a functional relation maintained between $\Delta x$ and $\Delta t$ as they approach zero. Normally, it is found that $\Delta t$ must be less than some function of $\Delta x$: $\Delta t \leq f(\alpha_i, \Delta x)$, where $\alpha_i$ represents parameters appearing in the differential equations.

In our example, the condition is that $\Delta t \leq \frac{\Delta x}{c}$, where $c^2 \equiv \left.\frac{\partial P}{\partial \rho}\right|_s$ is the local sound speed.

The normal procedure in solving the finite difference equations is to compute the quantity $f(\alpha_i, \Delta x)$ for every zone of the mesh, and, at the end of a time cycle, to use the smallest of these quantities as a time interval for the next time cycle. It is quite common for f to vary widely over the mesh, either because $\alpha_i$ varies or because of $\Delta x$. In our case, the sound speed might be much higher in some part of the mesh, or the spatial interval might be markedly decreased to give better spatial resolution in a particular region. It is normally necessary, in these cases, to calculate in the main part of the mesh with a $\Delta t$ much smaller than required locally for either stability or accuracy, and this can greatly increase the computing time required for a problem. Several distinct approaches can be made to this problem: (1) The stability condition can be relaxed. A different difference scheme permitting a larger $\Delta t$ or perhaps even $\Delta x$ can be used. (2) The spatial mesh can be varied during the course of the calculation to minimize fluctuations in the time interval. (3) The local time interval can be used in advancing the spatial mesh.

In the case of linear equations, unconditionally stable finite difference schemes can be found for most differential equations if implicit schemes are considered. Comparatively simple implicit schemes can also be obtained for both Euler and Lagrage hydrodynamic schemes which are unconditionally stable according to the usual first-order stability analyses. Unconditionally stable schemes, however, do not remove all restrictions on $\Delta t$, the time interval. They allow it to be chosen solely on the basis of accuracy. Nonlinear equations like those of hydrodynamics often permit the development of discontinuities: for example, hydrodynamic shocks. Contact discontinuities can also occur, even in linear equations. Normally, the difference equations and spatial mesh are chosen so that these discontinuities are spread over two or three zones, or a real distance which is as large as can be tolerated for the definition desired in the problem. Let us follow Richtmyer's terminology[1] and write our differential equation as $\frac{du}{dt} = Au$. Most difference schemes are based on integrating this in the form

$$U_j^{n+1} = U_j^n + \int_n^{n+1} (Au)\, dt.$$

In a simple, explicit, forward-time-centered scheme, the integral is approximated by $(Au)_j^n \Delta t$, where we have said nothing about the space centering. An implicit scheme normally approximates the integral by $(Au)_j^{n+1} \Delta t$ (backward time differencing) or by $\frac{1}{2} \left[ (Au)_j^n + (Au)_j^{n+1} \right] \Delta t$ (centered time differencing), and, if the spatial differencing is done properly, unconditionally stable difference equations will usually result. In most of our problems, Au represents spatial derivatives of u. As discontinuities travel through the mesh, these derivatives, taken at a point in the mesh, run from infinitesimal value through finite value back to infinitesimal value as the variable goes from its initial to final value. That is, $(Au)_j^o = (Au)_j = 0$. We may plot $(Au)_j$ as a function of time:

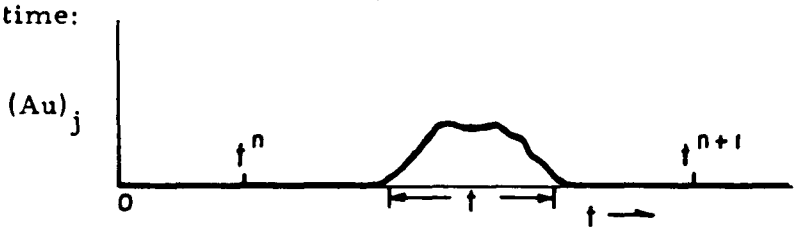


$\tau$ is on the order of two or three times $\Delta x/s$, where s is the propagation velocity of the discontinuity.

If the time interval is large compared to $\tau$ we can easily make a large error in the integration with any reasonable difference scheme. If $t^n$ and $t^{n+1}$ are as shown, any of the three schemes mentioned will give a zero value for the integral. For any degree of accuracy at all, the time interval must be less than $\tau$, i.e. about 1 $(\frac{\Delta x}{s})$.

In many cases, simpler explicit conditionally stable difference schemes will permit a comparable $\Delta t$, so that the more complex implicit schemes will not necessarily permit an appreciable reduction in computing time. Generally, the time interval in an implicit scheme might be expected to be determined by that region of the problem where quantities are rapidly varying, for example, in the vicinity of a shock front. The requirement may be that $\Delta t \leq h(\alpha_i, \Delta x)_j$ where j is a point in the shock region. An implicit scheme can be very valuable in cases where h has a reasonable value for most of the problem. That is, even if a small portion of the mesh is finely zoned for better detail, this portion of the mesh will only affect the time interval when a shock passes through it. Otherwise, it is not artificially slowing the computing merely to keep stability in its vicinity. Another approach which has been exploited in

solving other types of initial value problems, like diffusion problems, is the use of higher order schemes in the spatial differencing for the purpose of increasing the spatial interval necessary for a given desired definition. Such schemes have been used occasionally in hydrodynamics to reduce truncation errors in cases where the mesh size changes rapidly over the mesh, but have not been seriously exploited in the above sense.

There are many problems of interest where an explicit, conditionally stable scheme will have a local time interval which varies widely over the mesh and where the time interval required for accuracy in an unconditionally stable scheme will always be smaller than desired. In purely hydrodynamic problems, it has been found to be very profitable to use the local time interval in advancing the spatial mesh. The following logical scheme permits each zone of the mesh to have its own time interval, and advances the time by an arbitrary amount per machine cycle.

At the beginning of a cycle, all points of the mesh exist at the same time. Generally, after a further sweep through the mesh, the points will exist at different times. A point is not accelerated if any of its neighbors have not yet been advanced as far in time as the point in question. If, however, the point is at a time less than or equal to that of all neighbors, it is accelerated. The neighbors are relocated temporally by interpolation to the time of the point in question. Hydrodynamic quantities are calculated at the time of the point and the point is moved using as a time interval the smallest of the neighboring intervals.

Various special cases may arise. If any of the neighbors is to be accelerated at the same time as the point, the interpolation routine is redundant and is bypassed for that point. If the time interval is such as to advance the point beyond the end of cycle time, it is adjusted to just reach this time. No zone is allowed a time interval greater than the cycle time interval. This allows inactive points or points with a large natural time interval to be advanced to the end of cycle time in one sweep. If any of the neighbors (of a point which has been advanced to the end of cycle time with the cycle time interval) have not yet been advanced to this time, the inactive point is backed up to the earliest such time and reaccelerated. This test automatically activates points when a disturbance reaches them.

The above scheme has been applied to the Lagrange difference equations for one- and two-dimensional flow. We shall briefly describe the Aeronutronic HOP program for one-dimensional flow. This program was originally developed for use on Bureau of Ordnance contract NOrd 17945, concerning the detonability of propellants.

The HOP program is best explained by reference to the flow chart. (Figure 1.) Location I is the entry point to begin a macro cycle. Part of the left hand boundary conditions are set, registers are initialized, and the program proceeds to A. At A, the time at which the coordinates of point j exist is compared with the time for point j + 1. If $t_j > t_{j+1}$, the program exits to make an activity test at location M. If $t_j \leq t_{j+1}$, it proceeds to accelerate the point unless it is already at the end of cycle time, in which case another activity test is made. If $t_j < t_{j+1}$, $x_{j+1}$ is recomputed at the time of point j under the assumption that j+1 was accelerated with a constant acceleration. If $t_j = t_{j+1}$, this interpolation is bypassed and we proceed directly to calculate hydrodynamic quantities for zone j+½ at the time of the point j. If $t_j = t_{j+1}$, and if it turns out that we may also accelerate point j+1 during the same sweep, we will not need to calculate hydrodynamic quantities for the left hand zone when doing j+1. Sense light 1 is turned on to inform the program that this is so.

Location C is the exit from calculating hydrodynamic data for zone j+½. At this point, sense light 2 is checked. If it is on, it means that hydrodynamic data for zone j-½ at time j already exists. If it is off, $t_j$ is compared with $t_{j-1}$, and in either case hydrodynamic data are calculated for zone j-½. Location D is the exit from the hydrodynamic calculations for zone j-½. The program transfers directly to D if sense light 2 is on. At D, the smallest of the two time intervals $\Delta t_{j+1/2}$ and the cycle interval $\Delta t_c$ is chosen as the time interval for the point j. The time is advanced and checked against $t^{N+1}$. If the new time is less than the end of cycle time, sense light 3 is turned on as an indication that at least one point has not yet been advanced to the end of cycle time. The point is then accelerated and a new velocity and coordinate are calculated.

Sense light 1 is on if the old $t_j = t_{j+1}$. In this case, sense light 2 is turned on and the program transfers to B where it proceeds to process the next point. If sense light 1 is off, $t_j$ was less than $t_{j+1}$ and normally the pro-

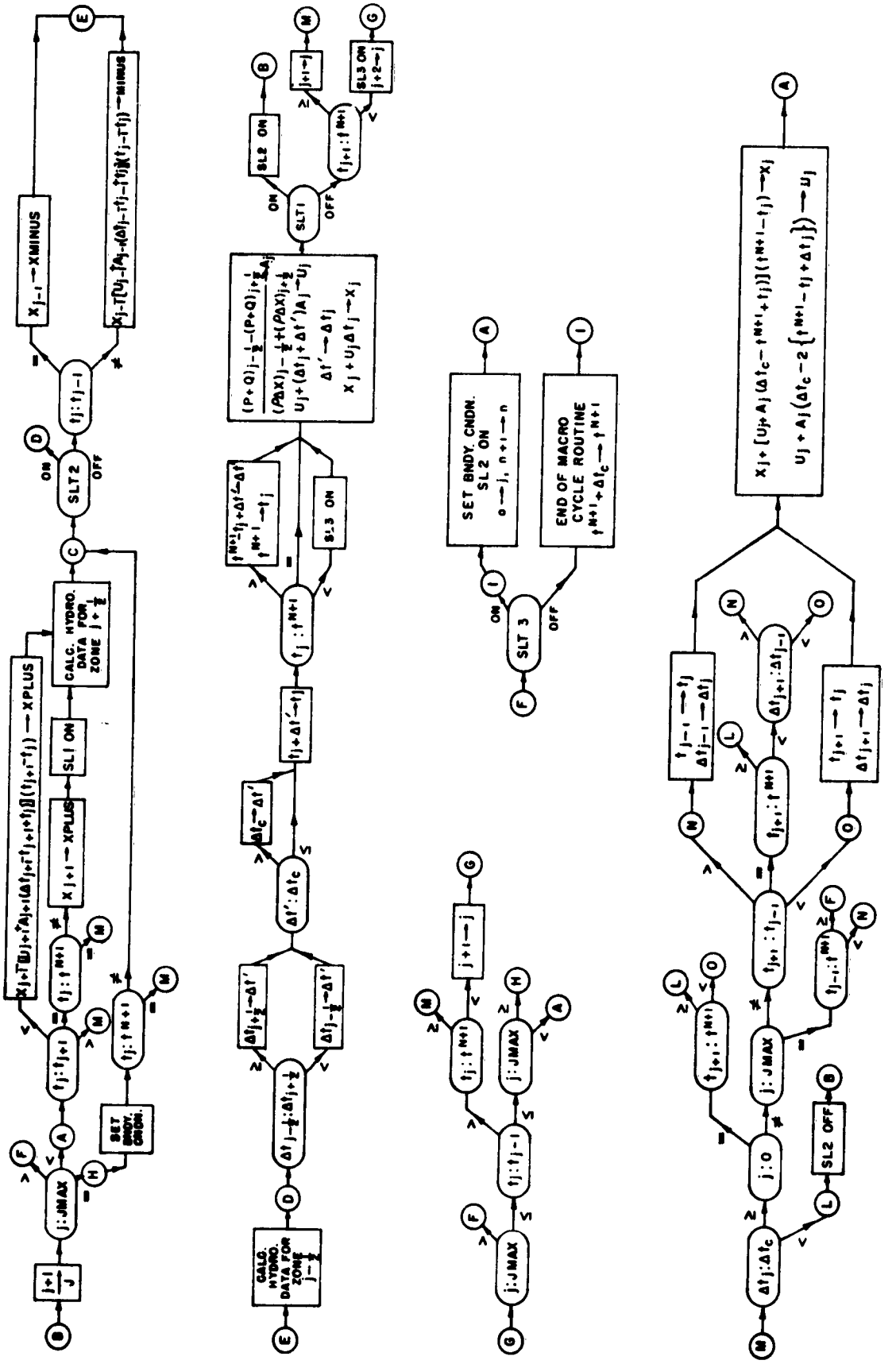
SET BNDY. CNDN. SL2 ON
o → j, n+1 → n
END OF MACRO CYCLE ROUTINE
SLT 3
ON
OFF
SLT1
SLT2
SL1 ON
SL2 ON
SL3 ON
SL2 OFF
CALC. HYDRO. DATA FOR ZONE j+½
CALC. HYDRO. DATA FOR ZONE j-½
SET BNDY. CNDN.
j:JMAX
XMINUS
XPLUS

Figure 1

gram skips and proceeds to test point j+2 unless $t_{j+1} = t^{N+1}$. If this is true, j is stepped by one and control passes to the activity test M. Normally j is stepped by two and the transfer is to location G where j is checked against JMAX. If j > JMAX, the program transfers to F to begin a new sweep through the mesh. If $j \leq$ JMAX, $t_j$ is compared with $t_{j-1}$. If $t_j > t_{j-1}$, it is compared with $t^{N+1}$. If these are equal, the activity test is made. If $t_j < t^{N+1}$, j is stepped by one and the program returns to G. If $t_j \leq t_{j-1}$, the point may be accelerated depending on $t_{j+1}$. If j = JMAX, the program transfers to H where the right-hand boundary conditions are set and an activity test made.

The activity test at location M first compares $\Delta t_j$ against $\Delta t_c$, the cycle interval. If $\Delta t_j < \Delta t_c$, the point has actively reached the end of cycle time and the program proceeds to step j+1 and does the next point. If the two intervals are equal, the program selects the smaller of times $t_{j-1}$ and $t_{j+1}$. If the smaller of these is equal to $t^{N+1}$, the program proceeds to do the next point. Otherwise, the point j is relocated to a time t, where t refers to the smaller of the adjacent times and $\Delta t$ is the corresponding time interval. Point j is then accelerated.

Location F begins a sweep through the mesh. If sense light 3 is on, at least one point is not yet at the end of cycle time and control passes through I. If sense light 3 is off, the entire mesh has been advanced to time $t^{N+1}$. Various end-of-cycle tests are made and the cycle time is stepped. The program then transfers to I to begin a new macro cycle.

One further departure is made from the standard difference equations. Since $P^{n+1} = g(\rho^{n+1}, e^{n+1})$, the time centered energy equation (3') is an implicit equation as $e^{n+1}$ occurs on the right hand side. If P is a linear function of e, which would be the case for a polytropic gas, equation (3') can easily be solved for $e^{n+1}$ and an explicit time centered equation obtained. Even a second order equation has some truncation error. In many problems, the $\int PdV$ must be performed over a change in density of several orders of magnitude, arriving at a final pressure many orders of magnitude less than the original pressure which must be given with an accuracy of at least several percent relative to its final value. It is impossible to get the desired accuracy using equation (3'). For this reason, we use the equation of state in the form $P = f(\rho, S)$. During the adiabatic expansion, S is constant, or at least slowly varying. For a polytropic gas, $P = A(S)\rho^{\gamma}$. This is our starting point

in integrating the energy equation and equation of state. Basically, with corrections for the von Neumann-Richtmyer Q and for other source or sink terms, the pressure equation is written as

$$P^{n+1} = \left(\frac{\rho^{n+1}}{\rho^n}\right)^{\gamma} P^n$$

where $\gamma$ is a slowly varying function of P and $\rho$ which incorporates the degree of ionization of the material.

## REFERENCES

1. Richtmyer, R. D., Difference Methods for Initial Value Problems, Interscience, 1957. (In particular, Chapter X)
2. Courant, R., Friedrichs, K. O., and Lewy, H., Mathematische Annalen, Vol. 100, page 32, (1928)

# SOME COMMENTS ON CONVAIR'S WORK ON NUMERICAL METHODS OF FLUID FLOW PROBLEMS

W. F. Brown
C. G. Davis
D. A. Hamlin
A. H. Schainblatt
Convair, San Diego

## 1. INTRODUCTION.

A discussion of some of the work on Numerical Methods of Fluid Flow Problems that has been carried out by the Physics Section of Convair-San Diego will be given. This discussion will include general philosophy, description of programs, techniques used, and results.

In order to avoid any semantic difficulties, let us state that when we talk about one- or two-dimensional hydrodynamics we mean one space variable and time or two space variables and time, respectively. For all other problems, it will be assumed that they are time independent unless otherwise noted; thus, when we talk about a one-dimensional non-equilibrium flow, we mean a time independent flow in one space variable. The areas which we will cover are one-dimensional and two-dimensional hydrodynamics and plane and axially symmetric non-equilibrium flows.

## 2. GENERAL.

It seems appropriate to give a few general statements of our philosophy regarding machine codes. We attempt a) to prepare our codes so that they are not the personal property of the individual scientists who developed them; b) to use, whenever possible, tested techniques; and c) to write our codes in such a way that they may be generalized but still specific enough to do the job at hand in a reasonable time. Furthermore, whenever possible, analytical and numerical techniques are used in a complimentary way.

Since we will have need of them later, let us now write the hydrodynamic equations in Lagrangian coordinates. In order to do this, we now represent the original Lagrangian coordinates of a fluid element as small $\{x_i\}$, $i = 1, 2, 3$, and the Eulerian coordinates as large $\{X_i\}$, $i = 1, 2, 3$.

The Eulerian coordinates which may be considered as functions $X_i = X_i(x_i, t)$, $i = 1, 2, 3$, give the positions at time t of the fluid elements which

were originally at $x_i$.

Under the above definitions the law of conservation of mass becomes

$$\frac{V}{V_0} = \frac{\partial\{X_i\}}{\partial\{x_i\}} \tag{2.1}$$

where $V = 1/\rho$ is the specific volume of the fluid element. $V_0$ is the original specific volume in the Lagrangian system and $\partial\{X_i\}/\partial\{x_i\}$ is the Jacobian of the transformation $\{x_i\} \longrightarrow \{X_i\}$

We may write the equation of motion as

$$\frac{\partial^2 X_i}{\partial t^2} = -V \frac{\partial P}{\partial x_i} \qquad i = 1,2,3 \tag{2.2}$$

Our basic set of differential equations are completed by the conservation of energy, which may be written as

$$dE = -p\,dv + \bar{S} \tag{2.3}$$

where E is the specific internal energy of the fluid and $\bar{S}$ is a quantity which contains sink as well as source terms.

In order to complete the above set of equations, an equation of state is needed. One may use for this

$$P = P(E,V) \tag{2.4}$$

## 3. ONE-DIMENSIONAL HYDRODYNAMICS.

By specializing the above equations to one space dimension and taking central differences, we obtain the difference form of the one-dimensional hydrodynamic equations when $\bar{S} = 0$.

$$U^{n+1}_{2m+1} = -\frac{\Delta t}{\rho_0 \Delta r}\left[P^n_{2m+2} - P^n_{2m} + q^n_{2m+2} - q^n_{2m}\right] \tag{3.1}$$

$$\left[\frac{R^n_{2m+1}}{r_{2m+1}}\right]^{\alpha-1} + U^n_{2m+1}$$

$$R_{2m+1}^{n+1} = \Delta t\, u_{2m+1}^{n+1} + R_{2m+1}^{n} \tag{3.2}$$

$$V_{2m}^{n+1} = \frac{1}{\rho_0} \frac{\left(R_{2m+1}^{n+1}\right)^{\alpha} - \left(R_{2m-1}^{n+1}\right)^{\alpha}}{\left(r_{2m+1}\right)^{\alpha} - \left(r_{2m-1}\right)^{\alpha}} \tag{3.3}$$

$$E_{2m}^{n+1} = E_{2m}^{n} - \left[\frac{P_{2m}^{n+1} + P_{2m}^{n}}{2} + q_{2m}^{n+1}\right] \left[V_{2m}^{n+1} - V_{2m}^{n}\right] \tag{3.4}$$

$$q_{2m}^{n+1} = \frac{2a^2}{V_{2m}^{n} + V_{2m}^{n+1}} \left(u_{2m+1}^{n+1} - u_{2m-1}^{n+1}\right)$$

$$\text{if } u_{2m-1}^{n+1} > u_{2m+1}^{n+1}$$

$$q_{2m}^{n+1} = 0 \quad \text{if } u_{2m+1}^{n+1} \geq u_{2m-1}^{n+1} \tag{3.5}$$

Here P is the fluid pressure, a is the "shock width constant," R = $X_i$, q is the pseudo-viscosity pressure term and $\alpha$ = 1, 1, 2, for slab, cylinder and sphere respectively. If we now consider the case of an ideal gas, we can write (3.4) as

$$P_{2m}^{n+1} = -\left[\gamma P_{2m}^{n} + (\gamma - 1) q_{2m}^{n}\right] \left[\frac{V_{2m}^{n+1} - V_{2m}^{n}}{V_{2m}^{n}}\right] + P_{2m}^{n} \tag{3.6}$$

Also, for our stability criteria, we have used the White number

$$\omega^2 = \left(\frac{C\Delta t}{\Delta R}\right)^2 + 4a\,\frac{|\Delta V|}{V} \leq 1 \qquad (3.7)$$

where C is the velocity of sound.

Let us now consider a spherical piston expanding into an ambient atmosphere and assume that the flow field external to the piston is represented by the one-dimensional hydrodynamic equations. We will now consider three models for the internal flow field.

The first will take the piston as a thin shell with constant mass and given initial energy. Interior to the mass shell, it will be assumed that P= 0. For this case, the equations governing the motion of the shell, which we represent as a mass point, are given in difference form as

$$U_1^{n+1} = U_1^n - P_2^n \frac{\Delta t}{M}\left(\frac{R_1^n}{r_1}\right)^2 \qquad (3.8)$$

$$R_1^{n+1} = \Delta t\, U_1^{n+1} + R_1^n$$

where $P_2^n$ (the external pressure) is found from the hydrodynamic equations and M is the total mass of the piston.

In the other two models which we have considered to date, an internal structure is assumed for the piston. The flow internal to the piston is considered to have a uniform initial density which is sufficiently low that particle-particle collision can be neglected and an expansion velocity initially given by

$$U = U_0 \frac{R}{R_1}$$

In the first case, it is assumed that the interface is a membrane and the internal particles reflect elastically from the membrane. Under these assumptions, the equation governing the motion of the piston is given by

$$(\lambda\tau)'' \lambda\left(1 - \lambda + \tfrac{1}{3}\lambda^2\right) = \alpha\tau^2(1-\lambda^2) - O\left([\lambda\tau]'''\right) \qquad (3.9)$$

where

$$\zeta = t/t_s$$

$$\lambda = \frac{1}{\zeta}\int_0^{\zeta} f(\eta)\,d\eta$$

$$\alpha = \left(\frac{4\pi}{3}\frac{U_0}{M}t_s^3 P_0\right)\frac{P_2}{P_0} = \alpha_r \frac{P_2}{P_0}$$

$$t_s = \left(\frac{3M\alpha_r}{4\pi P_0 U_0}\right)^{1/3}$$

$$f = 1 - \frac{U_2}{U_0}$$

Here f and $\lambda$ denote the fractional lag in velocity and position, respectively, of the actual interface behind the unretarded interface. and $t_s$ is a scale time.

The other case considered assumes that when a particle hits the interface it sticks to it. In this case, the governing equation becomes

$$(\lambda\zeta)''\lambda\left(1-\lambda+\frac{\lambda^2}{3}\right) = \alpha\zeta^2(1-\lambda)^2 - \zeta(\lambda')^2(1-\lambda)^2 \qquad (3.10)$$

where the variables are defined as before, except that $\alpha_r$ is replaced by $\alpha_s = 6$.

Based on the above equations, a series of codes have been written and a number of cases computed.

The first program solved the case of a spherical piston expanding into a constant ambient atmosphere. In this code, a fixed number of points were maintained in the flow field and only the points which were influenced by the piston motion were calculated. In figure 1, we see the results of some typical calculations. In this figure, the circled points denote calculations made for $\gamma = 5/3$ and triangles for $\gamma = 2$. As is clearly seen, the variation of $\gamma$ has a very small effect on the solution. Other calculations have been made for different initial conditions and the results are similar to those shown in figure 1. Typical pressure and velocity profiles obtained from our machine calculations are shown in figures 2 and 3 respectively.

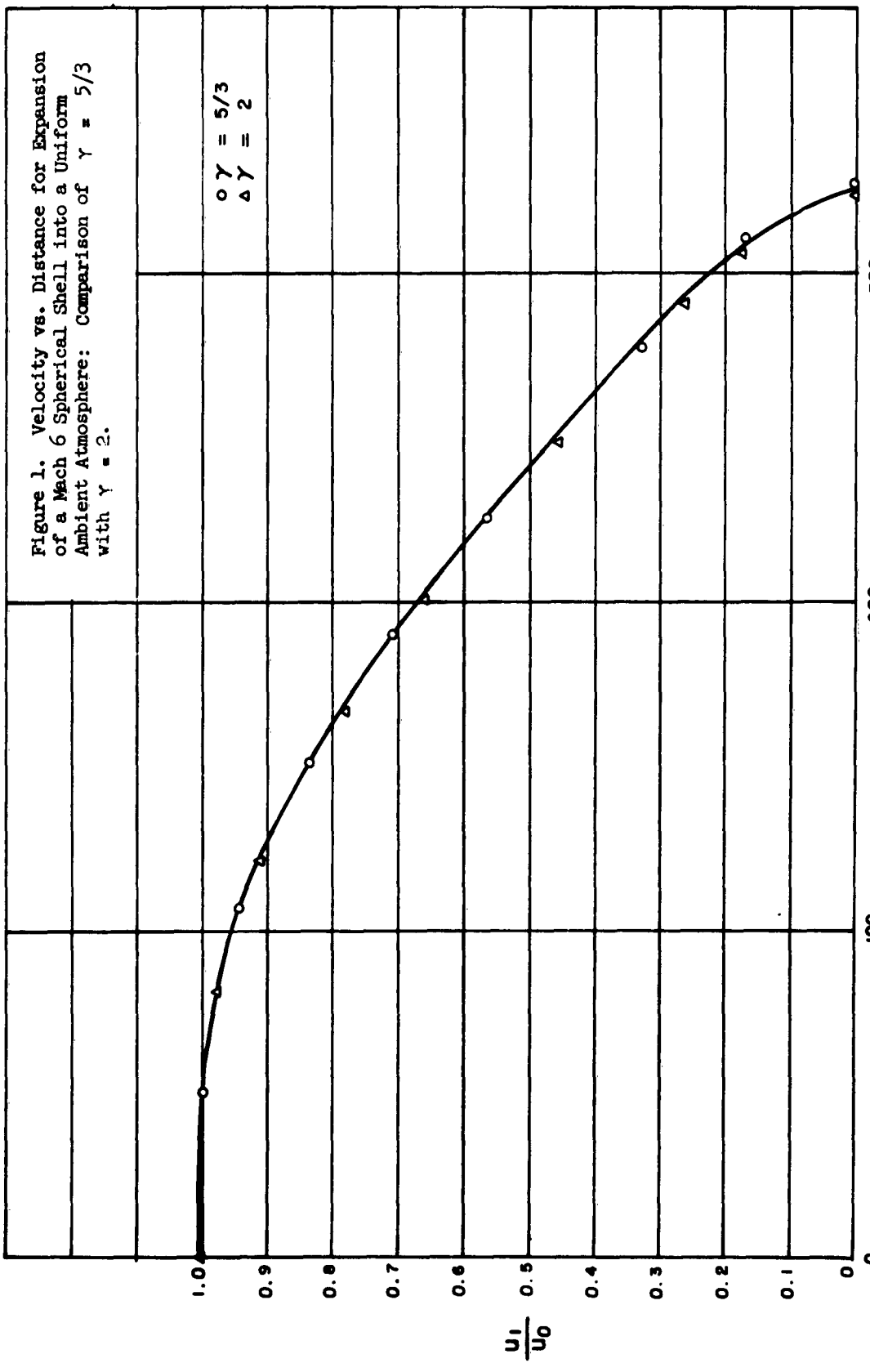
Figure 1. Velocity vs. Distance for Expansion of a Mach 6 Spherical Shell into a Uniform Ambient Atmosphere: Comparison of γ = 5/3 with γ = 2.
o γ = 5/3
Δ γ = 2
1.0
0.9
0.8
0.7
0.6
0.5
0.4
0.3
0.2
0.1
0
$\frac{u_1}{u_0}$
0
100
200
300
R

Figure 1

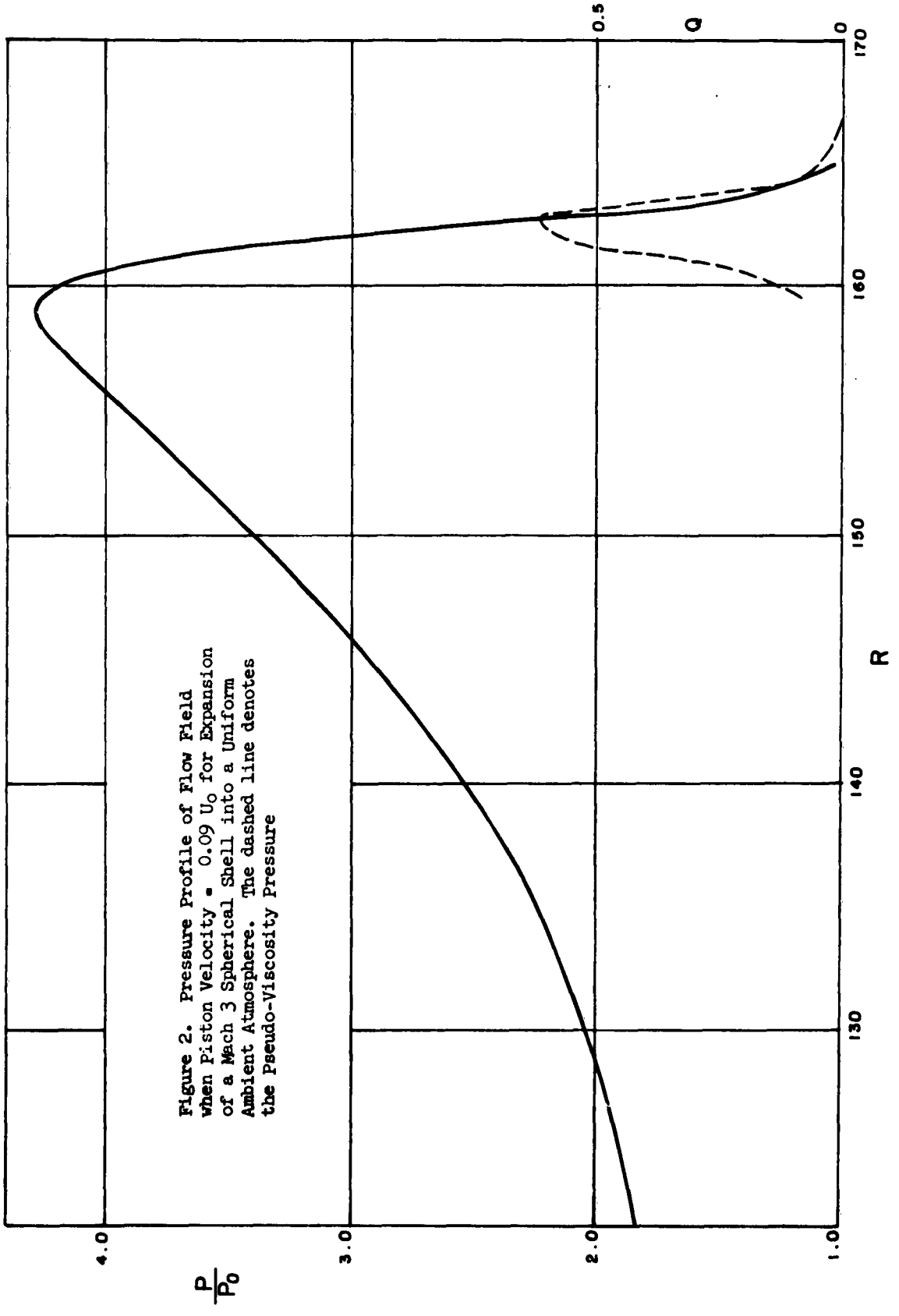


Figure 2. Pressure Profile of Flow Field when Piston Velocity = 0.09 $U_0$ for Expansion of a Mach 3 Spherical Shell into a Uniform Ambient Atmosphere. The dashed line denotes the Pseudo-Viscosity Pressure

Figure 2

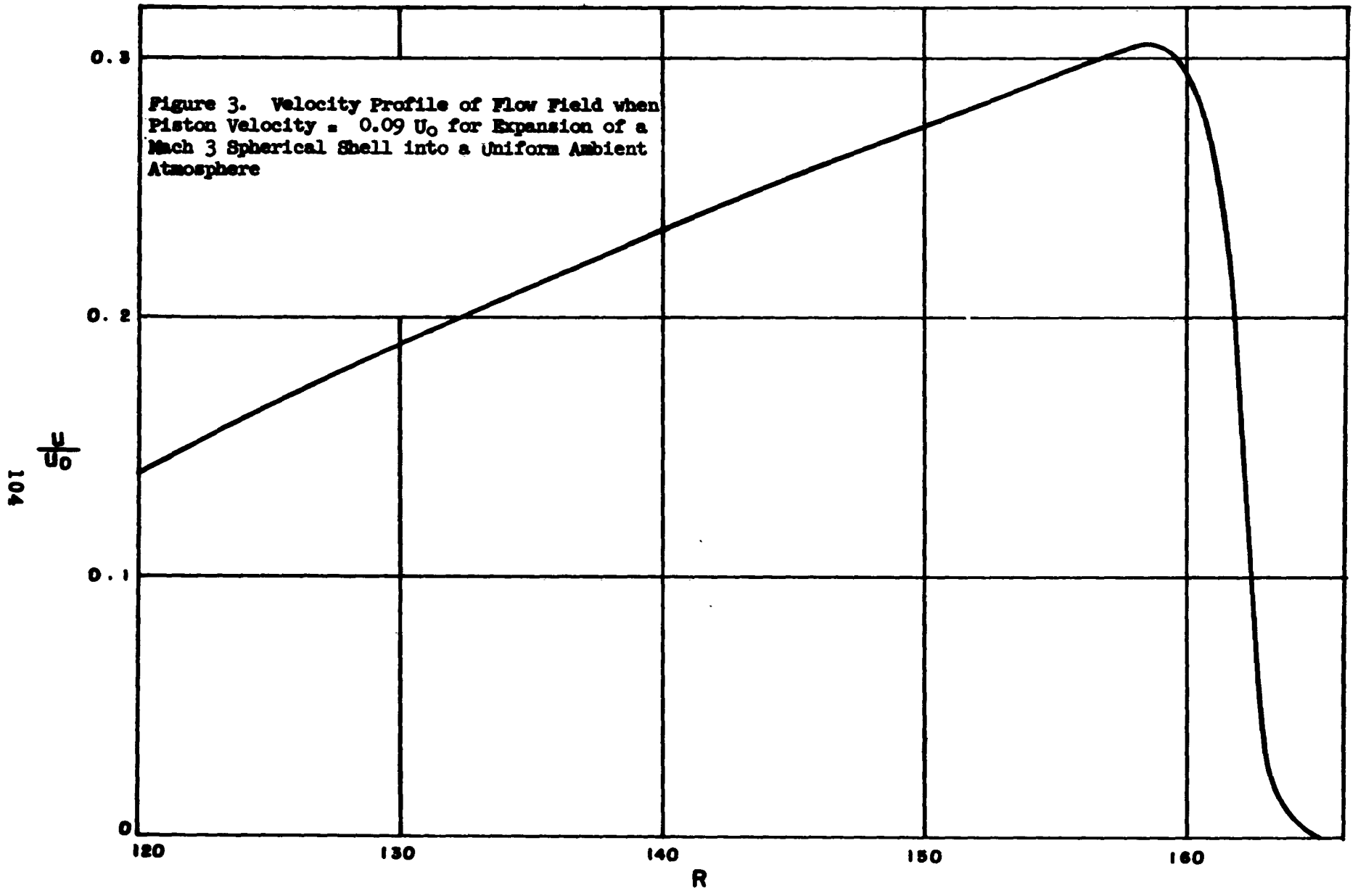


Figure 3. Velocity Profile of Flow Field when Piston Velocity = 0.09 $U_0$ for Expansion of a Mach 3 Spherical Shell into a Uniform Ambient Atmosphere

Figure 3

G. I. Taylor[1] has obtained a solution for a piston expanding with a constant velocity in an ambient atmosphere. From this solution, one can see that over a wide range of velocity we can represent the pressure on the piston in the form

$$\frac{P_2}{P_0} = 1 + \Gamma(\gamma)\left(\frac{u_1}{c}\right)^2 \tag{3.11}$$

where c is the velocity of sound in the ambient medium.

This can also be written as

$$\frac{P_2}{P_0} = 1 + \beta\left(\frac{u_1}{V_0}\right)^2 \tag{3.12}$$

where

$$\beta = \Gamma(\gamma)\left(\frac{V_0}{c}\right)^2$$

To determine $\Gamma(\gamma)$, we make use of numerical results obtained from the expansion of a spherical piston with constant velocity. These results are illustrated in figures 4, 5, 6.

Using this form of the pressure, one can obtain an analytic solution for the motion of the mass shell piston. The results are given in figure 7 and a comparison is made with a hydrodynamic calculation in figure 8.

Because of the applicability of the fitted pressure, it was decided to solve the other two piston models using this form of the pressure, but analytical solutions cannot be obtained as in the case of the shell model, except for the special case of a constant pressure for which a power series solution can be obtained. When the pressure equation (3.12) is substituted into equations (3.9) and (3.10), we have ordinary differential equations for the interface velocity. A program was prepared which integrates these equations and results of typical calculations are given in figure 9. Also, as part of these codes, the partition of energy was calculated and results of a typical case are shown in figure 10, where $E_1$ denotes the streaming energy, $E_2$ is the kinetic energy of the shell in the sticky model, $E_3$ is the heat produced in the shell because of the sticking, and $E_4$ is the work done against the total back pressure; $E_2$ and $E_3$ are not applicable to the reflecting model. For the sticking model, the total energy is clearly conserved to the accuracy of the calculation. The total energy for the reflecting model is very difficult to calculate and has not

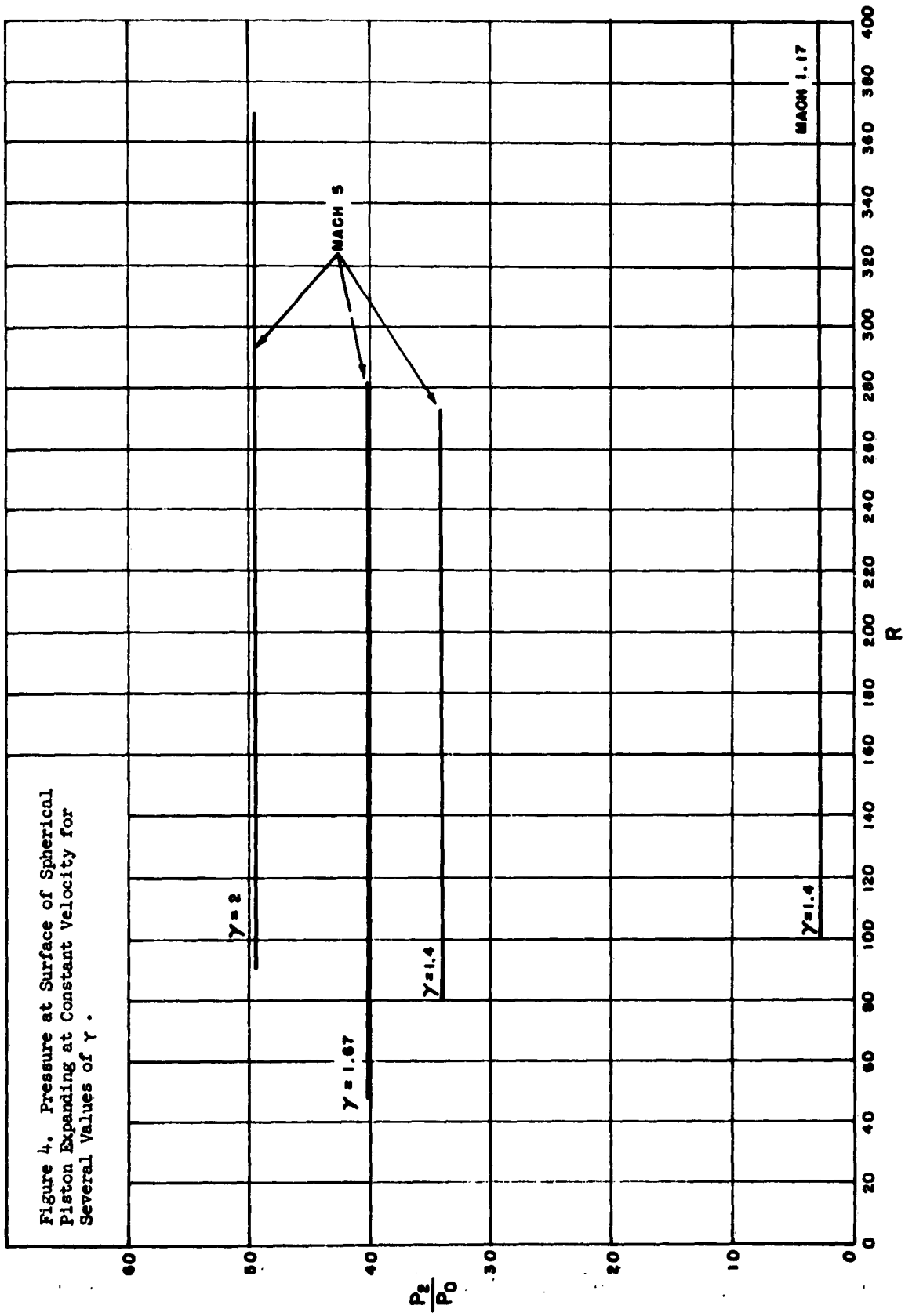


Figure 4. Pressure at Surface of Spherical Piston Expanding at Constant Velocity for Several Values of γ.

Figure 4

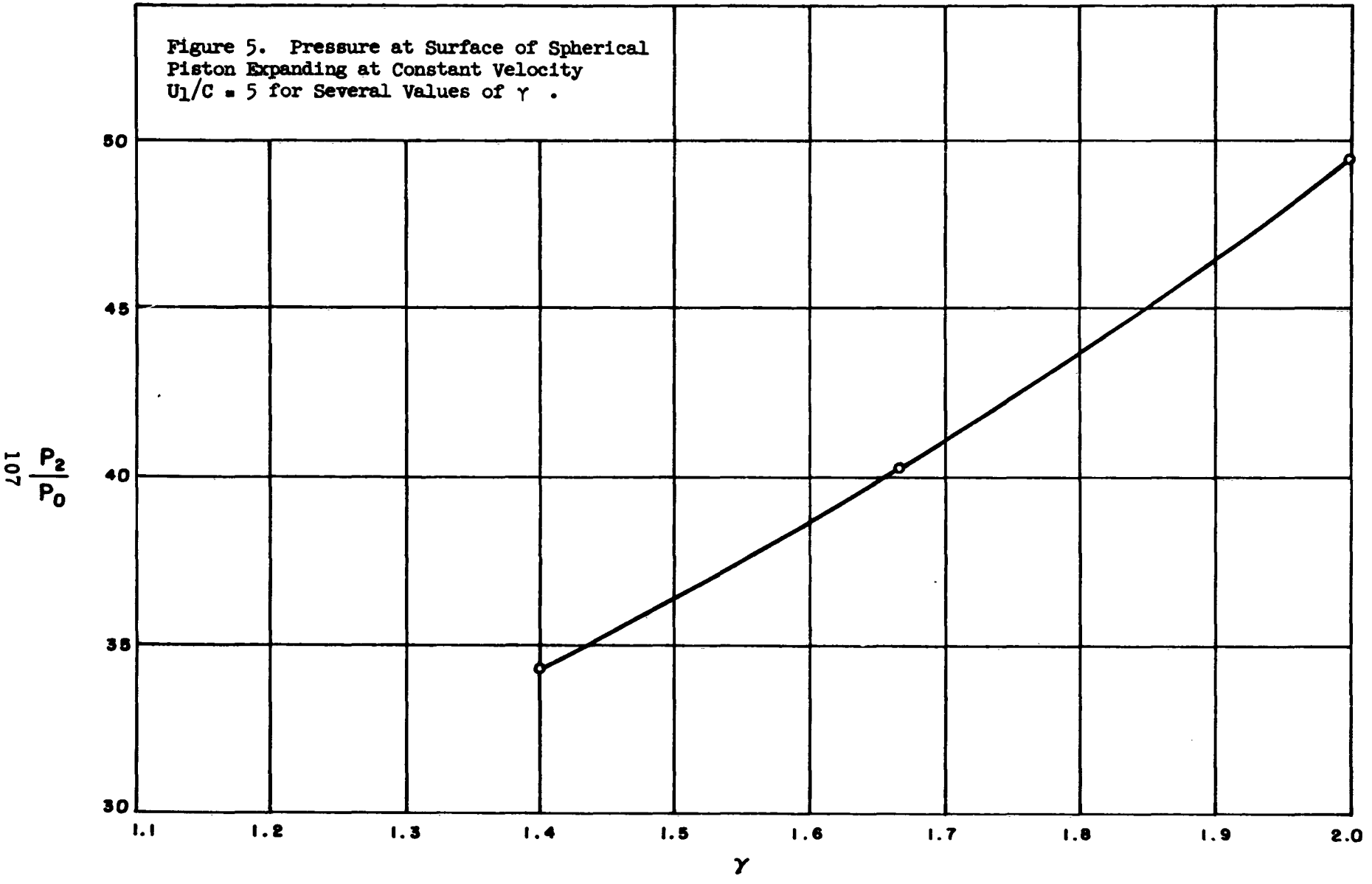
Figure 5. Pressure at Surface of Spherical Piston Expanding at Constant Velocity $U_1/C = 5$ for Several Values of $\gamma$ .
$10^7 \frac{P_2}{P_0}$
50
45
40
35
30
1.1
1.2
1.3
1.4
1.5
1.6
1.7
1.8
1.9
2.0
$\gamma$

Figure 5

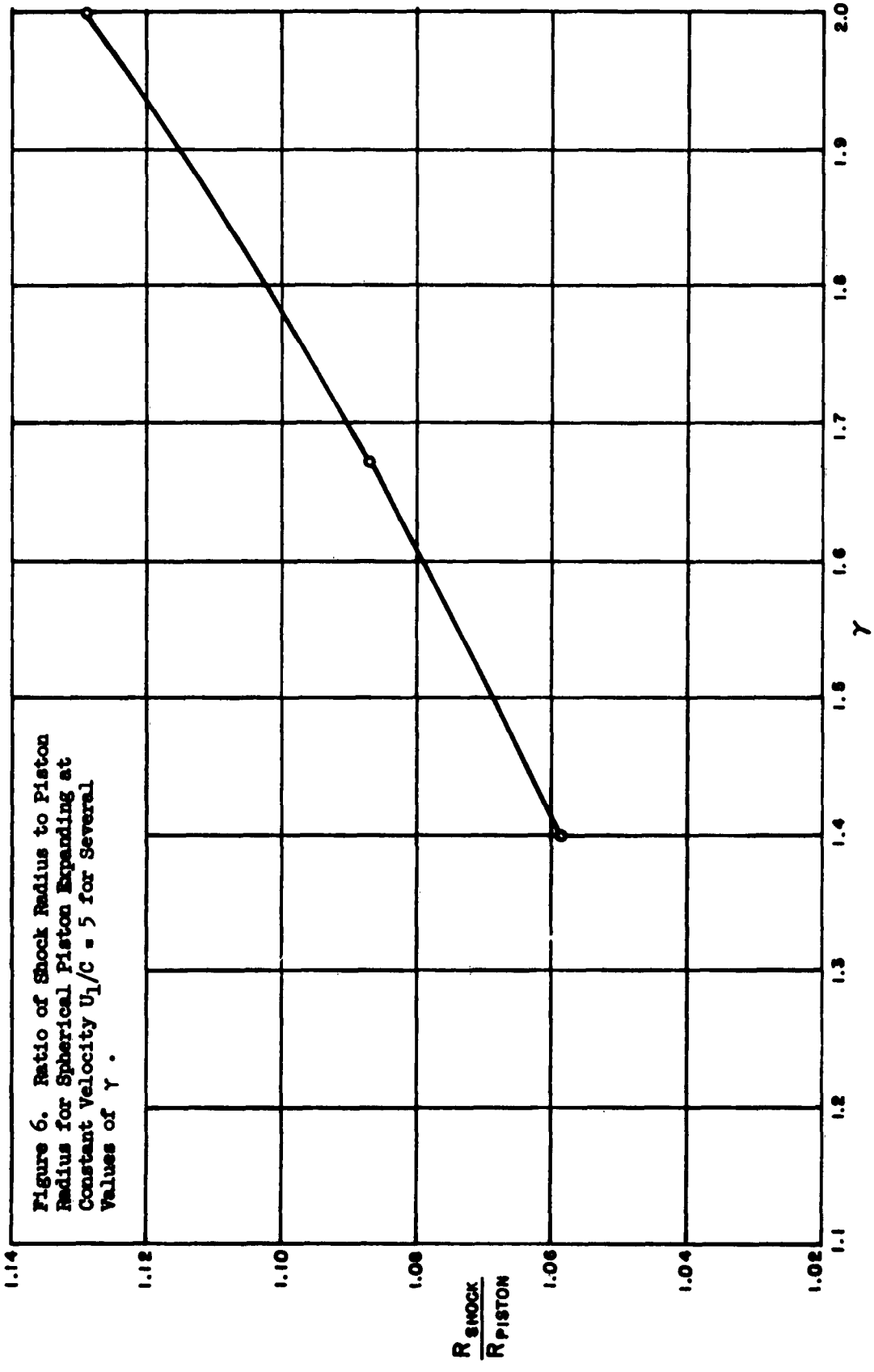
Figure 6. Ratio of Shock Radius to Piston Radius for Spherical Piston Expanding at Constant Velocity $U_1/C = 5$ for Several Values of $\gamma$.
1.14
1.12
1.10
1.08
1.06
1.04
1.02
$\frac{R_{SHOCK}}{R_{PISTON}}$
1.1
1.2
1.3
1.4
1.5
1.6
1.7
1.8
1.9
2.0
$\gamma$

Figure 6

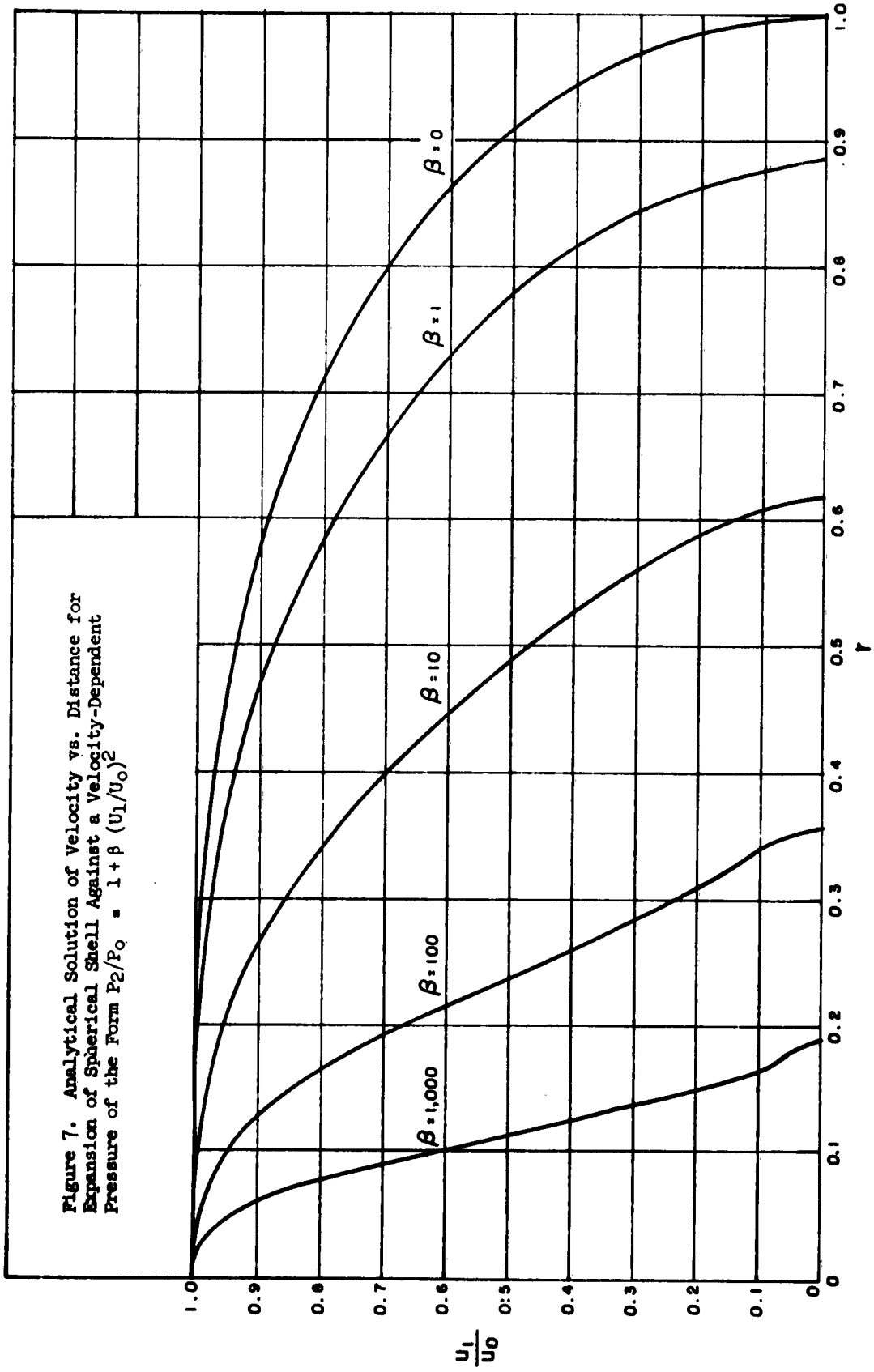
Figure 7. Analytical Solution of Velocity vs. Distance for Expansion of Spherical Shell Against a Velocity-Dependent Pressure of the Form $P_2/P_0 = 1 + \beta (U_1/U_0)^2$
$\beta = 0$
$\beta = 1$
$\beta = 10$
$\beta = 100$
$\beta = 1{,}000$
$\frac{U_1}{U_0}$
r
1.0
0.9
0.8
0.7
0.6
0.5
0.4
0.3
0.2
0.1
0

Figure 7

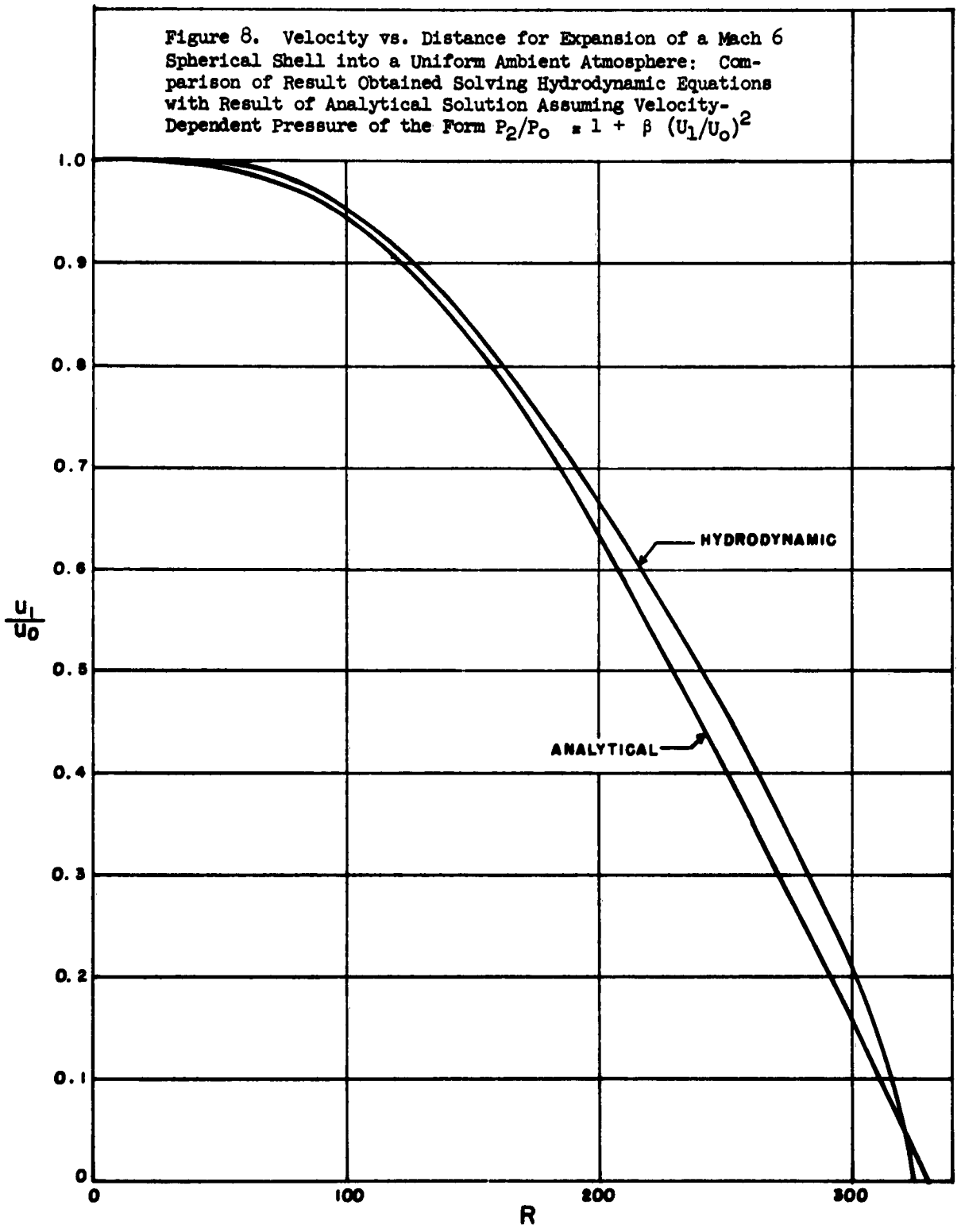


Figure 8. Velocity vs. Distance for Expansion of a Mach 6 Spherical Shell into a Uniform Ambient Atmosphere: Comparison of Result Obtained Solving Hydrodynamic Equations with Result of Analytical Solution Assuming Velocity-Dependent Pressure of the Form $P_2/P_o = 1 + \beta (U_1/U_o)^2$

Figure 8

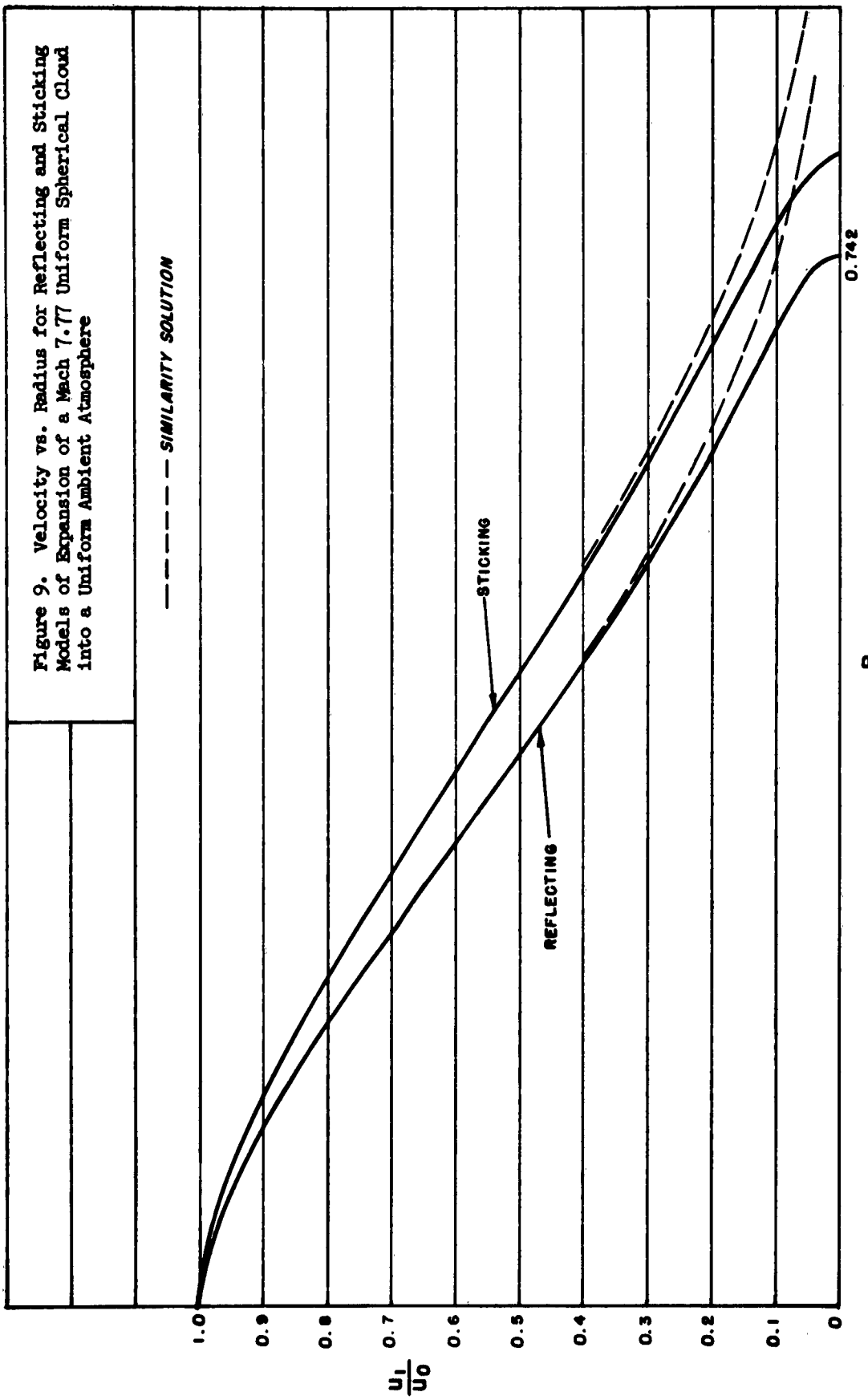
Figure 9. Velocity vs. Radius for Reflecting and Sticking Models of Expansion of a Mach 7.77 Uniform Spherical Cloud into a Uniform Ambient Atmosphere
— — — — — — SIMILARITY SOLUTION
STICKING
REFLECTING
0.742
1.0
0.9
0.8
0.7
0.6
0.5
0.4
0.3
0.2
0.1
0
$\frac{u_1}{u_0}$
$\frac{R}{V_0 t_s}$

Figure 9

Figure 10. Distribution of Energy vs. Radius for Reflecting and Sticking Models of Expansion of a Mach 7.77 Uniform Spherical Cloud into a Uniform Ambient Atmosphere.

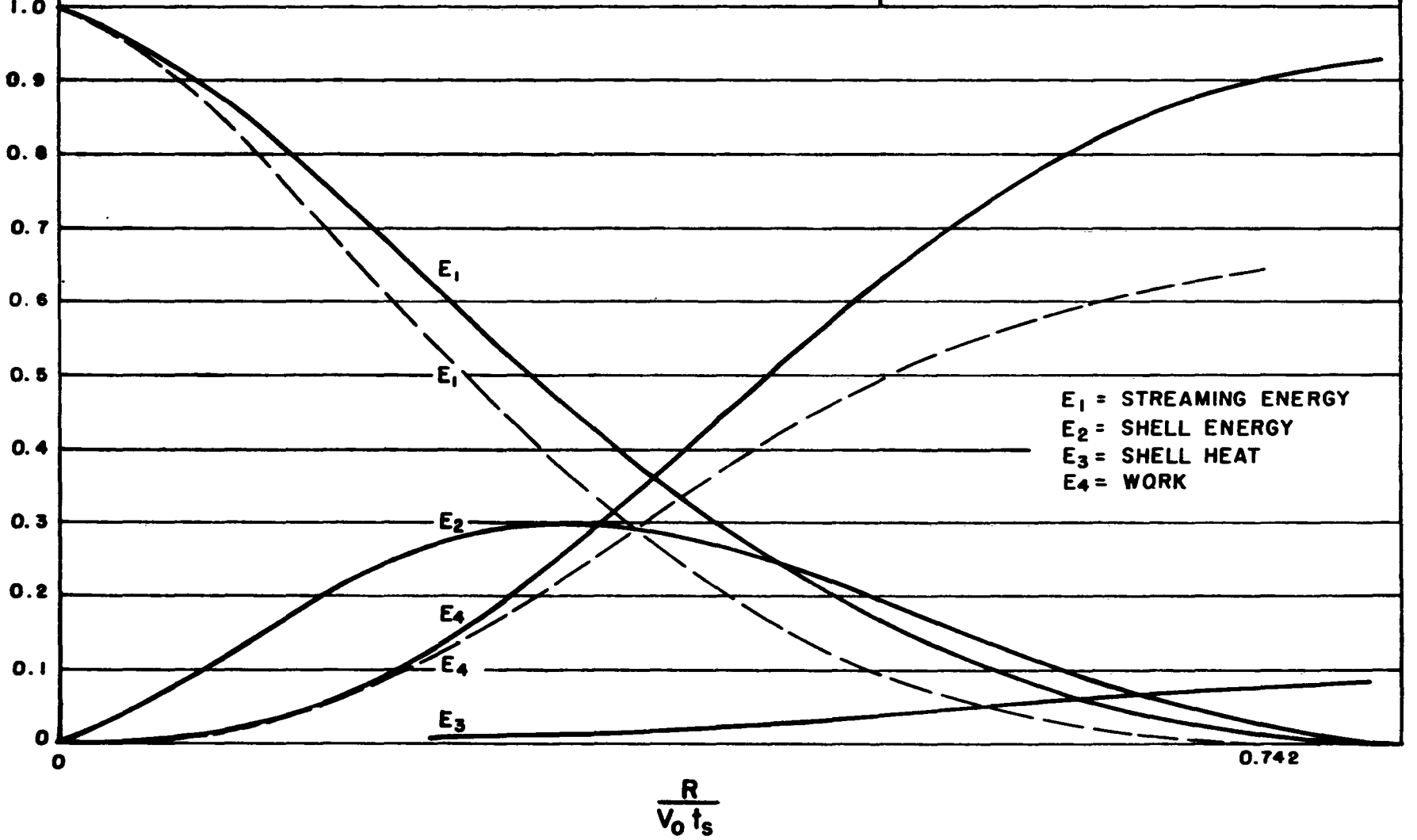


Figure 10

yet been done.

In order to check these results, a hydrodynamic program has been prepared which uses equation (3.9) and(3.10). Preliminary results from this code indicate that the pressure given by equation (3.11) is still a good approximation. In figure 11, a comparison is given between all three models for the pressure given by equation (3.11).

Programs have also been prepared which calculate the expansion into a non-uniform atmosphere for the three models under consideration. Presently, calculations are being made. It should be noted that with our present codes we could calculate piston motion when the internal flow is governed by the hydrodynamic equations.

In this work, we have an example of analytical and numerical methods complementing each other; also, of a machine program being flexible enough to permit extensions and yet give useful results at each stage of development.

Other problems in this area in which we are actively engaged are hydrodynamic flow with radiation. Our present work is limited to radiation diffusion. Thus, the only difference that occurs in our basic equations is in the energy equation which can be written in differential form as

$$\delta E = -p\delta V + \nabla\cdot(K\nabla\theta^4) + S \qquad (3.13)$$

where K is a function of the opacity, $\theta$ the temperature, and S a source term. Our present code is so constructed that the energy equation is solved in a subroutine, thus permitting different differencing techniques to be used in the diffusion term and use of different methods of solving the resulting nonlinear equations. In the present code, the Crank-Nickolson method is used. This is an implicit method which replaces the diffusion term at $n + 1/2$ by the average of term at n and $n + 1$. The radiation coupling is done by first letting the radiation flow from n to $n + 1$ with the hydrodynamics held fixed, and then using the temperature at $n + 1$, compute E and P. Now a number of other methods of coupling can be used but the method presently being used has been successfully tested and used on similar problems.

In our radiation-hydrodynamics effort, we have an example of a code which has developed from a fairly simple code to one of some complexity in which the

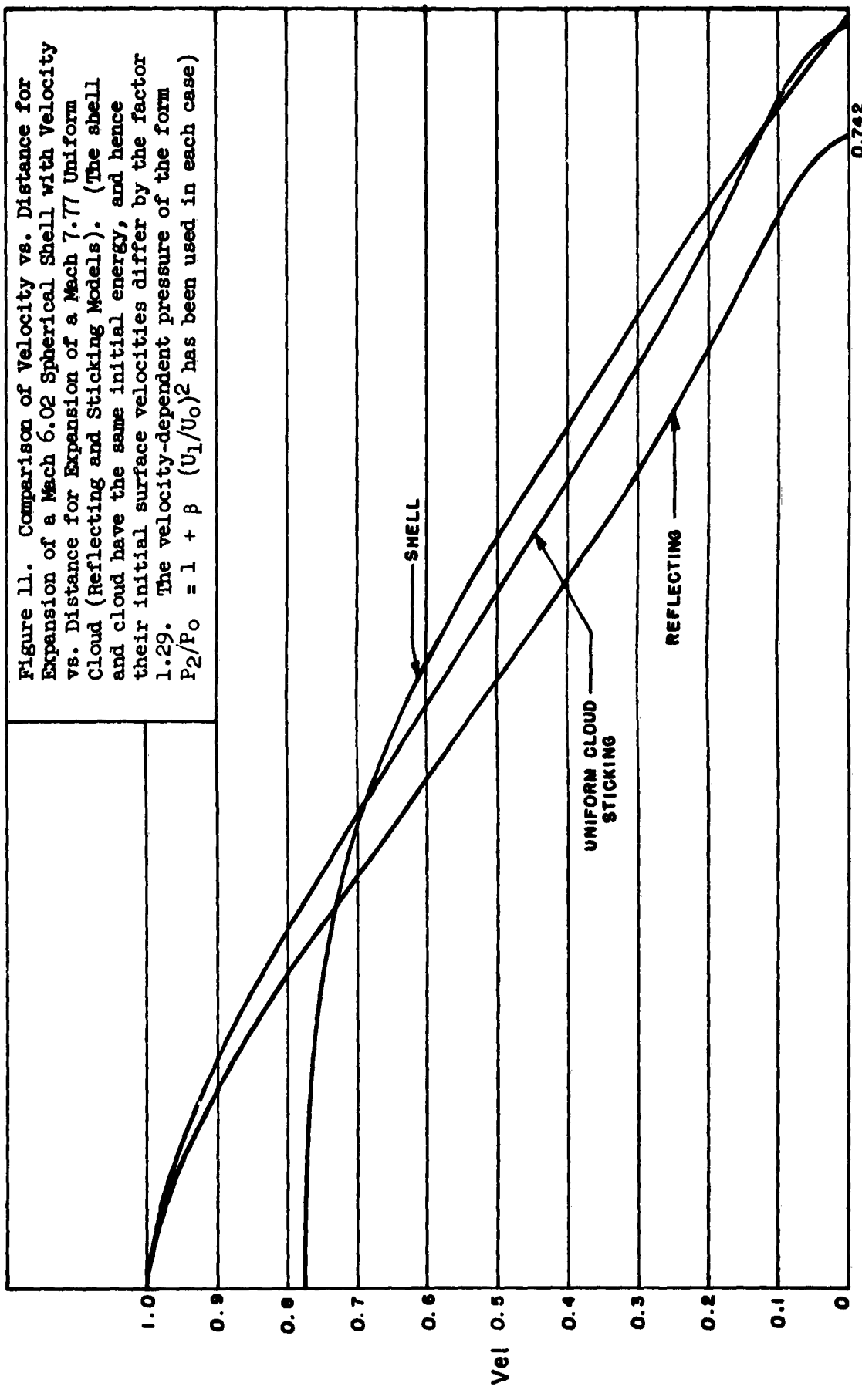


Figure 11. Comparison of Velocity vs. Distance for Expansion of a Mach 6.02 Spherical Shell with Velocity vs. Distance for Expansion of a Mach 7.77 Uniform Cloud (Reflecting and Sticking Models). (The shell and cloud have the same initial energy, and hence their initial surface velocities differ by the factor 1.29. The velocity-dependent pressure of the form $P_2/P_o = 1 + \beta \ (U_1/U_o)^2$ has been used in each case)

Figure 11

first methods being used are tested but the code is so constructed that basic changes can be made in the code without major reprograming.

4. TWO-DIMENSIONAL HYDRODYNAMICS.

In this area, we have been interested in both pure hydrodynamic as well as radiation-hydrodynamic calculations.

In order to achieve our goals, we first prepared a hydrodynamic code modeled after the Los Alamos Magee code.[2] Thus the difference equations used are

$$A^n_{I,J} = \frac{\left(P^n_{I-1,J+1} - P^n_{I-1,J-1}\right)\left(Y^n_{I-2,J} - Y^n_{I,J}\right)\left(X^n_{I-2,J} + X^n_{I,J}\right)}{2\left(m_{I-1,J+1} + m_{I-1,J-1}\right)}$$

$$+ \frac{\left(P^n_{I+1,J+1} - P^n_{I+1,J-1}\right)\left(Y^n_{I,J} - Y^n_{I+2,J}\right)\left(X^n_{I,J} + X^n_{I+2,J}\right)}{2\left(m_{I+1,J+1} + m_{I+1,J-1}\right)} \qquad (4.1)$$

$$+ \frac{\left(P^n_{I-1,J-1} - P^n_{I+1,J+1}\right)\left(Y^n_{I,J} - Y^n_{I,J+2}\right)\left(X^n_{I,J} + X^n_{I,J+2}\right)}{2\left(m_{I+1,J+1} + m_{I-1,J+1}\right)}$$

$$+ \frac{\left(P^n_{I-1,J-1} - P^n_{I+1,J-1}\right)\left(Y^n_{I,J-2} - Y^n_{I,J}\right)\left(X^n_{I,J-2} + X^n_{I,J}\right)}{2\left(m_{I-1,J-1} + m_{I+1,J-1}\right)}$$

$$B^n_{I,J} = \frac{\left(P^n_{I-1,J+1} - P^n_{I+1,J+1}\right)\left(X^n_{I,J+2} - X^n_{I,J}\right)\left(X^n_{I,J} + X^n_{I,J+2}\right)}{2\left(m_{I+1,J+1} + m_{I-1,J+1}\right)}$$

$$+ \frac{\left(P^n_{I-1,J-1} - P^n_{I+1,J-1}\right)\left(X^n_{I,J} - X^n_{I,J-2}\right)\left(X^n_{I,J} + X^n_{I,J-2}\right)}{2\left(m_{I+1,J-1} + m_{I-1,J-1}\right)} \qquad (4.2)$$

$$+ \frac{\left(P^n_{I-1,J+1} - P^n_{I-1,J-1}\right)\left(X_{I,J} - X_{I-2,J}\right)\left(X^n_{I,J} + X^n_{I-2,J}\right)}{2\left(m_{I-1,J+1} + m_{I-1,J-1}\right)}$$

$$+ \frac{\left(P^n_{I+1,J+1} - P^n_{I+1,J-1}\right)\left(X^n_{I+2,J} - X^n_{I,J}\right)\left(X^n_{I+2,J} + X^n_{I,J}\right)}{2\left(m_{I+1,J+1} - m_{I+1,J-1}\right)}$$

$$X^{n+1}_{I,J} = X^n_{I,J} + \Delta t\left[U^n_{I,J} - \Delta t\, A^n_{I,J}\right] \tag{4.3}$$

$$Y^{n+1}_{I,J} = Y^n_{I,J} + \Delta t\left[W^n_{I,J} - \Delta t\, B^n_{I,J}\right] \tag{4.4}$$

$$U^{n+1}_{I,J} = U^n_{I,J} - \Delta t\, A^n_{I,J} \tag{4.5}$$

$$W^{n+1}_{I,J} = W^n_{I,J} - \Delta t\, B^n_{I,J} \tag{4.6}$$

$$\left(A_{\Delta 124}\right)^{n+1}_{I+1,J+1} = \frac{1}{2}\left[X^{n+1}_{I,J}\left(Y^{n+1}_{I+2,J} - Y^{n+1}_{I,J+2}\right) + X^{n+1}_{I+2,J}\left(Y^{n+1}_{I,J+2} - Y^{n+1}_{I,J}\right)\right] \tag{4.7}$$

$$+ X^{n+1}_{I,J+2}\left(Y^{n+1}_{I,J} - Y^{n+1}_{I+2,J}\right)\Big]$$

$$\left(A_{\Delta 342}\right)^{n+1}_{I+1,J+1} = \frac{1}{2}\Big[X^{n+1}_{I+2,J+2}\left(Y^{n+1}_{I,J+2} - Y^{n+1}_{I+2,J}\right)$$

$$+ X^{n+1}_{I,J+2}\left(Y^{n+1}_{I+2,J} - Y^{n+1}_{I+2,J+2}\right) \qquad (4.8)$$

$$+ X^{n+1}_{I+2,J}\left(Y^{n+1}_{I+2,J+2} - Y^{n+1}_{I,J+2}\right)\Big]$$

$$\left(\bar{X}_{\Delta 124}\right)^{n+1}_{I+1,J+1} = \frac{1}{3}\left[X^{n+1}_{I,J} + X^{n+1}_{I+2,J} + X^{n+1}_{I,J+2}\right] \qquad (4.9)$$

$$\left(\bar{X}_{\Delta 342}\right)^{n+1}_{I+1,J+1} = \frac{1}{3}\left[X^{n+1}_{I+2,J+2} + X^{n+1}_{I+2,J} + X^{n+1}_{I,J+2}\right] \qquad (4.10)$$

$$V^{n+1}_{I+1,J+1} = \frac{\left(\bar{X}_{\Delta 124} A_{\Delta 124}\right)^{n+1}_{I+1,J+1} + \left(\bar{X}_{\Delta 342} A_{\Delta 342}\right)^{n+1}_{I+1,J+1}}{\left(R_0 A_0\right)_{I+1,J+1}} \qquad (4.11)$$

$$\Delta V^{n+1}_{I+1,J+1} = V^{n+1}_{I+1,J+1} - V^{n}_{I+1,J+1}$$

$$q_{I+1,J+1}^{n+1} = \frac{C_0 b \left[ \left(A_{\Delta 124}\right)_{I+1,J+1}^{n+1} + \left(A_{\Delta 342}\right)_{I+1,J+1}^{n+1} \right] \left(\Delta V_{I+1,J+1}^{n+1}\right)^2}{(\Delta t)^2 \left(V_{I+1,J+1}^{n+1}\right)} \quad (4.12)$$

$$q_{I+1,J+1}^{n+1} = 0 \qquad \text{if } \Delta V_{I+1,J+1}^{n+1} < 0$$

$$\text{if } \Delta V_{I+1,J+1}^{n+1} \geq 0$$

$$E_{I+1,J+1}^{n+1} = E_{I+1,J+1}^{n} - \Delta V_{I+1,J+1}^{n+1} \left[ \frac{P_{I+1,J+1}^{n+1} - P_{I+1,J+1}^{n}}{2} \right] \quad (4.13)$$

$$P_{I+1,J+1}^{n+1} = P\left(E_{I+1,J+1}^{n+1}, V_{I+1,J+1}^{n+1}\right) + q_{I+1,J+1}^{n+1} \quad (4.14)$$

$$\frac{\omega^2}{1.44}\Bigg|_{I+1,J+1}^{n+1} = \frac{2.6\, E_{I+1,J+1}^{n+1} (\Delta t)^2}{e_0 \left[ \left(A_{\Delta 124}\right)_{I+1,J+1}^{n+1} + \left(A_{\Delta 342}\right)_{I+1,J+1}^{n+1} \right]} + 4 \left| \frac{\Delta V_{I+1,J+1}^{n+1}}{V_{I+1,J+1}^{n+1}} \right| \quad (4.15)$$

The acceleration terms are those obtained by the so-called Force Gradient[2] Method. This code has the feature that the form of the acceleration terms can easily be changed as well as the equations of state; also, the overall logic is such as to minimize the time of calculations.

In order to develop our radiation hydrodynamics code, we first prepared a radiation diffusion code which can be coupled to the hydrodynamics in the same way as for the one-dimensional case. The basic equation solved in the radiation code is the energy which when written in integral form becomes

$$\frac{\partial}{\partial t}\int_{\tau_0} \mathcal{E}\,\delta\tau = -\int_S \vec{\phi}\cdot\delta\vec{s} \qquad (4.16)$$

where $\mathcal{E} = \mathcal{E}(\theta, v)$ is the specific internal energy, i.e., per unit original volume, $\vec{\phi}$ is the flux of radiation across the surface S bounding the element $\tau_0$.

By differencing these equations by the implicit alternating direction method, i.e., for one time step, the equations are differenced implicity in the X direction and, on the next time step, implicitly in the Y direction. We obtain

$$A^n_{I+1,J+1}\,\Delta\theta^{n+1/2}_{I-1,J+1} + B^n_{I+1,J-1}\,\Delta\theta^{n+1/2}_{I+1,J-1} + C^n_{I+1,J+1}\,\Delta\theta^{n+1/2}_{I+3,J-1} = D^n_{I+1,J+1} \qquad (4.17)$$

$$\bar{A}^n_{I+1,J+1}\,\Delta\theta^{n+1/2}_{I+1,J-1} + \bar{B}^n_{I+1,J+1}\,\Delta\theta^{n+1/2}_{I+1,J+1} + \bar{C}^n_{I+1,J+1}\,\Delta\theta^{n+1/2}_{I+1,J+1} = \bar{D}^n_{I+1,J+1}$$

$$\Delta\theta^{n+1/2}_{I+1,J+1} \equiv \theta^{n+1}_{I+1,J+1} - \theta^{n}_{I+1,J+1} \qquad (4.18)$$

where the coefficients $A^n_{I+1,J+1}$, $\bar{A}^n_{I+1,J+1}$ etc. are known functions of known quantities at time n.

These equations are solved by introducing the well known recursion relationship

$$\Delta\Theta^{n+1/2}_{I-1,J+1} = a^{n+1}_{I-1,J+1} + b^{n+1}_{I-1,J+1}\,\Delta\Theta^{n+1/2}_{I+1,J+1} \tag{4.19}$$

By substituting these into the above equations, one obtains

$$a^{n+1}_{I+1,J+1} = \frac{D^{n}_{I+1,J+1} - a^{n+1}_{I-1,J+1}\,A^{n}_{I+1,J+1}}{B^{n}_{I+1,J+1} + b^{n+1}_{I-1,J+1}\,A^{n}_{I+1,J+1}} \tag{4.20}$$

$$b^{n+1}_{I+1,J+1} = \frac{-C^{n}_{I+1,J+1}}{B^{n}_{I+1,J+1} + b^{n+1}_{I-1,J+1}\,A^{n}_{I+1,J+1}} \tag{4.21}$$

and a similar set for the Y implicit. Using these and the boundary conditions, one is able to solve the necessary equations. The code used to solve these contains the same feature as our one-dimensional code and the coupling is done in the same way as before.

Here again, we have used tested methods[2] but still allow for other methods to be easily used, and have developed our code in a step-wise manner.

## 5. NON-EQUILIBRIUM FLOWS.

Let us now briefly turn to the area of non-equilibrium gas flows. We have chosen as our model that given by Wood and Kirkwood[4] with the further assumption that we have local thermodynamic equilibrium between classes of degrees of freedom as well as within these classes. These equations could also have been obtained by specializing the Kirkwood-Crawford[5] equations to an inviscid nondiffusing gas. The equations are

$$\frac{\partial P}{\partial t} + \rho c_0^2\,\nabla\cdot\vec{u} = \rho c_0^2\left(\sum_\alpha \sigma_\alpha r_\alpha\right) - \delta\rho c_0^2\, v/y \tag{5.1}$$

$$\rho\frac{\partial\vec{u}}{\partial t} + \nabla P = 0 \tag{5.2}$$

$$\frac{\partial \lambda_\alpha}{\partial t} = r_\alpha' \tag{5.3}$$

$$T\frac{\partial S}{\partial t} = -\sum_\alpha \Delta_\alpha F r_\alpha \tag{5.4}$$

The density derivative has been eliminated from the mass equation by use of the differential form of the caloric equation of state

$$C_0^2 \frac{\partial \rho}{\partial t} = \frac{\partial P}{\partial t} - \rho C_0^2 \sum_\alpha \sigma_\alpha r_\alpha \tag{5.5}$$

where we have defined

$$\sigma_\alpha = [\rho \beta_0 / C_P^0]\left\{[C_P^0/\beta_0]\Delta_\alpha 1/\rho - \Delta_\alpha H\right\} \tag{5.6}$$

$$C_0^2 = \left(\frac{\partial P}{\partial \rho}\right)_{S,\{\lambda\}} \quad \text{(frozen velocity of sound)} \tag{5.7}$$

$$\beta_0 = \left(\frac{\partial (1/\rho)}{\partial T}\right)_{P,\{\lambda\}} \quad \text{(frozen expansion coefficient)} \tag{5.8}$$

$$C_P^0 = T\left(\frac{\partial S}{\partial T}\right)_{P,\{\lambda\}} \quad \text{(frozen specific heat at constant pressure)} \tag{5.9}$$

$$\Delta_\alpha F = \sum_s \mu_s \nu_s^\alpha \tag{5.10}$$

Also $\mu_s$ is the specific chemical potential of specie s and $\nu_s^\alpha$ the specific stoichiometric coefficient for the s specie in the $\alpha$th reaction.

In order to complete our set of equations, we introduce the equation of state for an ideal mixture

$$P = \rho R T Z \tag{5.11}$$

Here Z is the compressibility.

The above equations govern the flow in non-equilibrium. The equations

for frozen flow are obtained simply by setting $\nu_\alpha = 0$. It can be shown[6] that the equilibrium equations can be obtained from the frozen equations by replacing the frozen velocity of sound by $C^2$, the equilibrium velocity of sound, and evaluating all of the thermodynamic functions from equilibrium thermodynamics. It is easily seen that these basic equations are hyperbolic in character and that the difference between equilibrium and non-equilibrium equations is only in the coefficients and added flux type terms. Thus one can use the usual tools for calculation of hyperbolic equations. Limiting ourselves to plane and axially symmetrical flows, we find the characteristic relations to be

$$\left.\frac{dY}{dX}\right|_{\pm} = \left[\frac{-uv \pm C_o\sqrt{u^2+v^2-C_o^2}}{C_o^2-u^2}\right] = F^{\pm} \qquad (5.12)$$

where the plus sign denotes the right-running characteristic and the minus sign the left-running characteristic. Also, the streamlines are characteristic, i. e.,

$$\frac{dY}{dX} = \frac{v}{u} \qquad (5.13)$$

The compatibility equations become

$$\rho C_o^2(u\,dv - v\,du) + [(u^2 - C_o^2)F^{\pm} - uv]\,dP$$

$$+\rho C_o^2\left(\sum_\alpha \sigma_\alpha r_\alpha - \frac{v\delta}{u}\right)(v - uF^{\pm})\,dX = 0 \qquad (5.14)$$

where $\delta = 1$ for axially symmetrical flows and 0 for plane flows. Another method is to finite difference the basic equations in such a way that the calculation is carried out using the proper domain of dependence determined by the characteristics. This has been done but will not be listed here. In order to carry out calculations using the above equations, one needs the thermodynamics which for equilibrium can be found in essentially three different ways, (a) table look up, (b) analytical fits to the tables, and (c) calculation of the basic equilibrium equations. It has been shown[7] that for

a wide range of interest air can be represented as a simple gas governed by the reactions

$$O_2 \rightleftharpoons 2O$$
$$N_2 \rightleftharpoons 2N \qquad (5.15)$$
$$NO \rightleftharpoons O + N$$

Also, all the needed thermodynamic quantities can be expressed[8] in terms of G, the dimensionless internal energy Z and all their derivatives.

Using these concepts, subroutines have been prepared for calculation of the thermodynamics for equilibrium and non-equilibrium. The basic difference in these subroutines is that for equilibrium the species concentrations are calculated from the equilibrium equations which are nonlinear algebraic equations, while for the other cases they are obtained from the kinetics which are solved as part of the basic flow equations. Codes have been prepared which use these subroutines and the basic equations for calculating flow fields. It has been determined that it is wiser to develop separate programs for equilibrium and non-equilibrium rather than to try to calculate all cases with one code.

The one basic difficulty introduced by non-equilibrium flows over and above determination of reaction rates is the limitation placed on the mesh size by the kinetics. It has been found in some cases that the mesh size must be taken such that it corresponds to a flow time of a nanosecond. Consequently, large amounts of machine time must be expended for a calculation. At the present, we are investigating various methods of reducing the calculating time.

## REFERENCES


1. Taylor, G. I., The Air Wave Surrounding an Expanding Sphere, Proc. Royal Society, A 186, 273-92, 1946
2. White, G. N. Jr., Orr, S. R., Private Communication, Los Alamos Scientific Laboratory.
3. Browne, P. H., Private Communication, Los Alamos Scientific Laboratory
4. Wood, W. W., and Kirkwood, J. C., Hydrodynamics of a Reacting and Relaxing Fluid, Journal of Applied Physics, Vol. 28, No. 4, pp. 395-398, April 1957
5. Kirkwood, J. C., and Crawford, B., The Macroscopic Equations of Transport, Journal of Chemical Physics, 56, 1048, December 1952
6. Sulzmann, K. G. P., Flow Equations for Inviscid Adiabatic, Non-Diffusing Mixtures with Frozen and Equilibrium Reactions, Convair-San Diego, 26 January 1959, ZPh-037
7. Hochstim, A. R., Approximation to High-Temperature Thermodynamics of Air in Closed Form, Convair Report ZPh-050, pp. 43-74, 31 December 1959
8. Hochstim, A. R., Gas Properties Behind Shocks at Hypersonic Velocities. II. Introduction to General Thermodynamics of a Real Gas, Convair-San Diego Report ZPh-003, 15 May 1957

# PROBLEMS OF RADIATION TRANSPORT IN HEATED AIR

Dr. R. K. M. Landshoff
Dr. R. E. Meyerott
Lockheed Missiles and Space Division

Nuclear explosions in the air can be strongly influenced by the emission and absorption of radiation which transfers energy from one point of the fireball to another or to points in the exterior. The flow of radiation can be expressed in terms of the intensity $I_\nu$, where $I_\nu \cos\theta d\Omega d\nu dt dA$ is the energy passing through an area dA, during a time dt, in a frequency interval $d\nu$ and coming from an element of solid angle $d\Omega$ around a ray which makes an angle $\theta$ with the normal to dA. In general, the intensity $I_\nu$ is a function of position and time, direction of ray, and frequency or wavelength.

Along a given ray, the intensity changes in a manner which is determined by emission and absorption of the radiation by the material through which it passes. Such changes are calculated from the equation of radiative transfer. If the material is in local thermodynamic equilibrium, the equation of transfer is [1]

$$\frac{dI_\nu}{ds} = \mu_\nu \quad (B_\nu - I_\nu) \tag{1}$$

where

$$\mu_\nu = \rho K_\nu \quad (1 - \exp(-h\nu/kt))$$

is defined in terms of the absorption coefficient $K_\nu(\rho, T)$; s measures the distance traversed by the radiation along the ray; $B_\nu = \frac{2h\nu^3}{c^2}\left[\exp\left(\frac{h\nu}{kt}\right)-1\right]^{-1}$

The mathematical character of equation (1) is well known and leads to solutions where $I_\nu$ tends towards $B_\nu$. If the temperature remains constant in a large enough region of space rather than changing from point to point, i.e., if one has complete rather than local thermodynamic equilibrium, $B_\nu$ will also be constant and $I_\nu$ will become equal to $B_\nu$. This is the situation within a "Hohlraum" or blackbody, and $B_\nu$ is thus the blackbody intensity.

Equation (1) treats the radiative transfer problem for each instant as if the density and temperature distributions were held fixed. Such an adiabatic

treatment is justified because of the high velocity of light.

If the absorption coefficient $\mu_\nu$ is known as a function of $\rho$ and T, one can formally solve equation (1) in terms of the instantaneous spatial distributions of $\rho$ and T. To write this solution down, it is convenient to introduce the optical depth of a general point P on the ray.

$$T_\nu (P) = \int_P^{P_o} \mu_\nu ds$$

The upper limit $P_o$ is a point beyond the edge where the ray emerges from the absorbing region into the region where $\mu_\nu$ has gone to zero. The point $P_1$ shown in the figure also lies in the nonabsorbing region on a section of the ray which has not yet entered the absorbing interior.

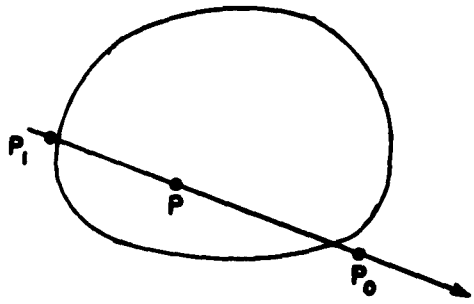


The intensity at a point P is then given by the integral

$$I_\nu = \int_{T_\nu}^{T_\nu (P_1)} B_\nu (P') \exp(T_\nu - T_\nu') \, dT_\nu' \qquad (2)$$

If $I_\nu$ has been determined for all rays going through a given point, the integral overall directions

$$\int \frac{dI_\nu}{ds} d\Omega = \int \mu_\nu (B_\nu - I_\nu) \, d\Omega \qquad (3)$$

is the difference between emitted and absorbed power per unit volume and frequency and determines the rate of cooling at that frequency.

In principle, carrying out integrals like (2) is quite straightforward but because of the strong frequency dependence of $\mu_\nu$, extensive calculations at many frequencies are involved. The difficulty which arises is that, even for frequencies which lie close together, the major contributions to the integral for $I_\nu$ may come from widely separated points on the ray. The variation of the point of origin (i. e. where the integrand in equation (2) is large) with frequency is particularly severe for transitions between bound states because they lead to spectral lines where the absorption coefficient is very much

larger at the center than in the wings.

Until a more satisfactory method has been found, one is forced to use approximate procedures. It is customary to use smoothed coefficients for the integration of the transport equation in which the contribution due to lines is distributed in frequency as if they were broad enough to overlap.

The current status of calculations to obtain the absorption coefficient of hot air is discussed in considerable detail in a forthcoming article by Meyerott and Armstrong[2]. Results of such calculations in the temperature range from 1,000° K to 12,000° K and for density ratios relative to sea level extending from 10 to $10^{-6}$ have been calculated and are tabulated as a function of wavelength between 1,200 A and 20,000 A[3]. The actual wavelengths appearing in the tables are those corresponding to values of $h\nu$ extending from 0.625 to 10.625 ev in steps of 0.25 ev.

In a higher temperature range extending from 22,000°K to 220,000°K and in nearly the same density range as before, absorption coefficients have been reported by Armstrong, Holland, and Meyerott[4]. The values of $h\nu$ extend from 1 ev to 1,000 ev, i.e., beyond the binding energy of the last K electron in O which is 871.1 ev.

A number of assumptions entering into the calculations of absorption coefficients, such as the use of the Born-Oppenheimer approximation, uncertain f-values, and the smoothing out prescriptions, make the use of these coefficients somewhat suspect. One way of testing them for the conditions where they are intended to be used is the calculation of the spectral distribution emerging from a nuclear fireball. Such a calculation has been carried out for a 1-KT airburst with temperature and density profiles taken from the report by Brode and Meyerott (ref. RM-1851). The results were compared with experimental spectral distributions observed from such small airbursts. There is good agreement on features like a sharp peak at 5,000 A and a sudden ultraviolet cutoff. By contrast, the computed spectral irradiances are significantly higher than the experimental values in the infrared region. This would result if the free-free absorption coefficients had been assumed too low. Recent theoretical and experimental results confirm that the free-free coefficients are indeed higher than the ones used in the calculation. Between the UV cutoff and the maximum of the observed spectral distribution, one finds a number of discrete spectra. Prominent among these are the $O_2$

Schumann Runge lines which appear in absorption. Other spectra, such as $N_2^+(1-)$ appear originally in absorption and change some time after the 2nd maximum to emission. The Schumann Runge bands are of particular interest because of a very strong sensitivity to temperature. Figure 1 shows the potential energy curves of the two electronic states of $0_2$ which give rise to the S-R band system. Transitions from low-lying levels of the $X^3 \sum g^-$ state are severely restricted by the Franck-Condon principle. Levels with vibrational quantum numbers $v''$ like 3, 4, or 5 are much more likely to make optical transitions, but these levels are not populated until the temperature is high enough. The relative intensities of the various lines can be used to calculate the population of the various levels. One can then attempt to interpret these populations in terms of temperatures. At early times in the history of an explosion, that attempt gives rise to contradictory results, which is an indication that these states are not present in thermodynamic equilibrium concentrations. At times around the first minimum the situation changes and from then on the various levels have a temperature-determined population.

The calculations reported in reference 3 show that the Schumann-Runge transitions are the dominant contributor to the absorption coefficient at low temperatures. At sea level density, this temperature range extends to about $6,000^\circ$ K and at $10^{-6}$ times s-l density to about $3,000^\circ$K, at which point the NO bands take over. It is important to note that there is no significant background of continuous transitions up to temperatures like $5,000^\circ$K. This fact, together with the appearance of bands in the observed spectra from explosions, indicates that line effects may invalidate the use of smoothed out absorption coefficients in calculating the radiative transfer of energy.

The Schumann-Runge and other band systems consist of exceedingly large numbers of lines which are characterized by their wavelength, width, and some measure of their intensity such as the value of $\mu_\nu$ at the center of the line or the integral $\int \mu_\nu \, d\nu$. The wave lengths can be calculated for given vibrational and rotational quantum numbers of the upper and lower state, $v' J'$ and $v'' J''$, with the aid of constants given by Herzberg[5]. The line widths are determined by pressure broadening and are assumed to be proportional to the pressure with a constant of proportionality which has been calculated by Margenau. The integrated absorption coefficient

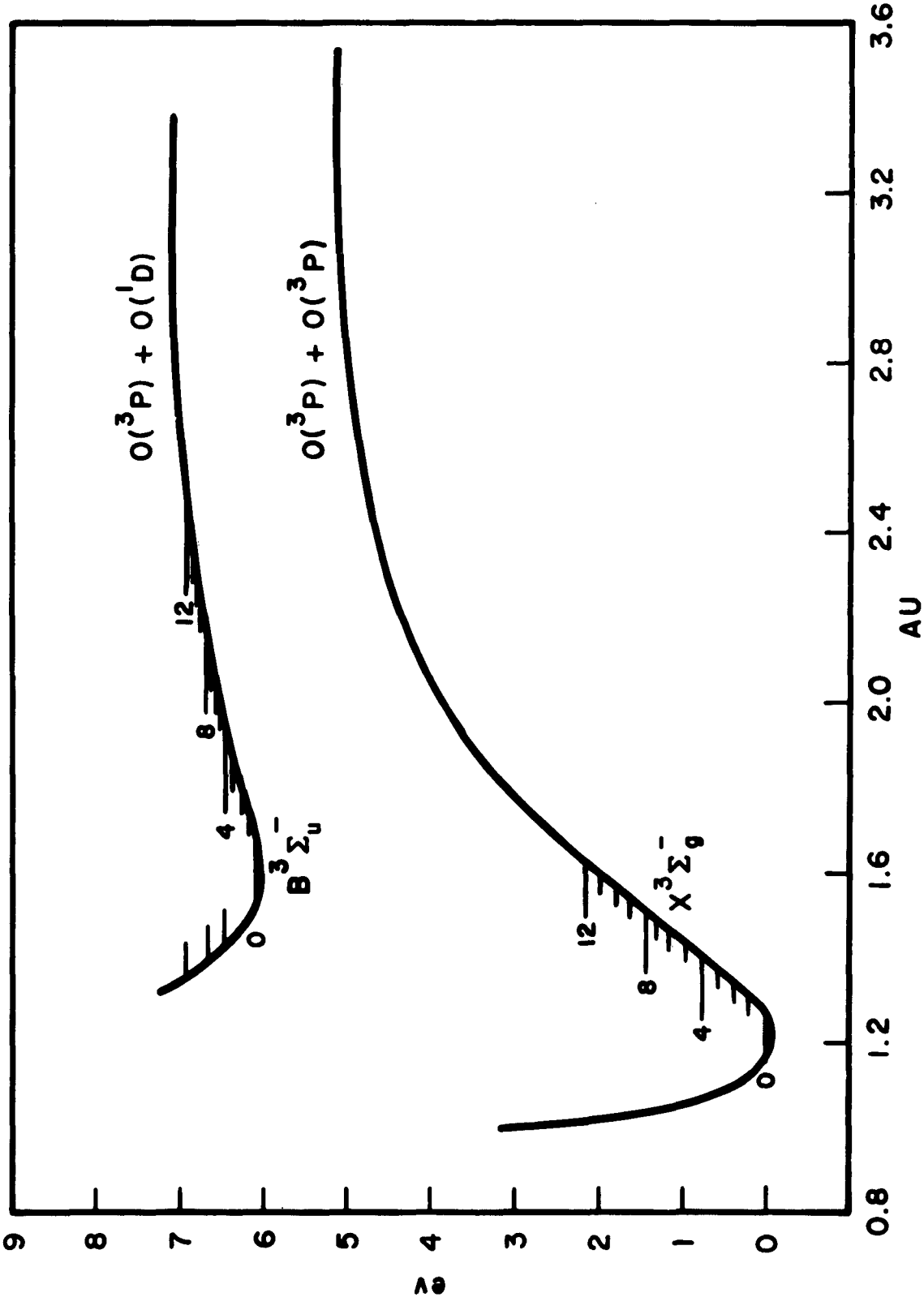


Figure 1. Levels for Schumann-Runge transitions

$$\int_{\text{line}} \mu_\nu d_\nu = \frac{\pi e^2}{m} N_{v'' J''} f g_{v'' v'} S_{J'' J'} \qquad (4)$$

requires a knowledge of four variable factors as follows:

1) The population $N_{v'' J''}$ of the lower level, which is assumed to be in thermal equilibrium and therefore obtained from the Boltzmann distribution

2) The electronic f value, which for $O_2$ (S-R) is assumed to be $f = 0.048$ as given by Treanor and Wurster[6].

3) The Franck-Condon factors $g_{v'' v'}$, as given by Fraser, Jarmain, and Nicholls[7].

4) The line strengths $S_{J'' J'}$ as quoted on page 208 of reference 5. The integral given in equation (4) and the maximum $\mu_m$ at the center of the line are directly proportional to each other. The factor depends on the line shape and varies like the line width $\Delta\nu$. Figures 2 and 3 show the envelopes of various bands at 1,000° K and at 3,000° K.

Figure 4 shows the fractional transmission for several thicknesses x of air of a number of lines in the (5-5) band. It is important to notice how these lines become wider with increasing thickness. For very thin samples the absorption $\mu_\nu x$ would be proportional to the thickness but this increase diminishes as the absorption becomes larger. Thus, the centers of lines where the absorption is the largest grow less strongly than the wings, and this makes the lines become wider. Since the absorption at the line center approaches its full value in a relatively thin sample, the major contribution to the transmission comes from the wings and the average transmission depends critically on the minimum of $\mu_\nu$.

The procedure of integrating the transport equation, so as to develop as much detail as shown in figure 4, is quite laborious and with more than 10,000 and possibly as many as 100,000 lines the amount of computation would be prohibitive. There are, however, certain regularities which can be readily noticed on inspection of band spectra, which suggest a simpler modification of the above procedure. Figure 5 shows the densitometer trace of a typical band spectrum attained with a high resolution Meinel spectrograph. The point which we want to make is that the average absorption changes quite slowly with wave length. The fact that figure 5 is an emission spectrum does

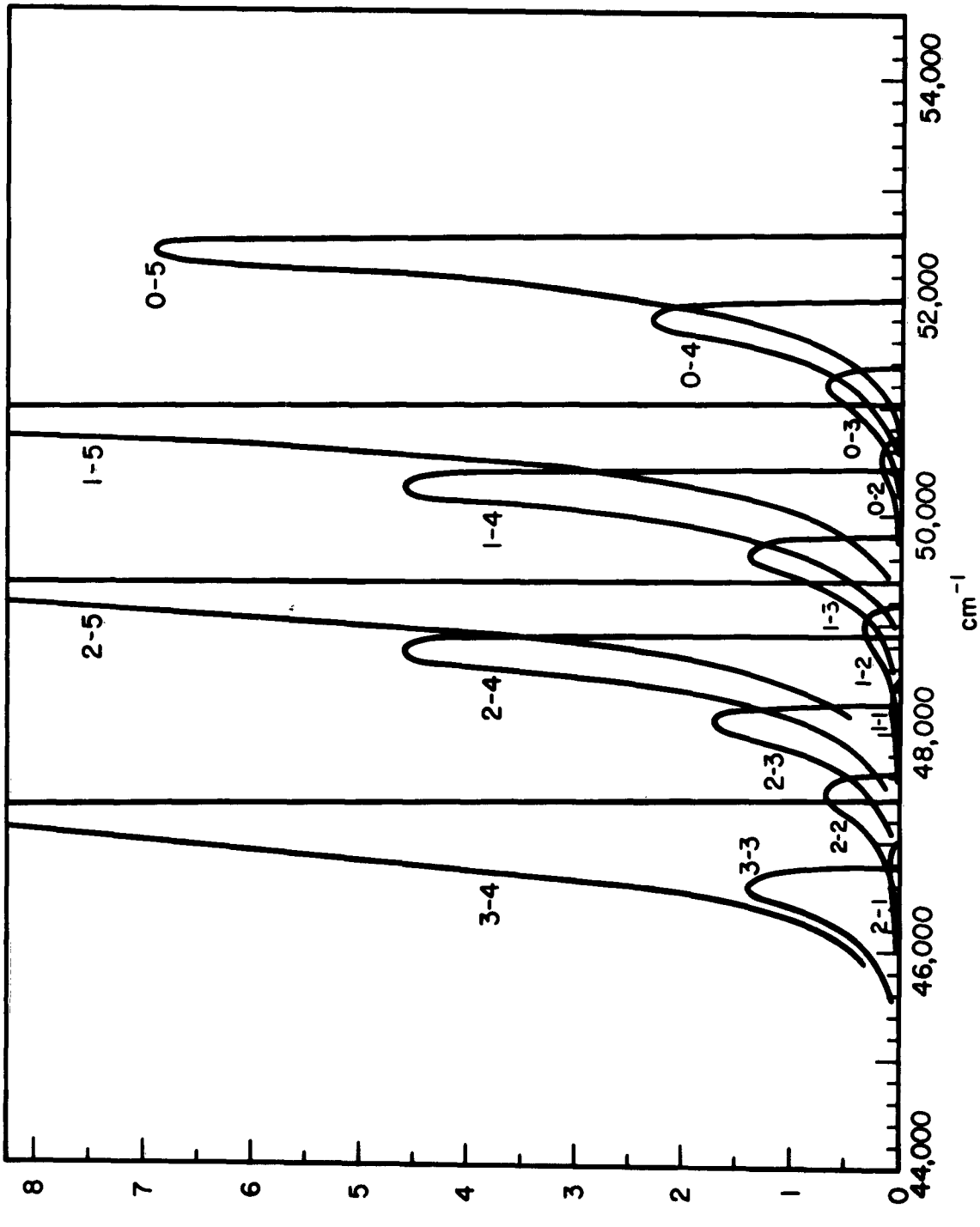


**Figure 2. Intensity distribution in $O_2$ Schumann-Runge bands at T = 1,000°K**

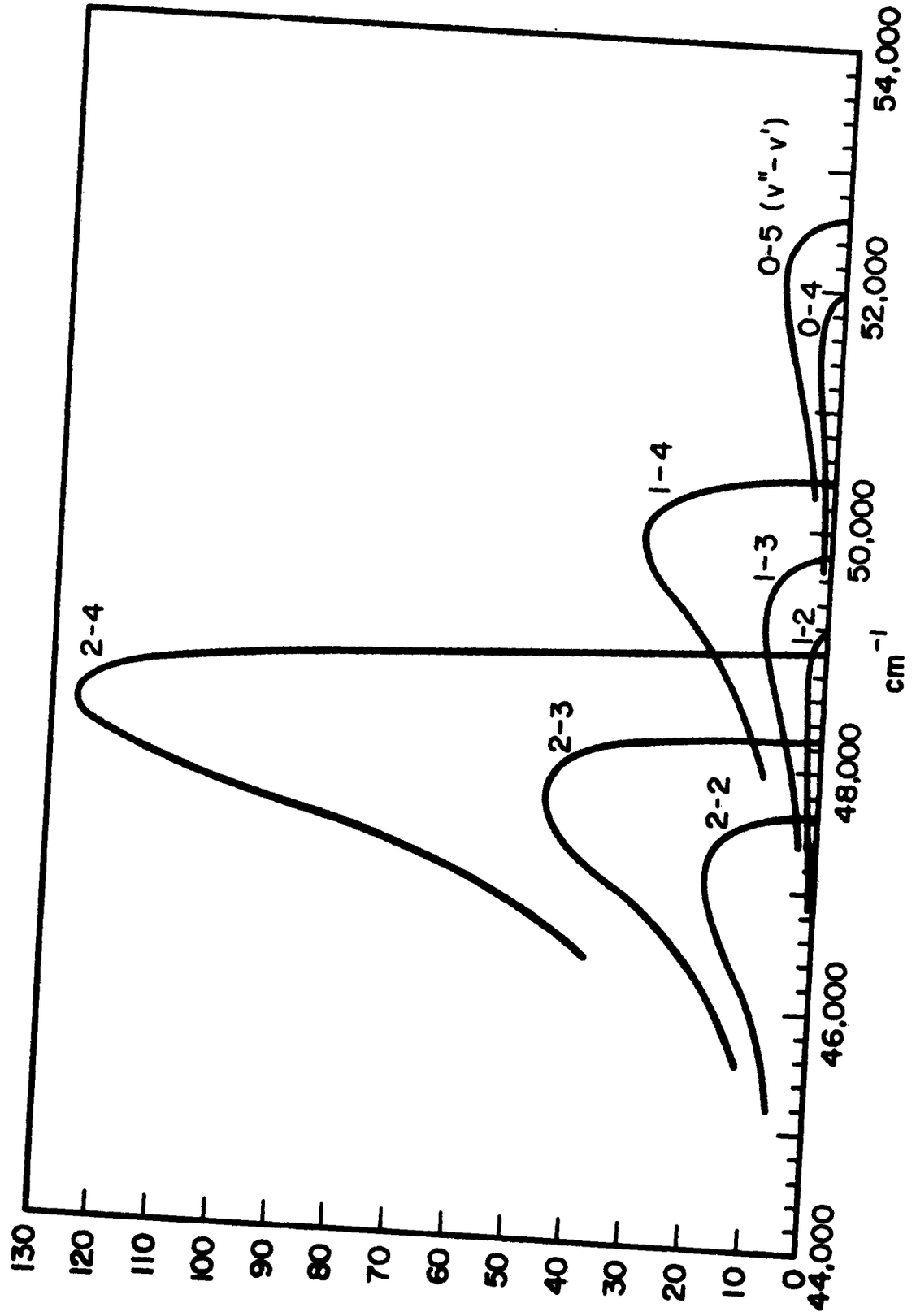


**Figure 3.** Intensity distribution in $O_2$ Schumann-Runge bands at $T = 3,000^{\circ}K$

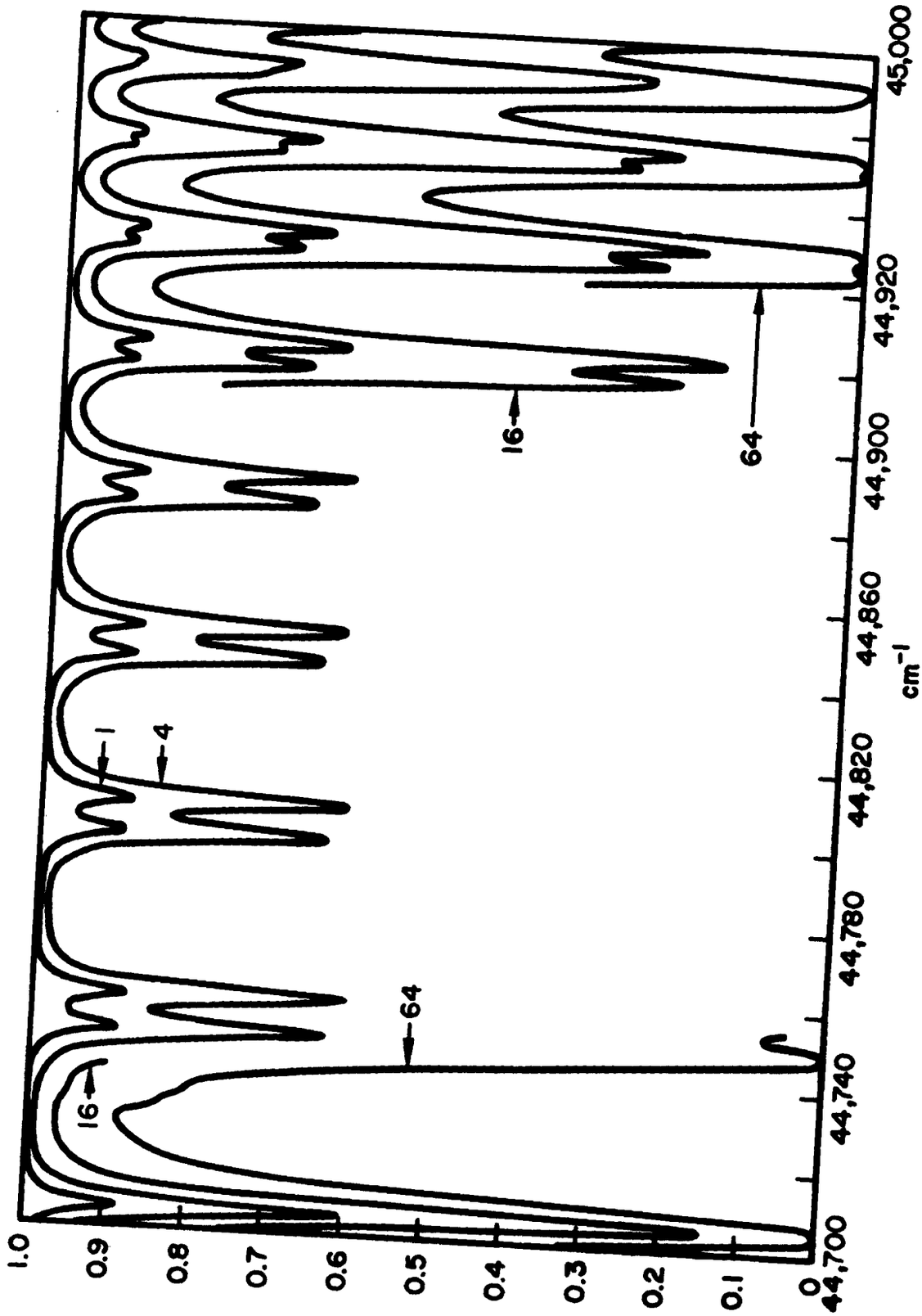


Figure 4. Fractional transmission in part of the 5-5 band for various path lengths

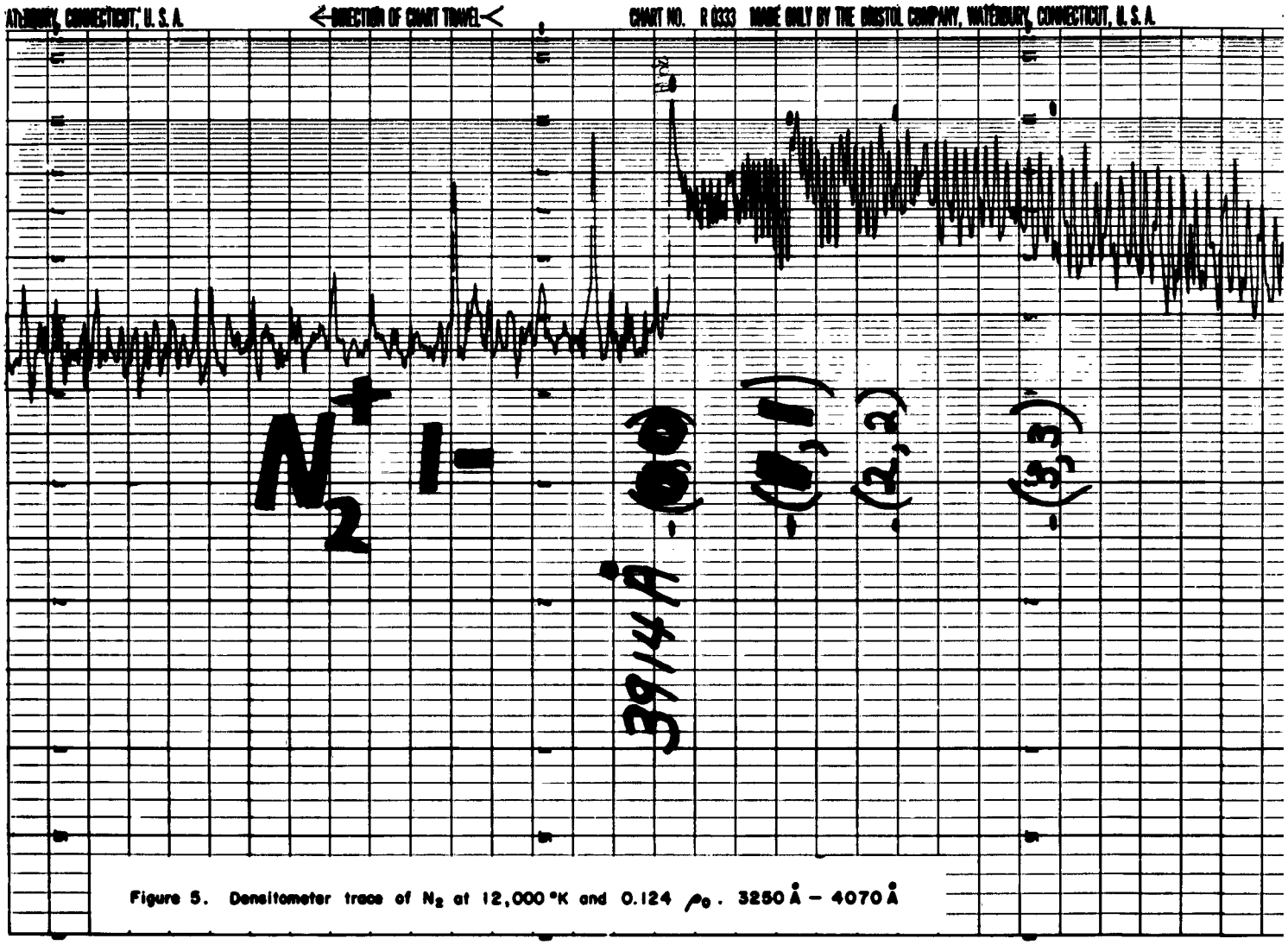


Figure 5. Densitometer trace of $N_2$ at 12,000 °K and 0.124 $\rho_0$. 3250 Å – 4070 Å

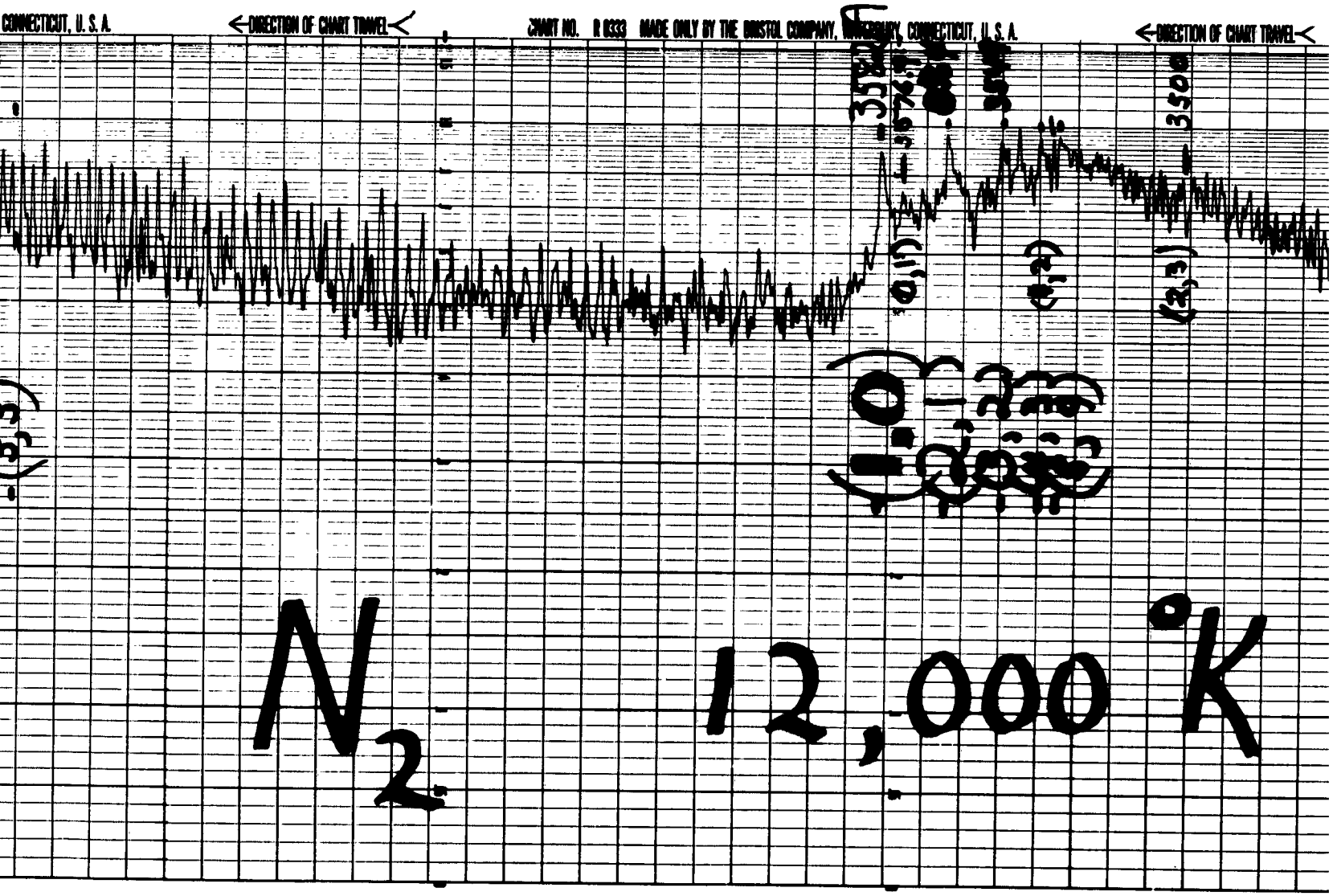
CONNECTICUT, U. S. A.
←DIRECTION OF CHART TRAVEL
CHART NO. B 6333 MADE ONLY BY THE BRISTOL COMPANY, WATERBURY, CONNECTICUT, U. S. A.
←DIRECTION OF CHART TRAVEL
$N_2$
12,000 °K

2

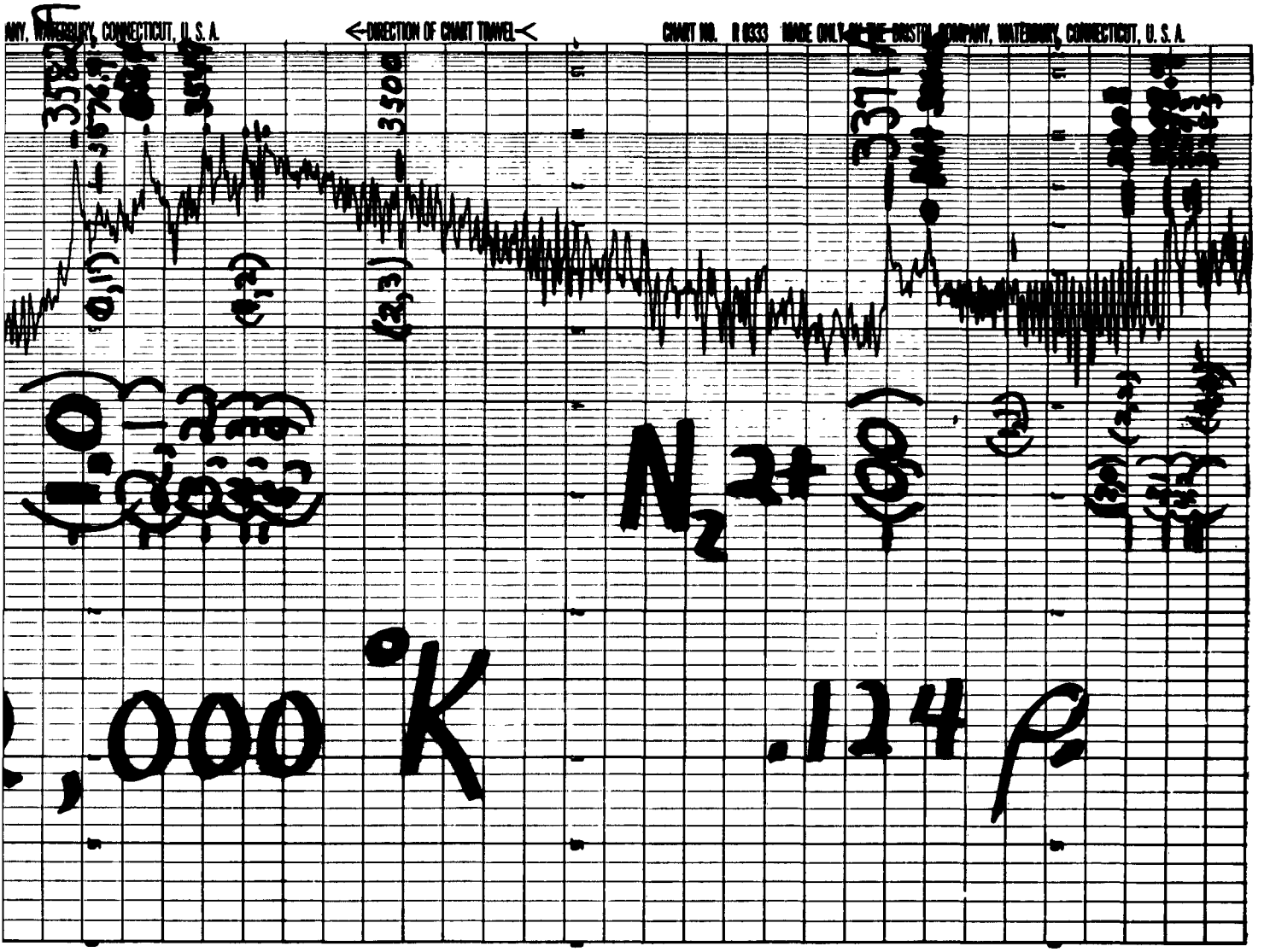
←DIRECTION OF CHART TRAVEL←
CHART NO. R 6553
$N_2 2+$
.124 μ

not affect this argument since the ratio of emission and absorption is also a slowly changing function of wave length. The gradual change of absorption suggests that it may be sufficient to solve the transport equation properly in a small number of fairly narrow frequency intervals such as the one shown in figure 4 and use these results to obtain averages for the entire spectrum.

A machine code to do this has been written and has been very nearly checked out. Details, such as optimal values for the width and the number of intervals, have to be found by experimenting with this code. It is estimated that an interval may contain an average of 20 and certainly less than 200 lines, and that there may be a total of 20 such intervals.

The general procedure then is as follows. For a given time in the history of the explosion at which density and temperature profiles are known, one can obtain densities and temperatures along any ray through the fireball. One can therefore calculate absorption coefficients along such rays for the selected frequencies within each one of the narrow intervals. By integrating the transport equation, one thus obtains the intensities $I_\nu$ which are then averaged for each narrow interval to form $\bar{I}_\nu = \frac{1}{\Delta\nu} \int I_\nu d\nu$. The next step is to interpolate $\bar{I}_\nu$ with respect to frequency, and some work is currently underway to devise a good procedure for doing this. The interpolated $I_\nu$ is then integrated over the entire spectrum to form

$I = \int_0^\infty \bar{I}_\nu d_\nu$. One can now calculate the cooling rate $\int \frac{dI}{ds} \, d\Omega$, enter this into the energy equation, and advance the hydrodynamic calculation.

## REFERENCES


1. Chandrasekhar, S., Radiative Transfer, Dover 1960
2. Meyerott, R. E., et al., Of Quantitative Spectroscopy and Radiative Transfer
3. Meyerott, R. E., Sokoloff, J., and Nicholls, R. A., Absorption Coefficients of Air. Geophysical Research Paper 68
4. Armstrong, B. H., Holland, D. H., and Meyerott, R. E., Absorption Coefficients of Air from 22,000° to 220,000°. SWC TR-58-36, August 1958
5. Herzberg, G., Molecular Spectra and Molecular Structure. I. Diatomic Molecules. D. Van Nostrand 1950
6. Treanor, C. E., and Wurster, W. H. Measured Transition Probabilities for the Schumann-Runge System of Oxygen. Journal Chemical Physics, 32, 758, 1960
7. Jarmain, W. R., Fraser, P. A., and Nicholls, R. W., Vibrational Transition Probabilities of Diatomic Molecules; Collected Results Astrophysics Journal 122, 55, 1955

# NUMERICAL METHODS FOR HYDRODYNAMICS WITH RADIATION TRANSPORT

Dr. R. A. Grandey
Aeronutronic Division, Ford Motor Company

## 1. THE EQUATIONS OF RADIATION TRANSPORT.

The integrodifferential equations of radiation transport are obtained by simultaneously solving the time dependent Boltzman transport equation for the radiation, which is a continuity equation, and the equation expressing overall conservation of material plus radiant energy. The energy equation is written in the form

$$\frac{dE_m}{dt} + P\frac{dV}{dt} + \frac{\partial E_r}{\partial t} + \nabla\cdot\vec{F} = 0.$$

Here $E_m$ is the material energy density, $E_r$ the radiation density, P the total pressure, V the specific volume and F the net flux of radiation. The third and fourth terms of this equation are expressed as integrals, over frequency and direction, of the Boltzman equation.

The Boltzman transport equation gives the time rate of change of intensity of radiation of frequency $\nu$ traveling in a direction $\vec{w}$. This intensity will be a function of time and position:

$$I_{\nu,w} = I_{\nu,w}(\vec{r}, t, \nu, \vec{w})$$

where $\vec{r}$ is the position vector and t the time. The transport equation may be written generally in the following form:

$$\frac{1}{c}\frac{\partial I_{\nu,w}}{\partial t} + (\vec{w}\cdot\nabla) I_{\nu,w} = -K_\nu^{(a)}\rho I_{\nu,w} + \rho j_{\nu,w} - K_\nu^{(s)}\rho I_{\nu,w} + \int \rho K_\nu^{(s)}(w,w') I_{\nu,w'}\, dw' \qquad (1)$$

The left side of this equation represents 1/c times the total time derivation of $I_{\nu,w}$. The first term on the right represents photons removed by absorption processes, $K_\nu^{(a)}$ being the absorption coefficient. The second term on the right represents photon production by emission from the material, the third term those photons lost by scattering, and the fourth those added by scattering from other directions, $\vec{w}'$, into the direction $\vec{w}$. In this equation P is the

material density, $j_{\nu,w}$ the emission coefficient and $K_\nu^{(s)}$, scattering coefficient.

Our problems will assume slab or spherical symmetry, in which case $I_{\nu,w}$ is a function of only one coordinate x and the angle $\theta$ between the direction of symmetry and the direction of travel of the photon in question:

$$I_{\nu,w} = I_{\nu,w}(x,t,\nu,\theta) = I_{\nu,\mu}(x,t,\nu,\mu)$$

where $\mu = \cos\theta$. We may write equation (1) as

$$\frac{1}{c}\frac{\partial I_{\nu,\mu}}{\partial t} + \mu\frac{\partial I_{\nu,\mu}}{\partial x} + \frac{\alpha(1-\mu^2)}{2x}\frac{\partial I_{\nu,\mu}}{\partial \mu} = \rho[-K_{\nu,\mu} I_{\nu,\mu} + j_{\nu,\mu}] + \int \rho K_\nu^{(s)}(\mu,\mu') I_{\nu,\mu'}\, d\mu' d\phi' \tag{2}$$

$K_{\nu,\mu}$ is the total "absorption" coefficient, i.e., the sum of the pure absorption and pure scattering coefficients. $\alpha = 0$ or 2 for slab or spherical geometry respectively.

The net monochromatic flux, $F_\nu$, traversing unit area is a vector in the x-direction with magnitude $2\pi c \int_{-1}^{1} I_{\nu,\mu}\,\mu\, d\mu$. The total flux F is defined by the $\int F_\nu d\nu$ or:

$$\bar{F} = F_x = 2\pi c \int_0^\infty \int_{-1}^{1} I_{\nu,\mu}\,\mu\, d\mu\, d\nu \tag{3}$$

The radiation energy density is the integral of $I_{\nu,\mu}$ over direction and frequency, i. e.

$$E_r = 2\pi \int_0^\infty \int_{-1}^{1} I_{\nu,\mu}\, d\mu\, d\nu \tag{4}$$

Thus the energy equation may be written as:

$$\frac{1}{c}\left(\frac{dE_m}{dt} + P\frac{dV}{dt}\right) + \frac{2\pi}{c}\int_0^\infty\int_{-1}^{1}\frac{\partial I_{\nu,\mu}}{\partial t}\, d\mu\, d\nu + 2\pi\int_0^\infty\int_{-1}^{1} x^{-\alpha}\frac{\partial (x^\alpha I_{\nu,\mu})}{\partial x}\,\mu\, d\mu\, d\nu = 0 \tag{5}$$

The transport equation is applied to assist in evaluating the integrals appearing in this equation.

The term $j_{\nu,\mu}$ in the transport equation represents both spontaneous and induced emission. Its form is sensitive to whether or not local thermodynamic equilibrium exists for the material. If local equilibrium is assumed, it may be expressed in terms of the absorption coefficient $K_\nu^{(a)}$ and the Planck spectrum. By combining this with the absorption term, equation (2) becomes

$$\frac{1}{c}\frac{\partial I_{\nu,\mu}}{\partial t} + \mu\frac{\partial I_{\nu,\mu}}{\partial x} + \alpha\frac{(1-\mu^2)}{2x}\frac{\partial I_{\nu,\mu}}{\partial \mu} = \tag{6}$$

$$\rho K_\nu^{(a)}\left(1-e^{-h\nu/kT}\right)\left[\frac{2h}{c^3}\frac{\nu^3}{\left(e^{h\nu/kT}-1\right)} - I_{\nu,\mu}\right] - \rho K_\nu^{(s)} I_{\nu,\mu}$$

$$+ \int \rho K_\nu^{(s)}(\mu,\mu') I_{\nu,\mu'}\, d\mu' d\phi'$$

In our problem, scattering may often be ignored in comparison with the emission process. In this case,

$$\frac{1}{c}\frac{\partial I_{\nu,\mu}}{\partial t} + \mu\frac{\partial I_{\nu,\mu}}{\partial x} + \alpha\frac{(1-\mu^2)}{2x}\frac{\partial I_{\nu,\mu}}{\partial \mu} = \rho K_\nu^{(a)}\left(1-e^{-\beta}\right)$$

$$\left[\frac{2h\nu^3}{c^3\left(e^{\beta}-1\right)} - I_{\nu,\mu}\right] \equiv \lambda_\nu^{-1}\left[J_\nu - I_{\nu,\mu}\right]. \tag{7}$$

Generally, we must solve equations (5) and (7) subject to the appropriate boundary conditions. Introduce an integrated intensity

$$I = 2\pi\int_0^\infty I_{\nu,\mu}\, d\nu$$

by integrating equation (7) over $d\nu$:

$$\frac{1}{c}\frac{\partial I}{\partial t} + \mu\frac{\partial I}{\partial x} + \alpha\frac{(1-\mu^2)}{2x}\frac{\partial I}{\partial \mu} = \frac{aT^4}{2\lambda_t} - \int_0^\infty \lambda_\nu^{-1} I_{\nu,\mu}\, d\nu \tag{8}$$

where $\lambda_t$, the transport mean free path, is defined by $\lambda_t^{-1} = \dfrac{\int_0^\infty \lambda_\nu^{-1} J_\nu\, d\nu}{\int_0^\infty J_\nu\, d\nu}$

and a is the Stefan-Boltzman constant. The second term in equation (5) may be eliminated by integrating (8) over $d\mu$:

$$\frac{1}{c}\frac{\partial}{\partial t}\int_{-1}^{1} I\, d\nu = \lambda_t^{-1} a T^4 - \int_0^\infty\int_{-1}^{1} \lambda_\nu^{-1} I_{\nu,\mu}\, d\mu\, d\nu - \int_{-1}^{1}\left[\mu\frac{\partial I}{\partial x} + \alpha\frac{(1-\mu^2)}{2x}\frac{\partial I}{\partial \mu}\right] d\mu \tag{9}$$

$$\text{or: } \frac{1}{c}\left(\frac{dE^m}{dt} + P\frac{dV}{dt}\right) + \lambda_t^{-1} a T^4 - \int_0^\infty\int_{-1}^{1} \lambda_\nu^{-1} I_{\nu,\mu}\, d\mu\, d\nu - \frac{\alpha}{2x}\int_{-1}^{1}\left[(1-\mu^2)\frac{\partial I}{\partial \mu} - 2I\mu\right] d\mu = 0$$

Our problem is to solve equations (8) and (9).

All equations are linear in the radiation intensities. Let us therefore write the monochromatic intensity as the sum of two terms: one including radiation due to material at a local temperature T, and the other radiation coming from an external source in transit through the material. The first term will include radiation flowing into the material from neighboring material not necessarily at exactly the same temperature. That is, define $I_{\nu,\mu} = I^P_{\nu,\mu} + I^E_{\nu,\mu}$; $I = I^P + I^E$, where the superscripts stand for Planck and external, and write separate continuity equations for the two components:

$$\frac{1}{c}\frac{\partial I^P}{\partial t} + \mu\frac{\partial I^P}{\partial x} + \frac{\alpha(1-\mu^2)}{2x}\frac{\partial I^P}{\partial \mu} = \frac{aT^4}{2\lambda_t} - \int_0^\infty \lambda_\nu^{-1} I^P_{\nu,\mu}\, d\nu \tag{10}$$

$$\frac{1}{c}\frac{\partial I^{E}_{\nu,\mu}}{\partial t} + \mu\frac{\partial I^{E}_{\nu,\mu}}{\partial x} + \frac{\alpha(1-\mu^2)}{2x}\frac{\partial I_{\nu,\mu}}{\partial \mu} = -\lambda_\nu^{-1} I^{E}_{\nu,\mu} \tag{11}$$

Specializing to the case of $\alpha = 0$ for simplicity, the energy equation (9) may be written as:

$$\frac{1}{c}\left(\frac{dE_m}{dt} + P\frac{dV}{dt}\right) + \left[\lambda_t^{-1} a T^4 - \int_0^\infty\int_{-1}^{1} \lambda_\nu^{-1} I^{P}_{\nu,\mu}\, d\mu\, d\nu\right] \tag{12}$$

$$- \int_0^\infty\int_{-1}^{1} \lambda_\nu^{-1} I^{E}_{\nu,\mu}\, d\mu\, d\nu = 0.$$

The diffusion approximation for the Planck spectrum is obtained by assuming that $\rho K_\nu^{(a)}$ is very large, or that $\lambda_\nu$ is small compared to dimensions over which quantities vary appreciably. In this case, an expansion of $I^{P}_{\nu,\mu}$ as a power series in $\mu$ converges rapidly. The result of such an approximation is the usual diffusion equation; plus an additional term involving $I^{E}$:

$$\frac{d}{dt}\left(E_m + aT^4\right) + P\frac{dV}{dt} - \frac{c}{3}\frac{\partial}{\partial x}\left(\lambda_r \frac{\partial (aT^4)}{\partial x}\right) - c\int_0^\infty\int_{-1}^{1} \lambda_\nu^{-1} I^{E}_{\nu,\mu}\, d\mu\, d\nu = 0 \tag{13}$$

where $\lambda_r$, the Rosseland mean free path, is defined by

$$\lambda_r = \frac{\int_0^\infty \lambda_\nu \frac{\partial J_\nu}{\partial T}\, d\nu}{\int_0^\infty \frac{\partial J_\nu}{\partial T}\, d\nu} = \frac{\pi}{aT^3}\int_0^\infty \lambda_\nu \frac{\partial J_\nu}{\partial T}\, d\nu$$

In several applications, it may be possible to make use of equation (13) in treating the Planck radiation, using equation (11) to treat the transport of external radiation through the material. In cases where the diffusion approximation is not valid for the Planck spectrum, a second appreciable simplification is still possible. Returning to equation (7), the right hand side of this equation may be written $\lambda_\nu^{-1}(J_\nu - I^{P}_{\nu,\mu} - I^{E}_{\nu,\mu})$. The integral of the first term

of this expression led to introduction of the transport mean free path, $\lambda_t$. It is seen to be appropriate to use this same mean free path as an approximation in equations (10) and (12) in the term involving $I^P$:

$$\frac{1}{c}\frac{\partial I^P}{\partial t} + \mu \frac{\partial I^P}{\partial x} = \lambda_t^{-1}\left(\frac{aT^4}{2} - I^P\right) \tag{14}$$

$$\frac{1}{c}\left(\frac{dE_m}{dt} + P\frac{dV}{dt}\right) + \lambda_t^{-1}\left(aT^4 - \int_{-1}^{1} I^P d\mu\right) - \int_0^{\infty}\int_{-1}^{1} \lambda_\nu^{-1} I^E_{\nu,\mu}\, d\mu\, d\nu = 0 \tag{15}$$

We shall have to follow the changing frequency spectrum of $I^E_{\nu,\mu}$ in time as it transports through the material. The number of frequency groups necessary and the expense of treatment will depend on the shape of the spectrum and the precise dependence of $\lambda_\nu$ on $\nu$.

Inclusion of the pure scattering terms and the extra terms for the spherically symmetric case do not introduce any difficulties and have been omitted only for convenience in the discussion.

## 2. NUMERICAL INTEGRATION OF THE TRANSPORT EQUATIONS.

Three approaches have been taken toward solving the transport equations. The chief problem is treating the angular integration. An immediate extension of the diffusion approximation is to use higher order terms in $\mu$, or, equivalently, to expand $I(\mu)$ in Legendre polynomials, since one can then make use of the various recursion and orthogonality relations existing. This approach leads to a set of $L + 1$ equations for the Legendre coefficients if polynomials up to order $L$ are used in the expansion. I may be defined by an $L + 1$ component vector consisting of the Legendre coefficients and finite difference methods applied to the resultant vector equation. The coefficients in the vector equation are $L + 1$ by $L + 1$ matrices. The difficulty of this so-called "Spherical Harmonic Method" is that an implicit difference scheme is required for unconditional stability and the scheme must be implicit both with respect to the space coordinate and the "1 coordinate," yielding very cumbersome equations.

A second approach is based on the "method of discrete ordinates." The distribution function is sampled in each of a finite number of directions, and

separate equations written for the individual directions. The two approaches are related, inasmuch as if L + 1 discrete angles are used for sampling, the solution can be fitted with the first L spherical harmonics. Wick and Chandrasekhar developed this approach independently using a Gaussian quadrature approximation for the angle integrals. It can be shown that the results from this approach are identical to results of the spherical harmonic method.

This method, which uncouples the equations angularly, is much more tractable than the spherical harmonic method if it is desired to obtain unconditionally stable finite difference equations.

3. THE CARLSON $S_n$ METHOD.

The $S_n$ method is also a discrete ordinate scheme in carrying out the integration over angle. It differs from the Wick-Chandrasekhar (W-C) method in several respects. The centering with respect to $\mu$ is done differently and a trapezoidal rather than Gaussian quadrature is used to perform the integration over angle.

The $S_n$ method divides the $\mu$ interval into n subintervals: $-1 = \mu_0 < \mu, < - - - < \mu_n = +1$. If $\mu_i = -1 + {}^{2i}/_{n}$, the $\mu$-mesh is said to be standard. Other choices may be appropriate to some problems.

In the W-C method, the transport equations are centered at the $\mu$-mesh points. $S_n$ centers these equations at the midpoint of the $\mu$-intervals:

$$\frac{1}{c}\frac{\partial I^{P}_{i+1/2}}{\partial t} = -\mu_{i+1/2}\frac{\partial I^{P}_{i+1/2}}{\partial x} - \frac{\alpha(1-\mu^{2}_{i+1/2})}{2x}\frac{\partial I^{P}}{\partial \mu}\bigg|_{i+1/2} \qquad (16)$$

$$+\lambda_t^{-1}\left(\frac{aT^{4}}{2} - I^{P}_{i+1/2}\right)\left(0 \le i < n\right)$$

This set of n equations in n + 1 unknowns is completed by adding the equation centered at i = o ($\mu = -1$):

(16a)

$$\frac{1}{c}\frac{\partial I^{P}_{o}}{\partial t} = \frac{\partial I^{P}_{o}}{\partial x} + \lambda_t^{-1}\left(\frac{aT^{4}}{2} - I^{P}_{o}\right)$$

Assume that $I^E$ may be represented by K frequency groups

$I^E_{\nu,\mu} \cong \sum_{K=1}^{K} I_{K,\mu}$ and write separate transport equations analagous to equations (16) and (16a) for the K components:

$$\frac{1}{c}\frac{\partial I_{K,j+1/2}}{\partial t} = -\mu_{j+1/2}\frac{\partial I_{K,j+1/2}}{\partial x} - \alpha\frac{(1-\mu^2_{j+1/2})}{2x}\frac{\partial I_K}{\partial \mu}\Big|_{j+1/2} \quad (17)$$

$$-\lambda_K^{-1} I_{K,j+1/2} \quad (0 \leq j < J)$$

$$\frac{1}{c}\frac{\partial I_{K,0}}{\partial t} = \frac{\partial I_{K,0}}{\partial x} - \lambda_K^{-1} I_{K,0} \quad (17a)$$

The number of angular groups required for accuracy may be different for $I^P$ and $I^E$. It is planned to allow for using an $S_I$ integration for the Planck spectrum and an $S_J$ integration for the "external" radiation.

3.1 The $S_n$ Difference Equations.

Equations (17) and (17a) will be used to illustrate Carlson's differencing methods. A more complicated procedure is required if anisotropic scattering (like Thomson scattering) is included but we shall not discuss this in the interests of simplicity and time. We shall drop the K subscript for simplicity.

Equation (17) is written in terms of the intensities at $\mu$-mesh points j and j+1 by performing an integration over $\mu$ under the assumption that the intensity I is linearly dependent on $\mu$ in the interval (a trapezoidal approximation):

$$I_\mu = I_{j-1} + (I_j - I_{j-1})\frac{\mu - \mu_{j-1}}{\mu_j - \mu_{j-1}}$$

$$\frac{\partial I_\mu}{\partial x} = \frac{\partial I_{j-1}}{\partial x} + \left(\frac{\partial I_j}{\partial x} - \frac{\partial I_{j-1}}{\partial x}\right)\frac{\mu - \mu_{j-1}}{\mu_j - \mu_{j-1}}$$

$$\frac{\partial I_\mu}{\partial \mu} = \frac{I_j - I_{j-1}}{\mu_j - \mu_{j-1}}$$

$$\frac{\partial I_\mu}{\partial t} = \frac{\partial I_{j-1}}{\partial t} + \left(\frac{\partial I_j}{\partial t} - \frac{\partial I_{j-1}}{\partial t}\right)\frac{\mu - \mu_{j-1}}{\mu_j - \mu_{j-1}}$$

The above are introduced into equation (17) and an integration performed over $\mu$ from $\mu_{j-1}$ to $\mu_j$. We note that

$$\int_{j-1}^{j} I_{k,\mu}\, d\mu = \tfrac{1}{2}(\mu_j - \mu_{j-1})(I_{k,j} + I_{k,j-1}) \equiv \tfrac{1}{2} l_j (I_{k,j} + I_{k,j-1})$$

$$\int_{j-1}^{j} \mu I_{k,\mu}\, d\mu = \tfrac{1}{2} l_j (a_j I_j + \bar{a}_j I_{j-1})$$

$$\int_{j-1}^{j} (1-\mu^2)\frac{\partial I_\mu}{\partial \mu}\, d\mu = \tfrac{1}{2} l_j b_j (I_j - I_{j-1})$$

where:

$$a_j \equiv \tfrac{1}{3}(2\mu_j + \mu_{j-1})$$

$$\bar{a}_j \equiv \tfrac{1}{3}(\mu_j + 2\mu_{j-1})$$

$$b_j \equiv \frac{2}{3}\frac{(3 - \mu_j^2 - \mu_j\mu_{j-1} - \mu_{j-1}^2)}{(\mu_j - \mu_{j-1})}$$

Introducing these into equation (17) and multiplying by $2/l_j$:

$$\left[\tfrac{1}{c}\frac{\partial}{\partial t} + a_j\frac{\partial}{\partial x} + \frac{\alpha}{2x} b_j + \lambda^{-1}\right] I_j + \left[\tfrac{1}{c}\frac{\partial}{\partial t} + \bar{a}_j\frac{\partial}{\partial x} - \frac{\alpha}{2x} b_j + \lambda^{-1}\right] I_{j-1} = 0 \qquad (18)$$

(17a) simply becomes:

$$\left[\tfrac{1}{c}\frac{\partial}{\partial t} - \frac{\partial}{\partial x} + \lambda^{-1}\right] I_o = 0 \qquad (18a)$$

Normally, in spherical systems the radiation streams in the direction of increasing $\mu$. The angular dependence is treated by arguing that the differencing should be backward with respect to the direction of flow. It is on this consideration that equations (16a) and (17a) are for $\mu = -1$ rather than for $\mu = +1$. Equation (18a) is solved for $I_o$ which is inserted into the equation involving $I_o$ and $I_1$ which is solved for $I_1$, etc.

We shall now introduce spatial coordinates $X_m$ which define a spatial mesh with an interval $\Delta_m = X_m - X_{m-1}$ and the temporal coordinates $t^\ell$ which define a temporal mesh with an interval $\delta_\ell = t^{\ell+1} - t^\ell$. Let us examine equations (18) and (18a) centered at time t and at the spatial coordinate $X_m$:

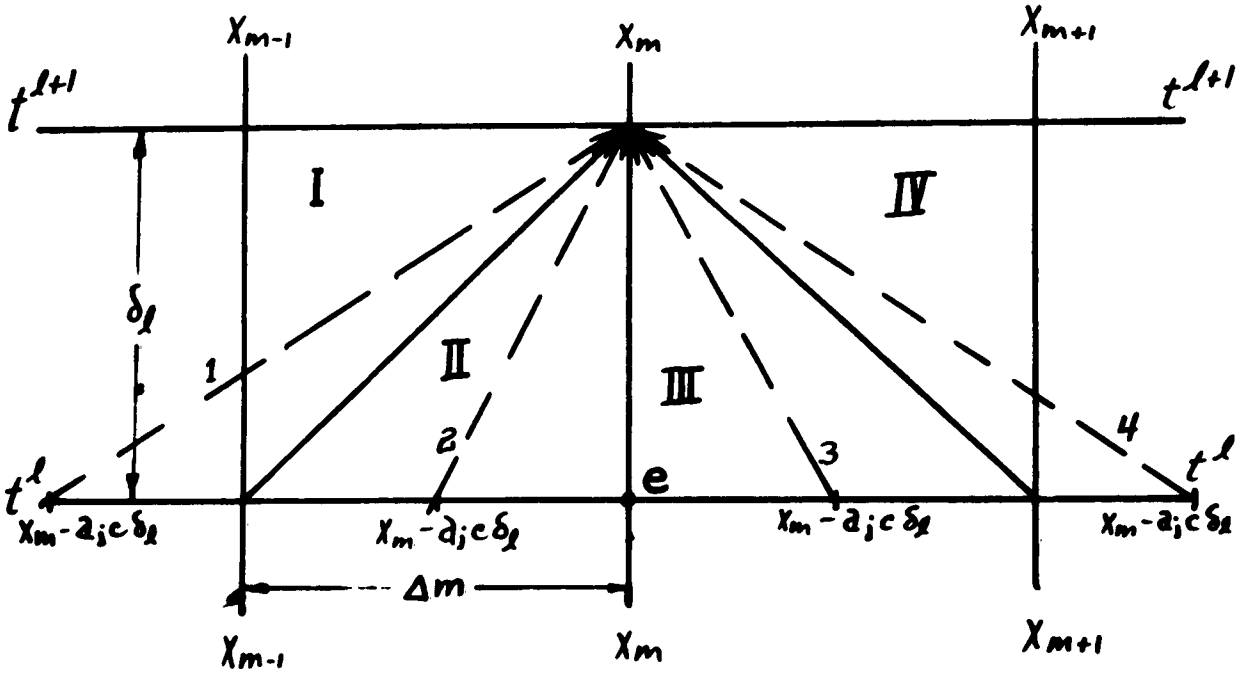


Photons arriving at point $X_m$ at time $t^{\ell+1}$ started from a point on the line $t^\ell$ a distance $ac\delta$ from point e. They traveled along path 1, 2, 3, or 4 depending on the value of $ac\delta$. The spatial and temporal derivatives occurring in equation (18) are formed along the appropriate legs of the triangle traversed by the photons in question. For example, if the photons follow path 1 (if $ac\delta > \Delta_m$), the $\frac{\partial I_j}{\partial x}$ appearing in (18) is differenced as

$$\frac{\partial I_j}{\partial X} \cong \frac{I_j(t^{\ell+1}, X_m) - I_j(t^{\ell+1}, X_{m-1})}{\Delta m}$$

and the $\frac{\partial I_j}{\partial t}$ as

$$\frac{\partial I_j}{\partial t} \cong \frac{I_j(t^{l+1}, X_{m-1}) - I_j(t^l, X_{m-1})}{\delta_l}$$

The result of the above will be an implicit finite difference equation for $I_j(t^{l+1}, X_m) \equiv I^{l+1}_{j,m}$ Generally, similar equations will exist for each frequency group, and it will be necessary to define $I^{l}_{k,j,m}$.

It should be noted that the transport equations are coupled angularly through the scattering integral and, in the case of spherical symmetry, through the term $\frac{(1-\mu^2)}{x} \frac{\partial I}{\partial \mu}$. In slab geometry with no scattering the equations are not coupled angularly and an $S_n$ -type calculation would not be required.

A third approach was mentioned. It is also possible to write the angular dependence in an integral form and apply iterative techniques which will converge to the correct solution[2].

## REFERENCES

1. Charlson, B. G., LA-1599, October 1953 and subsequent
2. Wilf, H. S., Journal of Mathematics and Physics, Vol. 1, p. 225

# SHOCK-INDUCED REACTIONS*

Dr. O. A. Nance
E. H. Plesset Associates, Inc.

In discussing the possibility of shock-induced reactions in condensed phases, we find that even reliance on the weak reed of chemical reaction theory eludes us. We can only hope to avoid the nonsequitur that experimental evidence provides many examples of this phenomenon.

The framework of gas phase reaction kinetics is dually supported, by thermodynamics and by the "absolute" rate theory. Classically, reactions are supposed to occur by "activation" of a molecule through collision or absorption of radiation. If the activated molecule simultaneously or subsequently encounters another appropriate molecule, a bimolecular reaction may occur. Alternatively, the activated molecule may decompose in a unimolecular reaction. To various degrees of sophistication, we may calculate the number of collisions occurring as a function of concentration and temperature.

Calculation of the rate of reaction from the number of collisions alone usually leads to a gross overestimate of the rate. The next level of approximation requires an estimate of the energy involved in collisions and an estimate of the probability of transferring an effective amount of energy to one of the colliding particles. The first formal expression is due to Arrhenius and takes the form $k = Ae^{-E_a/RT}$, where k is the specific rate constant, A is a frequency factor and $E_a$ is the energy of activation. This expression was inherently an empirical description of the variation of reaction rate with temperature. "A" can be related to the number of collisions but with only indifferent success except in the case of simple bimolecular reactions between atoms.

If we add the concept of the Maxwell distribution, we gain the concept of the fraction of molecules capable of undergoing effective collisions and the concept of at least a quasi-equilibrium state which will maintain the population of "hot" molecules. Use of this new information improved the calculation

* This report is based on preliminary results of work sponsored by the Richfield Oil Corporation. Potential applications to petroleum technology are subject to patent rights sought by that Company.

of the frequency factor in simple cases but gave no clue to the predictability of the energy of activation.

With the advent of the absolute rate theory, a major practical advance occurred; unfortunately the quantitative gains and theoretical validity were severely limited. In this theory we consider a potential energy surface representing the reacting system in the pertinent region of configuration and momentum space. One assumes a quasi-equilibrium distribution of the macro state with respect to this surface and examines those portions of the potential energy surface with which externally recognizable chemical changes may be correlated. In the customary notation, we write

$$k_r = \left(\frac{kT}{h}\right) e^{\Delta S^{\neq}/R_e} e^{-\Delta H^{\neq}/RT} = \frac{kT}{h} \frac{Q^{\neq}}{\pi Q_i} e^{-\Delta E_0^0/RT}$$

Where $k_r$ is the specific rate constant

T is absolue temperature

h is Planck's constant

$\Delta E_0^0$ is the difference in "ground state" between normal and activated species

Q represents a partition function

$\Delta S^{\neq}$ is the entropy of activation

$\Delta H_{\neq}$ represents part of the energy of activation

The superscript $\neq$ refers to the activated species and the subscript $\neq$ refers to the quantity after the "reaction coordinate" is removed. The product of $Q_i$ over "i" is necessary when several reactant species are involved. It will be necessary to refer the reader to standard texts or reference works for discussion of the development of these expressions.

The point of outlining the background briefly here is to permit a discussion of the situations in which misapplication is possible. The first set of terms defines the rate in thermodynamic variables; this is of value primarily in recognition of the source of a temperature dependent and a temperature independent term, together with clues to the application of statistical mechanical concepts. One will note that the factor $\frac{kT}{h}$ appears in both expressions and that it has been borrowed from $\Delta H^{\neq}$ in one case and from $Q^{\neq}$ in the other (noted by demotion of the symbol $\neq$ to a subscript).

In the second expression, the partition functions are taken with respect to a ground state in each case and the ground state factors are combined in the term $e^{-\Delta E_0^\circ}$. In addition, the partition function has been depleted by the factor $\frac{kT}{h}$; this factor is usually interpreted as the partition function of the "reaction coordinate", treated as a very "stiff" vibration. That is, it is assumed that an important characteristic of the activated complex is the occurrence of an appropriate amount of energy in a "degree of freedom" of the complex such that motion in that one coordinate can produce the observed macroscopic reaction. In terms of the potential energy surface, motion in this coordinate leads from "reactant" to "product" portions of the energy surface. Roughly speaking, $\Delta E_0^\circ$, is the least upper bound of the energy required to surmount the potential barrier and thus is in excess of the quantities $\Delta H^\neq$ or $E_a$ which are averages of the energy barrier from a given level to the transition level, weighted by the energy distribution for the reactant species.

For gas phase reactions of simple species, the partition functions may be approximated and estimates may be made of the partition functions for postulated activation configurations. Furthermore, we have a reasonable idea of the use of temperature, both to describe the energy partition and to calculate the number and effect of collisions. We can also estimate the effect of pressure on the rate of reaction and on the distribution of products, if several reaction paths are possible. Increasing the pressure on a gas raises the temperature and increases the concentration of reactant species; it also increases the probability of deactivation and, unless the activated complex is more compact than the separated reactants, may lead to increase or decrease in reaction rate, depending on the specific reaction mechanism.

In the gas phase, the probable collision orientations and transfer of energy between degrees of freedom is also somewhat amenable to treatment. In particular, the energy content is not readily exchanged between translation and either rotation or vibration, i.e., there is difficulty in transferring translational energy and there is a corresponding persistence of vibrational excitation when it does occur. The effectiveness of vibrational energy in complex molecules is complicated as well by the possibility of delocalization and localization which arises from anharmonic contributions to the potential functions.

Statistical theory of transport.

The fundamental questions which apply here simply emphasize the limitations of reaction theory in general. One of the fundamental difficulties heretofore has been that theories predicting reaction rates have postulated equilibrium states and used thermodynamic expressions more from desperation than sagacity. A fruitful and logical point of attack must lie in the larger question of description of the approach to equilibrium and irreversible processes in statistical mechanical terms.

In attempting to predict kinetic processes we are attempting to assess the behavior of perturbed regions, molecular aggregates, or individual molecules in a macroscopic system which may be at or near equilibrium. This point has long been recognized, e. g., Kirkwood made significant contributions and was, at the time of his death, a leader in this technique of approach.

It was the author's original intent to discuss nonequilibrium theory in some detail but it became increasingly obvious that such a discussion was impractical under the circumstances. The reader who wishes to pursue the matter is referred to an excellent review article by S. A. Rice and H. L. Frisch which appeared in vol. 11 of the Annual Review of Physical Chemistry (pps. 187 - 272) (Ann. Reviews, Inc., Palo Alto, Calif. - 1960) or to recent papers by Kirkwood and his collaborators, particularly S. A. Rice.

Reactions in condensed phases.

With the foregoing discussion in mind, great audacity is required in applying the theory of gas phase reactions to condensed phases and shock phenomena. To the extent that shocks can raise the local energy content substantially, we can begin to consider reactions in terms of the general theory. Activation leading to unimolecular reactions can probably be accomplished by collisions between neighboring atoms or molecular groups. In the sonic approximation, the transfer of energy to vibrational modes of a crystalline structure is known to be an effective means of energy transfer and we would expect individual species to be subjected to periodic disturbances. Since these disturbances have periods characteristic of the lattice modes, the coupling to atomic vibrations of much higher frequency would be of comparatively low efficiency. In the transonic and strong shock regimes, the efficiency of transfer should appreciably increase. Furthermore, loss of bond vibrational

excitation should be inhibited by the factors which by-passed molecular excitation in the sonic case. Some measure of the vibrational excitation can be obtained in gases by observing the dispersion of supersonic waves; there it is observed that vibrational excitation by one or more quanta can be obtained in the range of $10^2$ - $10^5$ sound-induced collisions. In solids, the situation is more complicated, theoretically and experimentally, but it has been observed that the lifetime of vibrational excitation is of the order of $10^{-9}$ seconds in many cases.

The partition functions for an organic material should be markedly different in gaseous and condensed phases because in condensed phases:

1. the translational modes are strongly coupled to the lattice modes;
2. the rotational degrees of freedom are severely restricted by the limited free space in condensed phases;
3. the vibrational modes of molecules probably have higher effective anharmonicity because of the intermolecular force fields, but are sufficiently different in frequency from the lattice modes to have appreciably different energy content;
4. there is a high degree of degeneracy in the lattice modes.

The entropy of activation in the gas phase may be considered in two parts. The first of these arises from the relative orientation of the colliding molecules at and during collision, and the second derives from configurations assumed during the free oscillation and rotation subsequent to the collision. In the case of condensed phases, both sources of variation of orientation are severely restricted by the nature of the state, particularly in cases where mechanical treatment or preferred bonding configurations are present during reaction or fabrication of the material.

By analogy with phenomena observed following irradiation of molecular aggregates, the predominant reactions appear to be unimolecular dissociation and reaction of activated sites with neighboring atoms or groups. A special case is that in which hydrogen atoms, produced by bond rupture, combine locally or diffuse to react at sites somewhat distant (usually 100 angstroms or less) from the point of origin.

Conventional reactions.

With the differences noted, it should be possible to treat reactions in

condensed phases by the same broad theoretical treatment and some techniques parallel to those used in gas phase kinetics. The temperature is now replaced by the internal energy of the material (with due regard to potential difference in partition functions); the expected duration of the reactions is that of the pulse duration plus one or more characteristic relaxation times which might be distinguishable by variation in product distribution.

The orientation factors are fairly stable and might be treated either by straightforward probability theory for isotropic material, or by considerations of random orientation plus the concept of crystallites familiar to workers in the field of plastics. Since some control over samples is possible, one might be able to use variation in sample fabrication to vary reaction rate and mechanism in experimental studies.

Experimental clues.

The facilities required for study of shock-induced reactions in condensed phases are not readily accessible. One requires instrumental bunkers in locations fairly remote from living areas, a supporting staff capable of sophisticated manipulation of high explosives, and rather elaborate sample containers which can survive the shocks and preserve the samples for post reaction analysis. Needless to say, the experiments are also rather expensive.

Some work has been done in support of the "Plowshare" program by LRL and some work has been supported by the Richfield Oil Corporation at SRI. There are also scattered bits of data which come as by-products of military programs.

One can summarize the available data crudely as follows:

1) severe decomposition of organic materials is produced in times of the order of microseconds by shocks of 250 kb or higher;
2) limited changes in materials occur in the same time intervals down to the order of 20 kb.

Calculation program.

Preparation of a numerical machine code is underway in support of this program. The code consists of a conventional Lagrangian hydrodynamics calculation supplemented by auxiliary sections for reaction calculation. For

materials in which reaction is possible, the logic of the hydrodynamic calculation is interrupted at the point where the pressure and internal energy have been calculated.

Two possible types of reaction have been provided. The first type is a "slow" reaction for which the rate equation has a unimolecular form and the rate constant is written in superficial Arrhenius form, i.e., the rate is first order in concentration and the rate constant consists of the product of a constant and an exponential function of internal energy. During each time cycle, the differential change in concentration and energy is calculated for the predicted reaction and the results used to correct the hydrodynamic quantities. In the event that changes produced by the reaction are comparable to changes produced by the mechanical factors of the shock, an additional iteration is required. In the cases investigated to date, the energy absorbed or produced by the reaction is a small percentage of the total and no additional references to the hydrodynamic portion are required. It is obvious, however, that highly endothermic or exothermic reactions could materially affect shock propagation. A limiting case is that encountered in detonation of explosives, in which the reaction energy is the mechanism for generation of the shock. It may be noted in passing that some of the difficulties in the theory of detonation which have been ascribed to state behavior are probably due to neglect of the effect of high pressure on the reaction rate.

Some preliminary calculations have been made on the effect of an underground nuclear explosion on petroleum bearing formations. An underground nuclear explosion is characterized by initially high attenuation of peak pressure with distance, because of both geometric and energy absorption factors. At the same time it is characterized by persistence of pressure which is greater by several orders of magnitude than the impulse duration of conventional experiments with high explosives. Using reaction constants derived from conventional petroleum technology, the calculations indicate extensive chemical reaction in regions near the detonation with a sharp decline in the amount of reaction at distances where the peak pressure is below about 100 kilobars. This result is to be expected because of the conservative approach in assigning reaction parameters, but the results compare well with the limited experimental data.

We have also proposed that there is probably another type of reaction accompanying shocks and which we have designated the "fast" reaction. It has been observed in shock tube experiments and in detonation of explosives that the observed rate of reaction is frequently higher than that predicted by the theoretical "temperature". J. von Neuman commented on this point in discussing detonation theory of explosives and remarked that the behavior seemed more like that resulting from a mechanical blow than from thermal excitation. He had calculated a reaction rate by a method comparable to our "slow" reaction and found the predicted rate to be less than the observed rate by a factor beyond that which could be explained by parametric ranges available in his theory. Unfortunately, he did not pursue the point.

We have made provision for this second type of reaction in the code but have not used that section, pending further theoretical work. One can, however, discuss some possibilities in phenomenological terms. One postulates that, as the shock strength increases, there is a point at which the particle velocity exceeds that for which the predominant energy transfer is to bulk modes of the material (lattice modes for crystals or crystallites). The effect would then be to transfer increasing fractions of the dissipated shock energy to vibrations of the molecules. On the basis of dispersion of supersonic waves, there is the indication that bond vibrational excitation persists with characteristic half-life of the order of $10^{-9}$ second. With vibration periods of the order of $10^{-13}$ second, there is ample time for reaction or internal transfer of the vibrational excitation. Since unimolecular decompositions are the result of localization of energy in vibrational modes, the effect of relatively direct transfer of shock energy to vibrational excitation would produce reaction rates far higher than those predicted on the basis of the bulk "temperature" of the material. At present, quantitative prediction of the effect seems impossible, and consideration of secondary factors such as the effect of orientation seems pointless except for speculation. Nevertheless, there is a possibility that recognition of the qualitative features of such a reaction might permit the design of fruitful experiments.

From the standpoint of the use of a hydrodynamic code, these considerations emphasize the limitations of a formulation which uses the Richtmyer - von Neuman "Q", since the region of the shock front which is so grossly distorted by the use of an artificial viscosity is just the region in which

accelerated reactions would occur. In addition to consideration of experiments to establish reaction parameters, we are considering known and pursuing novel techniques for treating the shock front phenomena in condensed phases. At present, we have no significant contribution to report.

# CALCULATION OF SPALL BASED ON A ONE-DIMENSIONAL MODEL

Mark Wilkins
Lawrence Radiation Laboratory

## INTRODUCTION.

Consider a one-dimensional model of an HE metal plate system. Since the pressure pulse from the HE at the HE-plate interface decays rapidly with time, a rarefaction wave proceeds forward into the plate, degrading the advancing pulse from the rear. Upon reaching the front surface of the plate where the normal stress must be zero, the pressure pulse is reflected as a receding rarefaction wave. This wave drops the pressure pulse from its initial value to zero; the rarefaction wave proceeding forward is already dropping the pressure such that when the two rarefactions cross the pressure falls below zero. The negative pressure or tension will be related to the amount the pressure has dropped behind the initial pulse when the rarefaction from the front surface has reached a given position. In figure 1 the tension will be approximately the pressure drop "h" that has entered the material before the receding rarefaction has reached the metal-HE interface and a pressure pulse has been transmitted back.

If either the magnitude or rate of increase of tension is great enough, the plate may fracture or spall.

## THE CALCULATIONAL MODEL.

The one-dimensional hydrodynamic equations were solved by the finite difference technique of Von Neumann and Richtmeyer.[1] The tension profiles for three different plate thicknesses were calculated using a high-speed computer together with an assumed equation of state and a method of simulating the burning of HE. The equation of state of the metal in compression was obtained from experimentally measured Hugoniot points. However, in the tension region, a Hooke's law of the form $P = \alpha(\frac{\rho}{\rho_o} - 1)$ was assumed. Here $\rho_o$ is the reference density expressed in gms per cc. A perfect gas law equation of state was used for the HE.[2]

Since the finite difference approximation is based on a Lagrangian description, the physical quantities of each mass element are known at any instant of time. Consequently it is possible to allow the material to split at a zone boundary by introducing the appropriate free surface boundary

conditions. By this technique material separation or spalling may be achieved when the tension falls below a specified amount. Other spall criteria based on strain rate, internal energy, momentum transferred, etc., may be easily introduced.

EXPERIMENTAL TECHNIQUE.

To measure the front surface velocity of HE-driven plates, the usual pin technique and optical methods were used. The experiments used 10cm of Composition B ignited by a plane wave generator. The other dimensions were chosen to maintain a one-dimensional model during the time of interest.

To measure the change in velocity of the front surface of a metal plate, a magnetic method was developed. The plate is the conductor advancing through parallel magnetic field lines. The voltage generated per unit length of the plate is described by

$$\frac{V}{L} = \vec{v} \times \vec{B}$$

V = voltage
L = length of plate
v = velocity
B = magnetic field

In order to measure the voltage and hence the plate velocity, two small wires are placed normal to the plate. As the plate advances into the wires, contact is maintained and the voltage as a function of time is recorded on oscilloscopes.

DISCUSSION.

By examining a plot of the front surface velocity time history of the plate, successive accelerations may be discerned. The time interval between consecutive pushes is equal to the transit time of a receding rarefaction wave plus the time of a compression wave. From the previously determined equation of state of the metal, the shock velocity at the pressure given by the HE can be calculated. The velocity of the rarefaction wave is very nearly equal to the shock velocity, so an easy calculation gives the time interval between consecutive accelerations of the plate front surface.

The time interval calculated from this simple model agrees with the solution given by the difference equations and also with the experimental results for thin metal plates. As the thickness of the plate increases, the time between consecutive accelerations is longer than the calculated times.

It is assumed that the plate has spalled or fractured and the previous simple calculation is no longer valid. A complete analysis of the wave interactions together with a criterion for fracture verifies this assumption. The results of the finite difference calculations which take into account the spall phenomenon correctly predict the time intervals between accelerations found experimentally.

Intuitively, increasing the thickness of the plate should have the following effects:

1. A larger part of the rarefaction wave could enter the material.
2. The pulse shape is changed, causing higher strain rates.
3. The time which a specified plane in the plate is under tension will increase because of the increase in transit time.

Any of the above mechanisms may cause the maximum dynamic strain in the plate to be exceeded, thus allowing the material to fracture or spall.

Other forms of the equation of state in the negative pressure region as well as different spall criteria have been investigated on the computer. The simple model presented here illustrated the effectiveness of the computer as a method of analysis.

RESULTS.

Figures 1, 1A; 2, 2A, and 3, 3A illustrate the results of finite difference calculations which do not contain a spall criterion and the corresponding experimental results. Figures 1 and 1A show the results of 10 cm of HE driving a 0.375 cm thick uranium plate. The agreement between the experiment and calculation is good and it is concluded that the plate did not spall. Figures 2, 2A, and 3, 3A show the corresponding results when the plate has a thickness of 0.545 cm and 0.75 cm. For these cases the acceleration times as measured by experiment do not agree with the calculated times. The conclusion is that the material has spalled and momentum can no longer be transferred. Thus the spalled portion of the plate flies off with the momentum characteristic of the pressure from the head of the original shock minus the amount of momentum transferred back by tension before spall occurred.

The decrease in front surface velocity between accelerations shown by the calculations results from the tensions in the plate. Experimentally this is not seen, since only average velocities are measured in the time interval between accelerations.

The calculations were repeated using a spall criterion of $-0.50 \times 10^{12}$ $\frac{\text{dynes}}{\text{cm}^2}$ ; i.e., the material was allowed to separate if the tension at any point in the material exceeded this amount. Figures 4 and 5 show the results of these calculations as compared to experiment.

Similar calculations using other thicknesses of plates, and a spall criterion based upon tension of about $-.050 \times 10^{12}$ $\frac{\text{dynes}}{\text{cm}^2}$ agreed with the experiment. The assumed equation of state in the region of negative pressure and the criteria for spall used are certainly not correct in every detail; however, the overall good agreement with experiment is justification for applying the technique to other HE metal plate systems.

CONCLUSION.

As stated in the first section, spall results when two rarefactions cross. An obvious method to defeat spall would be to cancel one of the rarefactions. To accomplish this a void can be placed between the HE and the metal. The transmitted shock into the material now has a rising profile instead of a profile that falls behind the shock front. Figures 6 and 6A show the results of calculation and experiment where a 1.5 cm void was introduced between the 0.75 cm plate and the HE.

The experimental methods, while accurate for measuring the changes in front surface velocity, only give average velocities during the intervals between accelerations. It would take separate experiments to establish the slowing down of the front surface as predicted by the calculations. Experiments of this type are presently being conducted.

(This document was originally released as UCRL 6356)

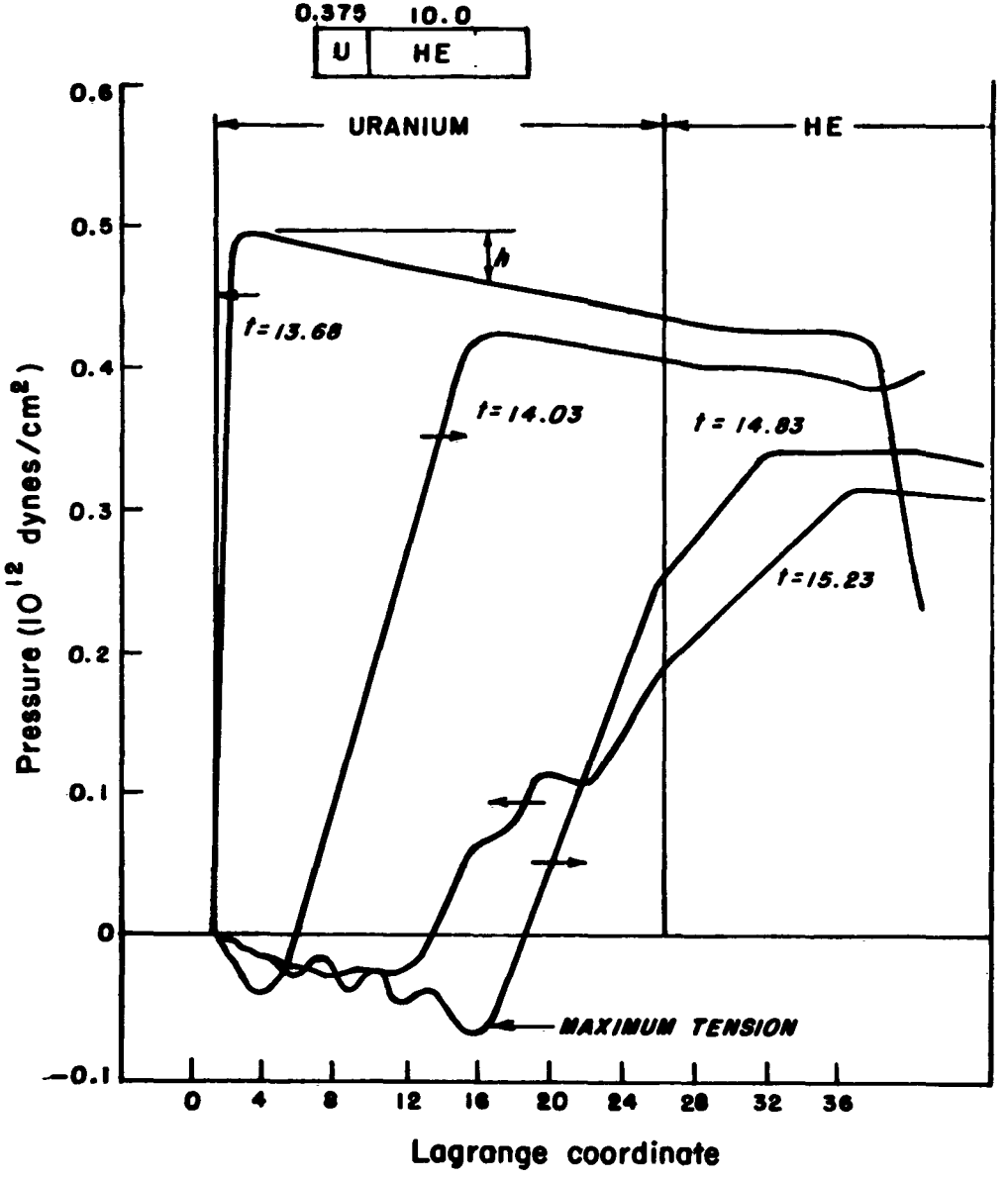
0.375
10.0
U
HE
URANIUM
HE
h
t=13.68
t=14.03
t=14.83
t=15.23
MAXIMUM TENSION
Pressure ($10^{12}$ dynes/cm$^2$)
Lagrange coordinate
0.6
0.5
0.4
0.3
0.2
0.1
0
-0.1
0
4
8
12
16
20
24
28
32
36

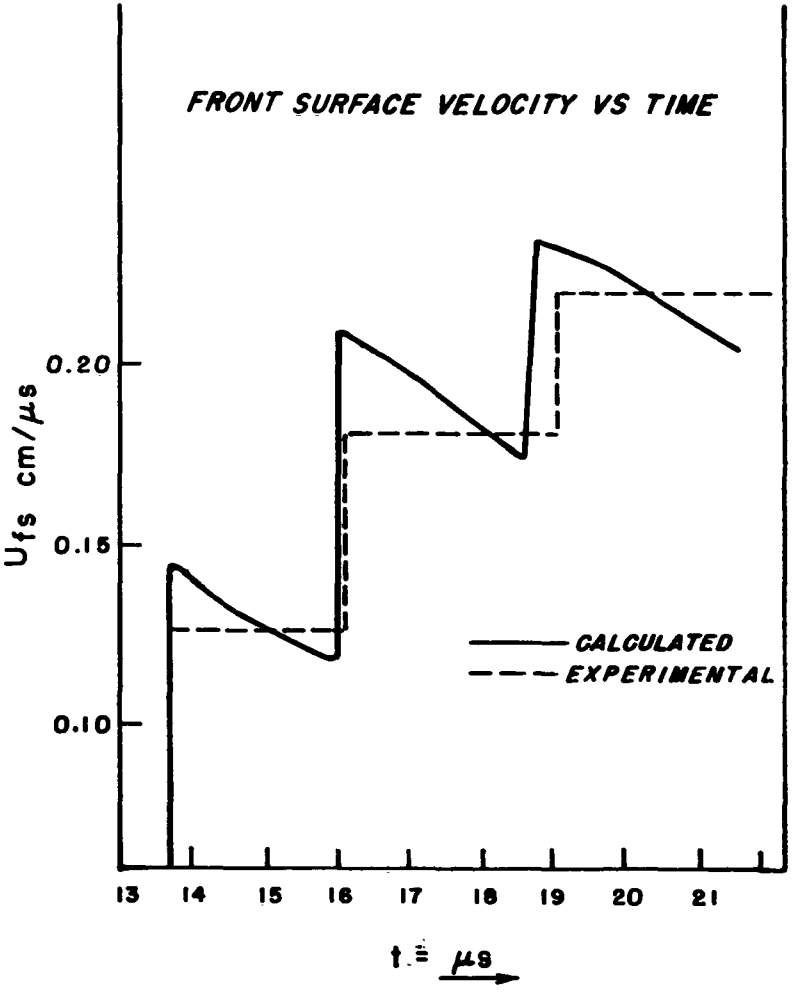
FRONT SURFACE VELOCITY VS TIME
$U_{fs}$ cm/μs
0.20
0.15
0.10
CALCULATED
EXPERIMENTAL
13
14
15
16
17
18
19
20
21
t = μs

Figure 1

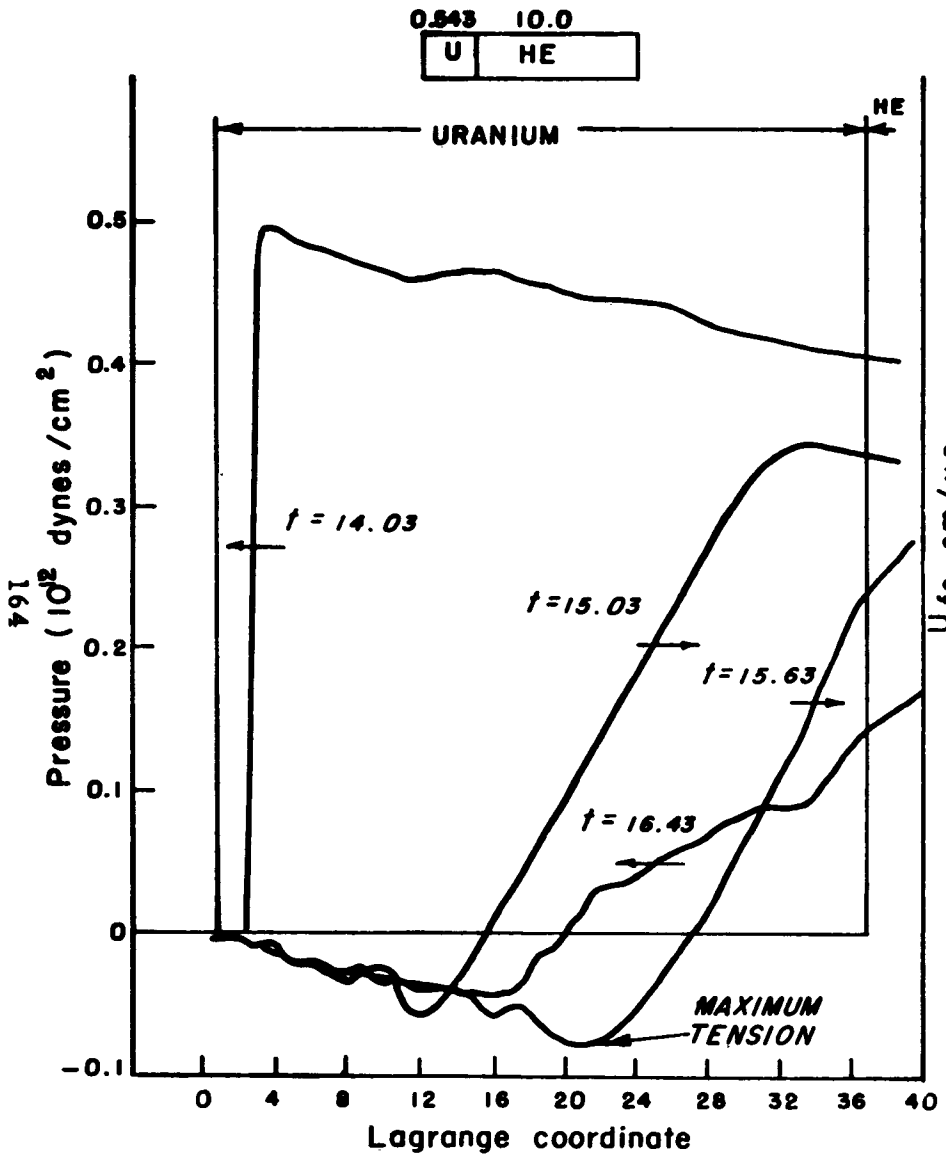
0.543
10.0
U
HE
URANIUM
HE
Pressure ( $10^{12}$ dynes /cm$^2$)
164
0.5
0.4
0.3
0.2
0.1
0
-0.1
t = 14.03
t=15.03
t=15.63
t = 16.43
MAXIMUM TENSION
0
4
8
12
16
20
24
28
32
36
40
Lagrange coordinate

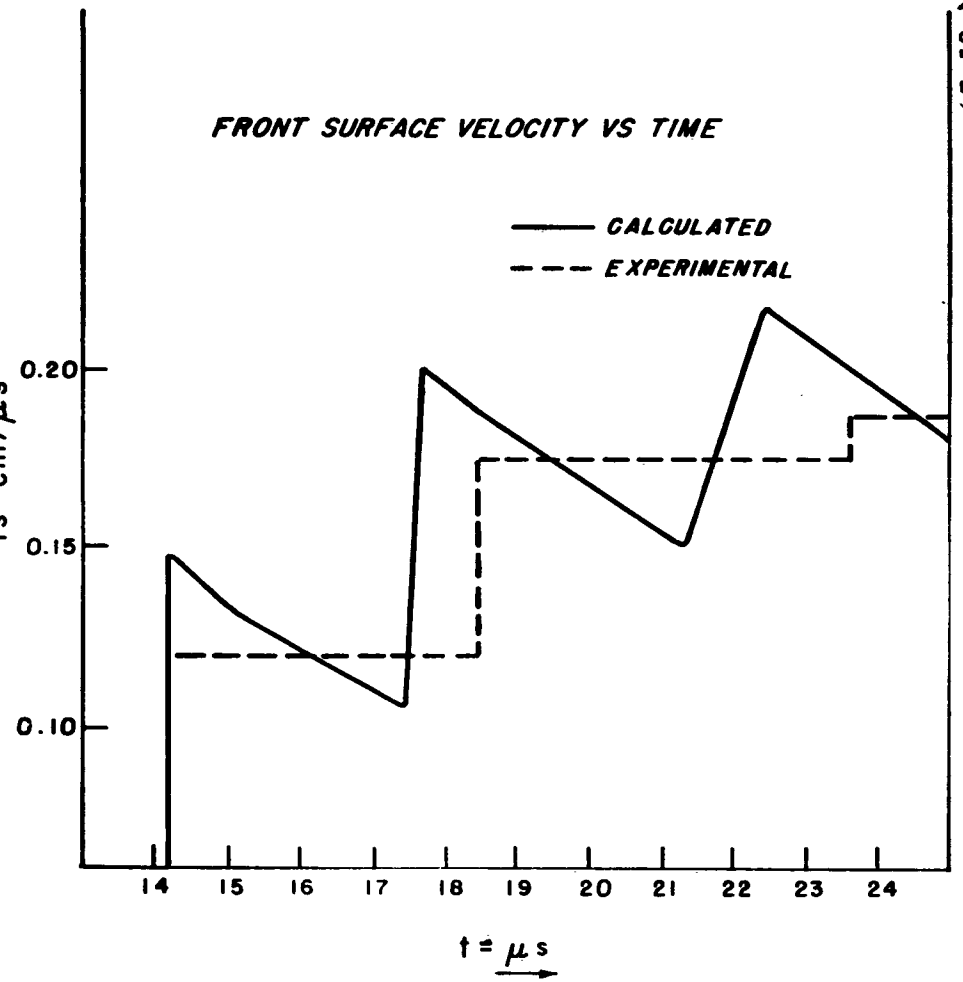
FRONT SURFACE VELOCITY VS TIME
CALCULATED
EXPERIMENTAL
$U_{fs}$ cm/$\mu$s
0.20
0.15
0.10
14
15
16
17
18
19
20
21
22
23
24
t = $\mu$s

Figure 2

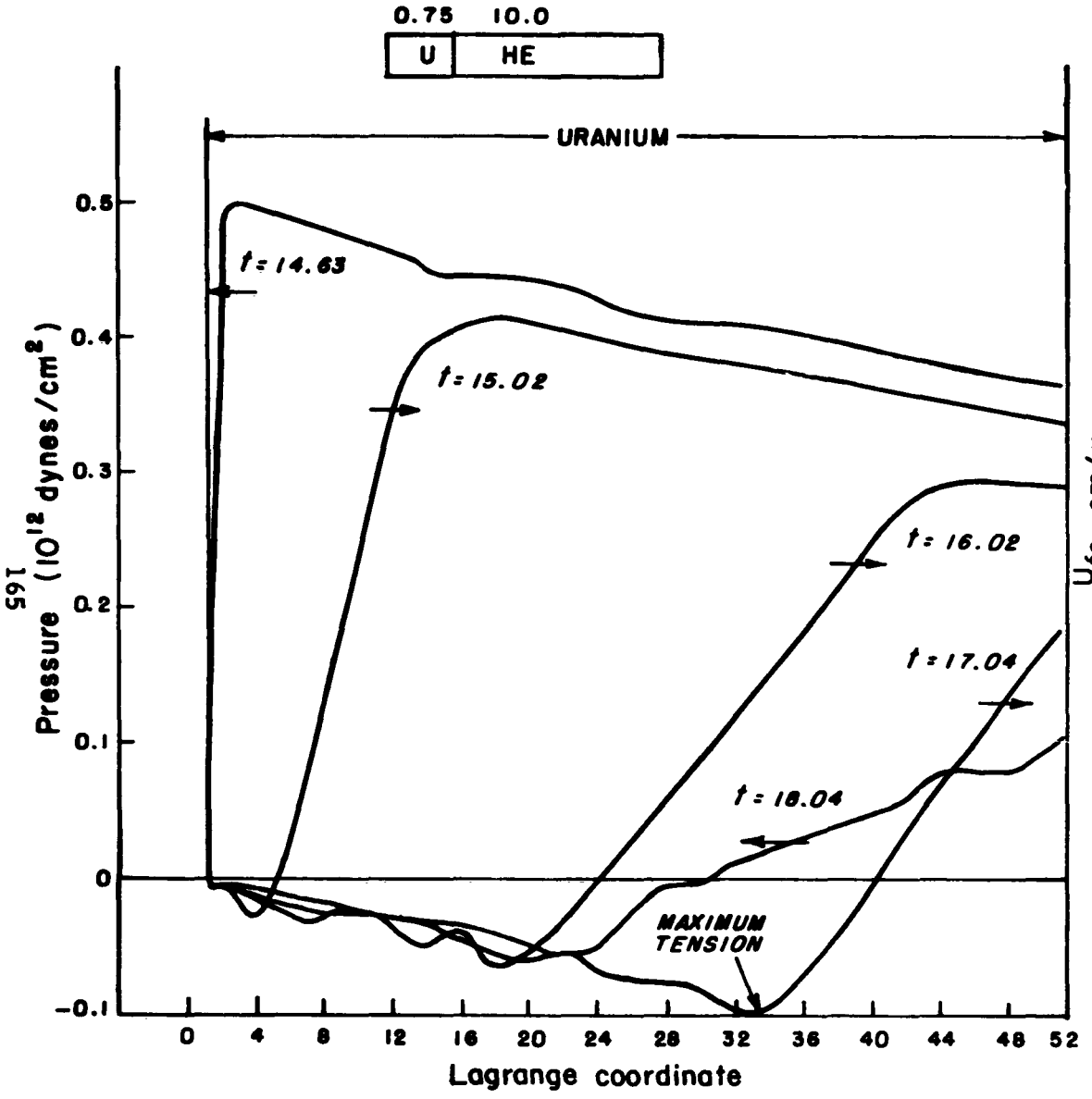


Figure 3

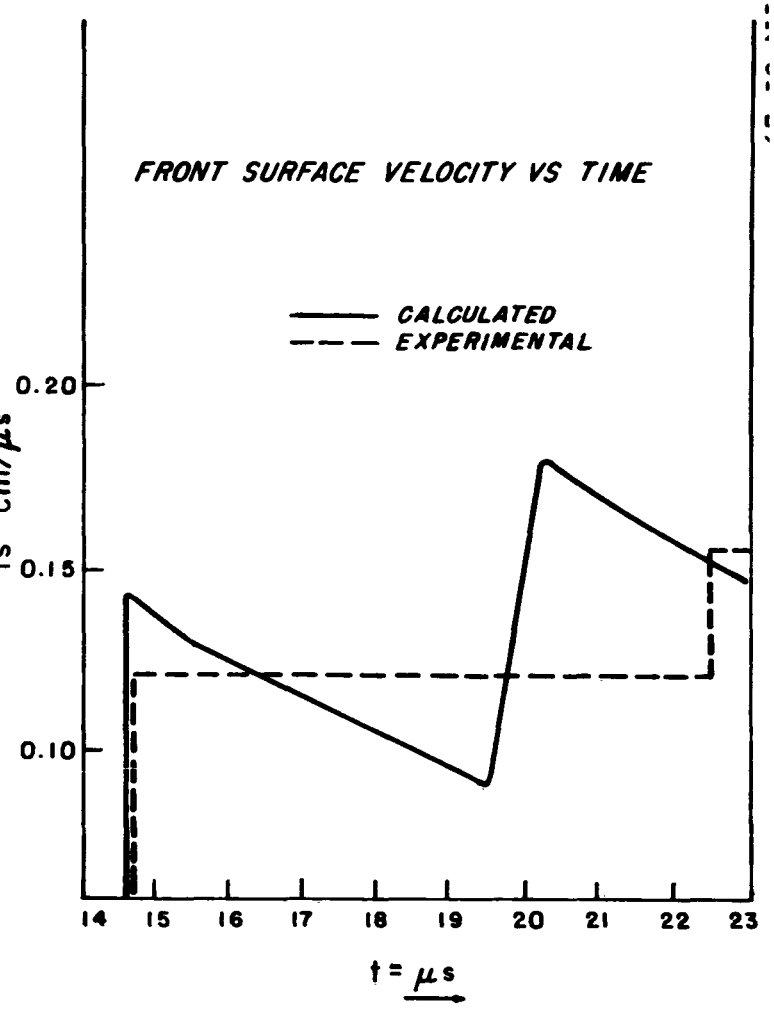


Figure 3-A

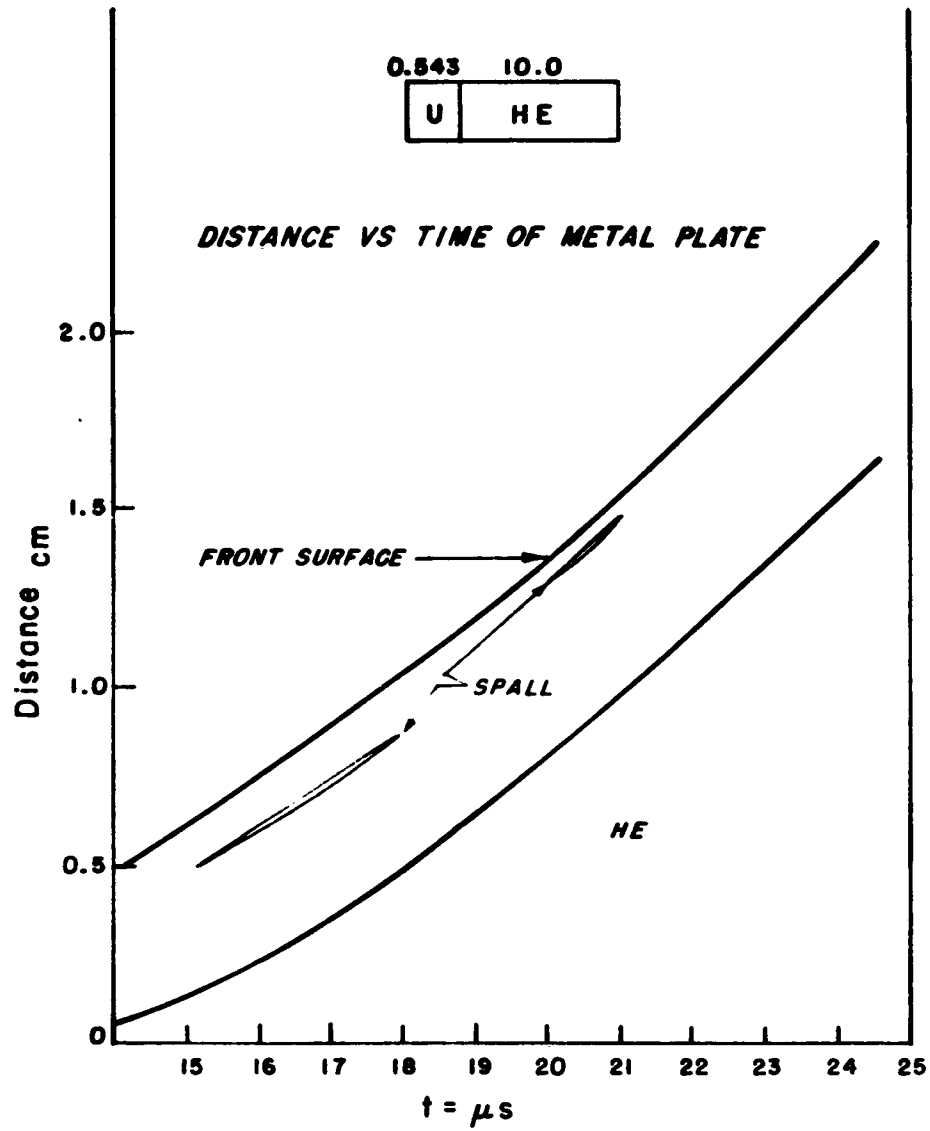


Figure 4

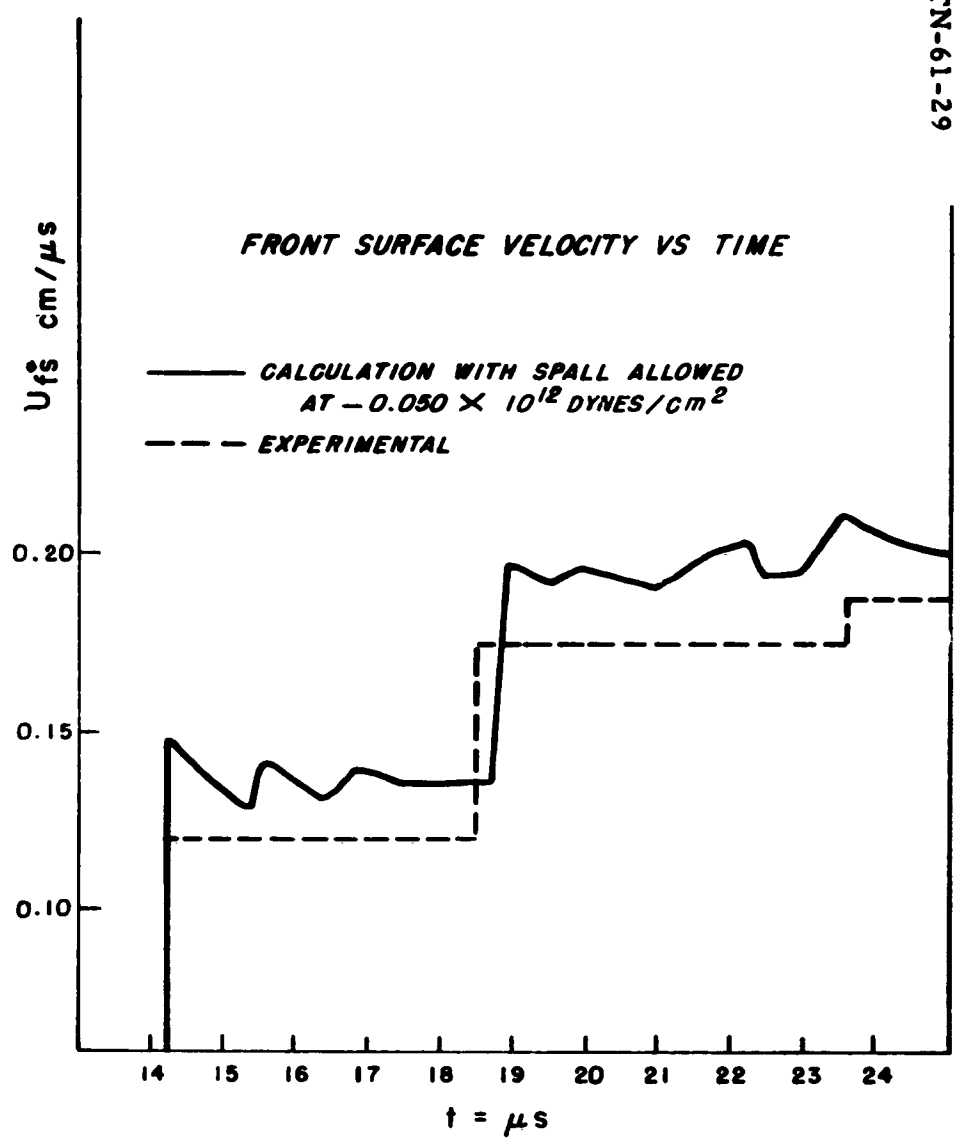


Figure 4-A

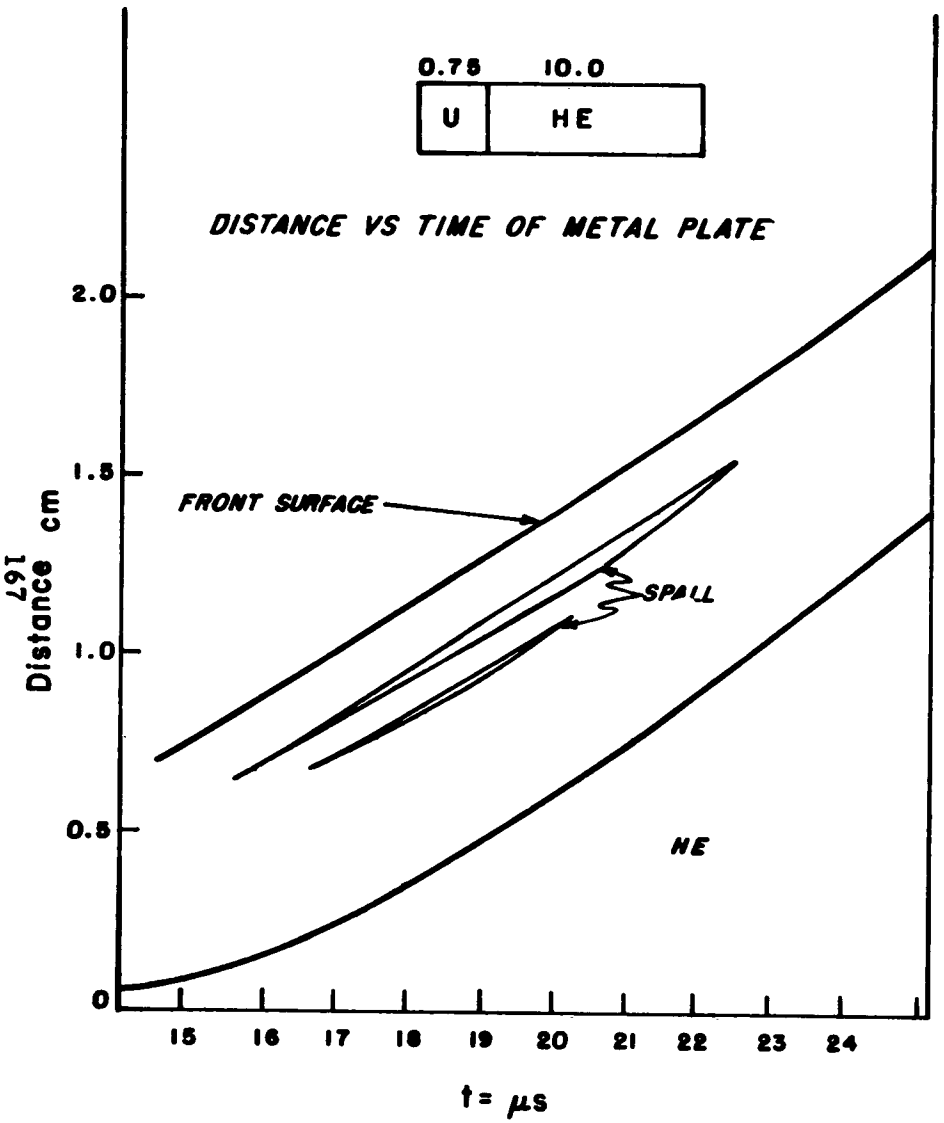


Figure 5

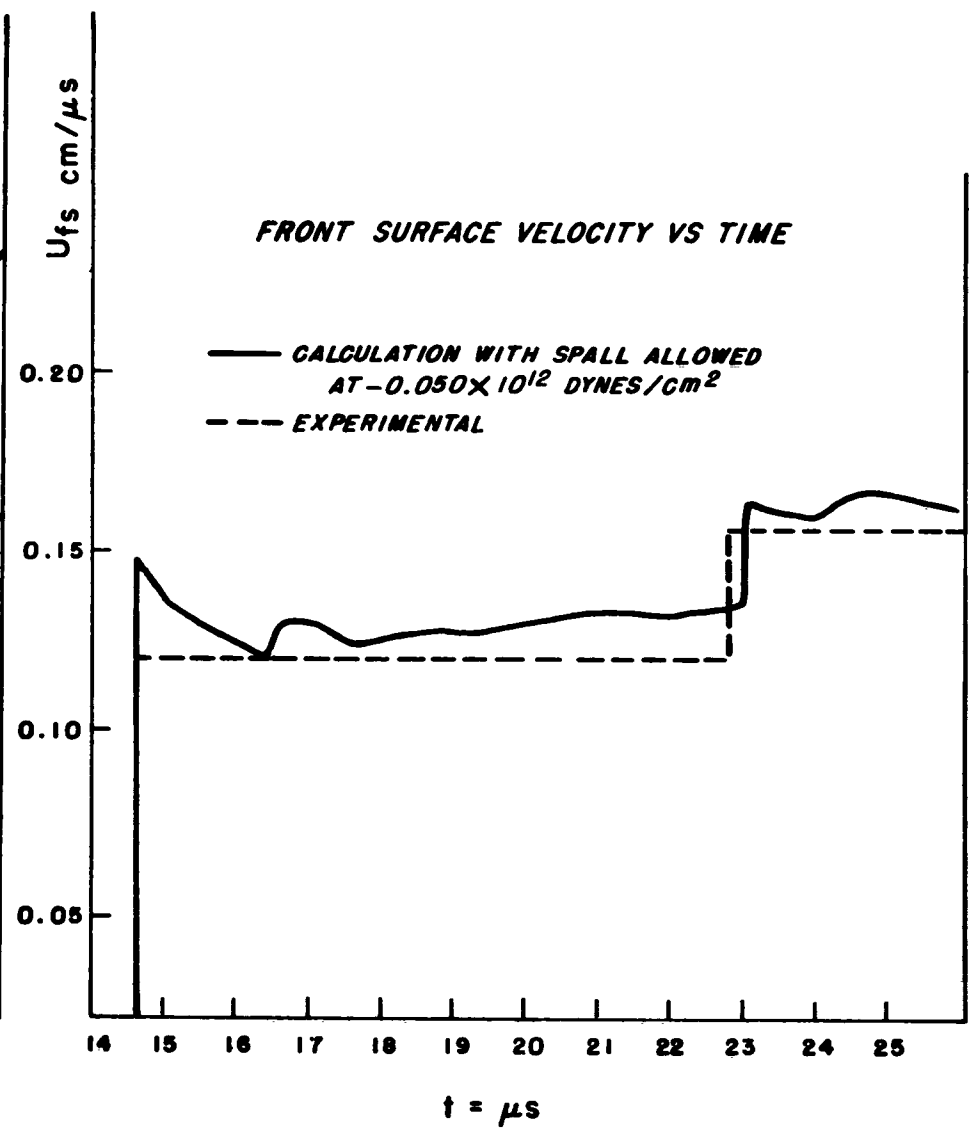


Figure 5-A

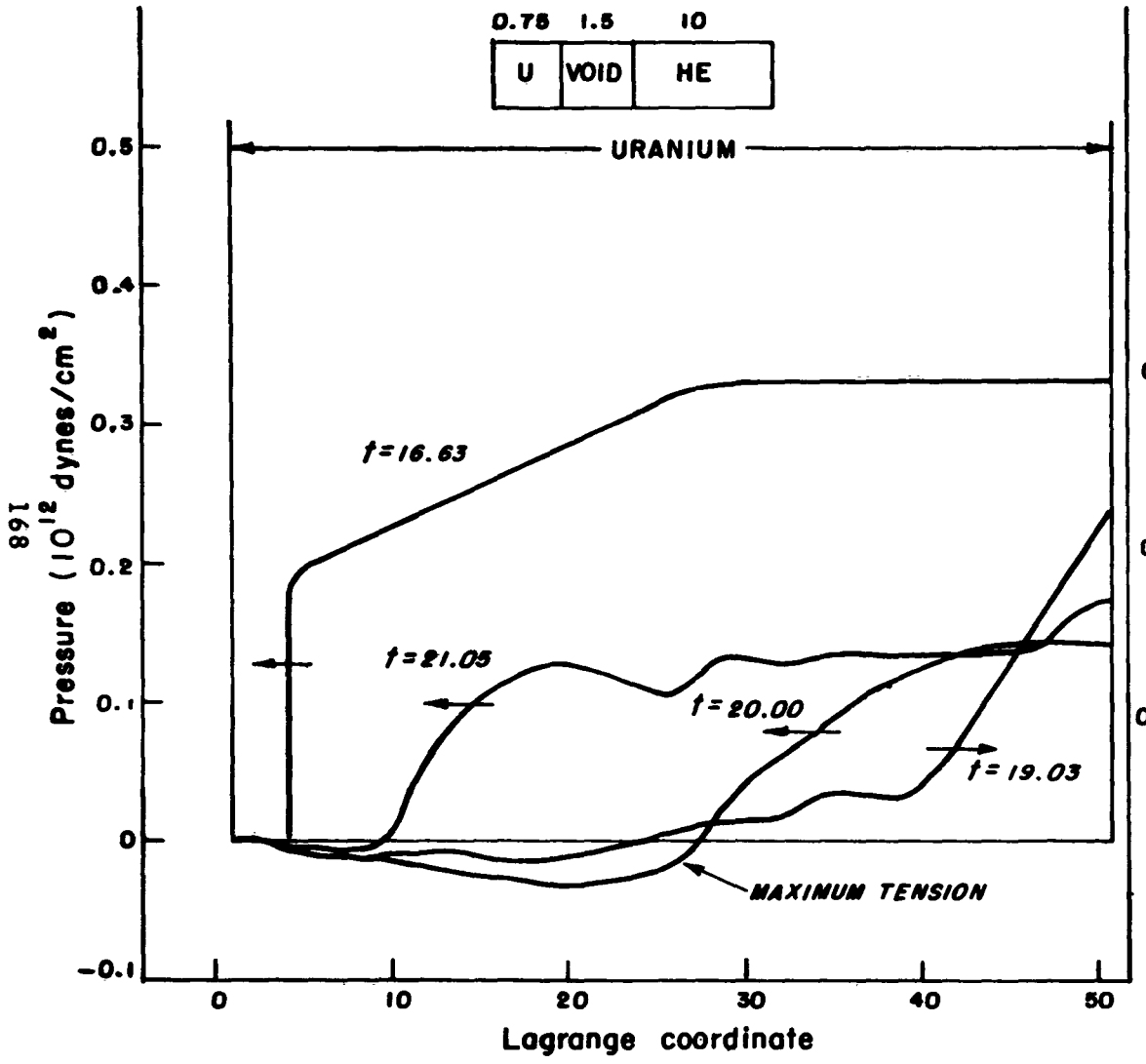


Figure 6

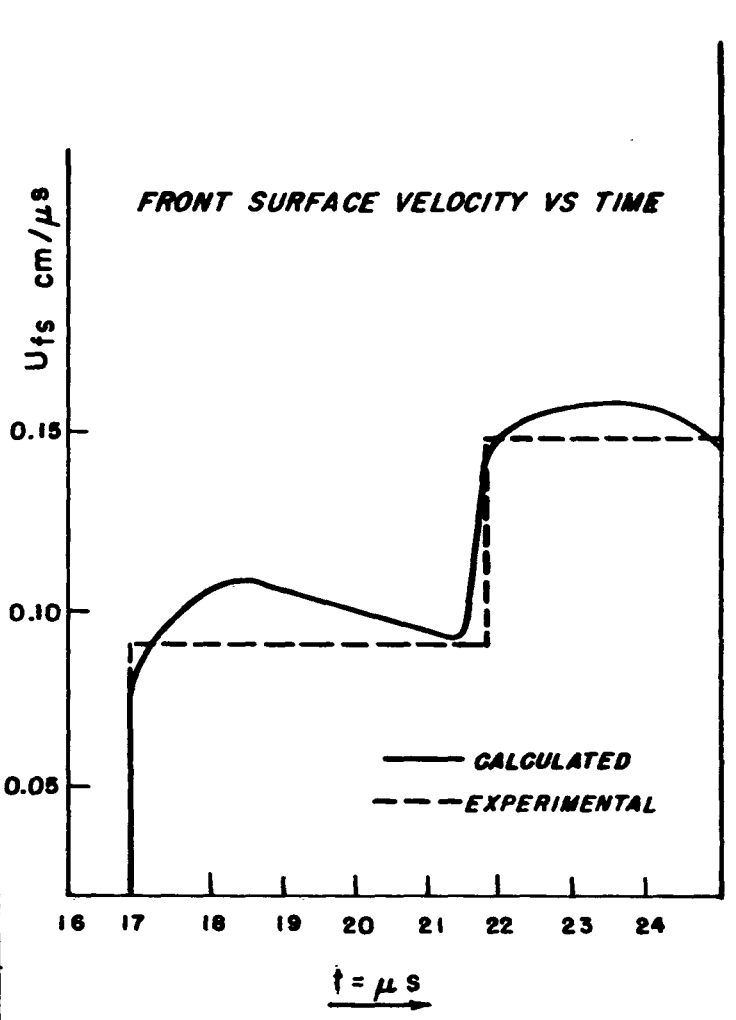


Figure 6-A

# DYNAMIC LARGE DEFLECTION OF SHELL STRUCTURES

Dr. W. Herrmann
T. H. H. Pian
J. W. Leech
Aeroelastic and Structures Research Laboratory
Massachusetts Institute of Technology

The problem considered concerns large deformations of shell-type structures subjected to non-uniformly distributed intense loads of very short duration. A brief review will be given of the methods and assumptions on existing dynamic analysis of elastic and plastic structures.

Where the impulse is sufficiently low, only elastic deformations result. The problem of lateral motion (normal to the shell surface) is somewhat more difficult than that of the longitudinal motion. In the case of elastic deformations, the equation of lateral motion involves a fourth-order differential equation while the equation for longitudinal motion involves only a second-order differential equation.

Transient solutions of lateral elastic motion can be obtained by the classical normal mode solution or by the wave solution. When the duration of the applied dynamic load is not too short, the normal mode method is the suitable choice. However, for problems which involve discrete pulse loads of very short duration, the convergence of the normal mode solution becomes questionable and the wave solution must be adopted. It has been shown, however, that if elementary beam theory is used the resulting flexual wave propagation leads to dispersion. The resulting phase velocity is found to be inversely proportional to the wavelength. For a wave of infinitely short wavelength the propagation velocity is infinite. One can thus conclude that elementary beam theory is inadequate for short impulsive loads because it leads to the physically impossible conclusion that disturbances are propagated instantaneously, throughout the beam. Refinements to elementary theory have been made by Rayleigh and by Timoshenko by taking into account the rotating inertia of the beam cross section and the transverse shear deformation. From this improved theory it can be shown that there are two types of waves propagated along the beam, one of which involves bending moment and

cross-section rotation while the other involves transverse shear force and lateral displacement. The two groups are traveling at different propagation velocities but they are coupled with each other, and the shape of each wave changes completely. The coupled wave equations can be solved by the method of characteristics.

Studies of plastic deformation of beams caused by lateral impulsive loading are of recent origin, having been initiated in this decade. Most of the studies have been based on simple beam theory with the moment-curvature relationship being considered as elastic-plastic (figure 1. a) or rigid-plastic, (figure 1. b) and the plasticity being described generally as either perfectly plastic (figure 1. a and b) or as linear strain-hardening (figure 1. c).

Analyses of elastic-plastic beams have also been made by using the normal mode approach. In this analysis the solution must be divided into individual phases. When the bending moment at any point reaches the yield bending moment, $M_o$, a single plastic hinge is formed and in the subsequent period the beam must be considered as two elastic beams connected by the hinge. By considering the proper continuity-relations between displacements and velocities at the joint, the solution can be established.

Solutions of lateral motion of plastic beams have also been obtained using the wave propagation approach. The solution by Duwez, Clark, and Bohnenblust is based on simple beam theory while the solution by Plass is based on an improved theory taking into account the rotational inertia and the shear deformation. These authors, however, consider only the problem of a semi-infinite beam subjected to a lateral disturbance at one end.

All the work on plastic beams to date has emphasized the permanent deformation due to the impulsive loading. For the cases where the plastic deformation is much larger than the elastic deformation, the simplified rigid-plastic analysis is justified. From the basic assumption of negligible elastic strain it can be concluded that the motion of the beam involves only rigid body motions of various beam segments which are connected by plastic hinges. This type of analysis was first developed by Lee and Symonds and was followed by other authors. A simple example using rigid-plastic analysis is given in the following.

Consider a simply supported beam acted on by a uniformly distributed

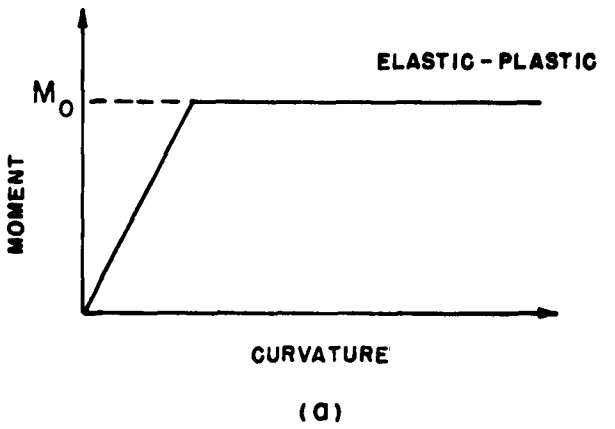


(a)

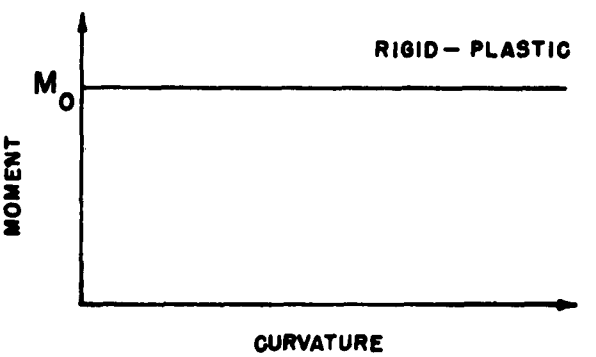


(b)

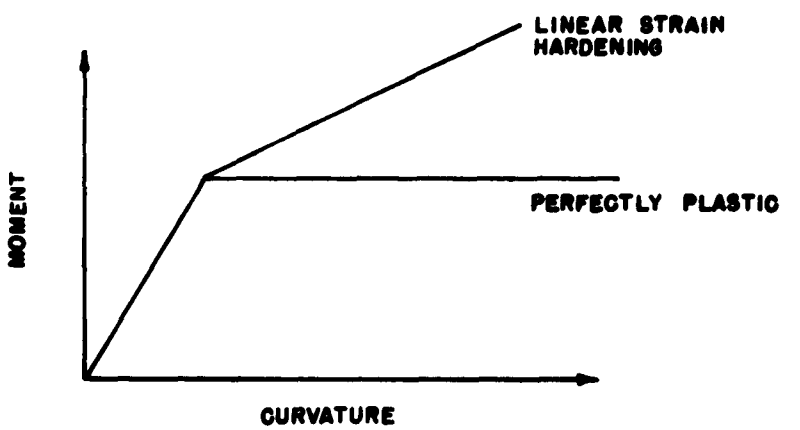


(c)

Figure 1. Idealized stress-strain relations

impulsive load p(t). (Figure 2) When the applied load is small, such that the maximum bending moment is less than the yield bending moment, the beam remains rigid. The maximum bending moment which occurs at the mid-span is equal to $\frac{p\ell^2}{8}$. Thus when $p = \frac{8 M_o}{\ell^2}$, a plastic hinge is formed at the mid-span. If the applied load further increases, the beam will move with two rigid segments rotating about the end supports. The magnitude of the angular acceleration of the rigid segments must be such that the bending moment at the mid-span is maintained at $M_o$. From figure 2 we obtain

$$\frac{p\ell^2}{8} - \frac{m\ddot{\theta}\ell^3}{24} = M_o$$

or

$$\ddot{\theta} = \frac{24}{m\ell^3}\left(\frac{p\ell^2}{8} - M_o\right)$$

When the impulsive load is increased continuously, a point will be reached when the location of maximum bending moment begins to spread outward from the mid-span point. This is the third phase of the motion, when two plastic hinges begin to appear and the beam will move with three rigid segments. Two of these segments rotate about the end support while the segment at the center undergoes uniform translation (figure 2. f.) The plastic hinges are moving away from the center when the load is increasing and they are moving toward the center when the load has been released. The rigid-plastic analysis involves essentially the determination of the motion in the various phases until the velocity of the beam becomes zero everywhere, and the final plastic deformation can be evaluated. The propagation of the plastic hinge in the rigid plastic analysis is not of the same nature as the propagation of elastic or plastic waves. In the present case, there is, in fact, no inertia associated with the moving plastic hinge.

Another refinement of the plastic beam analysis is the inclusion of the axial load effect on the yield bending moment. For a beam restrained at both ends from longitudinal displacements, axial tensile stress is developed when the deflection of the beam becomes larger than the thickness. For a rigid-plastic beam of rectangular cross section the magnitudes of the bending moment, M, and the axial force, N, at the yield condition are related by the following interaction equation:

1st PHASE

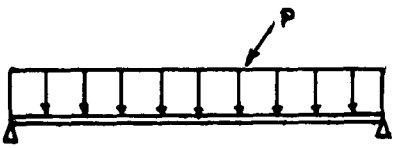


(a) INITIAL LOAD DISTRIBUTION

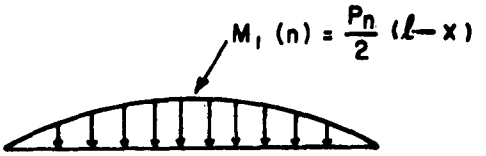


(b) B.M. DISTRIBUTION DUE TO P

2nd PHASE

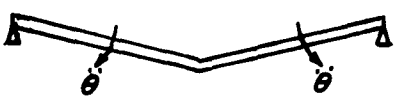


(c) MOTION OF BEAM

(d) DISTRIBUTED INERTIA FORCE

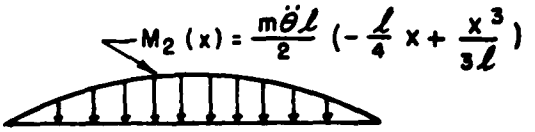


(e) B.M. DISTRIBUTION DUE TO INERTIA FORCE

3rd PHASE

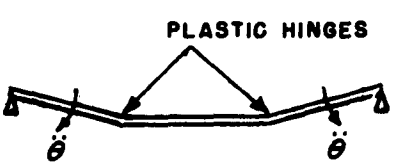


(f) MOTION OF BEAM

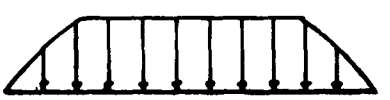

(g) B.M. DISTRIBUTION

Figure 2. Motion of perfecly plastic beam under impulsive load

$$\frac{M}{M_o} + \left(\frac{N}{N_o}\right)^2 = 1$$

where $M_o$ = yielding bending moment when the axial load N is zero and $N_o$ = yielding axial load when the bending moment M is zero.

It can be seen that in the initial phase where the deflection and the axial load are small, the plastic work involves essentially bending at the plastic hinge. However, when the deflection increases, the axial tensile load also increases, and the plastic work will involve mainly axial strain instead of bending strain. In the limiting case where the axial load becomes equal to $N_o$, the beam becomes a plastic string under constant tension $N_o$. (Thus this last phase must be treated differently). Such an analysis was made by Symonds and Mentel. A treatment of a low arch under lateral load was made by Chen, Hsu and Pian. In the latter case axial compressive stress is developed when the arch deforms inward.

All of the previously described plastic theories apply to small deflections in that geometrical nonlinearities are excluded; and in addition, they make further simplifying assumptions, either neglecting elastic effects by assuming rigid-plastic behaviour, or considering only infinitesimal deflections for which the axial (membrane) stress is negligible.

Extension to large deformations involves not only the introduction of axial (membrane) stresses but additional nonlinearities caused by the geometrical effects. The resultant equations require numerical solution. It was decided to retain elastic effects in this analysis since certain evidence was found to suggest that the energy stored in elastic strain in certain deformed shell configurations is not negligible. In particular an appreciable amount of energy appears to be stored in elastic strain in circular cylindrical and spherical shells when these have been deformed to the order of half the radius, as may be shown by cutting the shell at some convenient location and measuring the work required to close the gap.

The method of solution requires setting the equation of motion for the shell, written for large deflections, together with the stress-strain relations, in finite difference form. The resulting initial value problem is solved, subject to the boundary conditions describing the constraints on the shell. The load may be introduced as a varying boundary condition if the loading is of

relatively long duration. Alternatively if the load duration is very short, and the structure does not deform appreciably during the time of load application, the load may be characterised as an impulse, giving rise to an initial velocity distribution in the shell.

Initially only cylindrical shells (rings) are being considered, thus eliminating one space dimension. The ring need not be initially circular. The shell may also be open ended, with appropriate end constraints, and therefore equivalent to a curved beam.

The equilibrium equation in finite difference form may be described in physical terms as follows. The ring is considered to be composed of a number of links joined by hinges. The links are assumed rigid in bending but elastic-plastic in extension. The hinges are considered to be inextensible, but elastic-plastic in bending. The mass of the ring is divided into discrete masses concentrated at the hinges. (Figure 3.)

As in the finite-deflection analysis of Symonds and Mentel, mentioned previously, there is an interaction between bending moment and axial force at the yield condition. For the elastic-perfectly plastic stress-strain relation used here, the interaction equation cannot be written simply, for a rectangular cross section. Particular difficulty is experienced when stress reversals occur. The difficulties are circumvented by idealising the cross section into an I beam (or sandwich plate) of equivalent force and moment carrying capacity. The flanges are considered to behave in an elastic-perfectly plastic manner, and a relatively simple relation between extensional strain and curvature, and axial stress and moment, can be found.

Since stress reversals may occur, and unloading will occur elastically, a multivalued relation results, the correct relation depending on the previous loading history. It is therefore necessary to provide the correct logic in the program to keep track of the loading history, in order to choose the correct relation between the axial stress and strain, and the moment and curvature.

Preliminary results for the case of a beam subjected to a uniform initial velocity indicate that traveling hinges are formed, as in the rigid-plastic case of Lee and Symonds. It is anticipated that the program will give insight into the failure modes to be expected in various configurations, and information about the relative amounts of energy absorbed in elastic and plastic deformation.

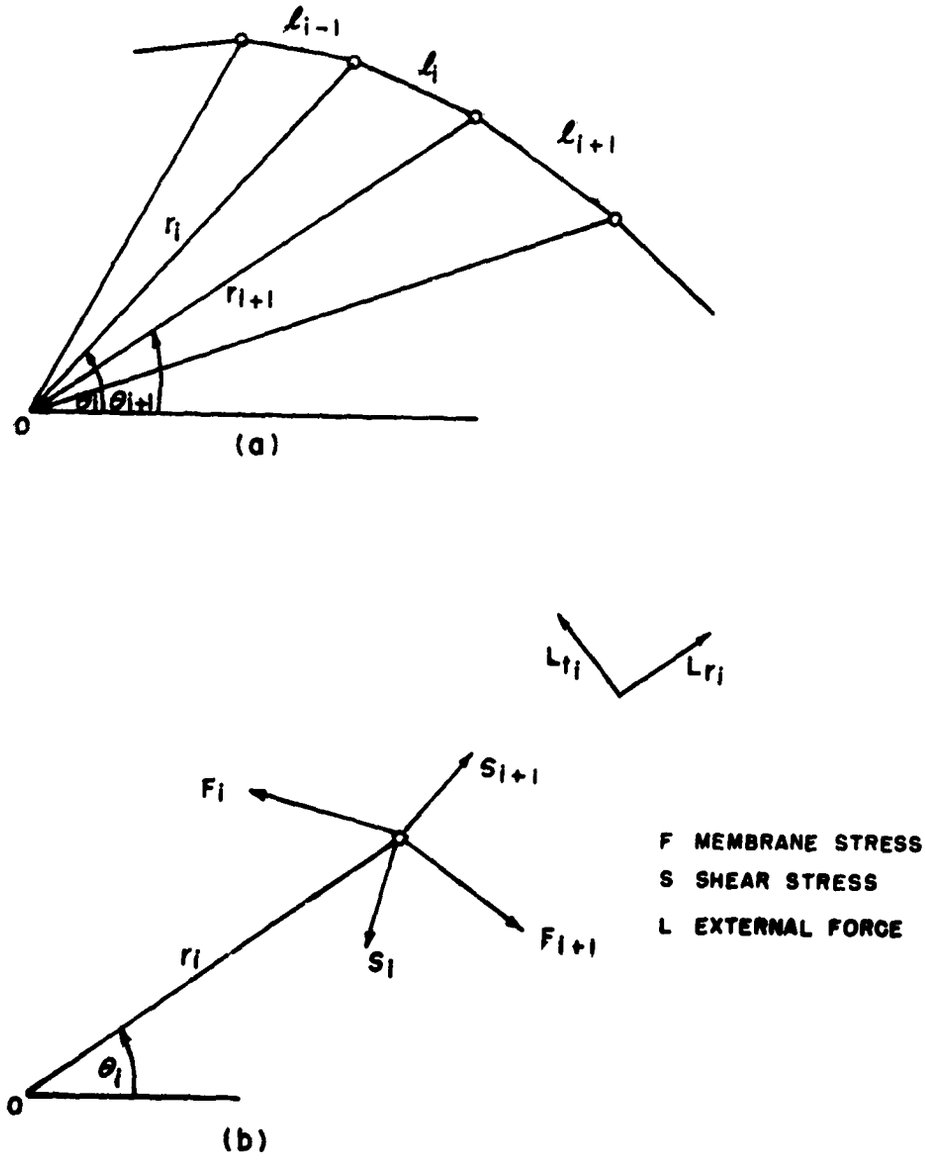


**Figure 3. Finite difference model for shell**

# MOTION OF AN ELASTIC HALF-SPACE

Dr. C. M. Ablow

Dr. Roy C. Alverson
Stanford Research Institute

Underground shelters are designed to withstand the motion of the earth under blast loadings caused by explosions on or above the earth's surface. A first approximation to that motion is obtained by computing the small motions of an isotropic elastic half space under circularly symmetric applied tractions. Features of the motion of major importance are preserved by a computing method which accurately predicts the strength and time of arrival of the first seismic shock. Such a method is at hand when shear and compressional wave motions are separated and independent variables are constant on wave fronts, i. e. when characteristic coordinates are introduced.

For axisymmetric motions of the elastic half space a cylindrical coordinate system $(r, \Psi, z)$ is appropriate. It is assumed that there is no rotation about the axis so that all functions appearing are independent of $\Psi$. It is then known[1] that the equations of motion and of Hook's law may be reduced to the solution of two equations for two potential functions $\varphi$ and $\theta$, function $\varphi$ determining the compression and function $\theta$ the shear:

$$\varphi_{rr} + \varphi_r/r + \varphi_{zz} = \varphi_{tt}/a^2$$

$$\theta_{rr} + \theta_r/r + \theta_{zz} - \theta/r^2 = \theta_{tt}/\beta^2$$

where $a^2 = (\lambda + 2\mu)/\rho$, $\beta^2 = \mu/\rho$, $\lambda$ and $\mu$ are the Lame elastic parameters, and $\rho$ is the density. Although the reduction to the above form is carried through in the reference only for constant $\lambda$, $\mu$, $\rho$, the same manipulations are permissible if $\lambda$ varies as a function of z. Thus the present analysis holds for an earth of constant density and shear wave speed but compressional wave speed varying with depth. Displacements in the radial direction, u, and in the axial direction, w, are determined by $\varphi$ and $\theta$ to be

$$u = \varphi_r - \theta_z, \qquad w = \varphi_z + \theta_r + \theta/r.$$

---

1 W. M. Ewing, W. S. Jardetzky, and F. Press, Elastic Waves in Layered Media, McGraw Hill, New York, 1957, Chapter I

If the surfaces in (r, z, t) space on which function f is constant are shear wave fronts then f is a solution of the characteristic equation

$$f_t^2 = \beta^2 (f_r^2 + f_z^2) .$$

Fundamental shear wave front surfaces are the right circular cones with arbitrary vertex, axis parallel to the time axis, and half vertex angle arc ctn $\beta$. It may be shown that any shear wave front is an envelope of such cones. For the characteristic coordinate surface $\bar{c} = 0$ there was taken the envelope of cones with vertices on the line marking the leading edge of the disturbance on $z = 0$, the surface of the earth. The location of $\bar{c} = 0$ in (r, z, t) space marks the progress of the initial shear disturbance throughout the medium.

The two other characteristic coordinate planes $\bar{a} = 0$ and $\bar{b} = 0$ were taken as the surfaces representing plane waves parallel to the surface of the earth, being at that surface at time zero, and, respectively, going out into the earth or returning from the depths. Thus $\bar{a} = 0$ is one planar envelope of the cones with vertices on the r-axis in (r, z, t) space while $\bar{b} = 0$ is their other planar envelope.

The same definitions give the $a = 0$, $b = 0$, and $c = 0$ characteristic surfaces for the compressional wave equation, except that the variability of $\alpha$ with depth distorts the right circular cones into surfaces of somewhat similar shape called conoids.

To obtain a complete coordinate system in (r, z, t) space, the surface $\bar{c} = k$ was taken as the $\bar{c} = 0$ surface moved k units parallel to itself in the direction of the t-axis, and similarly for the other coordinates. Analytically, if f(r, z, t) is that solution of the characteristic equation for which $f(r, z, t) = 0$ represents the $\bar{c} = 0$ surface, then the equation for $\bar{c} = k$ was taken to be $f(r, z, t-k) = 0$.

It is evident that there is a high degree of arbitrariness in the choice of characteristic coordinate system. The choice made above makes coordinate planes of the initial compressional and shear wave fronts and also provides simple plane surfaces in characteristic space for the surfaces $r = 0$ and $z = 0$ on which boundary conditions are applied as well as the surfaces $t =$ constant on which the computed output is conveniently displayed. Further, on the boundary $z = 0$, where compressional and shear waves satisfy combined

conditions, one has $a = \bar{a}$, $b = \bar{b}$, and $c = \bar{c}$ so that there is no interpolation problem.

| Physical surface | Characteristic surface | |
|---|---|---|
| | for compression | for shear |
| Initial wave | $c = 0$ | $\bar{c} = 0$ |
| $r = 0$ | $a = c$ | $\bar{a} = \bar{c}$ |
| $z = 0$ | $a = b$ | $\bar{a} = \bar{b}$ |
| $t = t_1$ | $a + b = 2t_1$ | $\bar{a} + \bar{b} = 2t_1$ |

Setting

$$\varphi_a = A, \qquad \varphi_b = B, \qquad \varphi_c = C,$$

$$\theta_{\bar{a}} = \bar{A}, \qquad \theta_{\bar{b}} = \bar{B}, \text{ and } \qquad \theta_{\bar{c}} = \bar{C}$$

permits the second-order potential equations to be replaced by the first-order systems

$$4A_b + 2(\alpha c_z + 1)A_c - 2(\alpha c_z - 1)B_c - \alpha^2 \nabla^2 c C = 0$$

$$A_b = B_a, \qquad B_c = C_b,$$

and

$$4\bar{A}_{\bar{b}} + 2(\beta \bar{c}_z + 1)\bar{A}_{\bar{c}} - 2(\beta \bar{c}_z - 1)\bar{B}_{\bar{c}} - \beta^2 \nabla^2 \bar{c}\bar{C} + \beta^2 \theta / r^2 = 0,$$

$$\bar{A}_{\bar{b}} = \bar{B}_{\bar{a}}, \qquad \bar{B}_{\bar{c}} = \bar{C}_{\bar{b}}$$

where the first set of equations replaces the potential equation for the dilatational waves and the second set replaces the potential equation for the shear waves. In these equations $\nabla^2 c$ stands for $c_{rr} + c_r/r + c_{zz}$, and it, as well as the other quantities appearing, needs to be expressed in the characteristic variables before the integrations can begin.

Finite difference approximations to the differential equations have been written using a cubical lattice in each characteristic coordinate system. As is to be expected with a hyperbolic system in characteristic form, the equations are explicit, the solution is obtained by a process of marching through the nodes of the lattice, and stability of this process is assured.

The initial wave fronts, being coordinate surfaces, are sharply defined in the finite difference calculation. No jump condition is needed across the wave front as the proper discontinuity is preserved in the finite difference forms.

The finite difference computation will smear sharp loading or unloading waves behind the initial front unless they fall along a characteristic coordinate surface, i.e., are plane waves parallel to the surface of the earth or are waves of the same speed and extent as the initial wave delayed in time.

The main disadvantage of the characteristic method is that three coordinate systems need to be carried along together, (r, z, t), (a, b, c), and ($\bar{a}$, $\bar{b}$, $\bar{c}$).

Displacements, velocities, and stresses in three different models of the earth under airburst loading are being computed and will appear in forthcoming reports. The three models all consider the earth as an isotropic, elastic, half space. In the first model the half space is homogeneous, in the second it is homogeneous with a homogeneous overburden, and in the third the compressional wave speed varies linearly with depth.

# GENERAL COMMENTS ON NUMERICAL INTEGRATION SCHEMES

Dr. John G. Trulio
Lawrence Radiation Laboratory

With regard to the numerical integration errors inherent in the von Neumann-Richtmyer equations, and the effect of these errors in spall calculations,* I would like to make the following comments.

First, as stated, the linear Q has the effect of eliminating oscillations behind a shock. It introduces much more damping than the quadratic Q. When velocity differences from zone to zone are not large, squaring them tends to produce Q's so small as to be ineffective for damping oscillations in density, etc.

However, a basic problem in describing rarefactions is that any signal which does not move with the velocity of the grid will diffuse. This appears in the rounding of the head of a rarefaction wave, and throws the timing off in rarefaction interaction problems. For most problems this is not a very important effect. However, it is important in any code calculation of the depth of spall, which is one of the main jobs of the (Boeing) code.

If a shock arrives at a free surface, the head of the reflected rarefaction wave may be 6 to 8 zones deeper in the material than it should be. (The error in the position of the rarefaction head is, of course, characterized by a fixed number of zones, and not a fixed distance.) An error of 6 or 8 zones is not serious if there are 600 zones in the spalled piece, but there is ordinarily a limit to the number of zones in these problems — a practical limit in calculation time. Also, a method which requires on the order of 1,000 zones to produce an acceptable solution to a one-dimensional problem is perhaps not the right method to use on the problem. For that reason, other methods are being investigated.

The various numerical integration procedures have application to a series of experiments which have been, and are being, carried out to investigate the

*Butler, Gunning, Jr., and Young, Daniel M., On the Treatment of Rarefaction Using a Dissipative Hydrodynamics Code

Wilkins, Mark, Calculation of Spall Based on a One-Dimensional Model

mechanism of the spall process. The purpose of the experiments is to determine whether or not the spall mechanism is time dependent. The experiments are based on the scaling laws of hydrodynamics, as described in the proceedings of last year's meetings (AFSWC-TR-60-12). In each experiment, one plate is driven at another plate. The absolute plate thicknesses are varied from experiment to experiment, keeping constant the ratio of plate thicknesses and the relative velocity of the plates before impact. Then the pressure distribution in the plates is the same in each experiment at corresponding positions and times. Therefore, if there is no delay time to fracture, one should observe threshold spall for the same relative velocity of the plates, regardless of their absolute thicknesses. So far, this does not seem to be the case, although we have drawn no firm conclusion as yet. Several sets of experiments have been done, for three or four plate thickness ratios. Results have been obtained both by exploding foil and air gun techniques; they agree rather closely.

If the spall mechanism is time dependent, then, in order to calculate the depth of spall, etc., as part of the problem of motion, it will be necessary to build into the code the experimental delay time to fracture, as a function of the applied stress. For stresses and strains outside the linear elastic range, the deduction of this delay time from the experimental data leads to the further problem of determining the stress-strain relation for large tensile stresses. If spall occurs instantly at a fixed tensile stress, the appropriate code modification is much simpler. In either case, a quantitative empirical (or semi-empirical) account of one-dimensional spall will result from experiements of the kind described. A technique for integrating the equations of motion is therefore acceptable only if it allows us to make full use of this knowledge to predict the occurrence of spall, the depth of spall, and other details of the spall process. On this basis, the equations of von Neumann and Richtmyer, unmodified, are inadequate.

I would like to comment also on an accuracy limitation inherent in any numerical scheme which integrates the hydrodynamic equations by stepwise advances in time. Many attempts have been made to increase the accuracy of the equations by "high-order differencing." That is, the difference analogs of the hydrodynamic equations are written in such a way that the error introduced in a dependent variable in a single timestep is of high order in the sense of a Taylor's Series expansion in powers of the space- and time-steps.

Efforts in this direction have had very limited success to my knowledge. There is, I think, a simple and basic reason for this: quite apart from shocks and contact discontinuities, the solutions of the equations of motion are not analytic for flows of even moderate complexity. For example, in one-dimensional motions of practical interest, the x - t plane is criss-crossed by curves across which the first derivatives of the sound speed or particle velocity with respect to x or t are discontinuous. Then the introduction of high-order differences into the difference equations can actually bring about a decrease in this accuracy of the equations, because the derivatives to which these differences tend in the limit of fine zoning are infinite at various points in the flow. Although the truncation error in a single time-step is reduced at most points by high-order differencing, the error introduced at the relatively few points on the singular lines of the flow can more than offset the gain in accuracy elsewhere. It seems that second-order accuracy is about the most that can or should be asked of a general purpose hydrodynamic code which operates through stepwise advances in time. To get around this difficulty, and thereby write rapidly convergent difference equations, one must see to it that differences are never taken across singular surfaces of a flow in the space-time continuum. Since the singular surfaces are characteristic surfaces (apart from shocks and contact discontinuities), the difficulty is overcome by using a set of characteristic coordinates as independent variables. This, it seems to me, is the basic reason for the much more rapid convergence obtained by differencing the equations in characteristic form. However, the use of the characteristic equations for numerical purposes has its own difficulties, especially in the treatment of shocks and contact discontinuities, and in two or three space dimensions.

Since the flow of a compressible fluid is a problem in wave motion (although nonlinear), it is natural to examine the question of accuracy from the point of view of a Fourier expansion as well as a Taylor's Series. Along these lines, the simple problem of linear wave propagation relative to a coordinate mesh has been studied. For concreteness, the motion can be thought of as the uniform translation of a bar of material with variable density and zero pressure, through an Eulerian grid. The difficulty is that the density is known basically at the Eulerian zone centers, while the mass flux needed to calculate changes in density must be defined at the zone boundaries. There are many ways in which the mass flux terms can be calculated from the basic densities, each

corresponding to a particular construction of a complete density profile from the basic discrete density field. Apart from some trivial cases, different definitions of the mass flux will produce different cycle-by-cycle density changes. Thus, instead of the correct undisturbed propagation of a density profile, the density profile will be distorted in the numerical calculations. It is worth noting that this transport problem appears whenever a disturbance propagates at a finite speed relative to the coordinate system used to describe it. In a Lagrangian frame, the problem arises for sound wave propagation.

One simple definition of the density used to calculate the mass flux at a zone boundary is the so-called "backward" definition, i. e., take the nearest zone-centered density in the direction corresponding to the tail of the velocity vector at the zone boundary. If this definition is used, it is found that the amplitude of an 8-zone sine wave decays by a factor of 10 by the time the wave has travelled two or three wavelengths relative to the grid. A cycle-by-cycle analysis of the results shows clearly why this rapid diffusion takes place; the point will not be pursued here. The rate of diffusion decreases as more zones are used per unit wavelength, so that the problem centers mainly on short waves.

To do a better job with sine-wave propagation, another simple definition of the transport density was adopted. This is the so-called "centered" definition, i. e., the zone-centered densities on either side of the zone boundary are averaged (a small correction term is added for purposes of numerical stability). With this definition, the 8-zone wave propagates with very little distortion and no noticeable diffusion. However, if the density profile is a step function, then the centered differencing scheme quickly leads to a train of large oscillations behind the step. The growth of these oscillations is easy to understand by following the calculation time-step by time-step. The initial spurious disturbance is a zone-by-zone oscillation. Thus, the problem again centers on the description of very short wavelengths. In a finite difference grid, the shortest possible sine wave is spread over four zones. These shortest waves, and even somewhat longer ones, are very coarsely defined, and do not propagate correctly through the grid. To eliminate errors from this source, an obvious stratagem is to suppress selectively all sinusoidal components shorter than some predetermined wavelength, without disturbing the others. One way this has been done, according to Dr. Cecil Leith at Livermore, is

actua lly to Fourier analyze the whole signal and subtract out the unwanted components. We have another scheme that accomplishes essentially the same thing - waves spread over any particular numbers of zones can be damped out. By suppressing the saw-toothed waves, all oscillations are wiped out but the first two, for a uniformly translating step function. The amplitude of the first oscillation behind the step is only slightly reduced, while the amplitude of the second oscillation is about halved. By suppressing the waves whose half-width is three zones or less, the second oscillation is eliminated, and the amplitude of the first oscillation is reduced by about a factor of 5 (relative to the amplitude characteristic of centered differencing with no suppression). At the same time, sine waves propagate exactly as in the case of centered differencing. The method is therefore fairly satisfactory for wave propagation in a finite grid.

The wave propagation study was undertaken largely to provide a means of handling the transport terms which appear when the equations of motion are written in a non-Lagrangian coordinate system. The treatment of transport resulting from this study has been put into a code which describes the one-dimensional linear motion of a single material with two Lagrangian boundaries, one of which is not allowed to move. Between the boundaries at any given time are a fixed number of zones of equal width. The grid is therefore neither Lagrangian nor Eulerian; the zone boundaries do not move with the particle velocity and they are not fixed in space. The most interesting problem run on the code to date is that of a steady shock and its reflection from a rigid wall. The error in the pressure behind the transmitted shock is about 50 percent greater than the error using the von Neumann-Richtmyer equations. This is actually better than it looks because the mass of a zone increases severalfold in crossing the shock. Only as the shock nears the rigid wall do the zone masses behind the shock approach their initial values; in the von Neumann-Richtmyer scheme, the masses do not change at all. When the shock gets close to the rigid wall, the zoning in the unshocked material is much finer than at the start of the problem, and the error in the reflected shock pressure is considerably less than in the von Neumann-Richtmyer case.

It can be seen that there are some very simple and fundamental problems which have not been solved adequately in the past — at least in the sense that the method of characteristics affords an adequate solution. In view of the

machine time spent on hydrodynamic problems, it would appear that a good deal more investigation of the difference equations themselves is in order.

## DISTRIBUTION

No. Cys

### HEADQUARTERS USAF

1 Hq USAF (AFCOA), Wash 25, DC

1 Hq USAF (AFDRT), Wash 25, DC

1 Hq USAF (AFDRT-GW-1), ATTN: Maj Lowry, Wash 25, DC

1 Hq USAF (AFCIN), Wash 25, DC

1 Hq USAF (AFTAC), Wash 25, DC

ATIC, Wright-Patterson AFB, Ohio

1 AFCIN 4FZA, Maj Pearce

1 AFCIN 41B1A, Library

AFOAR, Bldg T-D, Wash 25, DC

1 RROSA

1 RRONN, Maj Munyon

1 AFOSR (SREC, Technical Information & Intelligence Division), Bldg T-D, Wash 25, DC

2 AFOAR, Hq AFCRL, ATTN: Tech Library, L. G. Hanscom Fld, Bedford, Mass

### MAJOR AIR COMMANDS

AFSC, Andrews AFB, Wash 25, DC

1 (SCR)

1 (SCR-2) Capt Ray Berrier

1 AUL, Maxwell AFB, Ala

1 USAFIT, Wright-Patterson AFB, Ohio

### AFSC ORGANIZATIONS

ASD, Wright-Patterson AFB, Ohio

3 (ASRMDS-12)

ATTN: Capt Walker

ATTN: Lt Hershey

ATTN: Mr. Gilbert

2 Technical Library

1 DCAS (Tech Library), AF Unit Post Office, Los Angeles 45, Calif

BSD, AF Unit Post Office, Los Angeles 45, Calif

1 (WDTV) ATTN: Col Middlekauf

DISTRIBUTION (con't)

| No. Cys | |
|---|---|
| 2 | (Tech Library) |
| 1 | SSD (Tech Library), AF Unit Post Office, Los Angeles 45, Calif |
| | ESD, Hanscom Fld, Bedford, Mass |
| 1 | (Tech Library) |
| 1 | (ESAT) |
| 1 | (ESF) |
| 1 | AF Msl Dev Cen (MDGRT), Holloman AFB, N Mex |
| 1 | European Office of Research, ATTN: Maj Sullivan, Brussels, Belgium |

KIRTLAND AFB ORGANIZATIONS

| | |
|---|---|
| | AFSWC, Kirtland AFB, N Mex |
| 1 | (SWNH) |
| 100 | (SWOI) |
| 10 | (SWRP) |
| 2 | (SWRS) |
| 1 | US Naval Weapons Evaluation Facility (NWEF) (Code 404), Kirtland AFB, N Mex |

OTHER AIR FORCE AGENCIES

| | |
|---|---|
| | Director, USAF Project RAND, via: Air Force Liaison Office, The RAND Corporation, 1700 Main Street, Santa Monica, Calif |
| 2 | (RAND Library) |
| 1 | ATTN: Dr. O. A. Nance |
| 1 | Dr. Al Latter |
| 1 | Dr. R. L. Bjork |
| 1 | Dr. Carl Greifinger |
| 1 | Mr. Kenneth Schwartz |
| 1 | Lt Col Whitener |

ARMY ACTIVITIES

| | |
|---|---|
| 1 | Chief of Research and Development, Department of the Army (Special Weapons and Air Defense Division), Wash 25, DC |

DISTRIBUTION (con't)

| No. Cys | |
|---|---|
| | Director, Ballistic Research Laboratories, Aberdeen Proving Ground, Md |
| 1 | Library |
| 1 | ATTN: Mr. Frank J. Allen |
| 1 | Mr. E. D. Baicy |
| 1 | ARGMA (Tech Library), Huntsville, Ala |
| | NAVY ACTIVITIES |
| 1 | Chief of Naval Operations, Department of the Navy, ATTN: OP-36, Wash 25, DC |
| | Commanding Officer, Naval Research Laboratory, Wash 25, DC |
| 1 | (Tech Library) |
| 1 | ATTN: Mr. Walter Atkins |
| 1 | Mr. Carroll Porter |
| 1 | Commanding Officer, Naval Radiological Defense Laboratory (Technical Info Div), San Francisco 24, Calif |
| | OTHER DOD ACTIVITIES |
| | Chief, Defense Atomic Support Agency, Wash 25, DC |
| 1 | (Document Library) |
| 1 | ATTN: Lt Col Singer |
| 1 | Maj McCormac |
| | Commander, Field Command, Defense Atomic Support Agency, Sandia Base, N Mex |
| 1 | (FCAG3, Special Weapons Publication Distribution) |
| 1 | ATTN: Lt Col Morgan |
| | Director, Advanced Research Projects Agency, Department of Defense, The Pentagon, Wash 25, DC |
| 1 | ATTN: Dr. Charles Cook |
| 1 | Lt Col Roy Weidler |
| 1 | Director, Defense Research & Engineering, ATTN: Col Gilbert, The Pentagon, Wash 25, DC |
| 10 | ASTIA (TIPDR), Arlington Hall Sta, Arlington 12, Va |

DISTRIBUTION (con't)

| No. Cys | |
|---|---|
| | AEC ACTIVITIES |
| 1 | US Atomic Energy Commission (Technical Reports Library, Mrs. J. O"Leary for DMA), Wash 25, DC |
| | President, Sandia Corporation, Sandia Base, N Mex |
| 1 | (Document Control Division) |
| 1 | (ATTN: Mr. C. D. Lundergan) |
| | Director, University of California Lawrence Radiation Laboratory, Technical Information Division, P. O. Box 808, Livermore, Calif |
| 1 | ATTN: Mr. Clovis Craig |
| 1 | Dr. John G. Trulio |
| 1 | Dr. Mark Wilkins |
| 1 | Mr. Robert Banaugh |
| 1 | Mr. Joseph Fleck |
| 1 | Mr. James Quong |
| | Director, Los Alamos Scientific Laboratory, P. O. Box 1663, Los Alamos, N Mex |
| 2 | (Helen Redman, Report Library) |
| 1 | (J-15, Dr. Arthur Cox) |
| 1 | (T-5, Dr. George White) |
| 1 | (J-10, Dr. Herman Hoerlin) |
| | OTHER |
| 1 | Edgerton, Germeshausen, & Grier, ATTN: Dr. Marion Schuler, 150 Brookline Ave., Boston, Mass |
| 1 | General Dynamics/Convair, Physics Division, ATTN: Dr. C. G. Davis, Box 1950, San Diego 12, Calif |
| | Cornell Aeronautical Lab, 4455 Genessee Street, Buffalo 21, NY |
| 1 | ATTN: Dr. Walter Gibson |
| 1 | Dr. J. Gordon Hall |
| 1 | Institute of Aerospace Sciences, Inc., 2 E. 64th St., New York, NY |
| 1 | OTS, Department of Commerce, Wash 25, DC |
| | Stanford Research Institute, Menlo Park, Calif |
| 1 | ATTN: Dr. C. M. Ablow |
| 1 | Dr. George Abrahamson |
| 1 | Mr. John O. Erkman |
| 1 | Mr. G. R. Fowles |

DISTRIBUTION (con't)

| No. Cys | |
|---|---|
| | Aeronutronic, A Division of Ford, Ford Road, Newport Beach, Calif |
| 1 | ATTN: Dr. Raymond Grandey |
| 1 | Dr. Donald Sachs |
| 1 | Mr. John W. Lipford |
| | The Boeing Company, Aerospace Division, Box 3707, Seattle 24, Wash |
| 1 | ATTN: Dr. Donald Hicks |
| 1 | Dr. Donald Keller |
| 1 | Mr. Daniel Young |
| 1 | Massachusetts Institute of Technology, Aeroelastic and Structures Laboratory, ATTN: Dr. Walter Herrmann, Cambridge 39, Mass |
| | Aerojet General Corporation, 1711 Woodruff Ave., Downey, Calif |
| 1 | ATTN: Mr. Nigel Thomas |
| 1 | Mr. Mark Wagner |
| 1 | Dr. Louis Zernow |
| | General Dynamics / General Atomic, Box 608 San Diego 12, Calif |
| 1 | ATTN: Dr. Burton Freeman |
| 1 | Dr. Charles Loomis |
| | RCA, Advanced Military Systems Group, David Sarnoff Research Center, Princeton, NJ |
| 1 | ATTN: Mr. Fred Herzfeld |
| 1 | Dr. John Jarem |
| 1 | Geophysics Corporation of America, ATTN: Dr. Harry E. Stubbs, Bedford, Mass |
| 1 | AVCO-RAD, ATTN: Dr. Jerrold Yos, 201 Lowell Street, Wilmington, Mass |
| | Lockheed Missiles and Space Division, 3251 Hanover Street, Palo Alto, Calif |
| 1 | ATTN: Dr. R. E. Meyerott |
| 1 | Dr. R. K. M. Landshoff |
| 1 | Dr. Dan Holland |
| | Republic Aviation Corporation, Plasma Propulsion Laboratory, Farmingdale, NY |
| 1 | ATTN: Mr. Milton Halem |
| 1 | Dr. William McIlroy |

DISTRIBUTION (con't)

| No. Cys | |
|---|---|
| 1 | McAllister and Associates, ATTN: Dr. Louis E. Bothell, 203 Truman, N. E., Albuquerque, N Mex |
| 1 | Allied Research Associates, ATTN: Mr. Sheldon Kahalas, 43 Leon Street, Boston, Mass |
| 1 | General Electric Company, Aeroscience Laboratory, ATTN: Dr. F. A. Lucy, 3750 "D" Street, Philadelphia 24, Pa |
| | Stanford Research Institute, Menlo Park, Calif |
| 1 | ATTN: Dr. L. Evan Bailey |
| 1 | Dr. Ernest G. Chilton |
| 1 | American Science and Engineering, ATTN: Mr. Gilbert Fryklund, 79 Broadway, Cambridge, Mass |
| | Space Technology Labs, Box 95001, Los Angeles 45, Calif |
| 1 | ATTN: Dr. H. Leon |
| 1 | Dr. J. Maxey |
| 1 | California Institute of Technology, ATTN: Dr. Max Williams, Pasadena, Calif |
| 1 | Battelle Memorial Institute, ATTN: Mr. B. J. Brand, 505 King Avenue, Columbus, Ohio |
| 1 | Technical Operations, Inc., ATTN: Dr. Paul I. Richards, Burlington, Mass |
| 1 | Official Record Copy (SWRPA, Lt Rich) |

Air Force Special Weapons Center, Kirtland Air Force Base, N Mex

AFSWC SECOND HYDRODYNAMIC CONFERENCE; NUMERICAL METHODS OF FLUID FLOW PROBLEMS (U), Compiled by John C. Rich, 16-18 May 1961. 206 pages including illus. (Project 5776) AFSWC-TN-61-29, Part I UNCLASSIFIED Report

The second AFSWC Hydrodynamic Conference was held at Kirtland Air Force Base for the purpose of discussing numerical techniques which have become an important and widely used tool for solving fluid flow problems. A large number of the papers presented dealt with the problems of the finite difference analogs of the differential equations of motion. A few papers discussed work toward analytic solutions of these equations. Topics included hydrodynamics, magnetohydrodynamics, radiation transport, and solid material motion. (U)

The Proceedings are published in two parts: Part I is unclassified and Part II is classified. (U)

UNCLASSIFIED

1. Astrophysics
2. Boundary layers
3. Fluid flow
4. Gases
5. Hydrodynamics
6. Ionization
7. Kinematics
8. Magnetic fields
9. Plasma
10. Radiation flow
11. Shock hydrodynamics
12. Shock waves
13. Spalling
14. Structural elements - Effects of blast
15. X-Radiation

I. Rich, John C., Comp.
II. AFSWC, Kirtland AFB, N Mex
III. Project 5776

UNCLASSIFIED

Air Force Special Weapons Center, Kirtland Air Force Base, N Mex

AFSWC SECOND HYDRODYNAMIC CONFERENCE; NUMERICAL METHODS OF FLUID FLOW PROBLEMS (U), Compiled by John C. Rich, 16-18 May 1961. 206 pages including illus. (Project 5776) AFSWC-TN-61-29, Part I UNCLASSIFIED Report

The second AFSWC Hydrodynamic Conference was held at Kirtland Air Force Base for the purpose of discussing numerical techniques which have become an important and widely used tool for solving fluid flow problems. A large number of the papers presented dealt with the problems of the finite difference analogs of the differential equations of motion. A few papers discussed work toward analytic solutions of these equations. Topics included hydrodynamics, magnetohydrodynamics, radiation transport, and solid material motion. (U)

The Proceedings are published in two parts: Part I is unclassified and Part II is classified. (U)

UNCLASSIFIED

1. Astrophysics
2. Boundary layers
3. Fluid flow
4. Gases
5. Hydrodynamics
6. Ionization
7. Kinematics
8. Magnetic fields
9. Plasma
10. Radiation flow
11. Shock hydrodynamics
12. Shock waves
13. Spalling
14. Structural elements - Effects of blast
15. X-Radiation

I. Rich, John C., Comp.
II. AFSWC, Kirtland AFB, N Mex
III. Project 5776

UNCLASSIFIED

Air Force Special Weapons Center, Kirtland Air Force Base, N Mex

AFSWC SECOND HYDRODYNAMIC CONFERENCE; NUMERICAL METHODS OF FLUID FLOW PROBLEMS (U), Compiled by John C. Rich, 16-18 May 1961. 206 pages including illus. (Project 5776) AFSWC-TN-61-29, Part I UNCLASSIFIED Report

The second AFSWC Hydrodynamic Conference was held at Kirtland Air Force Base for the purpose of discussing numerical techniques which have become an important and widely used tool for solving fluid flow problems. A large number of the papers presented dealt with the problems of the finite difference analogs of the differential equations of motion. A few papers discussed work toward analytic solutions of these equations. Topics included hydrodynamics, magnetohydrodynamics, radiation transport, and solid material motion. (U)

The Proceedings are published in two parts: Part I is unclassified and Part II is classified. (U)

UNCLASSIFIED

1. Astrophysics
2. Boundary layers
3. Fluid flow
4. Gases
5. Hydrodynamics
6. Ionization
7. Kinematics
8. Magnetic fields
9. Plasma
10. Radiation flow
11. Shock hydrodynamics
12. Shock waves
13. Spalling
14. Structural elements - Effects of blast
15. X-Radiation

I. Rich, John C., Comp.
II. AFSWC, Kirtland AFB, N Mex
III. Project 5776

UNCLASSIFIED

Air Force Special Weapons Center, Kirtland Air Force Base, N Mex

AFSWC SECOND HYDRODYNAMIC CONFERENCE; NUMERICAL METHODS OF FLUID FLOW PROBLEMS (U), Compiled by John C. Rich, 16-18 May 1961. 206 pages including illus. (Project 5776) AFSWC-TN-62-29, Part I UNCLASSIFIED Report

The second AFSWC Hydrodynamic Conference was held at Kirtland Air Force Base for the purpose of discussing numerical techniques which have become an important and widely used tool for solving fluid flow problems. A large number of the papers presented dealt with the problems of the finite difference analogs of the differential equations of motion. A few papers discussed work toward analytic solutions of these equations. Topics included hydrodynamics, magnetohydrodynamics, radiation transport, and solid material motion. (U)

The Proceedings are published in two parts: Part I is unclassified and Part II is classified. (U)

UNCLASSIFIED

1. Astrophysics
2. Boundary layers
3. Fluid flow
4. Gases
5. Hydrodynamics
6. Ionization
7. Kinematics
8. Magnetic fields
9. Plasma
10. Radiation flow
11. Shock hydrodynamics
12. Shock waves
13. Spalling
14. Structural elements - Effects of blast
15. X-Radiation

I. Rich, John C., Comp.
II. AFSWC, Kirtland AFB, N Mex
III. Project 5776

UNCLASSIFIED

Air Force Special Weapons Center, Kirtland Air Force Base, N Mex

AFSWC SECOND HYDRODYNAMIC CONFERENCE; NUMERICAL METHODS OF FLUID FLOW PROBLEMS (U), Compiled by John C. Rich, 16-18 May 1961. 206 pages including illus. (Project 5776) AFSWC-TN-61-29, Part I UNCLASSIFIED Report

The second AFSWC Hydrodynamic Conference was held at Kirtland Air Force Base for the purpose of discussing numerical techniques which have become an important and widely used tool for solving fluid flow problems. A large number of the papers presented dealt with the problems of the finite difference analogs of the differential equations of motion. A few papers discussed work toward analytic solutions of these equations. Topics included hydrodynamics, magnetohydrodynamics, radiation transport, and solid material motion. (U)

The Proceedings are published in two parts: Part I is unclassified and Part II is classified. (U)

UNCLASSIFIED

1. Astrophysics
2. Boundary layers
3. Fluid flow
4. Gases
5. Hydrodynamics
6. Ionization
7. Kinematics
8. Magnetic fields
9. Plasma
10. Radiation flow
11. Shock hydrodynamics
12. Shock waves
13. Spalling
14. Structural elements - Effects of blast
15. X-Radiation

I. Rich, John C., Comp.
II. AFSWC, Kirtland AFB, N Mex
III. Project 5776

UNCLASSIFIED

Air Force Special Weapons Center, Kirtland Air Force Base, N Mex

AFSWC SECOND HYDRODYNAMIC CONFERENCE; NUMERICAL METHODS OF FLUID FLOW PROBLEMS (U), Compiled by John C. Rich, 16-18 May 1961. 206 pages including illus. (Project 5776) AFSWC-TN-61-29, Part I UNCLASSIFIED Report

The second AFSWC Hydrodynamic Conference was held at Kirtland Air Force Base for the purpose of discussing numerical techniques which have become an important and widely used tool for solving fluid flow problems. A large number of the papers presented dealt with the problems of the finite difference analogs of the differential equations of motion. A few papers discussed work toward analytic solutions of these equations. Topics included hydrodynamics, magnetohydrodynamics, radiation transport, and solid material motion. (U)

The Proceedings are published in two parts: Part I is unclassified and Part II is classified. (U)

UNCLASSIFIED

1. Astrophysics
2. Boundary layers
3. Fluid flow
4. Gases
5. Hydrodynamics
6. Ionization
7. Kinematics
8. Magnetic fields
9. Plasma
10. Radiation flow
11. Shock hydrodynamics
12. Shock waves
13. Spalling
14. Structural elements - Effects of blast
15. X-Radiation

I. Rich, John C., Comp.
II. AFSWC, Kirtland AFB, N Mex
III. Project 5776

UNCLASSIFIED

Air Force Special Weapons Center, Kirtland Air Force Base, N Mex

AFSWC SECOND HYDRODYNAMIC CONFERENCE; NUMERICAL METHODS OF FLUID FLOW PROBLEMS (U), Compiled by John C. Rich, 16-18 May 1961. 206 pages including illus. (Project 5776) AFSWC-TN-61-29, Part I UNCLASSIFIED Report

The second AFSWC Hydrodynamic Conference was held at Kirtland Air Force Base for the purpose of discussing numerical techniques which have become an important and widely used tool for solving fluid flow problems. A large number of the papers presented dealt with the problems of the finite difference analogs of the differential equations of motion. A few papers discussed work toward analytic solutions of these equations. Topics included hydrodynamics, magnetohydrodynamics, radiation transport, and solid material motion. (U)

The Proceedings are published in two parts: Part I is unclassified and Part II is classified. (U)

UNCLASSIFIED

1. Astrophysics
2. Boundary layers
3. Fluid flow
4. Gases
5. Hydrodynamics
6. Ionization
7. Kinematics
8. Magnetic fields
9. Plasma
10. Radiation flow
11. Shock hydrodynamics
12. Shock waves
13. Spalling
14. Structural elements - Effects of blast
15. X-Radiation

I. Rich, John C., Comp.
II. AFSWC, Kirtland AFB, N Mex
III. Project 5776

UNCLASSIFIED

Air Force Special Weapons Center, Kirtland Air Force Base, N Mex

AFSWC SECOND HYDRODYNAMIC CONFERENCE; NUMERICAL METHODS OF FLUID FLOW PROBLEMS (U), Compiled by John C. Rich, 16-18 May 1961. 206 pages including illus. (Project 5776) AFSWC-TN-62-29, Part I UNCLASSIFIED Report

The second AFSWC Hydrodynamic Conference was held at Kirtland Air Force Base for the purpose of discussing numerical techniques which have become an important and widely used tool for solving fluid flow problems. A large number of the papers presented dealt with the problems of the finite difference analogs of the differential equations of motion. A few papers discussed work toward analytic solutions of these equations. Topics included hydrodynamics, magnetohydrodynamics, radiation transport, and solid material motion. (U)

The Proceedings are published in two parts: Part I is unclassified and Part II is classified. (U)

UNCLASSIFIED

1. Astrophysics
2. Boundary layers
3. Fluid flow
4. Gases
5. Hydrodynamics
6. Ionization
7. Kinematics
8. Magnetic fields
9. Plasma
10. Radiation flow
11. Shock hydrodynamics
12. Shock waves
13. Spalling
14. Structural elements - Effects of blast
15. X-Radiation

I. Rich, John C., Comp.
II. AFSWC, Kirtland AFB, N Mex
III. Project 5776

UNCLASSIFIED